THE UNIVERSITY OF OKLAHOMA

GRADUATE COLLEGE

ANGULAR DISTRIBUTION OF SCATTERED INTENSITY FROM VARIOUS AEROSOLS

A DISSERTATION

SUBMITTED TO THE GRADUATE FACULTY

in partial fulfillment of the requirements for the

degree of

DOCTOR OF PHILOSOPHY

BY

JAMES F. BEATTIE

Norman, Oklahoma

1965

ANGULAR DISTRIBUTION OF SCATTERED

INTENSITY FROM VARIOUS AEROSOLS

APPROVED BY

S. T. Sa...

J. J. Eubank

Orrin K. Crosser

Darrell G. Harden

Robert M. St. John

DISSERTATION COMMITTEE

ABSTRACT

Under sponsorship of the United States Air Force an investigation was undertaken to obtain experimentally the monochromatic mass extinction and the monochromatic mass scattering coefficients for several real substances dispersed in air. These substances were aluminum oxide powder, carbon powder, carbonyl iron, glass beads, and silica powder.

Curves of the normalized axially-symmetric conservative scattering functions for each powder are plotted as a function of the polar angle into which energy is being scattered for each wave length investigated. Also included are plots of the experimentally determined mass extinction coefficients (β) and the ratio of σ/β for each powder.

Tables of the integrated axially-symmetric conservative scattering functions for aluminum oxide powder only are also included. These functions were calculated using the finite difference method.

ACKNOWLEDGMENTS

The research for this dissertation was conducted by the author while serving as an instructor in the Mechanical Engineering Department at the University of Oklahoma. The research equipment was made available by grant GP 360 from the National Science Foundation, and funds for the research by the Aeronautical Research Laboratories, Office of Aerospace Research, United States Air Force, (contract AF33(657)-8859), and the Ford Foundation.

The author also wishes to thank Dr. Tom J. Love, Jr. for his continued advice and encouragement throughout the course of this study as major advisor.

All members of the author's Graduate Committee, Dr. O. K. Crosser, Dr. D. Harden, Dr. R. M. St. John, and Professor W. J. Ewbank.

Mr. Han Min Hsia, for his assistance in programing and development of the theory.

To my wife, Kathryn, I will be eternally grateful, for whose infinite patience and understanding made this work possible.

TABLE OF CONTENTS

LIST OF TABLES

LIST OF ILLUSTRATIONS

ANGULAR DISTRIBUTION OF SCATTERED INTENSITY FROM VARIOUS AEROSOLS

CHAPTER I

INTRODUCTION

Since the initial space probes and satellites were designed, there has been an increasing interest in more detailed knowledge of the radiation properties of a polidisperse media. This interest has been primarily prompted by the need for more accurate predictions of the thermal balances of spacecraft which includes the region surrounding the vehicle that contains high temperature particles of ablative material. In particular, precise knowledge of the angular monochromatic scattering function, mass scattering and extinction coefficients and the spectral absorption and emission coefficients of these polydisperse particles will be required if accurate thermal balances are achieved.

Thermal energy affecting the temperature of a spacecraft in flight is derived from two sources--(i) energy generated internally, and (ii) absorption of incident radiation from the sun and other celestial bodies. Radiation from the background of space itself is negligible, since its

effective temperature is so low as to be insignificant. Therefore, temperatures encountered by spacecrafts are determined by an energy exchange between these two sources.

By establishing and maintaining a proper energy balance between absorbed solar radiation and the radiant energy emitted from the vehicle to space, almost any required temperature within the vehicle may be readily maintained. This balance, then is a function of the optical properties and the temperature of the exterior of the spacecraft. Further, there are two spectral regions of major interest, one between approximately 0.3 micron and 3.0 microns, where over 98 per cent of the sun's energy is emitted (111)[1], and the other beyond 3.0 microns, a region in which a spacecraft operating at a moderate temperature emits more than 99 per cent of the emitted thermal radiation.

The exact calculation of the angular distribution of the intensity of light scattered by an element of mass illuminated by a parallel beam of light is extremely complex. For spheres, this calculation has been carried out by Mie; using Van de Hulst's formulation of Mie's equations (145), the intensity scattered per unit of solid angle and per unit area of cross section of the particle may be expressed in terms of $\alpha = 2\pi r/\lambda$ (where r is the radius of the spherical particle and λ is the wave length of the incident light in

---

[1]Numbers in parentheses refer to items in bibliography.

the medium surrounding the particle), the relative refractive index m, and the angle θ between the direction of propagation of the incident and scattered beam.

Accounts of "Mie's theory" are so readily available (144), that it will suffice here to give only the barest outline. Mie gave his solution in series form. The terms thereof correspond to the electromagnetic waves scattered by a sphere due to an incident plane electromagnetic wave. The movement of free and bound electrons in the sphere that is induced by the incident wave gives rise to radiation that is decomposable into dipole, quadrupole, and higher radiation, each described by a partial wave.

This general theoretical solution by Mie covers the behavior of spheres of all sizes and colors. For very small spheres of colorless matter his solution reduces to that given by Lord Rayleigh (89). For large particles such as those occurring in haze, smog, and fog, where particle diameters may range from about 0.1 micron to over 100 micron, the "Mie scattering theory," for colorless spheres reduces to the rainbow phenomena which can be deduced by geometric optics. Application of this theory to atmospheric scattering involves the classification of particle size and index of refraction by statistical methods. The "Mie scattering functions," which are converging infinite series, have been calculated on electronic computing machines, for a wide range of particle sizes and refractive indexes and are

available in tabular form (56).

Atmospheric scattering by large particles, unlike Rayleigh scattering which is strongly wave length dependent, is nonselective or independent of wave length. It also assumes negligible absorption, and is applicable therefore to the intervals of negligible atmospheric absorption.

In the atmosphere, transmission of infrared radiation is reduced or attenuated by both absorption and scattering, which occur together. Absorption may be much greater than scattering, or vice versa, depending upon the nature of the atmosphere, the particle size, and the wave length considered, but both phenomena are present. Furthermore, the combined sum of percents of absorption, scattering, and transmission always totals 100. The combined total of the absorption and scattering coefficients is often referred to as the extinction coefficient. Thus, for a given wave length

$$I = I_o\, e^{-(k_a+k_s)d} = I_o\, e^{-k_e d} .$$

For particles smaller in diameter than the wave length of the incident radiation, Rayleigh's law indicates that spectral radiance due to scattering decreases rapidly with increasing wave length. Under these conditions Rayleigh's law states that

$$I_s = I_o k V^2 \lambda^{-4}$$

where I_s = intensity of scattered radiation

I_o = intensity of incident radiation

V = volume of the scattering particles

λ = wave length of incident radiation

k = a constant

This shows that visible light is scattered more than the longer-wave length infrared radiation. This also accounts for the blue color of the sky, since scattering by the earth's atmosphere is greater at the blue end of the visible spectrum. The red and yellow coloring of sunsets and sunrises is due to increased scattering of the longer-wave lengths in the visible spectrum caused by particles of dust and smoke and the longer path length near the horizon. In the infrared spectrum, scattering is greatest in the near-infrared region adjoining the visible spectrum, and decreases rapidly for longer wave lengths. The Rayleigh scattering theory is limited however, to scattering by particles whose diameters are considerably smaller than the wave lengths of the incident radiation. Thus, in the visible region of the spectrum, Rayleigh's scattering theory applies to molecular scattering.

For particles of diameter greater than the wave length of the incident light however, Mie's equations are too cumbersome to apply in their standard form. For these particles one or the other of two approximations which have been proven to give very accurate results in this region may be used. The approximations available are those of: (i) Rayleigh and Gans (55) (applicable to transparent particles if

$2\alpha(M-1)<<1$, and (ii) Mecke (144) applicable if $2\alpha(M-1)>>1$ and $\alpha>10$, approximately). Where M is the complex index of refraction.

CHAPTER II

LITERATURE SURVEY

In recent years, scores of papers have been written in which the scattering properties of perfect spheres as a function of both the size and the electrical properties of the scatterer have been evaluated. The basic formulas which are used are almost without exception referred to as the "Mie solution," "Mie formulas," or "Mie theory."

The reason that these formulas are associated with the German physicists Gustav Mie in a classic paper published by Mie in 1908 (101) in which he developed the spherical harmonic series which describes the energy scattered by a perfect sphere due to the passage of an incident plane electromagnetic wave in terms of partial electric and magnetic waves.

An examination of the literature of the late 1800's reveals that the formulas which came to be known as the "Mie solution" were first presented in a memoir published by a Danish physicist Ludwig Lorenz in 1890 (88), in which he solved the vector-wave equation by using a pair of potential functions which are identical with the Debye potentials

which are said to have been first introduced by P. J. Debye in a paper published in 1909 (29).

Most authors seem to be aware of the fact that the solution of the boundary value problem for the scattering of acoustic waves by a perfect sphere was first given by Lord Rayleigh in 1872 (89). However, it is apparently not well known that Lamb (84) acknowledged that his vector-wave solution of 1881 (or, its equivalent, the Lorenz - Debye potential), had been discovered by Alfred Clebsch as early as 1861. Clebsch showed how to solve exactly, for any ratio of particle size to wave length, the problem of determining what, in modern vector terminology, is known as the dyadic Green's function for the elastic wave equation for the case of a perfectly rigid sphere.

In 1962 Rudolf Penndorf (116) developed a series of approximation formulas for small spherical particles in absorbing and nonabsorbing aerosols in which the radius of the spherical particles contained within the aerosols are much smaller than the wave length of the light under consideration. These formulas were derived by using the spherical harmonic series expansion of "Mie's theory" and they give the total scattering coefficient K for real, complex, and infinite indices of refractors. Thus, by using these approximation formulas one is able to calculate the scattering and absorption coefficients faster than by using the "Mie formulas" with an error of less than 10 per cent.

Also, in 1962 Penndorf (114) by using the cross section theorem, developed an approximation formula for the scattering of light in the forward direction which proved to be valid for perfect spherical particles contained within aerosols if the radius of the particles in question were larger than the wave length of the incident light. This function is called the approximated phase function pM' and is equal to $\frac{1}{4}\alpha^2 K$ where K is again the total scattering coefficient developed by Mie and α is the size parameter of the aerosol and is equal to $2\pi r/\lambda$. The limit however is that α must be greater than 5.0.

J. R. Hodkinson and I. Greenleaves (69) in 1963 presented a series of graphs which would enable one to make quick estimation of the scattering and extinction of light by a media of transparent spheres. These graphs are based on the external reflection and transmission of light geometrically incident on the spherical particles and scattering by classical diffraction.

The index of refraction for these particles ranged from 1.10 to 2.00. Their investigation for scattering angles up to 40 degrees proved that if the particles were 3 or 4 times larger than the wave length of the incident light, and if the particle size range was 2:1 so that phase effects averaged out, the scattering and extinction coefficients calculated using their graphs agreed well with the scattering and extinction coefficients calculated directly from "Mie's

theory" and by the diffraction approximation of Gumprecht and Sliepcevich (56). Thus, from their investigation they concluded that their results should also hold for irregular particles and to some extent with nontransparent particles.

Measurements of the optical scattering coefficients of the atmosphere at ground level and altitudes up to 14,000 feet have been made by Crosby and Koerber (26). In their work they used an integrating nephelometer. The principle of the nephelometer is as follows: a ray of light from a FA. 10 electronic flash tube transmitted by an opal glass window is passed through the conical view of a photometer. The light is scattered by atmospheric particles (dust, smoke, water droplets, and air molecules) and some of the light is then directed toward the photometer at some angle ϕ. Since the light source is a plane diffuse source, light scattered by the particles from the other rays of light is also received by the photometer at some other anle ϕ'. Then by knowing the radiant intensity along the normal to the light source, the scattering coefficient is determined.

From the comparisons of results obtained for the case of homogeneous spherical scatterers by Born's approximation with those of the exact analysis obtained by Mie's formulas, F. A. Albini (2) concluded that consistent application of the Born approximation to the case of inhomogeneous spherical particles will give accurate values of the differential and total scattering cross section. Also, Albini concludes that

Born's approximation is not restricted to perfectly spherical particles as are several of the other approximations. However, at the present this has not been proven.

In 1961 Curcio (27) was able to determine the particle size distribution for atmospheric aerosols by using measured values of the monochromatic scattering coefficients in the wave length region of 0.40 micron to 2.27 micron. From this investigation Curcio found that aerosol size distribution is in error if calculations are based only on extinction and scattering measurements in the visible region. Thus, for size distribution of atmospheric aerosols extinction and scattering measurements in the infrared region are required along with those made in the visible region of the spectrum.

Durmendjian, Clasen and Viezee (32) in 1961 developed a new set of exact Mie functions which are related to the scattering of electromagnetic waves on dielectric and partially absorbing spheres. By means of an IBM - 1410 computer system numerical results for particles having complex indexes of refraction and size corresponding to atmospheric particles illuminated by visible and infrared radiation are given. Their investigation also includes diagrams on the effects of an increase in absorption indexes on the extinction and absorption cross section and the intensity of the scattered flux.

In the last few months, Fraser (45) has published a paper which deals with the specific intensity and polarization

of sunlight that is scattered by the surface of the earth due to an overlying aerosol. The data presented in this paper is valid only for moderate optical thickness ($\tau < 0.25$). Fraser assumed that the incident light is parallel and the light falling on the earth's surface is reflected by the earth's surface.

Stein, Welson, and Stidham (131) in their work, extended the Rayleigh - Gans approximation theory (55) for light scattered by homogeneous spheres having an internal heterogeneous density. These internal heterogeneities are described by a Debye-type exponential function. By considering the effects of internal heterogeneities, their scattering results consisted of a sum of two terms; one representing the contribution from the homogeneous spheres and the second representing the contribution to the scattering intensity caused by the internal heterogeneities. Their predicted results were found to have the same trends as the scattering intensity measured experimentally for heterogeneous spheres.

Speyer (130) designed and built a cloud chamber for measuring the various optical properties of aerosols. In his paper he explains the design of the optical system, the cloud chamber, and two radiation detector systems. He also explains the procedure for determining the transmissivity vs distance measurements and the scattering vs transmissivity measurements along with the method used in calculating the

absorptivities of the aerosols.

Recent work by L. M. Romanova (122) describes the angular spatial scattering or radiation in plane layers of a homogenous turbid medium with a pronounced forward scattering index. In his paper he gives experimental and theoretical data for a turbid medium of nearly spherical dielectric particles which have a refractive indices slightly different than unity and are dispersed in a solid medium. Polarization effects were neglected. His experimental and theoretical data is compared with experimental measurements made by Limofeeva (138) upon whose work Romanova theory is based.

A. P. Prishivalko (119) in 1962 studied light scattering from large highly absorbing spherical particles by the geometrical optics approximation. Since in his paper scattering is completely determined by the reflection of the incident light at the surface of the particle; Prishivalko explains in detail the dependence of the scattering diagrams, the degree of polarization of the scattered light, and the scattering coefficient on the optical constants of the scattering particles. In comparing his work to that of Fedorova (40) and Pribytkova (118), Prishivalko found his results to be in agreement if they were multiplied by a correction factor. The reason for this correction factor is that Fedorova and Pribytkova measurements were made using particles having the shapes of splinters rather than spherical shapes.

A. P. Ivanov (71) presented in 1962 a theoretical study on the phenomena of opacity decrease, luminescence, amplification and self-excitation as a function of the optical characteristics of light scattering substances. He discussed in detail the effects that a positive absorption coefficient has upon the reflection and transmission in a dispersing layer and the effects of light being generated in a dispersing media and the influence that heterogenetics have upon energy generated by particles having a negative absorption coefficient in plane-parallel layers. His results showed that the intensity of the energy generated due to this negative absorption coefficient is more intense in scattering substances than in nonscattering substances and that for the self-exciting system of plane-parallel layers that contain inhomogeneities there is a maximum value for the intensity of the energy generated.

Wyatt (150) in the last few years has written several papers on scattering from inhomogeneous particles or objects that are spherically symmetrical (148, 149). In 1962 he solved Maxwell's equations in terms of transverse magnetic and transverse electric fields. The two potential functions that describe these fields were reduced to those used by Van de Hulst (144) who worked with the similar case of uniform refractive index. However, this exact theory was derived earlier by Nomura and Takaku (110).

In Wyatt's theory the equations were solved for an

inhomogeneous sphere by a numberical method. The only assumption made was that the optical properties and their first derivatives are continuous throughout the scatterer with a possible exception being at the outermost surface. Also, in this theory the refractive index was presented in a special form as a function of the radius of the sphere.

Wyatt's theory has a great variety of possible applications. A few of the more important ones are problems that are concerned with an accurate description of the transition region within spherical scatterers such as dimetallic particles, microwave scattering from plasma surrounded re-entry vehicles, soft x-ray scattering, scattering from planetary atmospheres, and radiowave scattering from plasmoids such as nuclear bursts. In addition, the general theory would simplify the physical calculations of determining the scattering coefficients associated with multi-layer concentric spheres.

Levine and Kerker (87) used the general theory for light scattered by spherically symmetric inhomogeneous objects derived by Wyatt for a particular model. This model consisted of a central core which had a uniform refractive index and a surrounding shell having a refractive index which varied with the radius of the sphere according to some power law. The medium surrounding the shell also had an uniform refractive index.

A problem similar to this was solved analytically by Nomura and Takaku (110). Thus by combining the work of

Wyatt and Nomura and Takaku, Levine and Kerker were able to obtain an analytical solution. The scattering coefficients given in the results are in a form similar to that used by Aden and Kerker (1).

Van de Hulst (144) states that the oscillatory Mie theory extinction coefficient curve for a single spherical particle would be a much smoother curve for a polydisperse media of transparent spheres. The new curve would rise from zero to a maximum value of about 3 where the mean particle diameter was in the neighborhood of $2\lambda/\pi(M-1)$ and then decline smoothly to a constant value of 2 as the mean particle size increased. Hodkinson (68) in his experimental work with transparent irregular particles that were larger than 2 or 3 wave lengths of light did not find this to be true. A plot of his data showed that the total extinction coefficient increased monotonically from zero to a constant value of two as the mean particle size increased. Hodkinson contributes the absence of the maximum point that Van de Hulst stated would be found in a plot of Mie's extinction coefficient for a polydisperse media of transparent spheres to the superposition of the results of many individual particles of various shapes, orientations and sizes.

Napper and Ottewill (108) in working with four monodisperse polystyrene latex dispersions of different diameter particles, found that multiple scattering would be present unless the distance between the centers of the spherical

particles was greater than 200 times their radius. From their results they also state that for particles whose size fall within the Mie region of light scattering that the scattered intensity at any given angle may not be directly proportional to the number of scattering units. However this may not be true for all wave lengths because in their experiment the only wave length involved was 5,461 A.

Napper and Ottewill worked with the four different dispersions and the size of the particles used varied from 0.264 micron to 1.171 microns. The concentration per unit volume was determined by particle counting using optical microscopy and the average distance between particles was then calculated from the concentration.

Much work has been done in the last year on determining the size of particles by light scattering techniques. Maron, Elder, Ulevitch, and Pierce (93, 94, 95, 96, 97) have published five papers in which five different theories and test procedures are discussed. They also present the results for an extensive number of latex systems of varying particle size and degree of size distribution. The method used in the first four papers utilizes absorption of incident light. In the last paper the electron microscopy is used to determine the polarization ratio at 90 degrees and thus the particle size. However in all five papers various light scattering techniques are used.

CHAPTER III

DEVELOPMENT OF THE TERMINOLOGY AND EQUATIONS

For the development of the terminology and equations used within this report, the author has elected to use the symbols and definitions that were utilized by Love (89).

It has been shown experimentally that when a pencil of rays from a light source is passed through certain media its intensity will decrease. This decrease in the intensity of the light ray is called extinction.

There are two factors which account for this decrease in intensity. One is that a small portion of the energy will be absorbed by the matter which is within the media. The second factor is that a portion of the incident energy may be reflected, refracted or diffracted by the matter and redistributed or scattered. If the energy were absorbed, it will cause an increase in the internal energy of the media, which in turn may remit energy at a different wave length. If the media redistributes or scatters the incident energy, the scattered energy like the reemitted energy may be at a different or possibly the same wave length as the incident energy. If the media scatters the incident energy at the

same wave length as that of the incident energy, the effect is called coherent scattering.

Coherent scattering may also be independent scattering. Since coherent scattering only indicates the wave length at which energy is reemitt or scattered whereas independent or multiple scattering indicates whether the scattering media causes the wave lengths of the remmitted or scattered energy to interfere with each other due to the density of the scattering media. Independent scattering prevailed throughout the work as will be verified in a later chapter.

There are several ways of expressing the mass extinction coefficient, the mass scattering coefficient and mass absorption coefficient. The most direct way is as follows: consider a media which has a mass per unit volume ρ and a thickness Δx. Let $I_o(x)$ be the intensity of the incident monochromatic energy that is traveling in the x-direction. Let $I(x)$ be the intensity of the monochromatic energy which is leaving the media after traversing through the media a distance Δx. As was mentioned earlier, energy when traversing certain media may be either scattered, absorbed or both. Thus one may account for the difference in $I_o(x)$ and $I(x)$ by writing the equation

$$I_o(x) - I(x) = + \rho(\sigma + \kappa) \quad I_o(x)\Delta x \qquad (1)$$

or

$$\frac{\Delta I(x)}{I_o(x)} = + \rho \beta \Delta x \qquad (2)$$

The negative sign indicates a decrease in $I_o(x)$ in the positive x-direction,

where κ = monochromatic mass absorption coefficient

σ = monochromatic mass scattering coefficient

$\beta = (k+\sigma)$ = monochromatic mass extinction coefficient.

The energy which is scattered from a pencil of rays will effect the intensity of radiation in other directions. Therefore, equations other than equations (1,2) are required to completely describe the phenomena known as radiation scattering.

In order to fully account for the effect of radiation scattering, a means for describing the scattering of energy as a function of the incident and scattering angle is required. Referring to Figure 1, the rate at which energy is scattered by an element of mass dm from a pencil of rays of which the intensity is $I(\theta,\phi)$ is

$$I(\theta,\phi)S(\theta,\phi,\theta'\phi')\frac{d\omega'}{4\pi}d\nu\, d\omega\, dm = I(\theta',\phi') \qquad (3)$$

where $I(\theta,\phi)$ = intensity of a pencil of rays with a frequency interval $(d\nu)$ having a direction θ,ϕ with respect to an arbitrary reference direction contained in a solid angle $(d\omega)$,

$d\omega'$ = solid angle into which energy is being scattered, having a direction θ',ϕ' with respect to an arbitrary reference direction.

θ = polar angle,

ϕ = azimuthal angle,

$S(\theta,\phi,\theta',\phi')$ = scattering function defined by equation (3).

Another way to look at the scattering function is to consider the terms

$$S(\theta,\phi,\theta',\phi') \frac{d\omega'}{4\pi}$$

as a probability function. This expression then gives the probability that energy which is incident on an element of mass dm from a direction θ, ϕ contained within the solid angle $d\omega$ having a frequency interval $d\nu$ will be scattered in the direction θ', ϕ' having a solid angle $d\omega'$. Then if β is the probability that the incident energy will either be absorbed or scattered or both by the element of mass dm and k the probability that the incident energy will be absorbed by dm, one can readily see that the probability that the incident energy is scattered is

$$\sigma = \int_0^{4\pi} S(\theta,\phi,\theta',\phi') \frac{d\omega'}{4\pi} \qquad (4)$$

where σ is again the mass scattering coefficient.

As was mentioned earlier if the media absorbs energy it will cause an increase in the thermal energy and may then be reemitted at a different or possibly the same wave length. If the element of mass dm does absorb part of the incident energy and this energy is completely converted into thermal energy and is then reemitted having a spectral energy

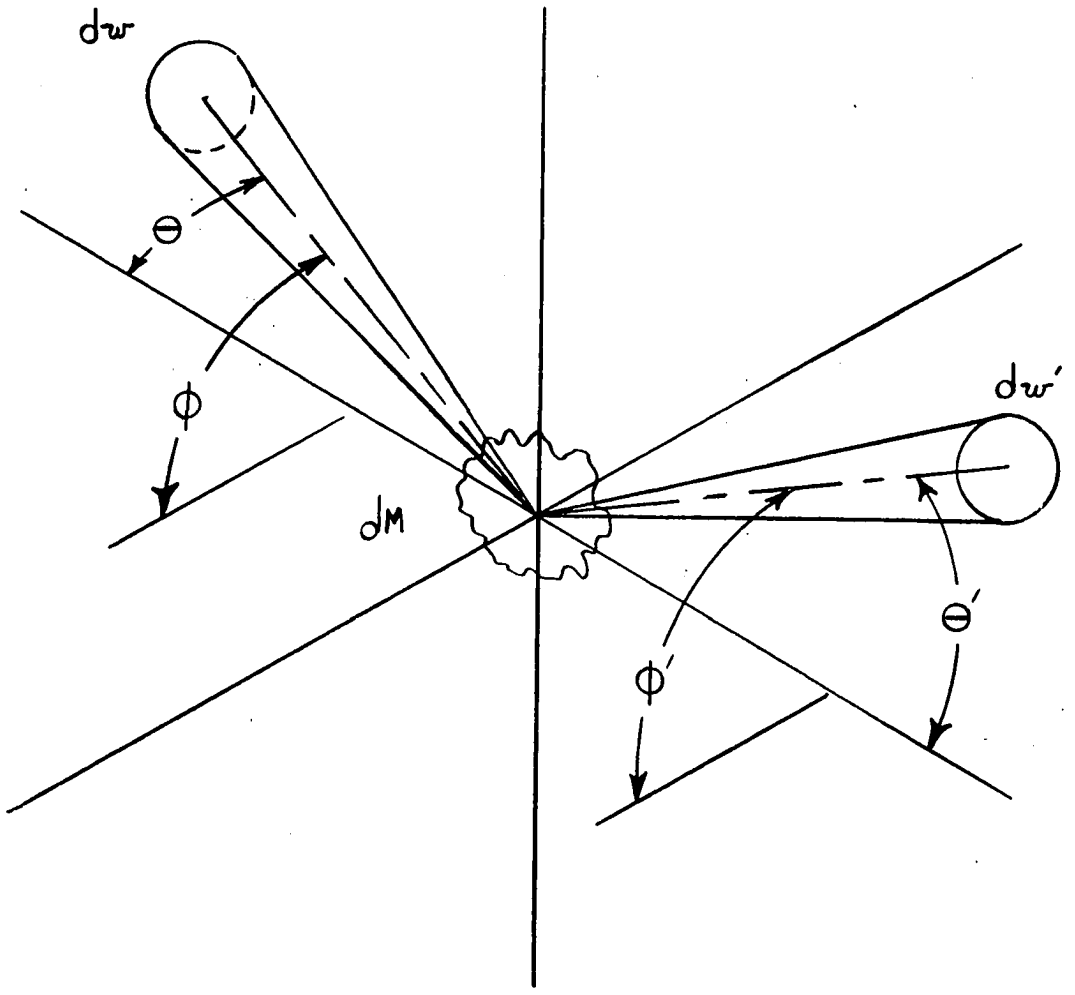

Coordinate Scheme for Scattering Function

Figure 1

distribution corresponding to the Planck function with the same frequency interval as the incident energy; the intensity of the thermal emission may be written as

$$I_{\nu}(T) = \varkappa I_{bb,}(T) \qquad (5)$$

where $I_{bb,}(T)$ = Planck's function at a temperature T, and a frequency ν, for an element of mass dm.

Thus by applying the conservation of radiant energy for an element of mass, an integro-differential equation takes form. This equation may be written as:

$$\frac{dI(S,\theta,\phi)}{dS} = -\rho\beta I(S,\theta,\phi) +$$

$$+ \int_0^{\pi}\int_0^{2\pi} \frac{\rho\sigma}{4\pi} S(\theta,\phi,\theta',\phi')I(S,\theta,\phi)\,\mathrm{Sin}\theta'd\theta'd\phi' + \rho\varkappa I_{bb,}(S) \qquad (6)$$

where the term on the left is the change in intensity with respect to distance. The first term on the right is the extinction of the incident energy as defined by the mass extinction coefficient. The second term is the energy which is scattered in the direction θ', ϕ' by radiant energy transversing the element of mass from all directions. The third and last term on the right-side accounts for the radiant energy which is emitted by the element of mass dm.

It should be noted that the scattering function $S(\theta.\phi,\theta',\phi')$ is a normalized function and the mass scattering function σ represents an average effect over all directions

and is not an exact expression for real cases. Also, the conservation of radiant energy equation is restricted to coherent scattering, because there is no way to acknowledge the contribution of energy scattered from other wave lengths.

CHAPTER IV

EQUIPMENT

The equipment used throughout this experiment was designed and built by Wheasler (147). Its function was to measure the intensity of energy scattered and absorbed by a polydispersed system of fluidized particles from a small pencil of incident rays. In this case the polydispersed fluidized particles were irregular in shape and size and were dispersed vertically in an air stream under pressure to form a column of fluidized particles bounded by ambient air. The stream tube was a highly polished 0.375-inch I.D. aluminum tube which was positioned concentrically through a 1.5-inch hole located in the center of a 36-inch rotating platform. The rotating platform held the energy sources and the source optics. The energy sources were a vertical filament tungsten lamp which was used in the 0.6 to 1.4 micron wave length region and a "glo-bar" which was used in the wave length region from 1.4 to 15.0 micron. The source optics consisted of a spherical mirror so positioned that one focus was on the energy source while the other focus was on the fluidized particles. As the platform rotated the

energy that was scattered by the cloud of particles focused by another spherical mirror and a front surface plane mirror on the "Littrow Mirror" within the monochromator. The monochromator used was a Perkin-Elmer Model 112, single-beam, double pass, infrared spectrometer equipped with an internal chopper. Due to the unusually wide spectral range to be investigated more than one prism material was required for full wave length coverage. The selection of the prism materials was based mainly on the wave length to be scanned and the low energy level available for detection at both the short and long wave length ends of the scanned spectrum. For these reasons fused silica was used for the wave length of 0.6 to 1.4 micron and sodium chloride for the 2 to 15 micron region. The monochromatic scattered energy was detected by a lead sulfide cell in the short wave lengths (0.6 to 1.4 micron) and by a thermocouple in the long wave length (2.0 to 15 micron) region of the spectrum. This signal was then amplified and recorded on a Leeds and Northrup Speed ox strip chart recorder. After the fluidized particles were ejected and had passed through the incident beam of energy they were collected by a "bell-mouth" attached to a Black and Decker industrial-type vacuum cleaner. For sampling the stream of fluidized particles a General Electric home vacuum cleaner with a filter attachment was used. The filter material used was a fiberglass material that would eliminate particles down to 0.5 micron and was furnished by

the Fram Corporation.

For a better understanding of the experimental equipment used, one is referred to figures (2, 3, 4).

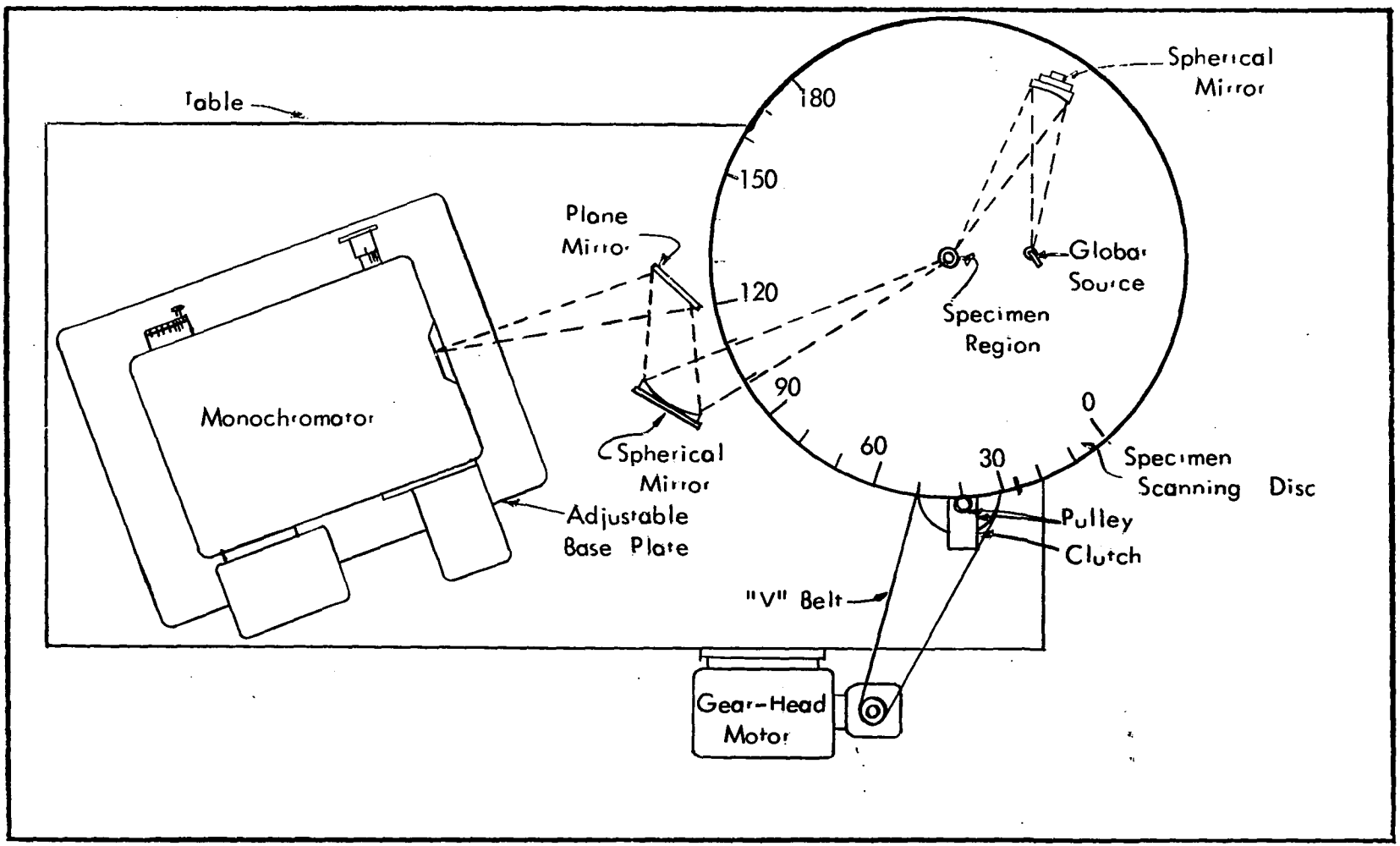

Figure 2 PLAN VIEW SCHEMATIC OF EQUIPMENT

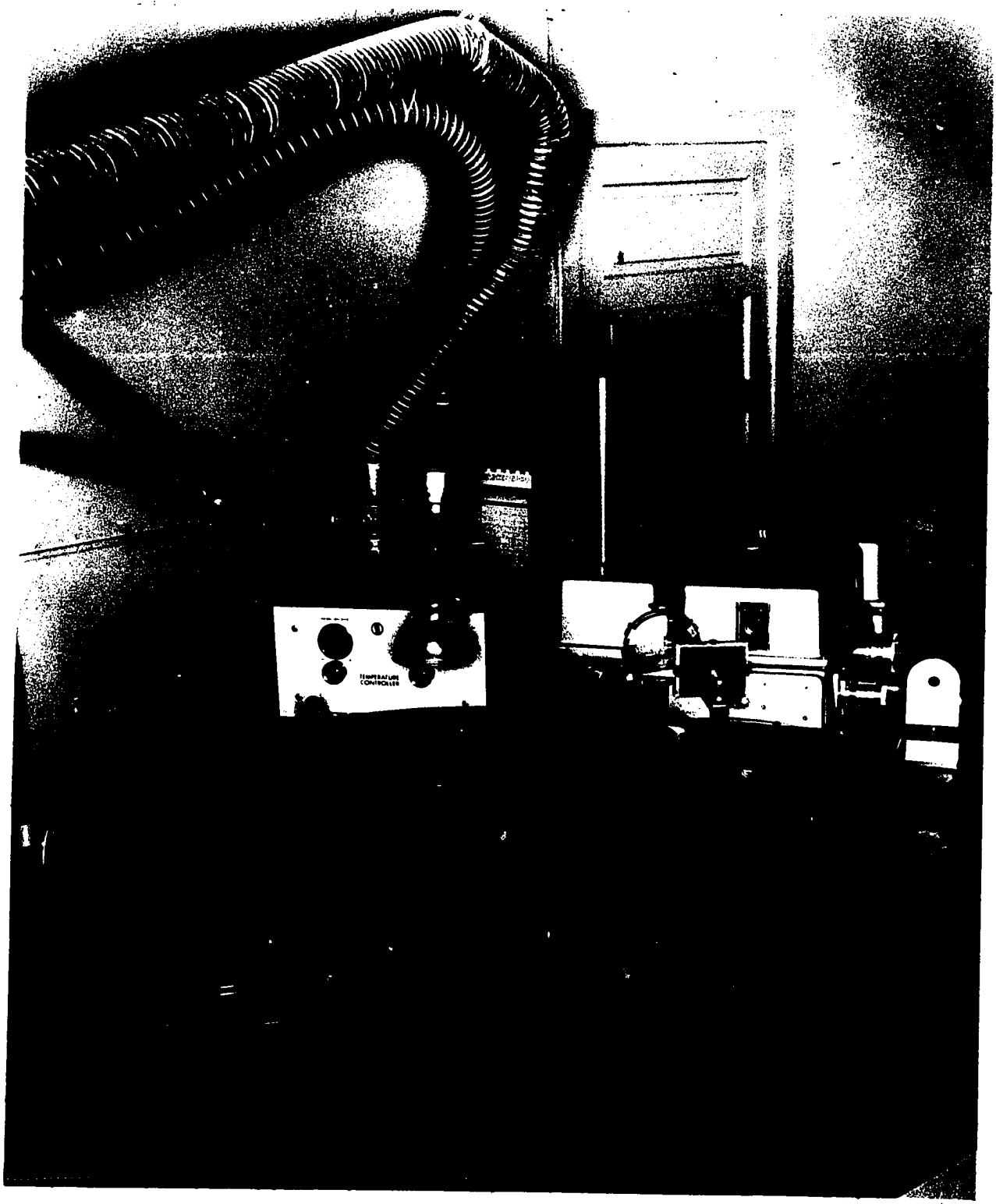

Radiation Scattering Detection Equipment

Figure 3

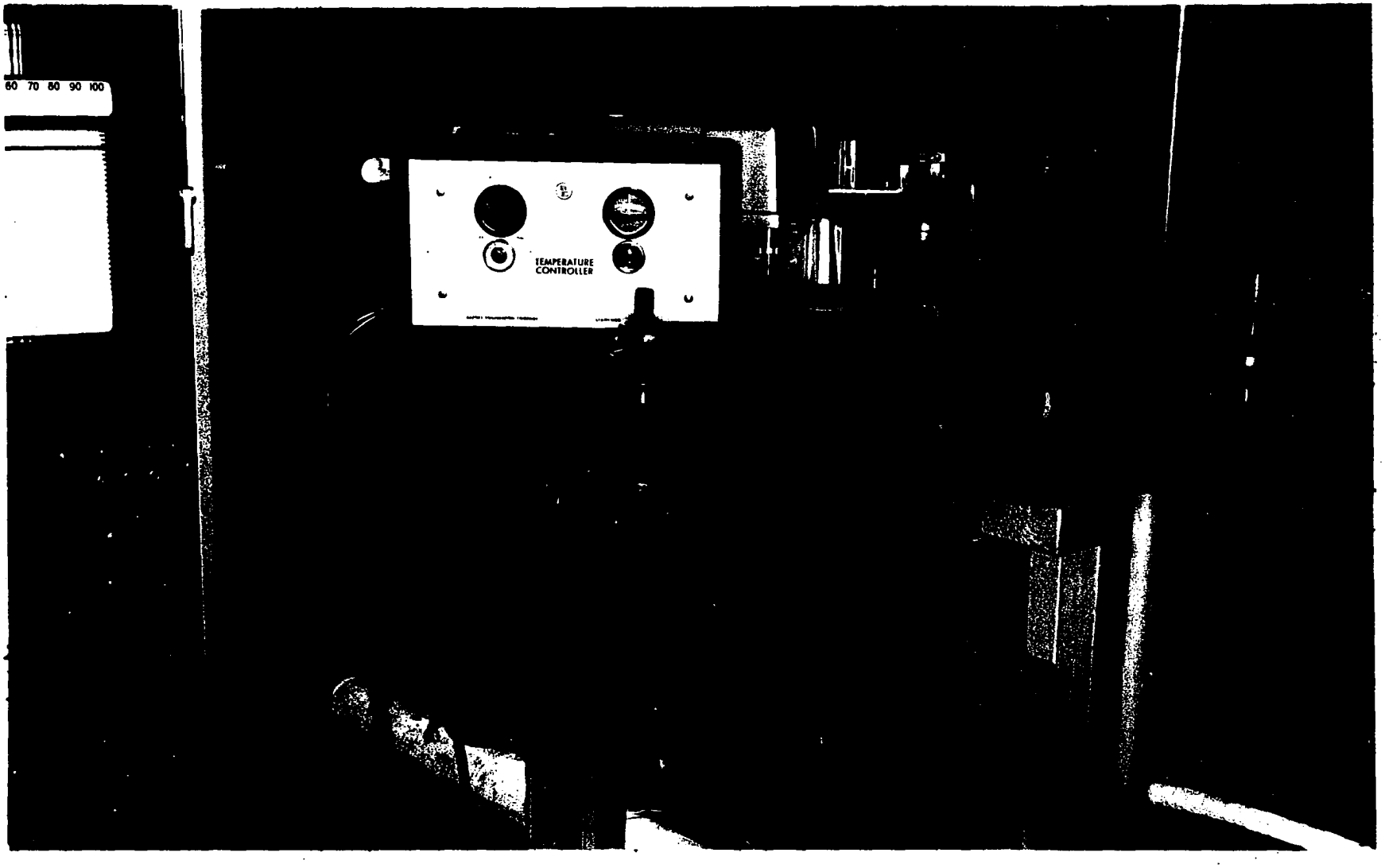

Radiation Scattering Detection Equipment

Figure 4

CHAPTER V

THE AEROSOL

The media used throughout this experiment was a polydisperse system. It consisted of particles which not only varied in size, but were irregular in shape. Also, for the wave lengths at which this experiment was conducted, it was desirable that the size range of the particles fall within 1 to 20 micron, of which 90 per cent be equal to or less than 5 micron.

Several different types of powder were used to produce the desired polydisperse media. They were: Aluminum powder 40-XD furnished by the Reynolds Aluminum Company, Carbonyl Iron powder SF furnished by the Antara Chemical Company, Silica powder furnished by the Pennsylvania Glass Sand Corporation, Carbon powder type Mogul A furnished by the Cabot Corporation, and Glass Beads furnished by the Pall Corporation. Each company also furnished a set of specifications which gave the average and maximum particle size, particle density, and the apparent density of the powder. However before testing was started, a complete analysis of each powder was performed to confirm the information supplied

by the manufactures.

The average particle size was determined for each powder by microscopic analyses, using a 400-power Bausch and Lamb microscope, a KE 10 power Unitron Micrometer eyepiece and a hemacytometer. The actual volume of the different particles was determined by a volumetric displacement of a fluid of a known volume and density, thus giving the relative density of the particles.

Since the average particle size not only determines the concentration of the aerosol but also whether multiple or single scattering is involved, several measurements were made and the mean particle size used. The procedures used are outlined by Robert A. Wheasler and James H. Ingram (147). The average particle size and average particle density of each different powder are given in Table 8.

The flow rate of the air used to produce the aerosols varied from 0.80 cfm to 2.50 cfm depending upon the type of powder being used. Therefore, for a 0.375-inch ID tube, turbulent flow conditions prevailed throughout the experiment insuring that the powder particles were well mixed in the air stream. The air flow rate was measured by a Stabil-Vis Flowrater, 0-2.55 cfm, manufactured by Fischer and Porter, Hatboro, Pennsylvania.

According to Van de Hulst (144) the intensity of a pencil of rays passing through a sample is reduced by extinction to $e^{-\tau}$ of its original value, where τ is the

optical depth of the sample and is defined as

$$\tau = \int_0^x \rho\beta dx \qquad \tau = \rho\beta x$$

assuming that ρ and β are constant and x represents the distance the rays of energy traveled through the sample. Thus, with this definition of the optical depth; Van de Hulst states that if $\tau < 0.1$, single scattering prevails. Boll and Sliepcevich (11) found from experimental results that single scattering will exist if the log of I_o/I is less than approximately 2.5 to 3, and the half-angle reception, θ, for the light received is less than about 1 degree to 1.4 degree. Using the above mentioned definition of single scattering, several experimental runs were made to determine the mass flow rate of the different powders and the rotor speed of the particle generator which would give the maximum value of $\Delta I_{ext.}$ and still be within the limits defining single scattering.

CHAPTER VI

PARTICLE GENERATOR

The particle generator used throughout this experiment was not the same generator that was designed and used by Wheasler (147) in his work. However, much of the earlier work of Wheasler's was incorporated in the present design. Wheasler's design did not give a uniformly dispersed aerosol for powders other than aluminum and in some cases (iron and silica) would not work at all. As was mentioned earlier the main criteria of the generator design was that it be able to produce a cloud of particles for a given period of time which has a constant density within preset limits.

A general description and principle of operation of the generator follows.

The particle generator consisted basically of a stirring or mixing chamber, rotor or stirring paddles, a screen or sets of screens, an AC constant speed motor, and a dispersion chamber. The stirring or mixing chamber was a copper tube which is 6 inches long and has an inside diameter of 2 inches and screws into a 2 x 1 - inch sweat fitting with the other end of the mixing chamber having a cap plug on it

for refilling the chamber. The 2 x 1 - inch sweat fitting was silver soldered to the "plugged" side of a 1 inch copper "tee" which served as part of the dispersion chamber. A 3/16-inch brass shaft was then passed through the mixing chamber and dispersion chamber and was used to turn the stirring paddles. To insure against leakage an "o-ring" seal was placed on the shaft as it passed through the dispersion chamber. The stirring motion was obtained by means of a 1/100 horsepower constant speed electric motor. To control the speed of rotation which directly governed the density of the aerosol, the power train between the motor and the stirring paddles was connected by a variable speed transmission and flexible couplings. Before the powder can pass from the mixing chamber or stirring chamber into the dispersion chamber it must pass first through a screen or series of screens, of which the size and number of screens depends upon the type of powder being used and the desired density of the cloud.

One advantage of this design is that in controlling the density of the cloud, there are three variables any one of which may be changed to give the desired density. They are screen size, stirring paddle speed, and the flow velocity of the air. This author did not find in any of the available literature a means for calculating screen size or mixing paddle speed that would give a preset mass flow rate of powder through a screen or series of screens. Therefore, before

a data run was made a test run was always made and the screen size, mixing paddle speed, and flow velocity of the air was determined which would give a given mass flowrate by trial and error methods.

For a better understanding of the particle generator described, one is referred to figures (5, 6, 7).

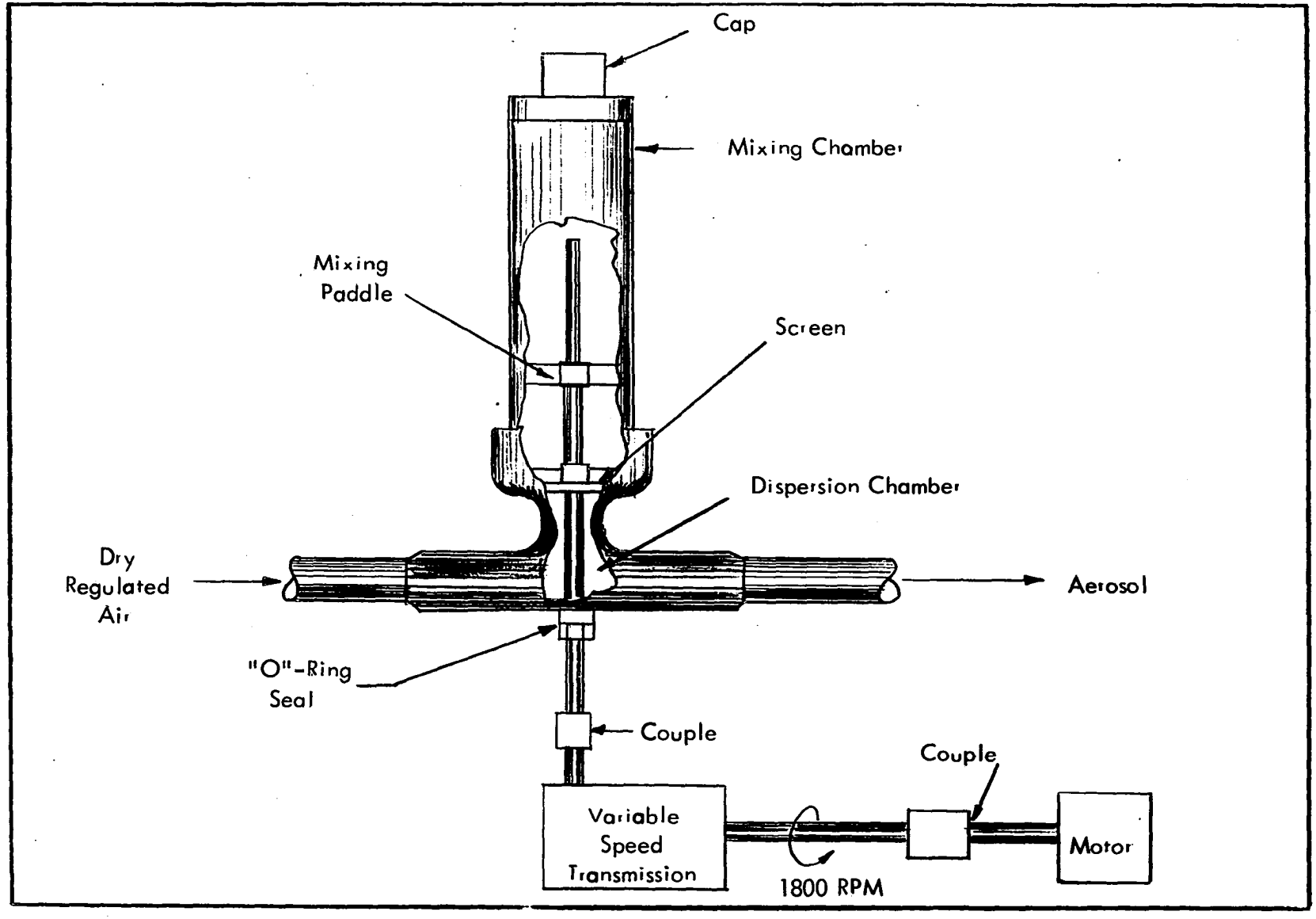

Figure 5

SCHEMATIC -- PARTICLE GENERATOR

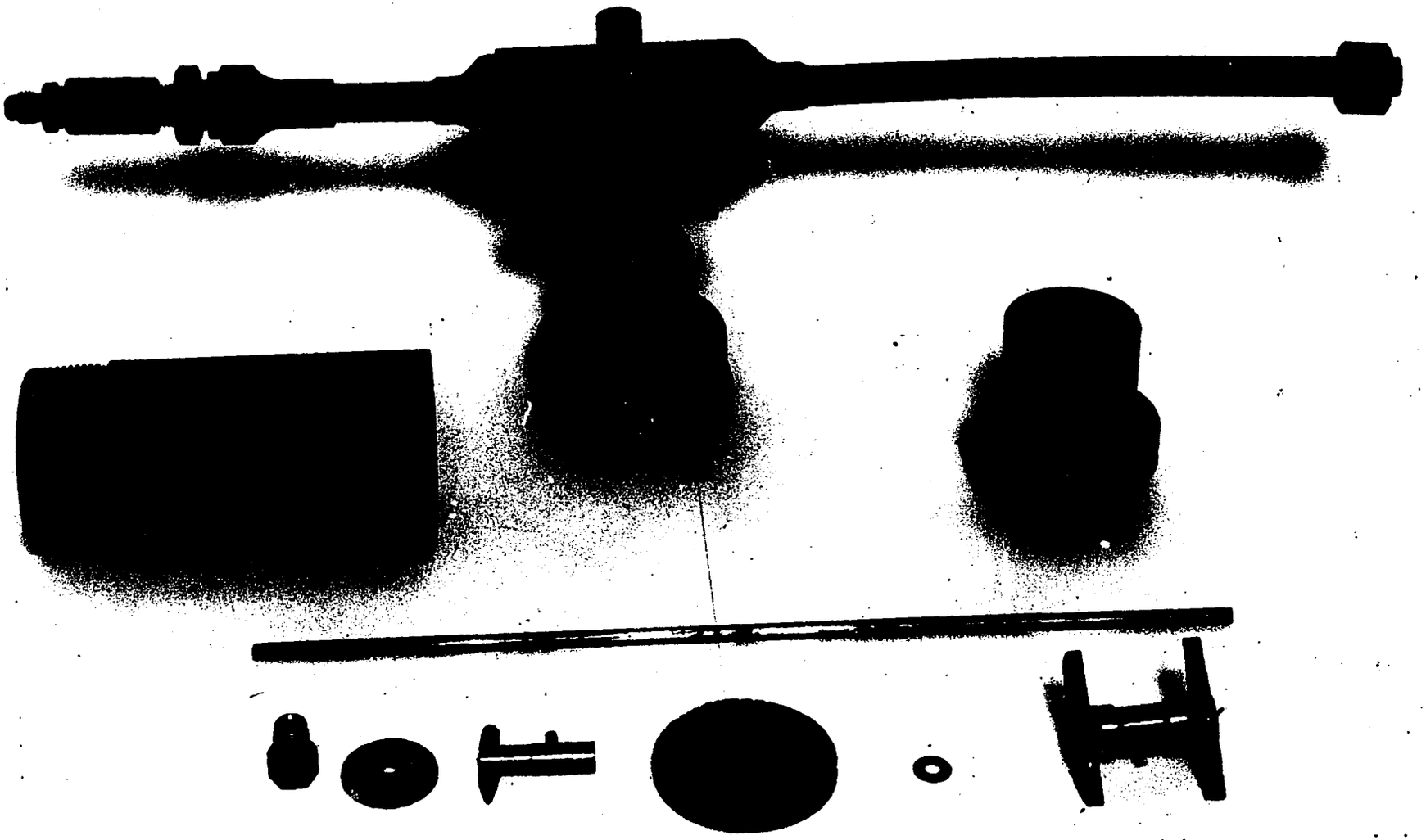

Particle Generator -- Exploded View

Figure 6

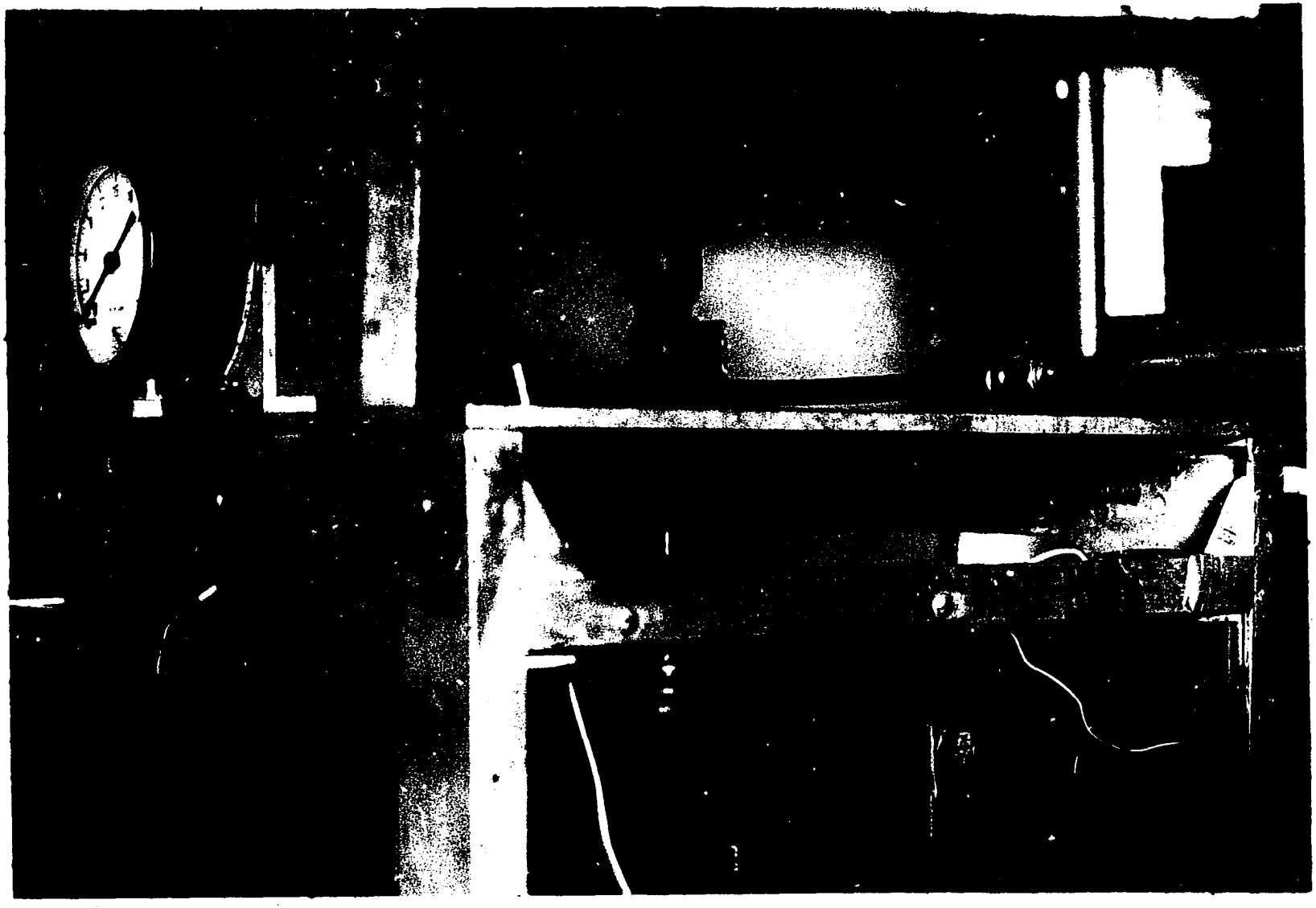

Particle Generator and Feed Mechanism

Figure 7

CHAPTER VII

EXPERIMENTAL RESULTS

The experimental data consisted of chart recordings of the signal from the lead sulfide cell or thermocouple of the monochromator as a function of the particle cloud density, angle of observation, and wave length of the radiation. Measurements consisted of a recorded signal with and without the cloud, combined with measurements of the particle diameter, and cloud density.

Extinction Coefficients

Extinction measurements were made on all five aerosol powders in 0.1 micron intervals over wave lengths ranging from 0.6 to 1.4 microns, in 0.5 micron intervals between 1.5 and 3.0 microns, and in 1.0 micron intervals between 3.0 and 15.0 microns. The following procedure was used to calculate the mass extinction coefficients. The incident energy intensity $I_o(x)$ at $\theta = 0$ and with the particle generator turned off was first recorded on the strip chart (see Figures 8, 9) for a particular wave length setting. After several runs were made of the incident energy to determine whether the recorder was balanced and if the energy level

Data Extinction

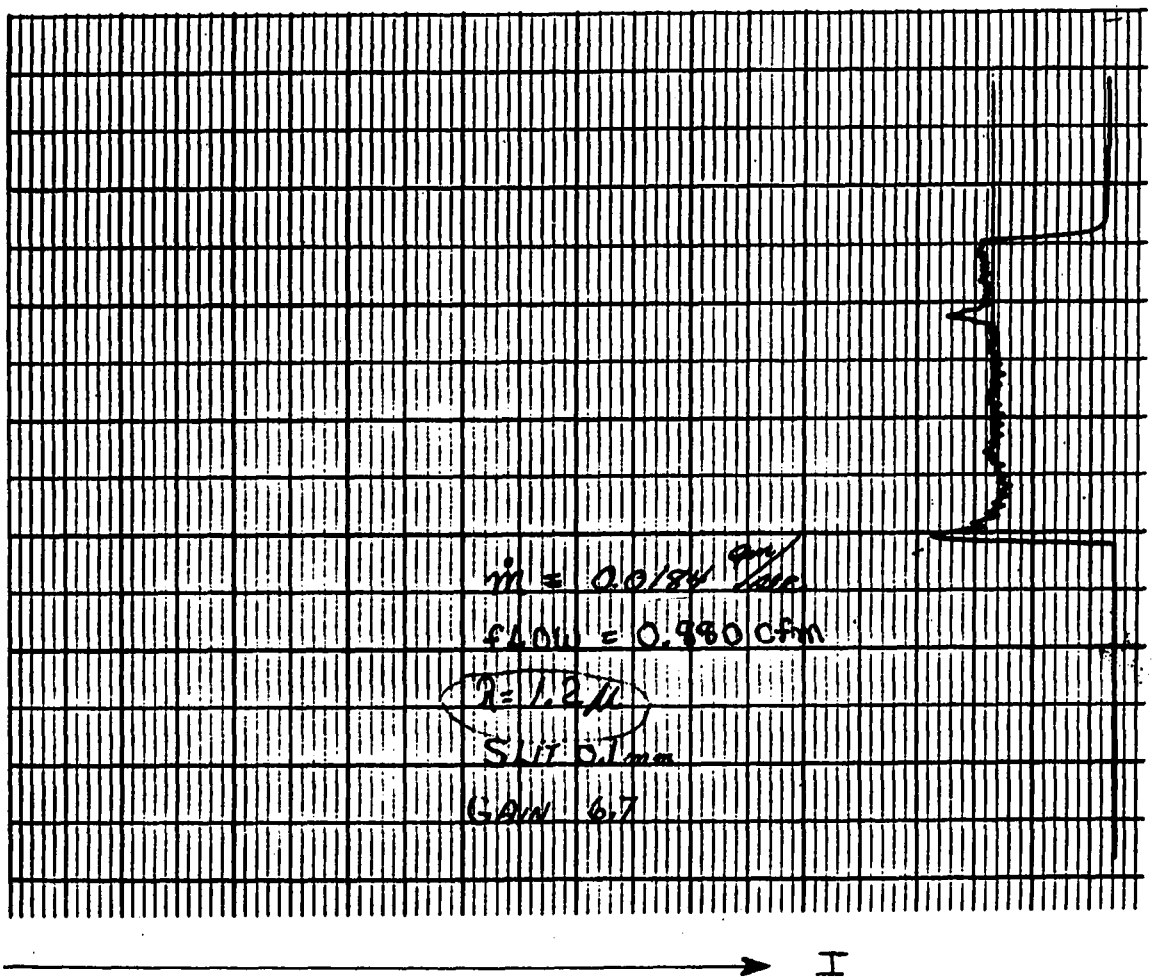

Figure 8

Data Extinction

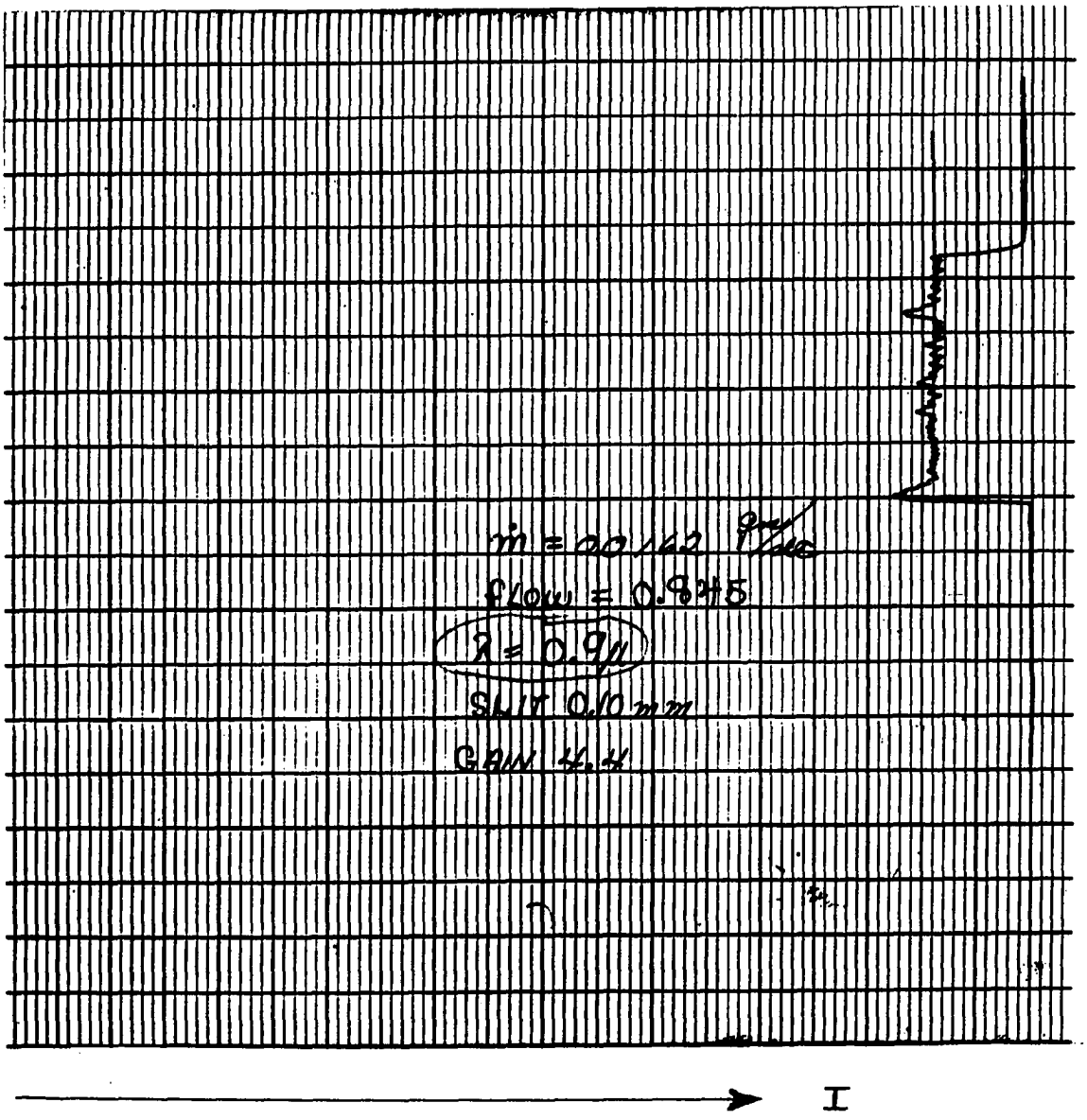

Figure 9

was constant, the particle generator was started. The absorption and scattering of the incident energy caused by the cloud of particles reduced the incident energy $I_o(x)$ to $I(x)$ their difference being $\Delta I(x)$. In equation 2 to calculate the mass extinction coefficient, the mass per unit volume ρ, of the aerosol and the distance Δx which the incident energy traveled in passing through the aerosol must be known. To determine the mass density a "bell mouth" funnel which contained a filter was placed completely over the aerosol discharge tube for a given period of time, then by dividing the weight of the aerosol trapped by the filter by the sampling time, the mass flow rate was determined. Since the aerosol was generated by injecting powder into an air stream of uniform velocity, the cloud density was found by dividing the mass flow rate of solid material by the volume flow rate of the air. Due to the method used to determine the mass flow rate and the accuracy to which the flowrater used to measure the airflow could be read, it is estimated that the deviation in density measurements was less than 1 per cent. A plate graduated in 1/40 inch divisions was placed an inch behind the aerosol discharge tube in order to measure the cloud thickness Δx. When the aerosol was struck by a ray of light, bright and dark fringe bands appeared on each side of the cloud. The average distance between these bright and dark fringe bands on each side of the cloud was determined as the cloud thickness Δx. In

general, these measurements were not affected by changing the flow rates or the flow ratio over the ranges used, and were always reproducible to 1/40 inch. The value of the thickness found was 0.376 inch.

The extinction data were obtained at each wave length a minimum of seven times, and, at some points in the longer and shorter wave lengths where atmospheric absorption was prevalent, as many as eleven times on separate occasions sometimes a full month apart. The values plotted in Figures 10 and 11, represent the average values of the extinction coefficients. For example, the mass extinction coefficient for aluminum at a wave length of 3 microns was plotted as an average value of 6,891 ft^2/lbm. At this particular wave length, the mass extinction coefficient was determined eight times and had a maximum value of 6,928 ft^2/lbm and a minimum value of 6,849 ft^2/lbm. For aluminum at a wave length of 4 microns, the mass extinction coefficient was determined ten times and was plotted as an average value of 5,263 ft^2/lbm with a maximum value of 5,317 ft^2/lbm and a minimum value of 5,244 ft^2/lbm. The variation in the results for the extinction coefficients was, therefore, less than 1 per cent. On occasional tests the calculated values of the mass extinction coefficient at a particular wave length would be as much as 20 per cent higher or lower than all other calculations made at the same wave length. This was always traceable to clogging in the particle generator. Therefore, these values

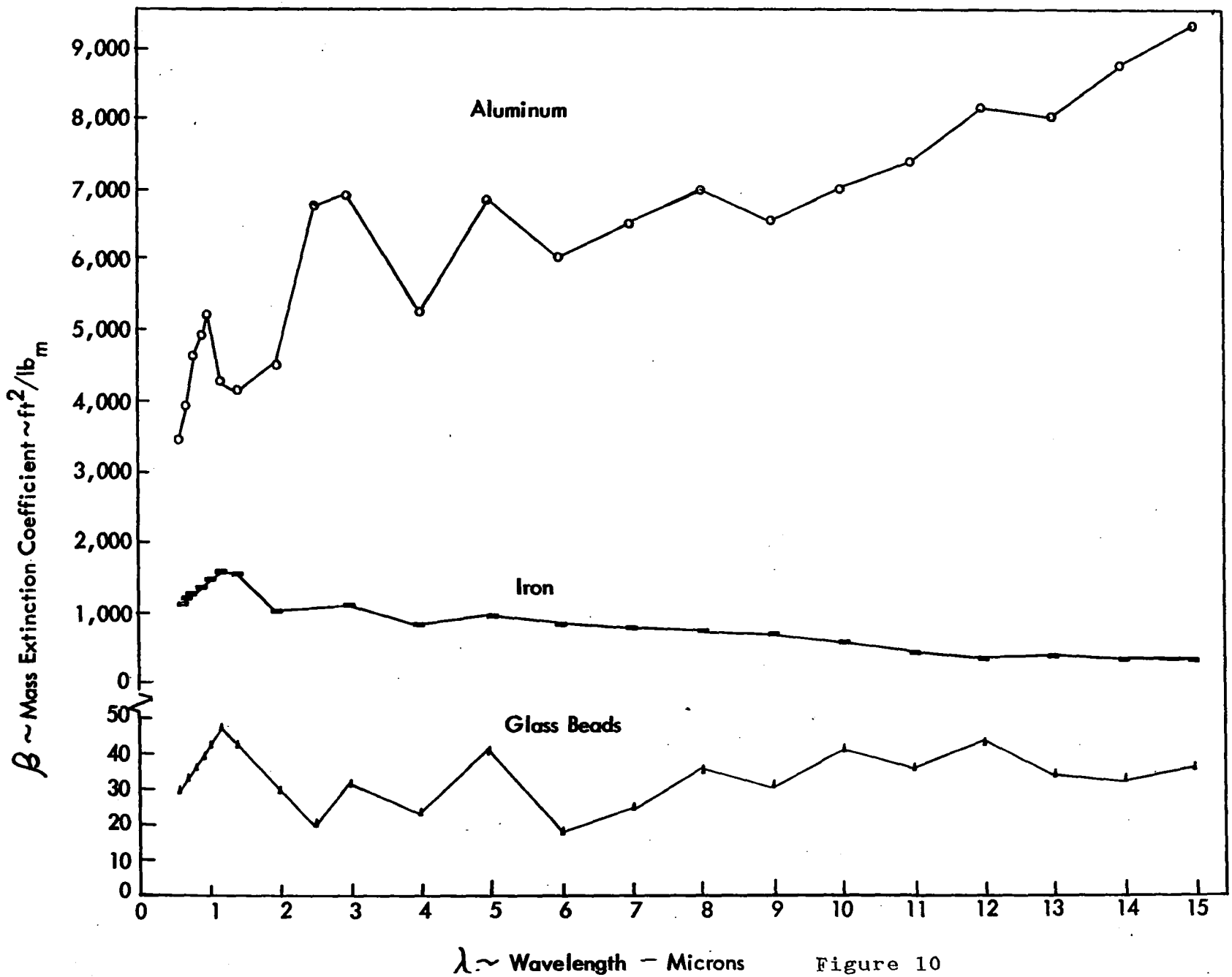

Figure 10

Variation of Mass Extinction with Wave Length

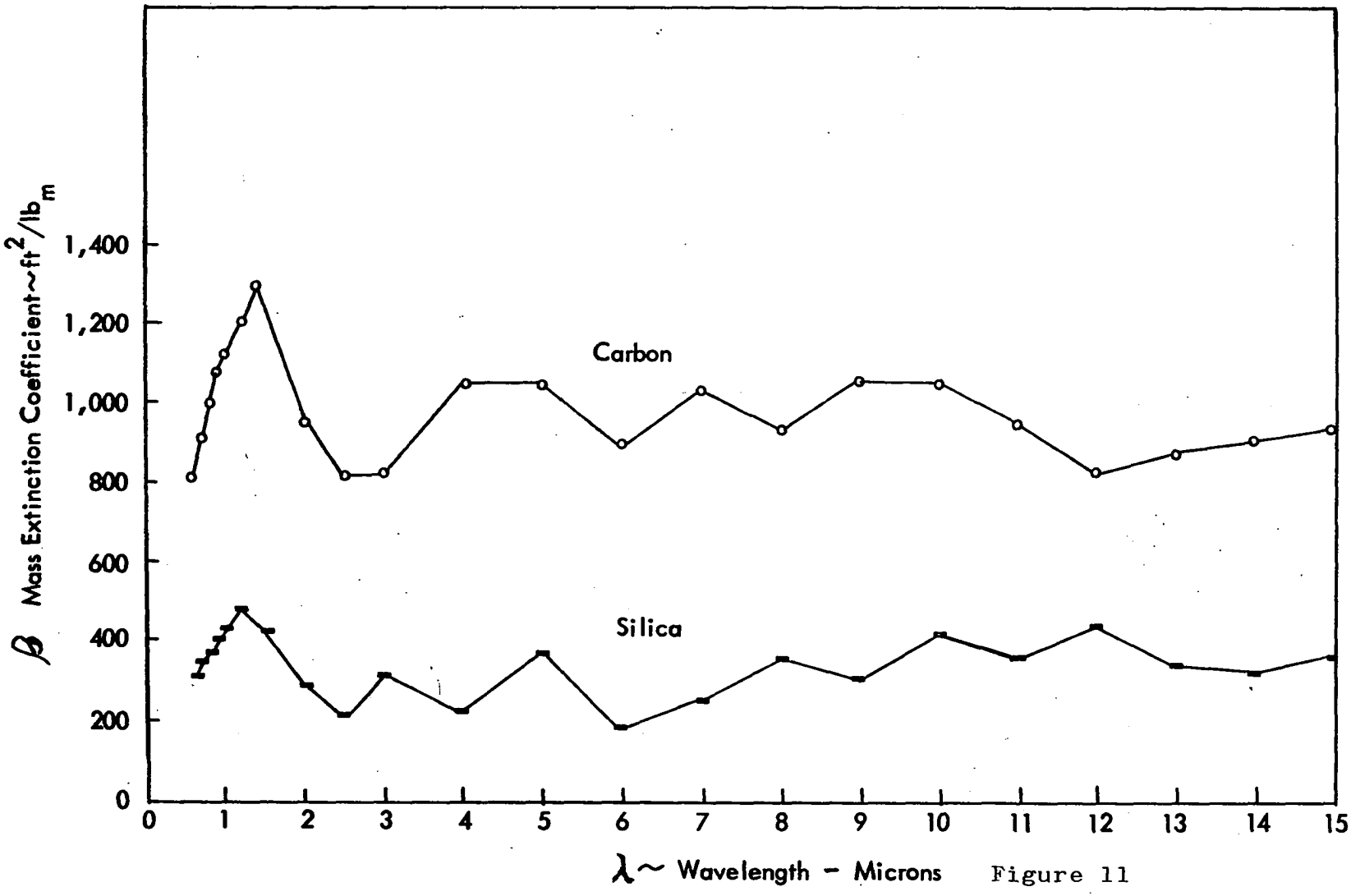

Figure 11

Variation of Mass Extinction with Wave Length

were not included in calculating the average values.

Scattering Measurements

The scattered radiation measured was energy scattered from a well defined axial-symmetric cloud of particles. An energy balance over the cloud neglecting emission yields:

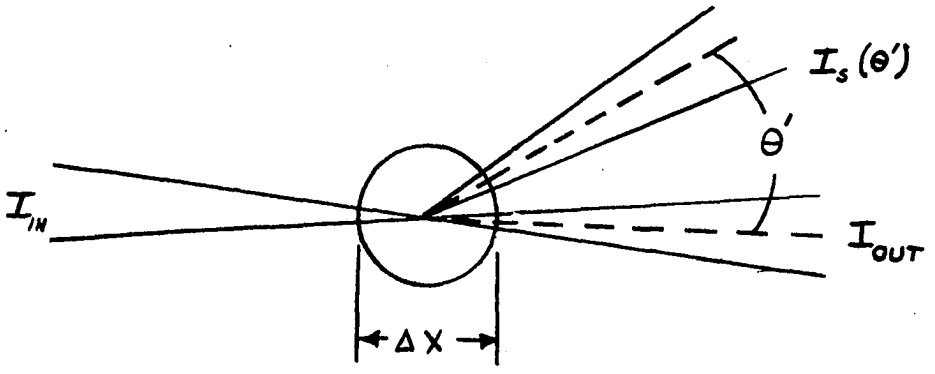

$$I_{in} - I_{out} = \Delta I_{scatt} + \Delta I_{abs} = \Delta I_{ext} \qquad (7)$$

where: ΔI_{scatt} = decrease in the incident intensity due to scattering

ΔI_{abs} = decrease in the incident intensity due to absorption

ΔI_{ext} = decrease in the incident intensity due to extinction.

It was found that emission could be neglected because increasing the particle temperature 40 degrees did not change the scattering intensity at $\theta = 90$ degrees. According to the elementary radiation theory, the emissive power would increase by 30 per cent for such a temperature change.

Writing ΔI_{scatt} for a unit solid angle with the limits of integration being the boundary of the hemispherical surface gives

$$\Delta I_{scatt} = \frac{1}{4\pi} \int_o^{2\pi} \int_o^{\pi} I_s(\theta') \, \mathrm{Sin}\theta' d\theta' d\phi' \qquad (8)$$

which for the axial-symmetric scattering may be rewritten as

$$\Delta I_{scatt} = \tfrac{1}{2} \int_o^{\pi} I_s(\theta') \, \mathrm{Sin}\theta' d\theta' . \qquad (9)$$

Beer's law may be written as

$$\frac{\Delta I_{ext}}{I_{in}} = \rho \, \beta \, \Delta x \qquad (10)$$

or

$$\frac{\Delta I_{scatt}}{I_{in}} = \rho \, \sigma \, \Delta x \qquad (11)$$

and if I_{in}, ρ and Δx are the same in both equations 10 and 11, then

$$\frac{\Delta I_{scatt}}{\Delta I_{ext}} = \frac{\sigma}{\beta} = \frac{1}{\Delta I_{ext}} \left[\tfrac{1}{2} \int_o^{\pi} I_s(\theta') \, \mathrm{Sin}\theta' d\theta' \right] . \qquad (12)$$

Using the same reasoning and rewriting equation 7 gives

$$\frac{\Delta I_{scatt}}{\Delta I_{ext}} + \frac{\Delta I_{abs}}{\Delta I_{ext}} = 1 \qquad (13)$$

or

$$\frac{\sigma}{\beta} + \frac{\kappa}{\beta} = 1 . \qquad (14)$$

From equation 4 and the definition of the scattering function $S(\theta',\phi)$ as being that portion of the scattered radiation directed into a solid angle $d\omega'$ in the direction θ', ϕ'; one may rewrite equation 12 for the case of non-conservative scattering ($\sigma \neq \beta$) as

$$\frac{\Delta I_{scatt}}{\Delta I_{ext}} = \frac{\sigma}{\beta} = \frac{1}{\Delta I_{ext}} \left[\frac{1}{4\pi}\int_0^{2\pi} \int_0^{\pi} \rho \Delta x I_{in} S(\theta',\phi') \sin\theta' d\theta' d\phi'\right] \tag{15}$$

where for the axial-symmetric case

$$S(\theta') = \frac{1}{4\pi} \int_0^{2\pi} S(\theta',\phi)\, d\phi'$$

and

$$I_s(\theta') = \rho\ \Delta\ x\ I_{in}\ S(\theta')\ .$$

However, since $\Delta I_{ext}/I_{in} = \rho\ \beta\ \Delta\ x$ equation 15 becomes

$$\frac{\Delta I_{scatt}}{\Delta I_{ext}} = \frac{\sigma}{\beta} = \frac{\rho \Delta x}{2\beta\rho\Delta x} \int_0^{\pi} S(\theta') \sin\theta' d\theta'$$

which reduces to

$$\sigma = \tfrac{1}{2}\int_0^{\pi} S(\theta') \sin\theta' d\theta'. \tag{16}$$

Equations 12 and 16 combined with the assumption that ΔI_{ext} is also a function of θ', the scattering function for the axial-symmetric case is

$$S(\theta') = \frac{\beta I_s(\theta')}{\Delta I_{ext}} = \frac{I_s(\theta')}{\rho \Delta x I_{in}}\ . \tag{17}$$

For the axial-symmetric case of conservative scattering ($\sigma = \beta$), the conservative scattering function can be defined as

$$S(\theta')_{cons} = \frac{I_s(\theta')}{\Delta I_{scatt}} \qquad (18)$$

which may be derived from equation 16 by dividing both sides of the equation by :

$$1 = \tfrac{1}{2}\int_0^{\pi} \frac{1}{\sigma} S(\theta')\mathrm{Sin}\theta' d\theta'$$

and setting

$$\frac{S(\theta')}{\sigma} = S(\theta')_{cons} \, . \qquad (19)$$

To experimentally determine the angular distribution of the scattered intensity $I_s(\theta')$, a blank run was first made to determine the magnitude of background scattering and noise level at different gain settings. After these two factors were determined, the particle generator was started and the cloud of particles were scanned from an angle of 180 degrees to approximately 20 degrees at which the scattering intensity was usually of such magnitude as to exceed the chart range, especially for data recorded in the lower wave lengths. In the longer wave lengths it was possible to record the scattered intensity over a larger angular range before exceeding the limits of the chart. Therefore, for each wave length the scattered intensity was recorded for an angular range which remained within the recorder range on one gain setting, and the remaining angular range

to 0 degrees was recorded at a different gain setting (see Figures 12, 13, 14). In this manner data was obtained at angles common to both gain setting's in order to provide sufficient information to locate the scattering intensity in the neighborhood of 0 degrees.

As one can see in Figures 12, 13, 14 the noise level varied with each gain setting. Thus to determine the scattering intensity, the noise level was averaged out.

Considering the change in the gain setting in the region from 20 degrees to 0 degrees, it was estimated that the accuracy of the scattered intensity $I_s(\theta')$ was within 12 per cent. This is a conservative value based on the maximum difference between traces taken on several different occasions. Since the decrease in the incident intensity due to scattering ΔI_{scatt} represents the area under the $I_s(\theta')$ curve, the values of the decrease in the incident intensity due to scattering used to calculate the ratio of the mass scattering coefficient to the mass extinction coefficient will also have a deviation of $\pm$ 12 per cent. This occurs because 80 per cent of the area under the $I_s(\theta')$ curve lay between the angles of 0 and 20 degrees.

For a given wave length, data for the distribution of angular intensity was obtained a minimum of four times, with some wave lengths in the longer and shorter regions of the spectrum being observed as many as eight times. The results were obtained in random order on different days.

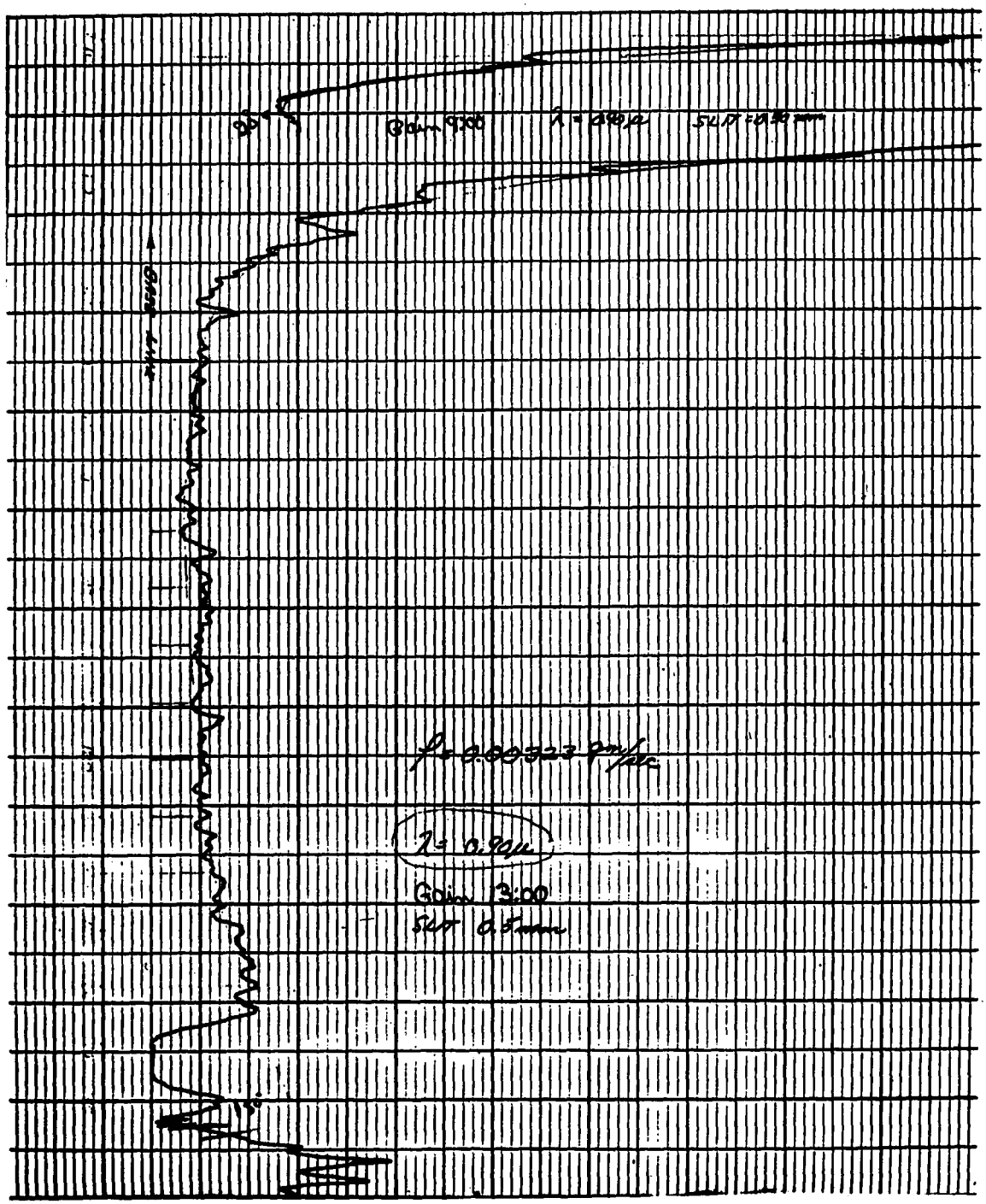

Data Scattering

Figure 12

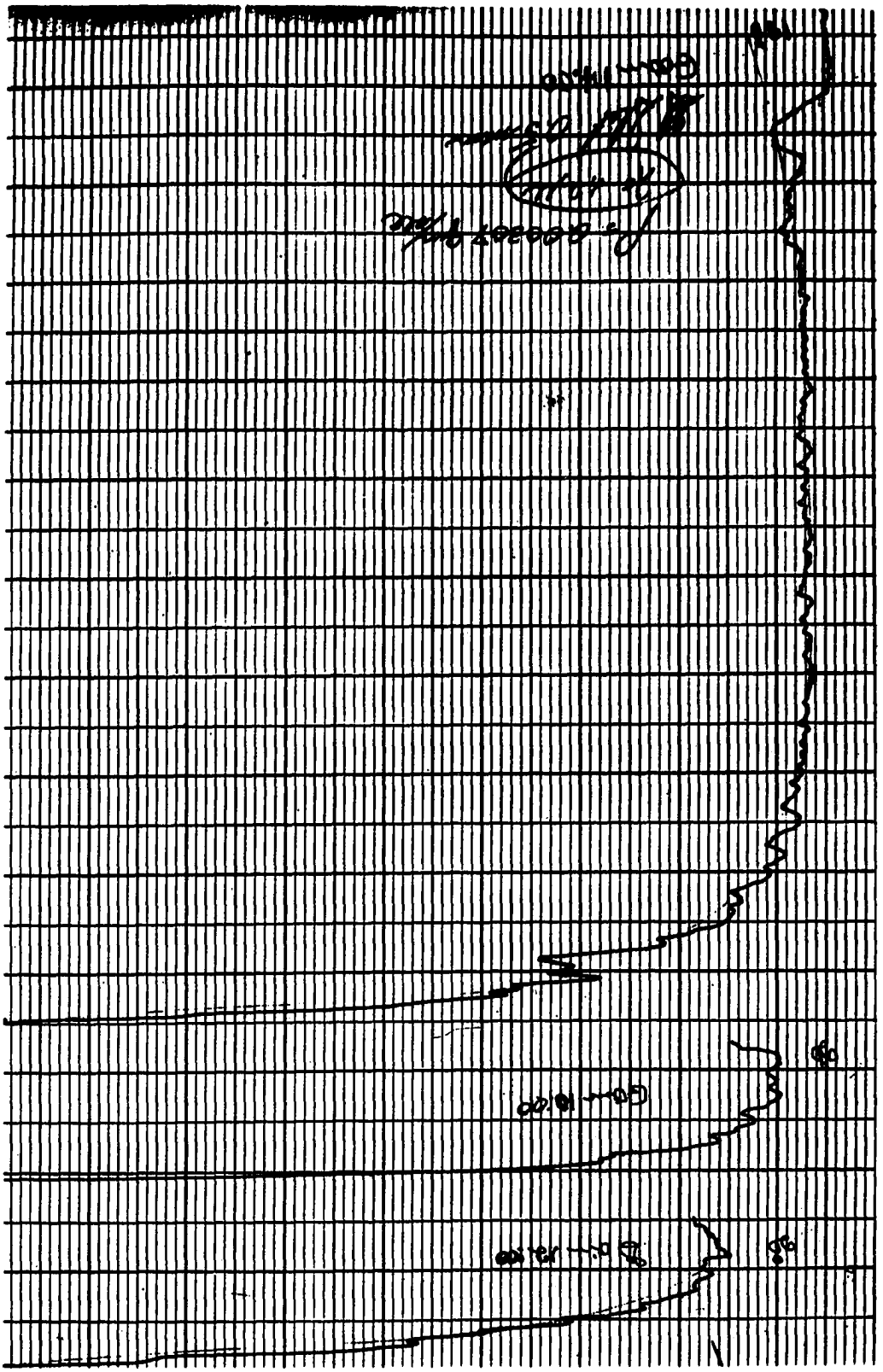

Data Scattering

Figure 13

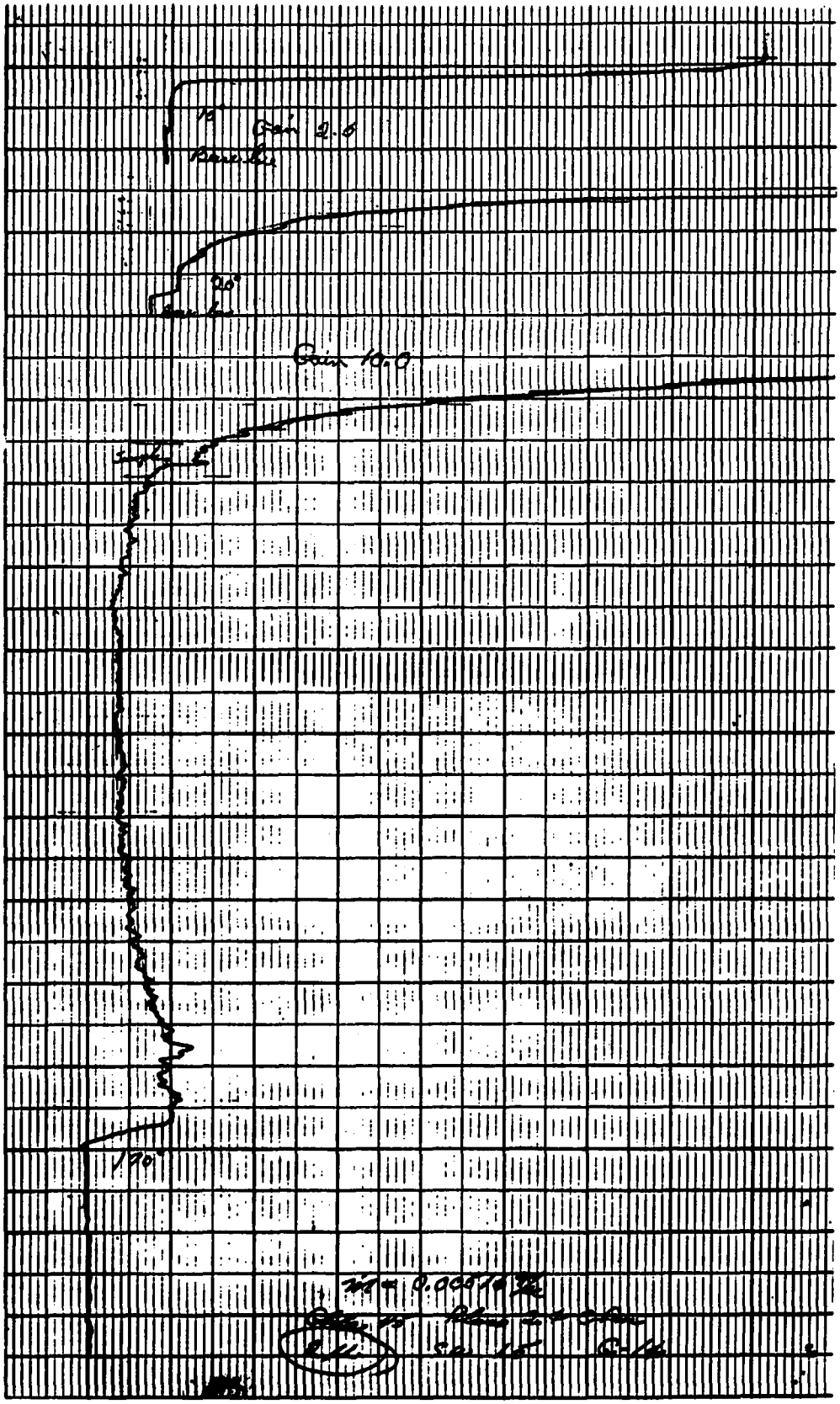

Data Scattering

Figure 14

Comparison of the distribution of angular scattered intensity for a given wave length on different occasions indicated the reproducibility was within 12 per cent. It was impossible to generate the same aerosol density, and the distribution of angular scattered intensity would not have identical values. Since conditions for single scattering phenomena were always maintained the relative shape were the same independent of the mass density of the aerosol.

The ratio of the mass scattering coefficient to the mass extinction coefficient was calculated for all five different aerosols using equation 12. These results are shown in Figures 15, 16, 17, 18, 19. There was a possible deviation of $\pm$ 12 per cent in these ratios due to ΔI_{scatt}. In calculating the decrease in incident intensity due to scattering from equation 9 one would need to know the mathematical expression for $I_s(\theta')$ in terms of θ' if direct integration were to apply. To overcome this obstacle, the decrease in incident intensity due to scattering was calculated by the finite difference method. By letting $d\theta = \Delta\theta = \pi/180$ radians, equation 9 becomes

$$\Delta I_{scatt} = \tfrac{1}{2} \sum_{N=1}^{180} I_s(\theta_N (\mathrm{Sin}\theta_N \frac{\pi}{180} . \qquad (20)$$

As was mentioned earlier, the ratio of the mass scattering coefficient to the mass extinction coefficient was calculated using equation 12

$$\frac{\sigma}{\beta} = \frac{\Delta I_{scatt}}{\Delta I_{ext}} . \qquad (12)$$

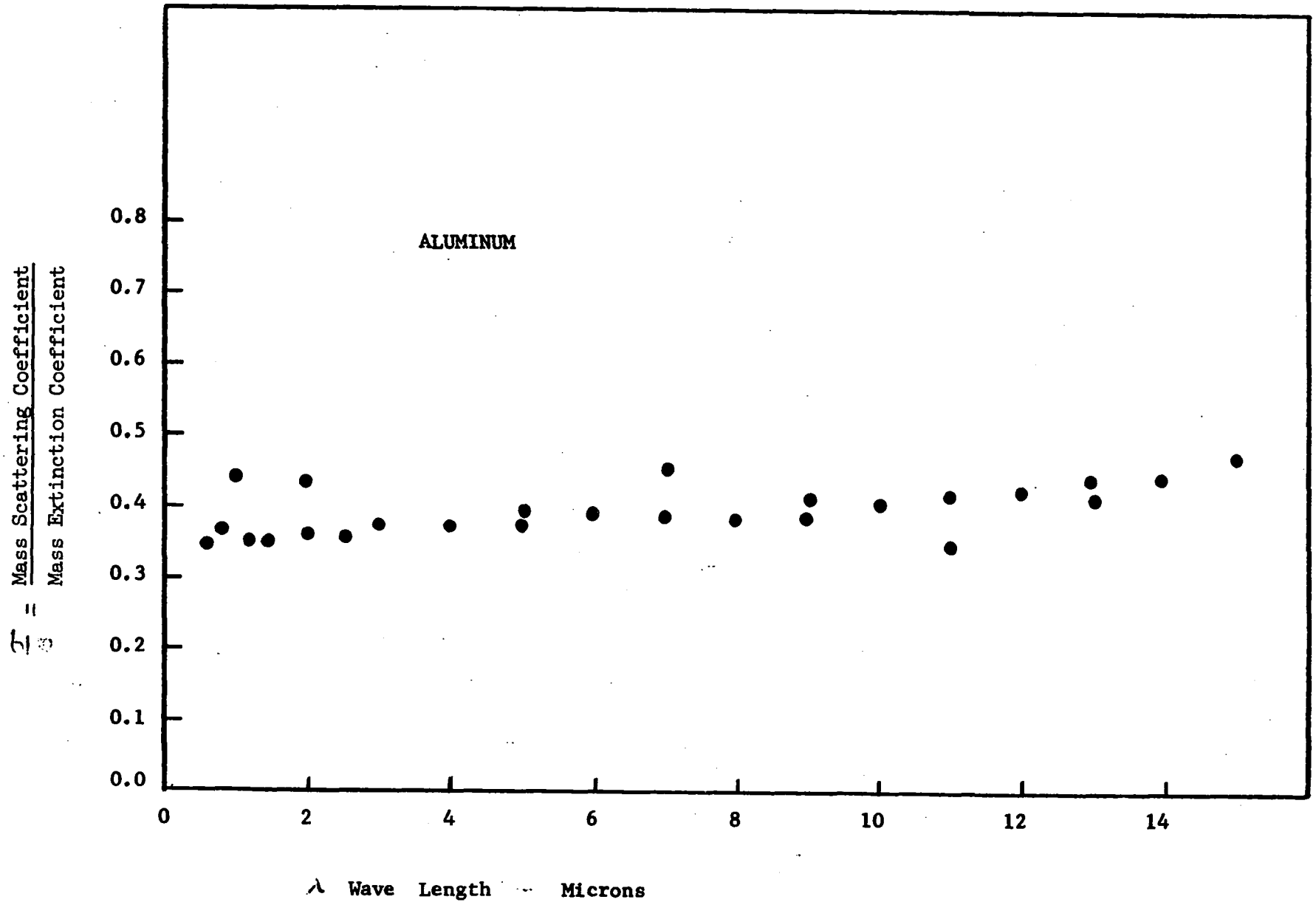

$\frac{\text{Mass Scattering Coefficient}}{\text{Mass Extinction Coefficient}}$ =

Figure 15 Variation of $\frac{\sigma}{\kappa+\sigma}$ with wave length

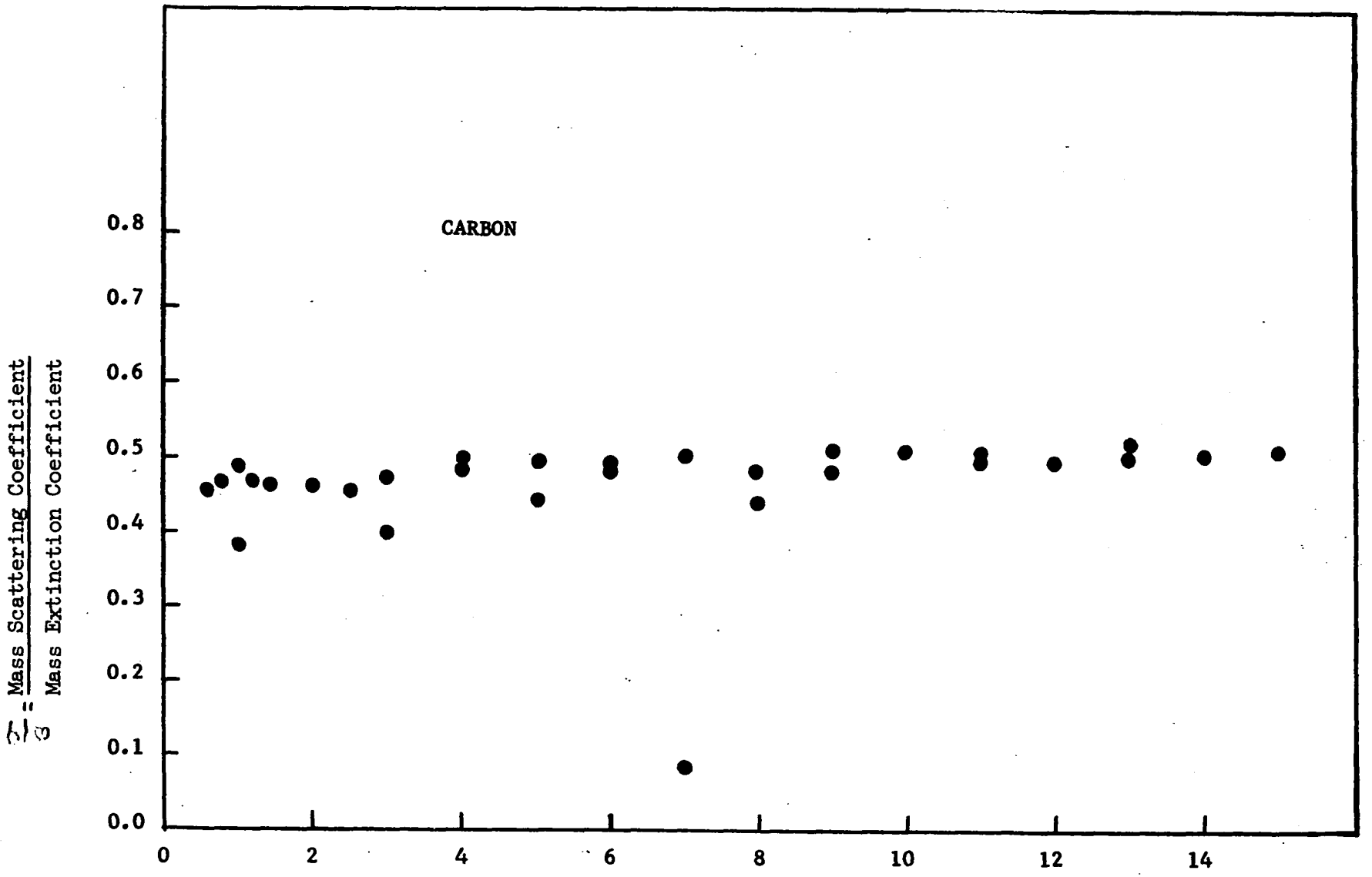

$\frac{\sigma_s}{\sigma}$ = Mass Scattering Coefficient / Mass Extinction Coefficient

Figure 16 Variation of $\frac{\sigma_s}{\sigma}$ with wave length

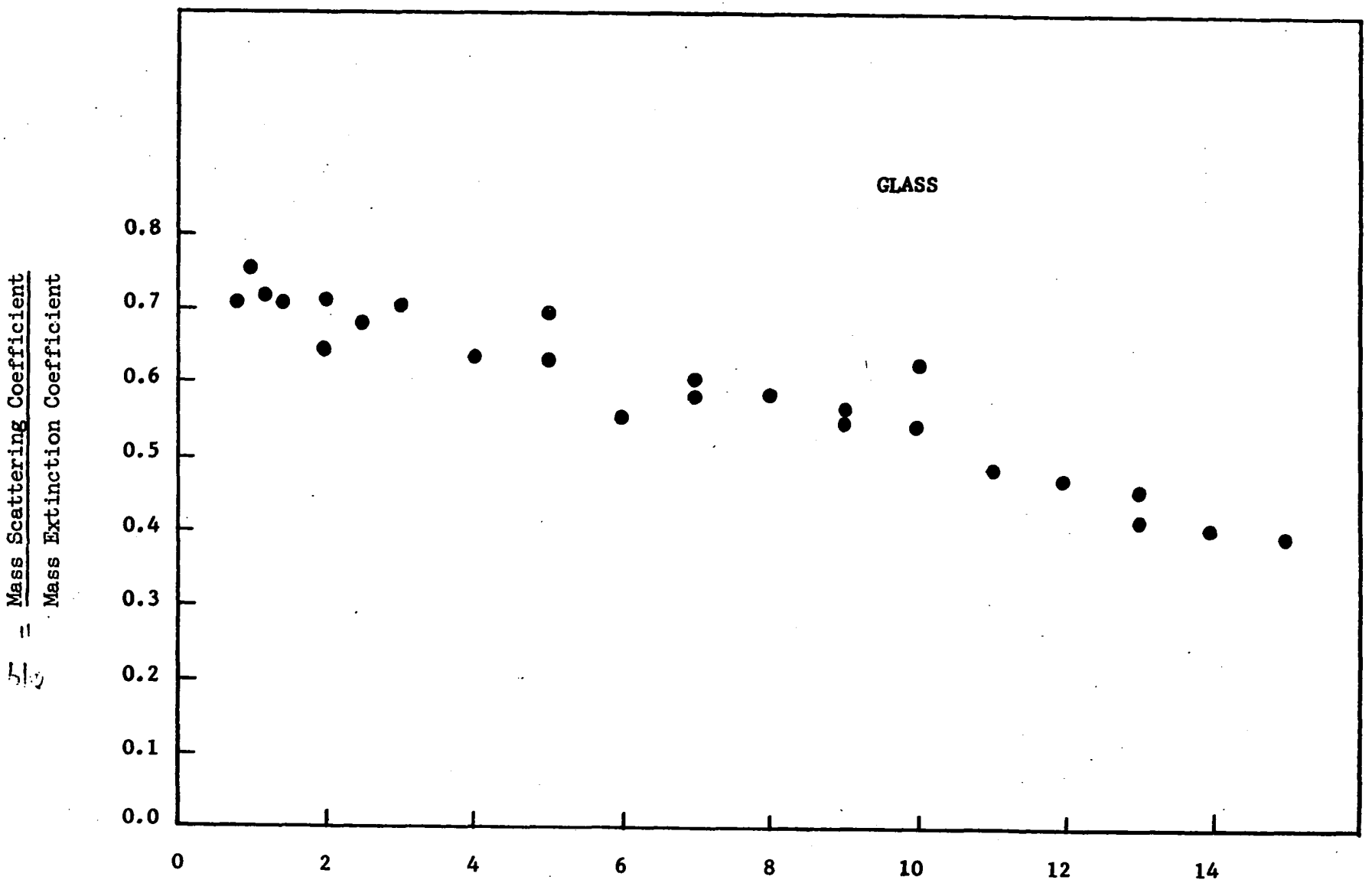

$\bar{\sigma}$ = Mass Scattering Coefficient / Mass Extinction Coefficient

Figure 17 Variation of $\bar{\sigma}$ with wave length

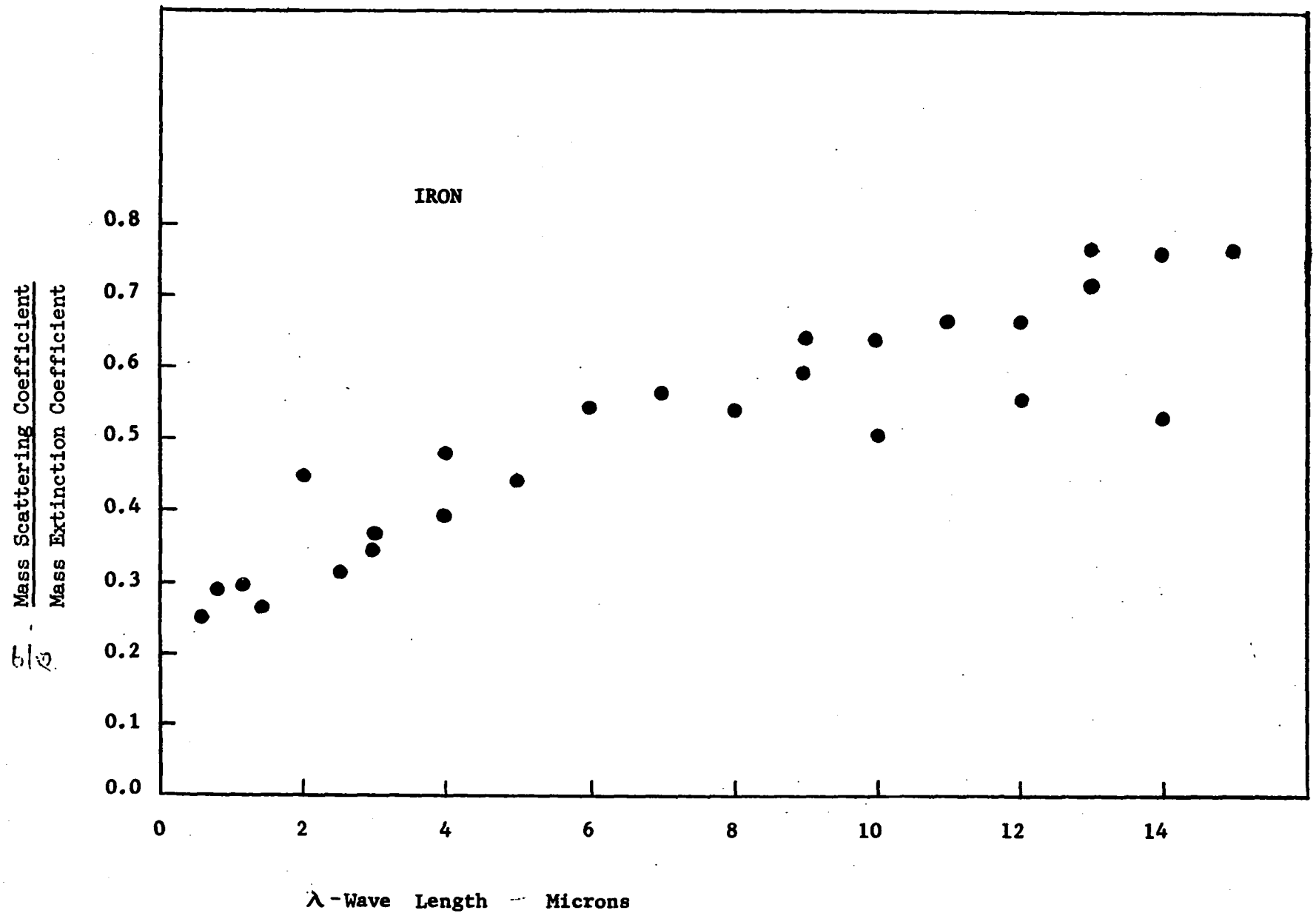

Figure 18 Variation of $\frac{\sigma}{\beta}$ with wave length

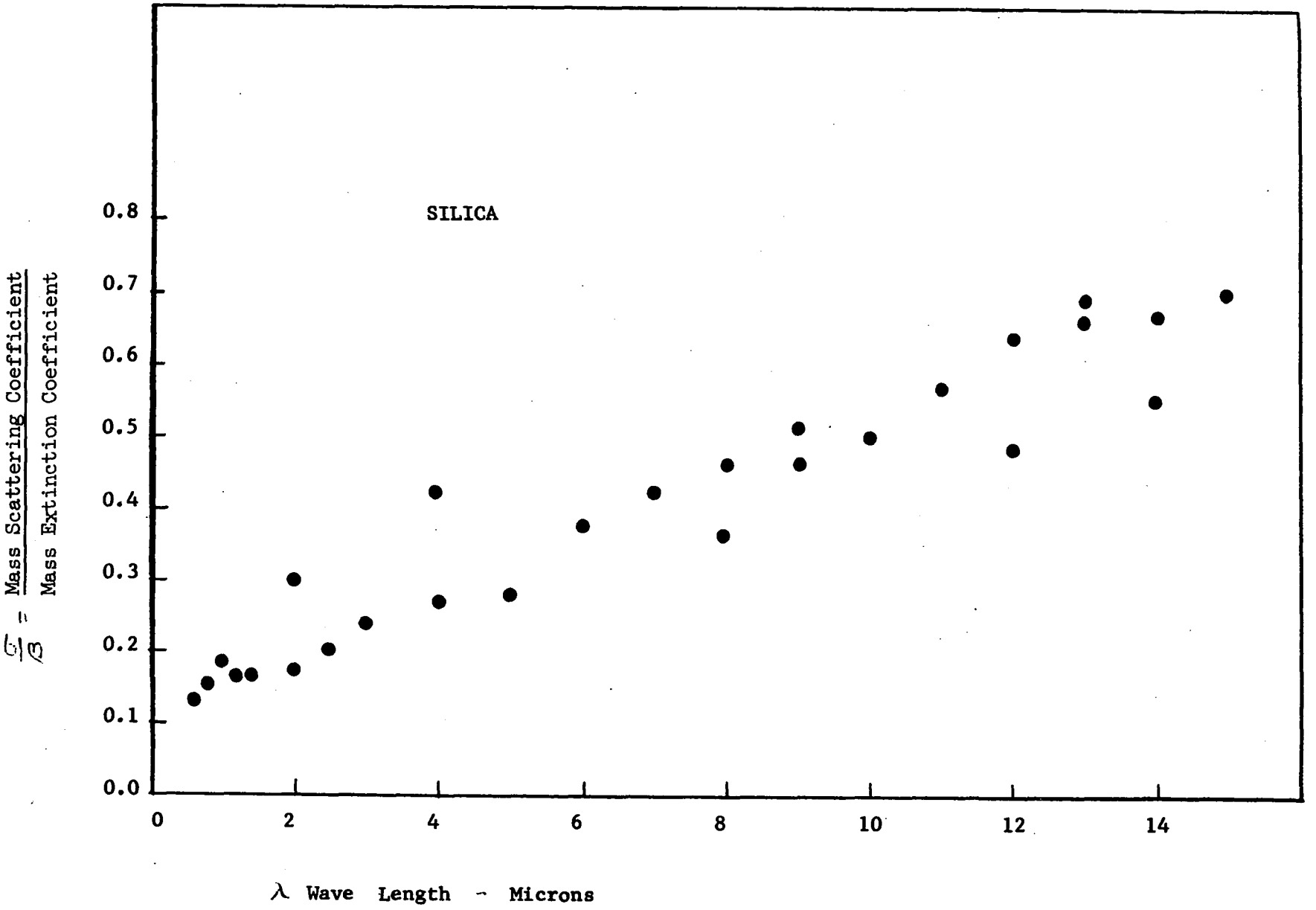

Figure 19 Variation of $\frac{\sigma}{\beta}$ with wave length

However, since the decrease in intensity due to extinction was determined for a given mass density and cloud thickness, equation 12 implies that ΔI_{scatt} must also be determined for the same density and optical thickness.

Since the decrease in intensities due to scattering and extinction were obtained independently, it was impossible to obtain the mass extinction coefficient or the decrease in intensities due to scattering and extinction for the same experimentally measured value of the mass density. Therefore, before the ratio of the mass scattering coefficient to the mass extinction coefficient may be calculated, the decrease in intensity due to extinction must be corrected to a mass density corresponding to the density at which the decrease in the intensity due to scattering was measured. From the definition of single scattering, the amount of energy scattered will be directly proportional to the density of the aerosol. By plotting the ratio of the decrease in incident intensity due to extinction and the incident intensity against the mass density for the five different aerosols, a set of curves were obtained which showed the decrease in incident intensity due to extinction to be directly proportional to the mass density. Therefore, if the mass density of the aerosol were increased or decreased by a given per cent, the change in incident intensity due to extinction would also increase or decrease by the same given percentage. Thus, by knowing the mass density at which the

decrease in incident intensity due to scattering was measured, the decrease in the incident intensity due to extinction for the same mass density could be calculated, and then, from equation 12, the ratio of the mass scattering coefficient to be the mass extinction coefficient may be calculated.

To summarize the procedure by which the ratios of the mass scattering coefficient to mass extinction coefficient were calculated, the following outline is given.

1. ΔI_{scatt} was obtained from the numerical integration of

$$\Delta I_{scatt} = \tfrac{1}{2} \int_0^{\pi} I_s(\theta')\mathrm{Sin}\theta' d\theta'$$

where $I_s(\theta')$ is experimentally determined for a particular wave length, aerosol density, and cloud thickness.

2. The value for the change in incident intensity due to extinction was correct to correspond to the same mass density at which the change in incident intensity due to scattering was measured by the method outline earlier.

3. Calculate

$$\frac{\sigma}{\beta} = \frac{\Delta I_{scatt}}{\Delta I_{ext}} \qquad (12)$$

This procedure was used to calculate the ratios of the mass scattering coefficient to the mass extinction coefficient for each of the five different aerosols. These ratios are plotted in Figures 15, 16, 17, 18, 19, as a

function of wave length.

By knowing the values of the experimentally measured scattered angular intensity $I_s(\theta')$ and applying equation 20 to equation 18 gives

$$S(\theta_N)_{cons} = \frac{360\ I_s(\theta_N)}{\sum_{N=1}^{180} I_s(\theta_N)\sin\theta_N} \quad . \qquad (21)$$

The numerical values of the conservative scattering function $S(\theta_N)_{cons}$ for each of the five different aerosol powders used were calculated using the IBM 1410 digitial computer. These values are presented in Figures 20 to 115 and are also in tabular form in Tables 1, 2, 3, 4, and 5.

The general shape of the conservative scattering functions were smooth curves from 180 to 0 degrees with a steep slope in the region of 20 to 0 degrees. The minimum value of $S(\theta')_{cons}$ usually occurred at 90 degrees, however for the carbon and glass beads aerosols the minimum varied from 60 degrees to 180 degrees. From the minimum point to 180 degrees the slope was small.

The plots of the conservative scattering functions shown in Figures 20 to 115 represent normalized data and are average values of all data taken.

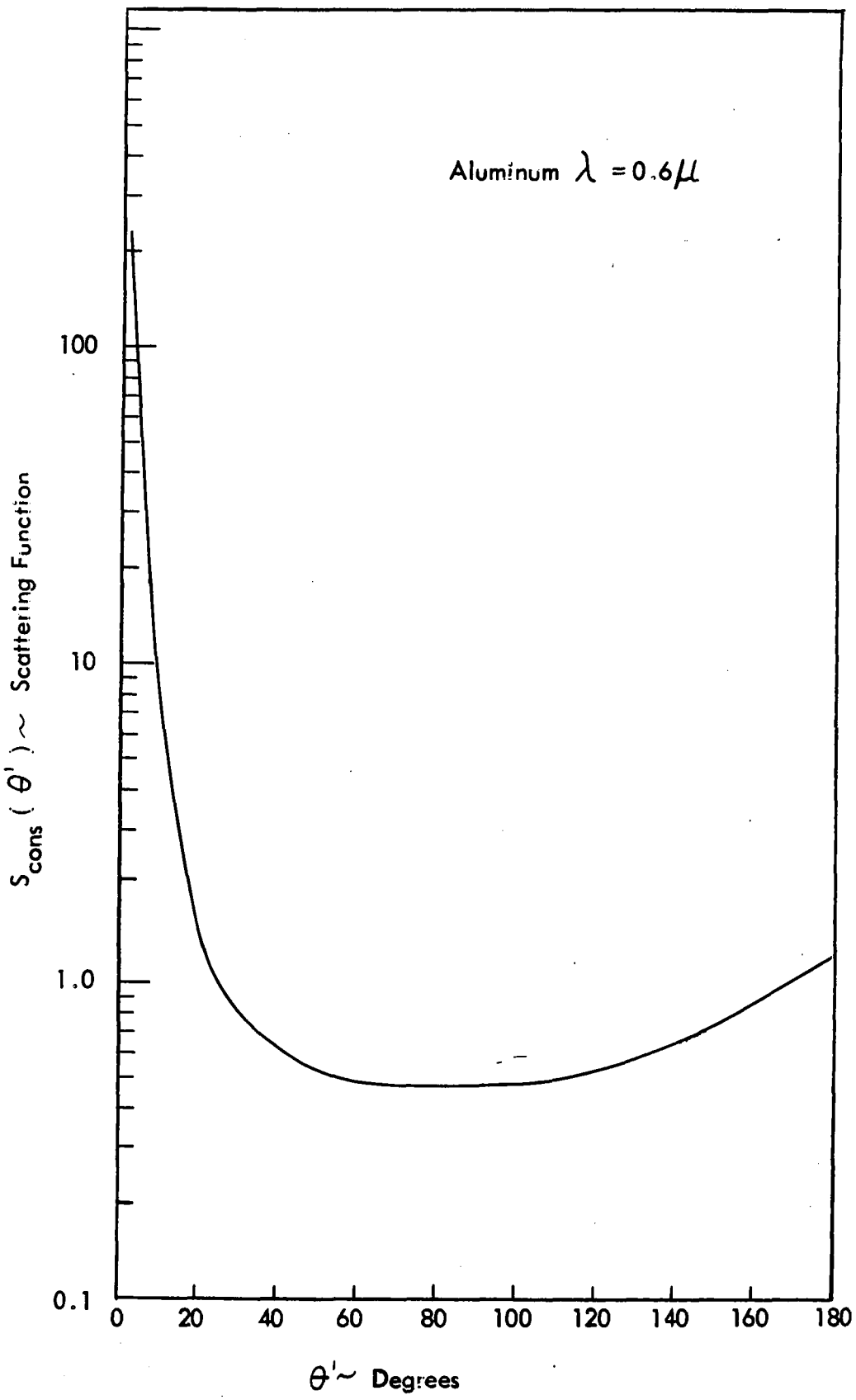

Figure 20
Angular Distribution of Scattering Function -- Experimental Data

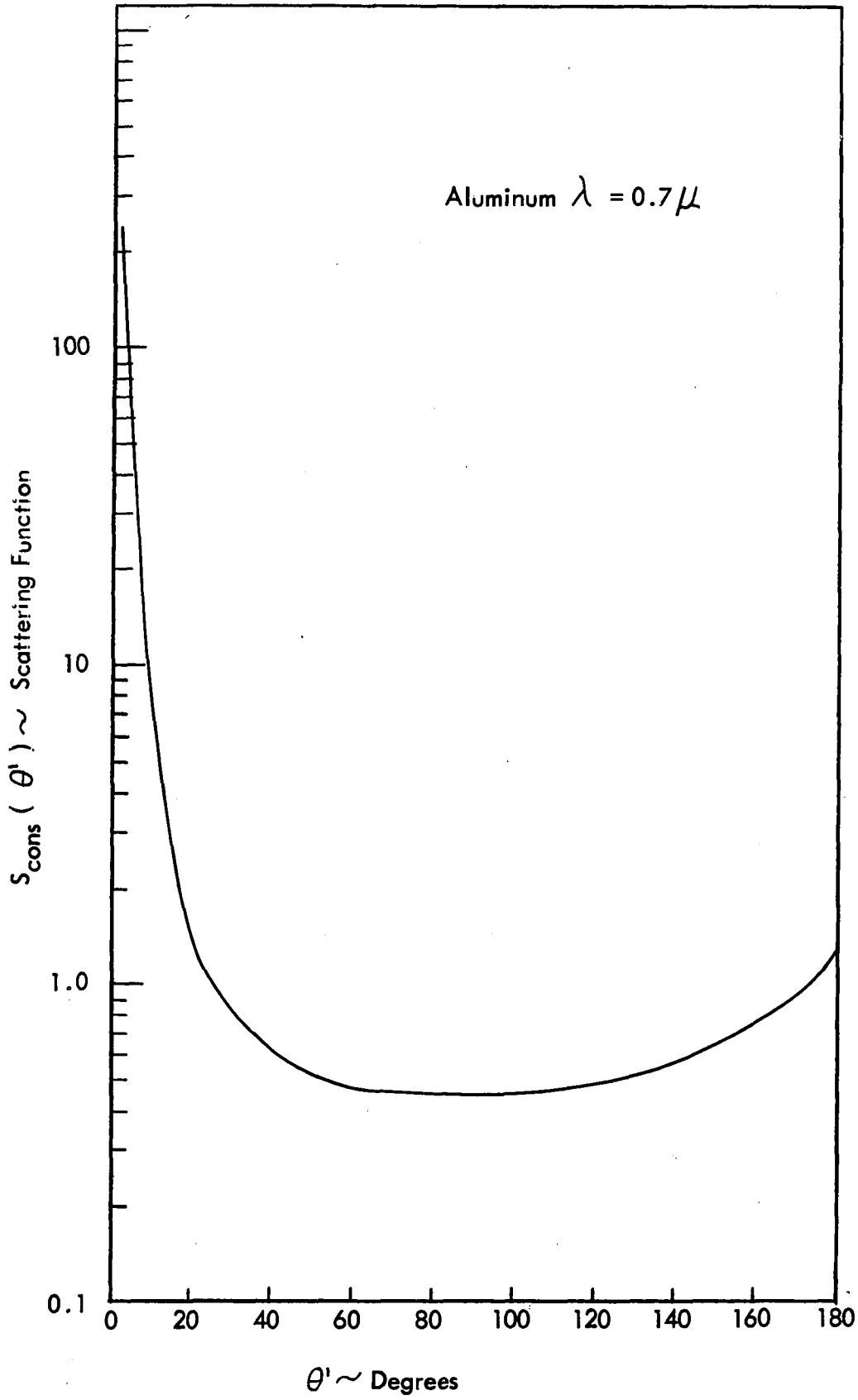

Figure 21
Angular Distribution of Scattering
Function -- Experimental Data

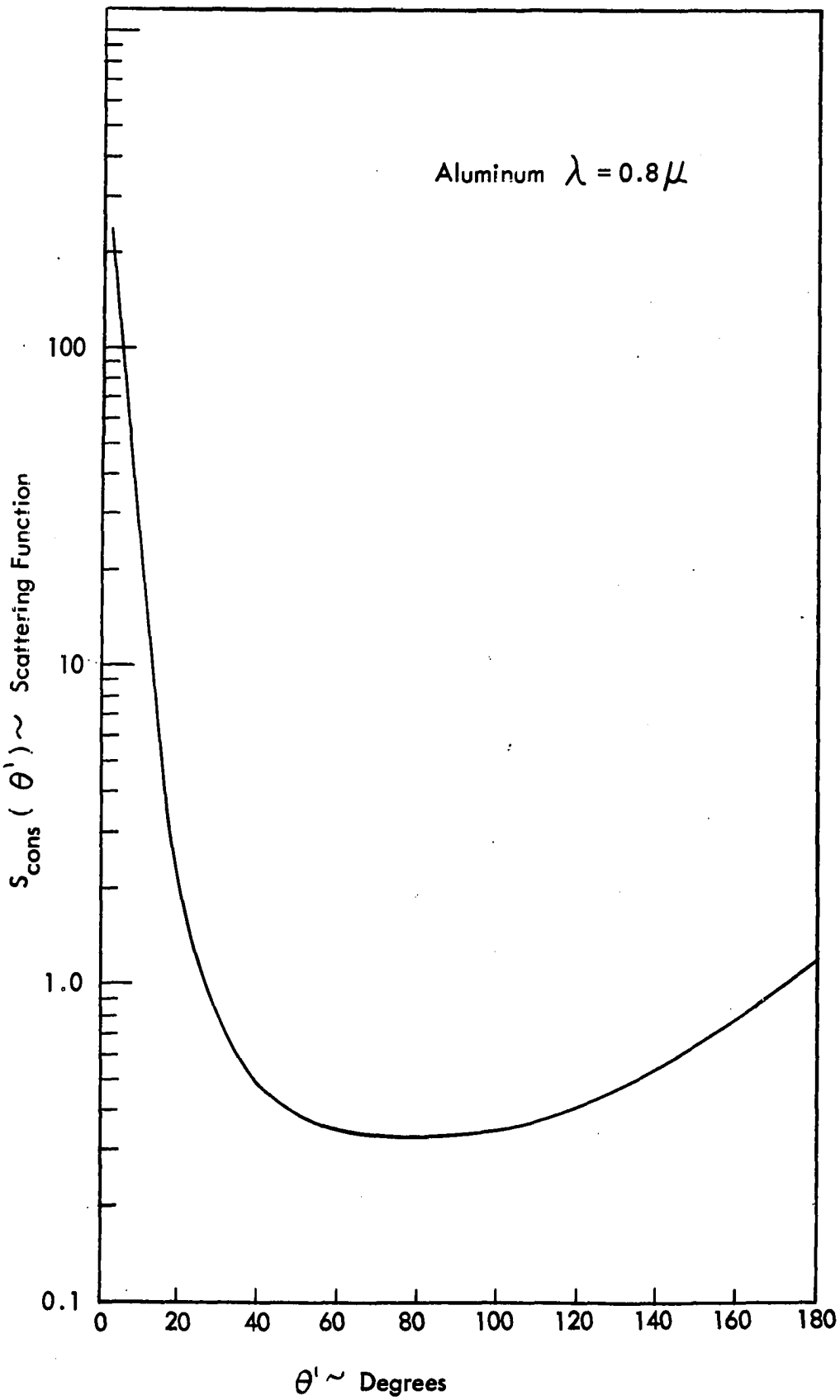

Figure 22
Angular Distribution of Scattering
Function -- Experimental Data

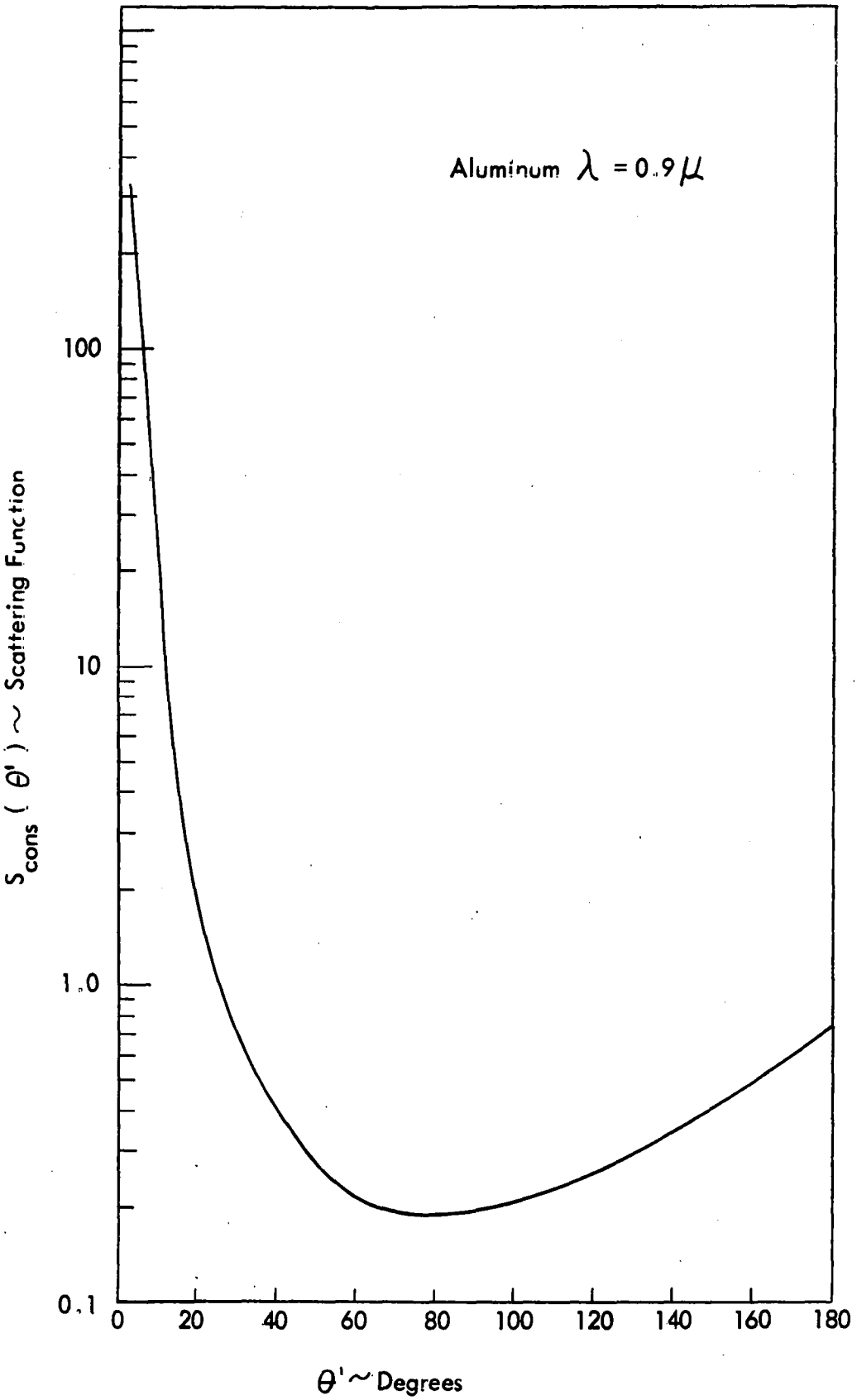

Figure 23
Angular Distribution of Scattering
Function -- Experimental Data

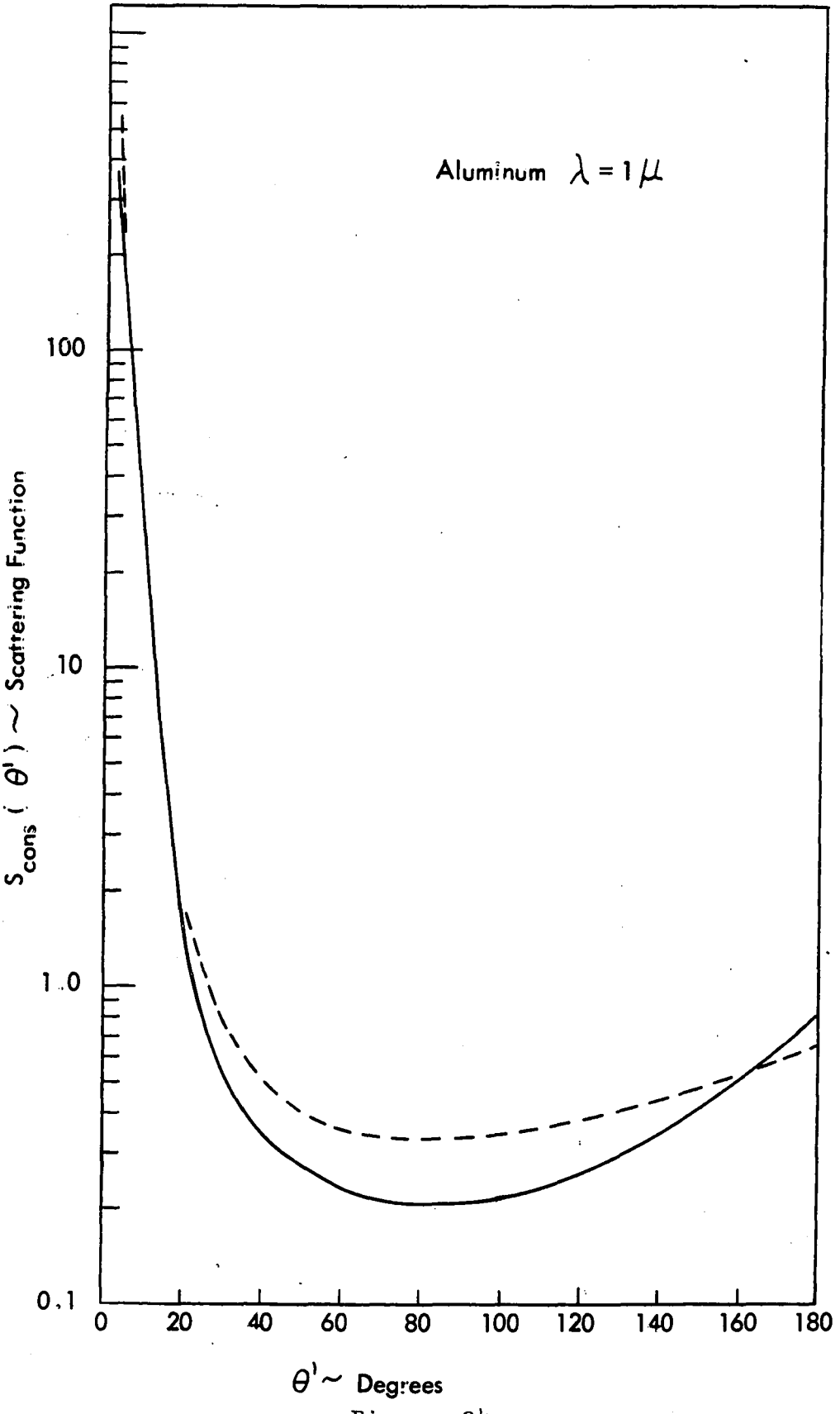

Figure 24
Angular Distribution of Scattering Function -- Experimental Data

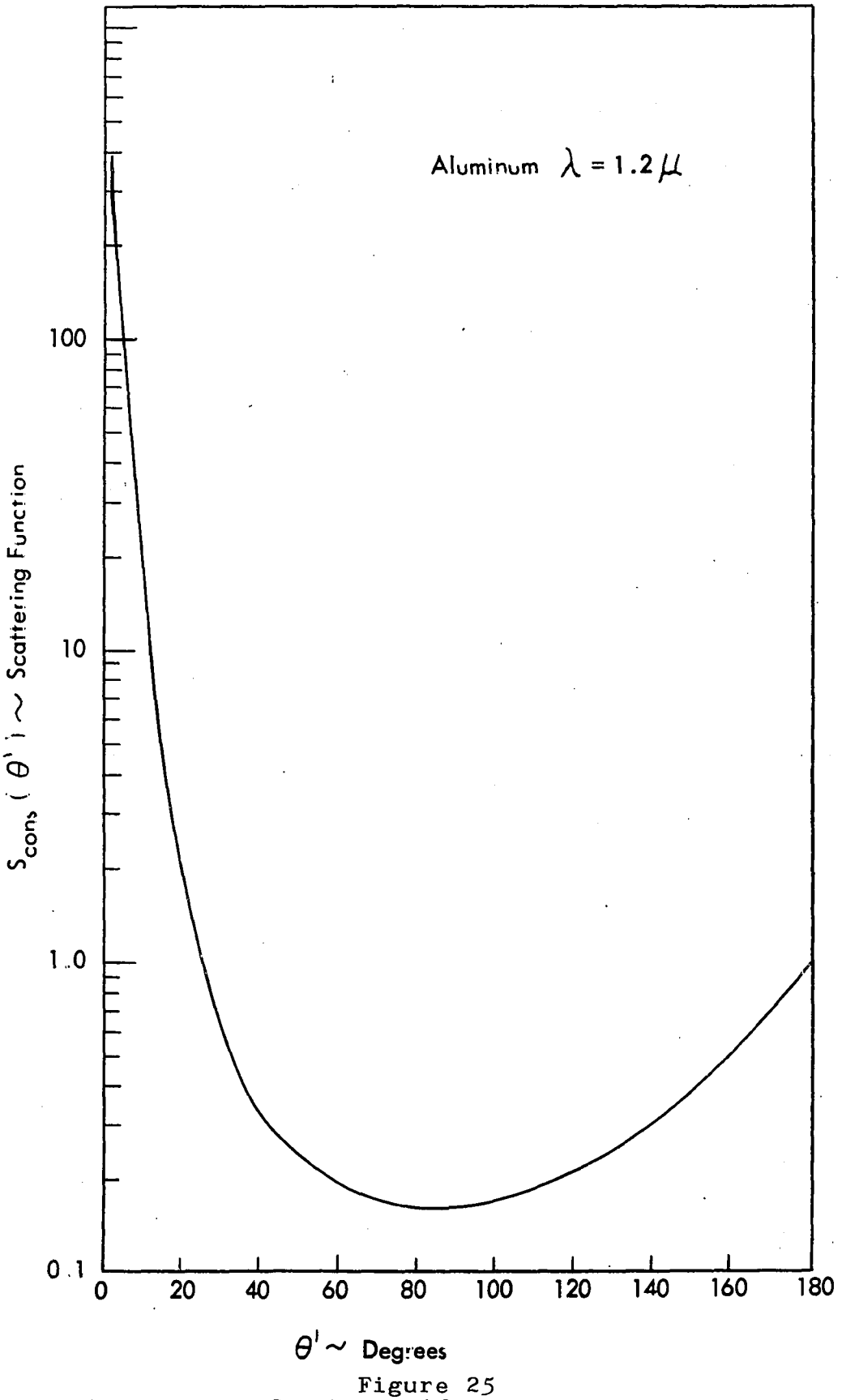

Figure 25
Angular Distribution of Scattering
Function -- Experimental Data

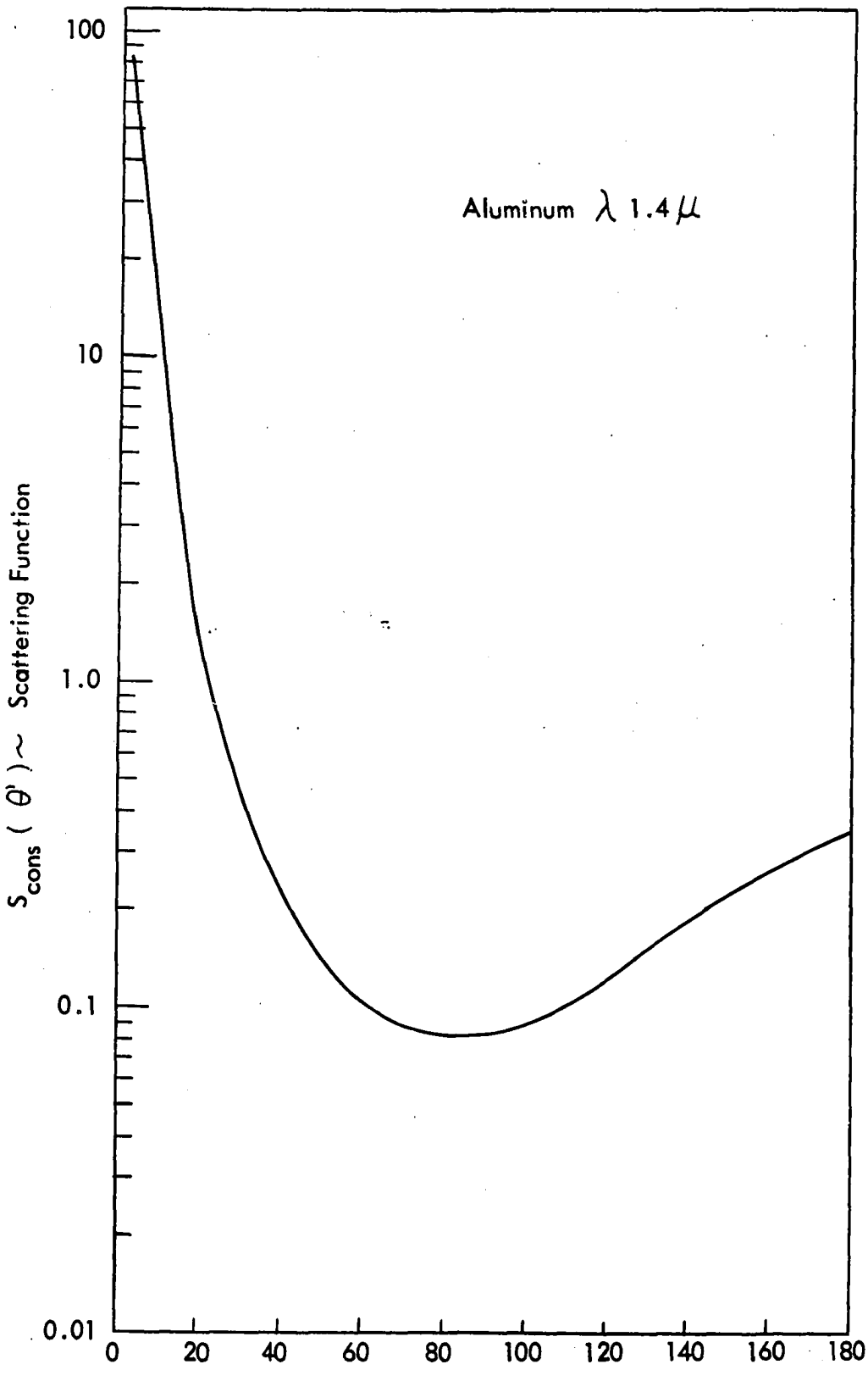

Figure 26
Angular Distribution of Scattering Function -- Experimental Data

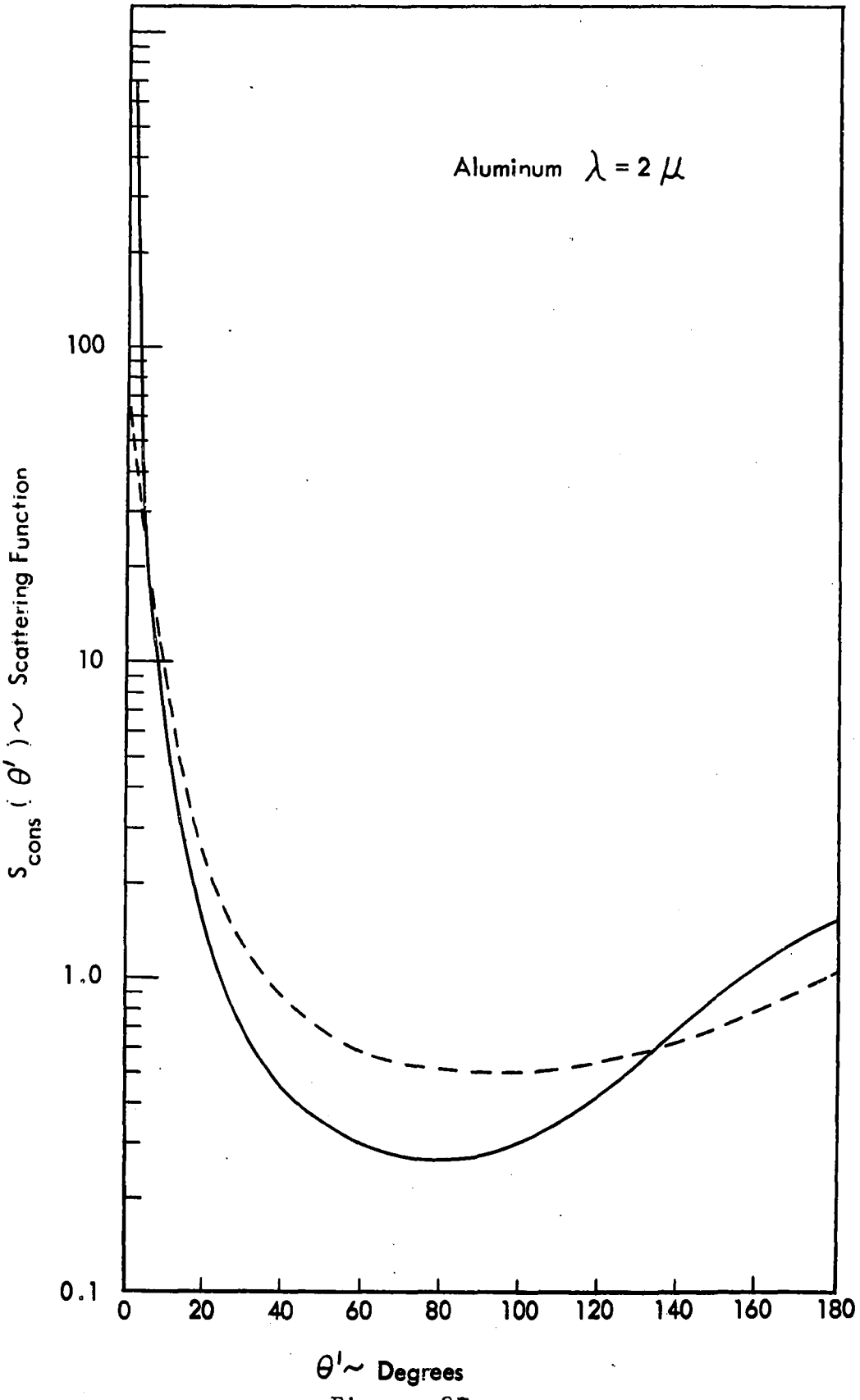

Figure 27
Angular Distribution of Scattering Function -- Experimental Data

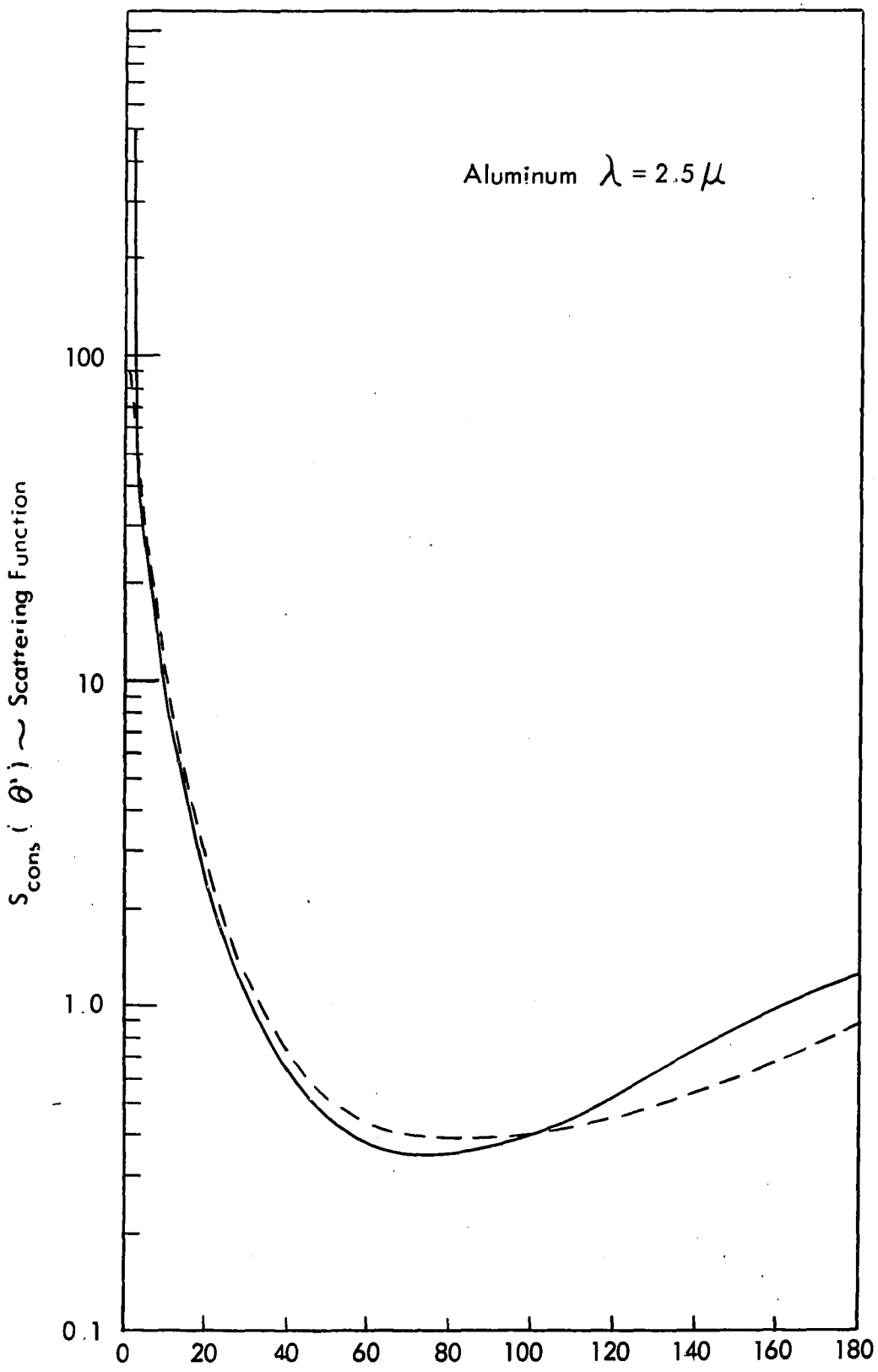

Figure 28
Angular Distribution of Scattering
Function -- Experimental Data

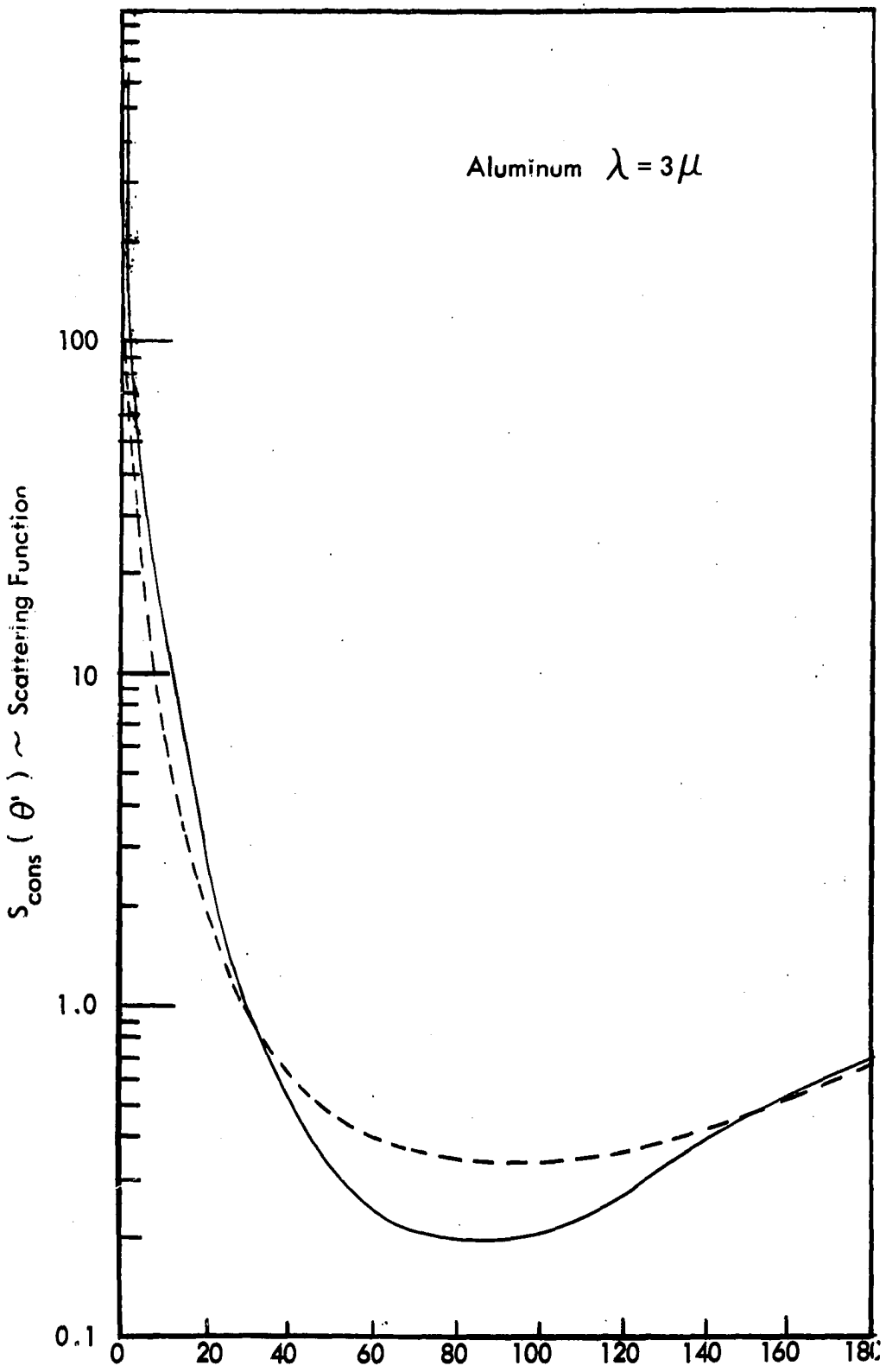

Figure 29
Angular Distribution of Scattering
Function -- Experimental Data

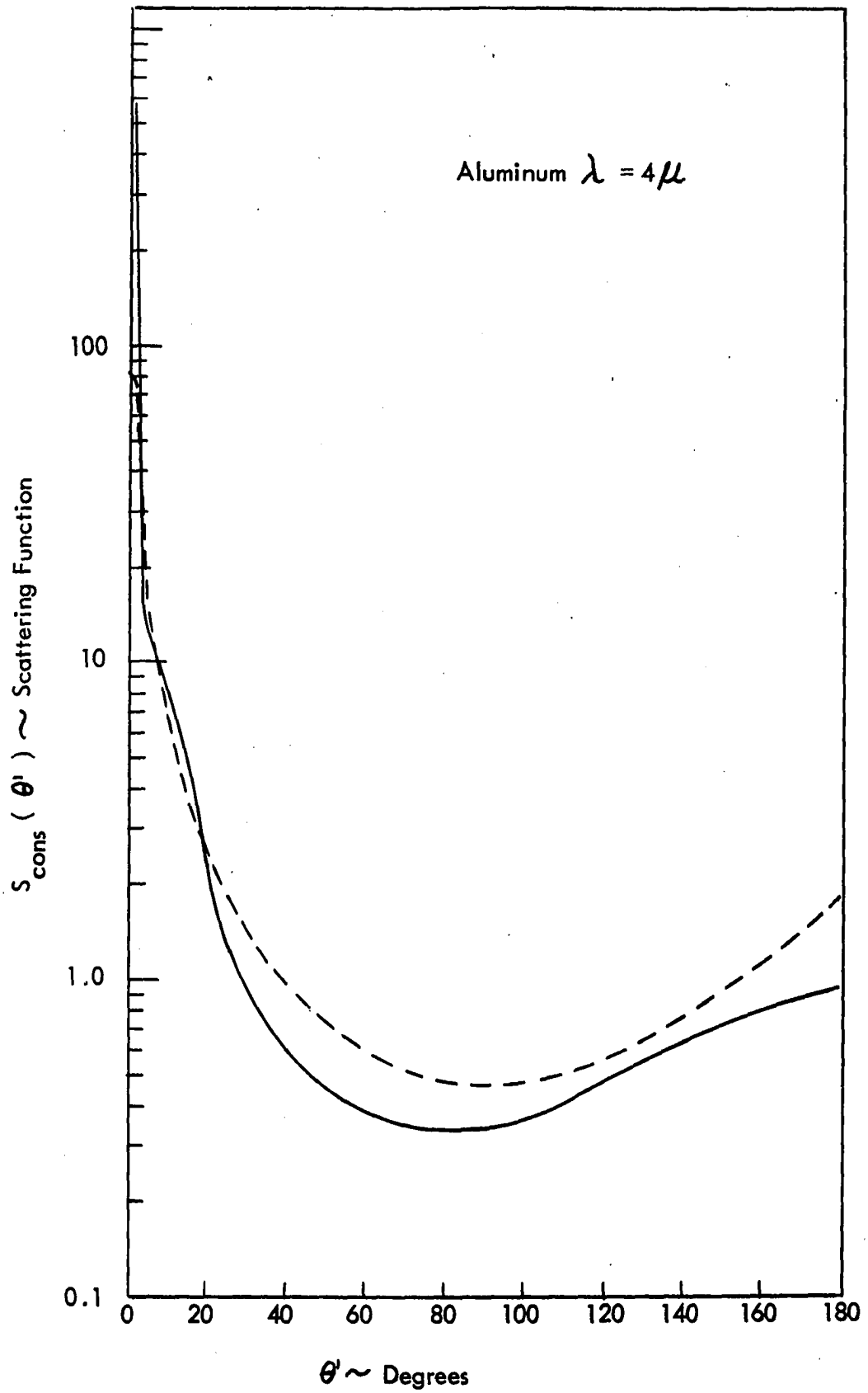

Figure 30
Angular Distribution of Scattering
Function -- Experimental Data

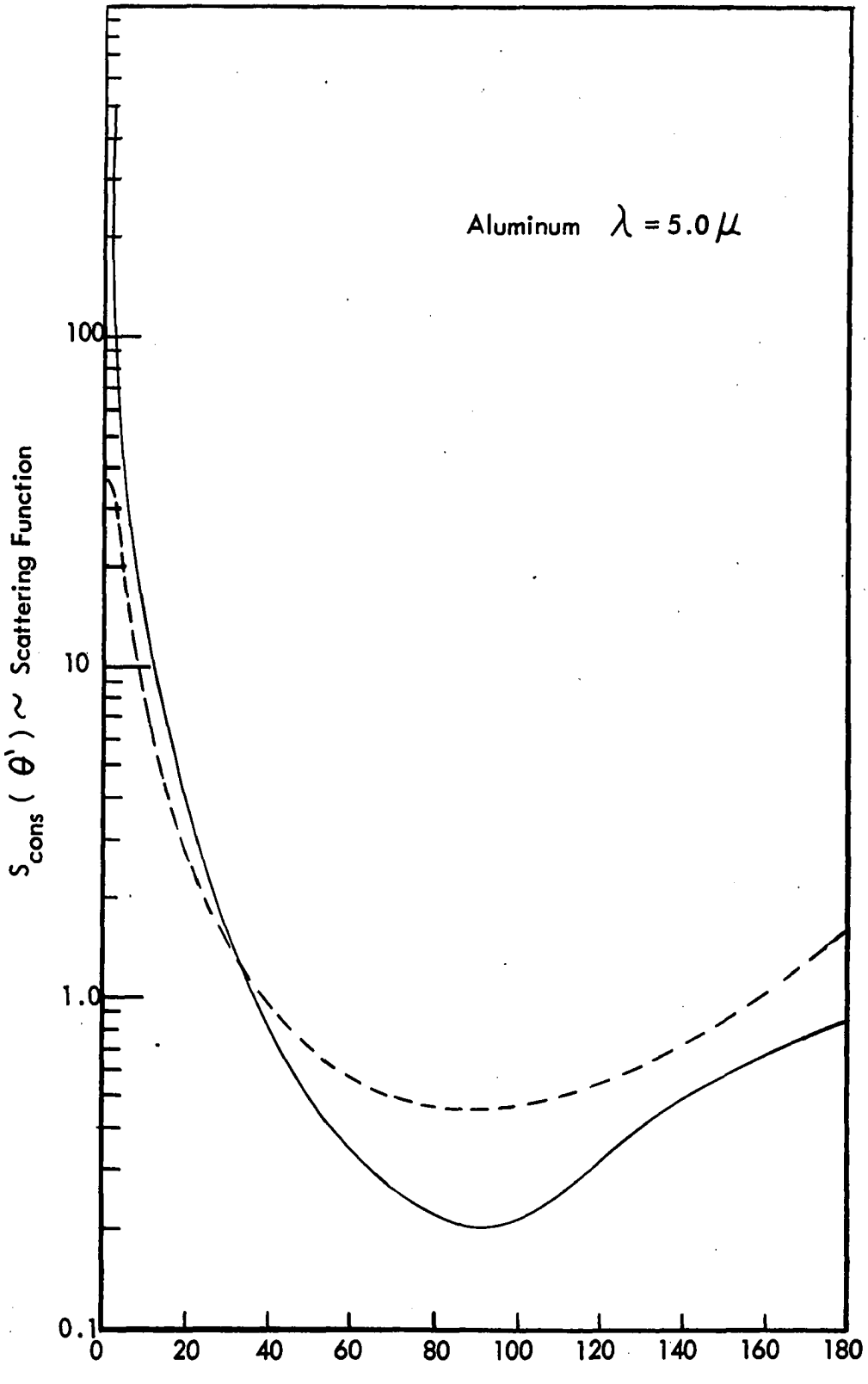

Figure 31
Angular Distribution of Scattering Function -- Experimental Data

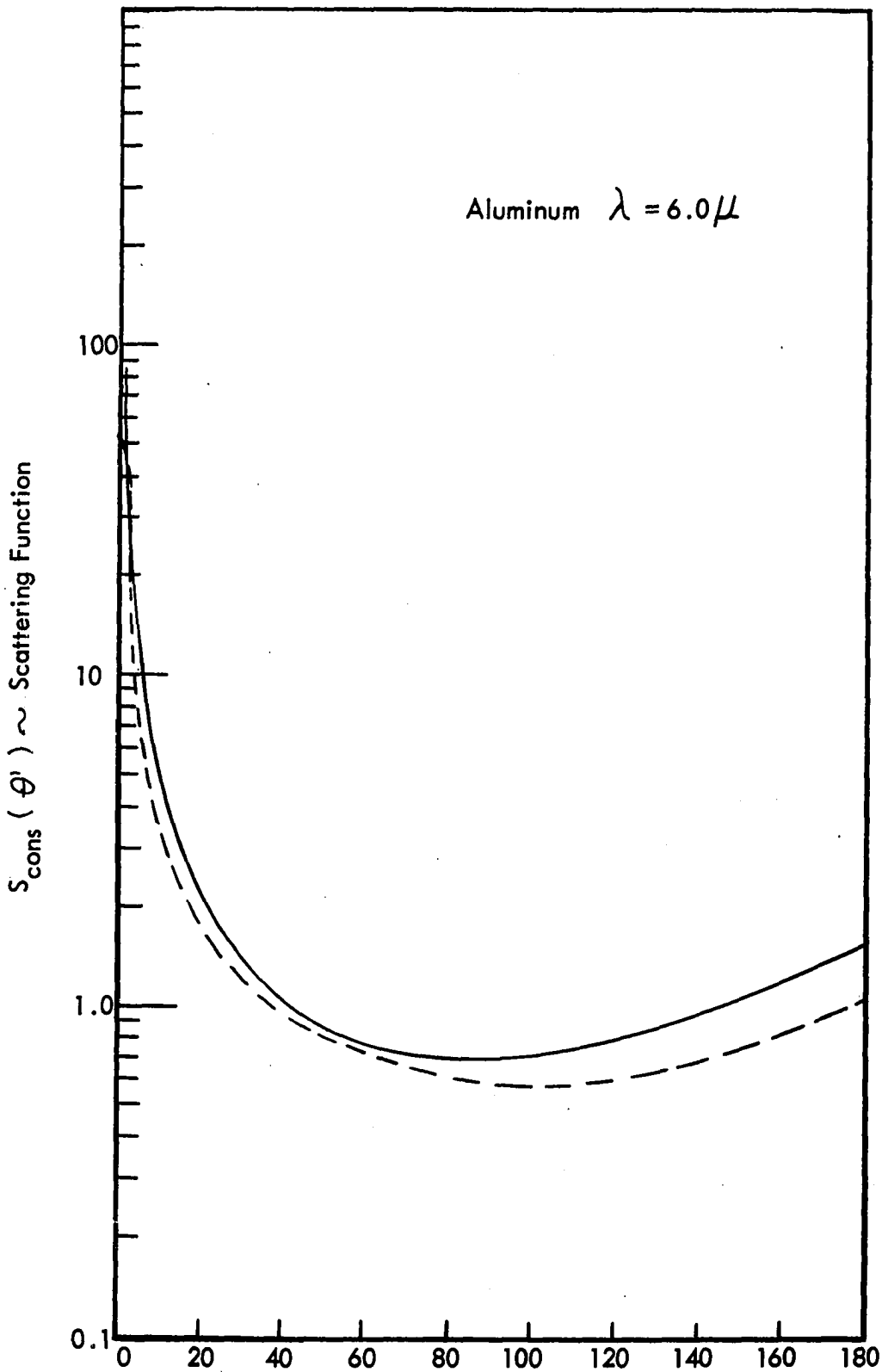

Figure 32
Angular Distribution of Scattering Function -- Experimental Data

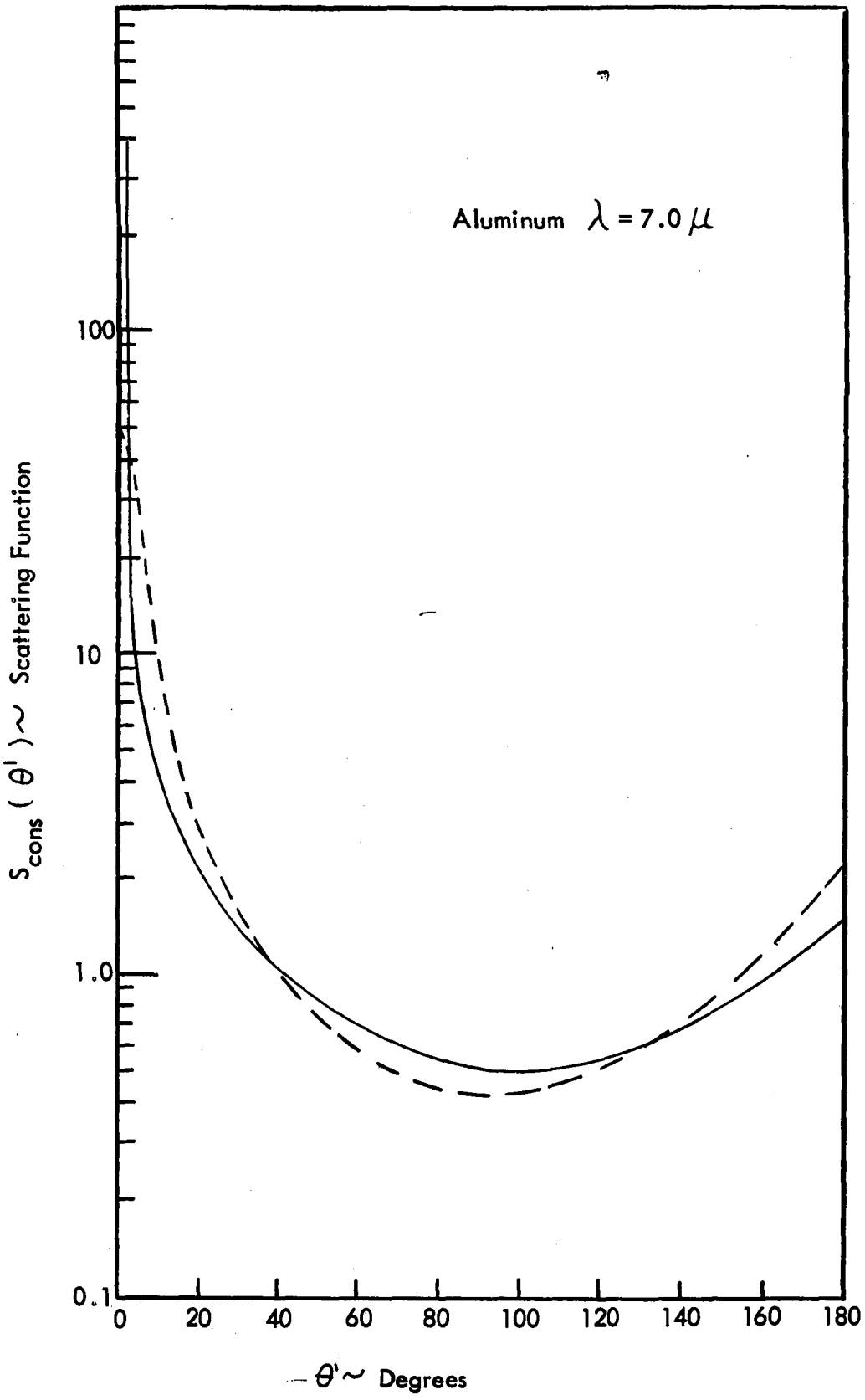

Figure 33
Angular Distribution of Scattering
Function -- Experimental Data

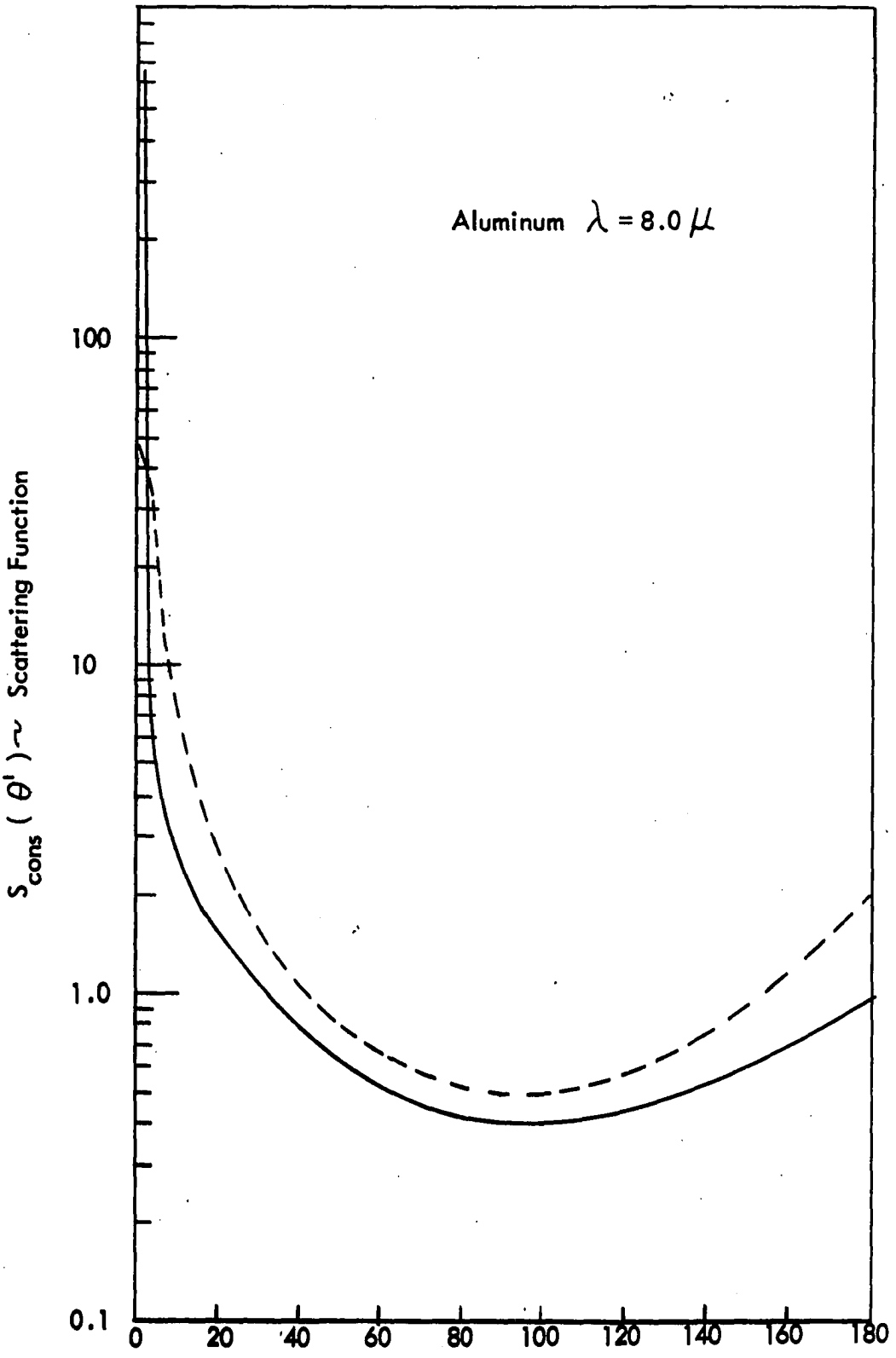

Figure 34
Angular Distribution of Scattering Function -- Experimental Data

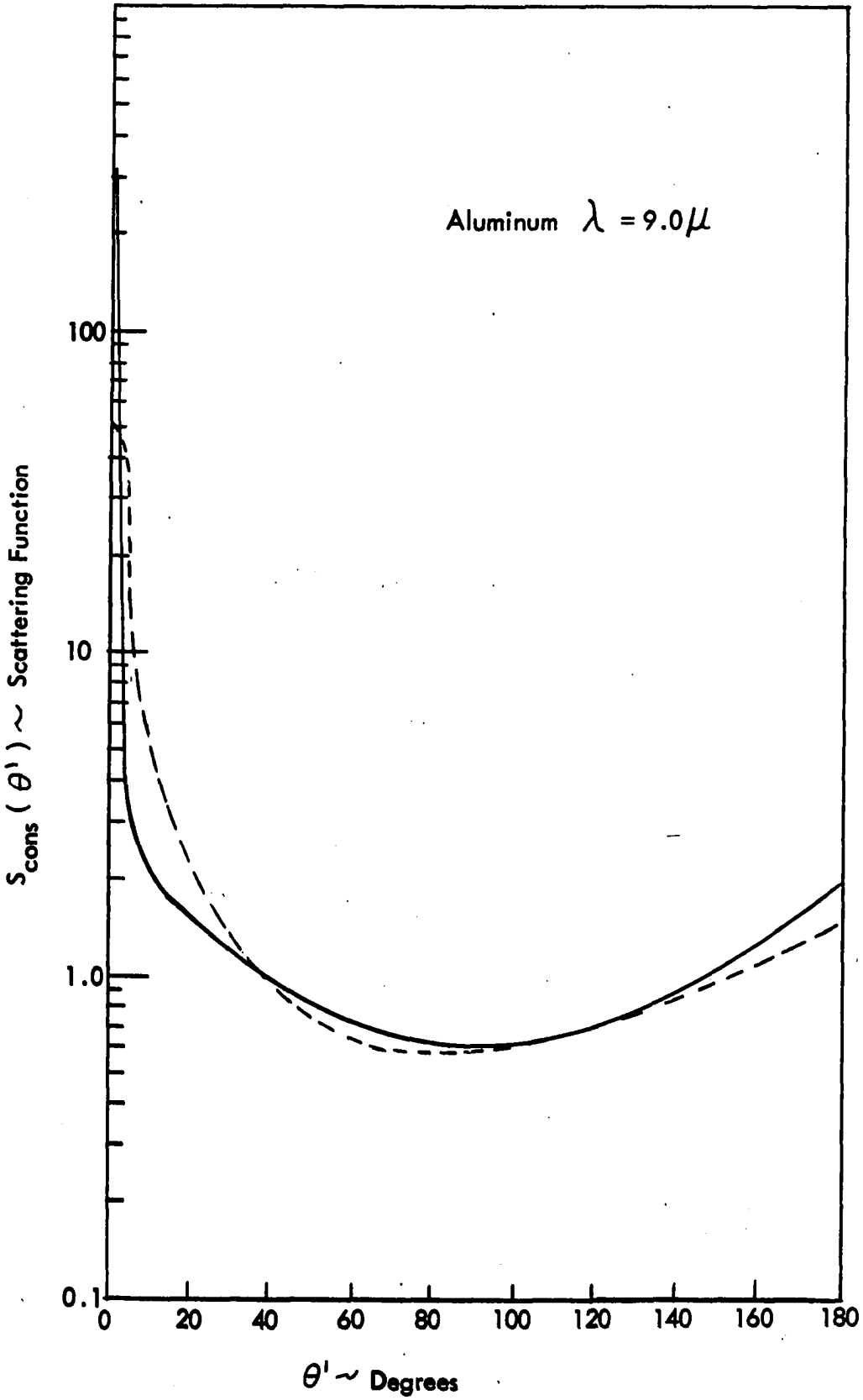

Figure 35
Angular Distribution of Scattering Function -- Experimental Data

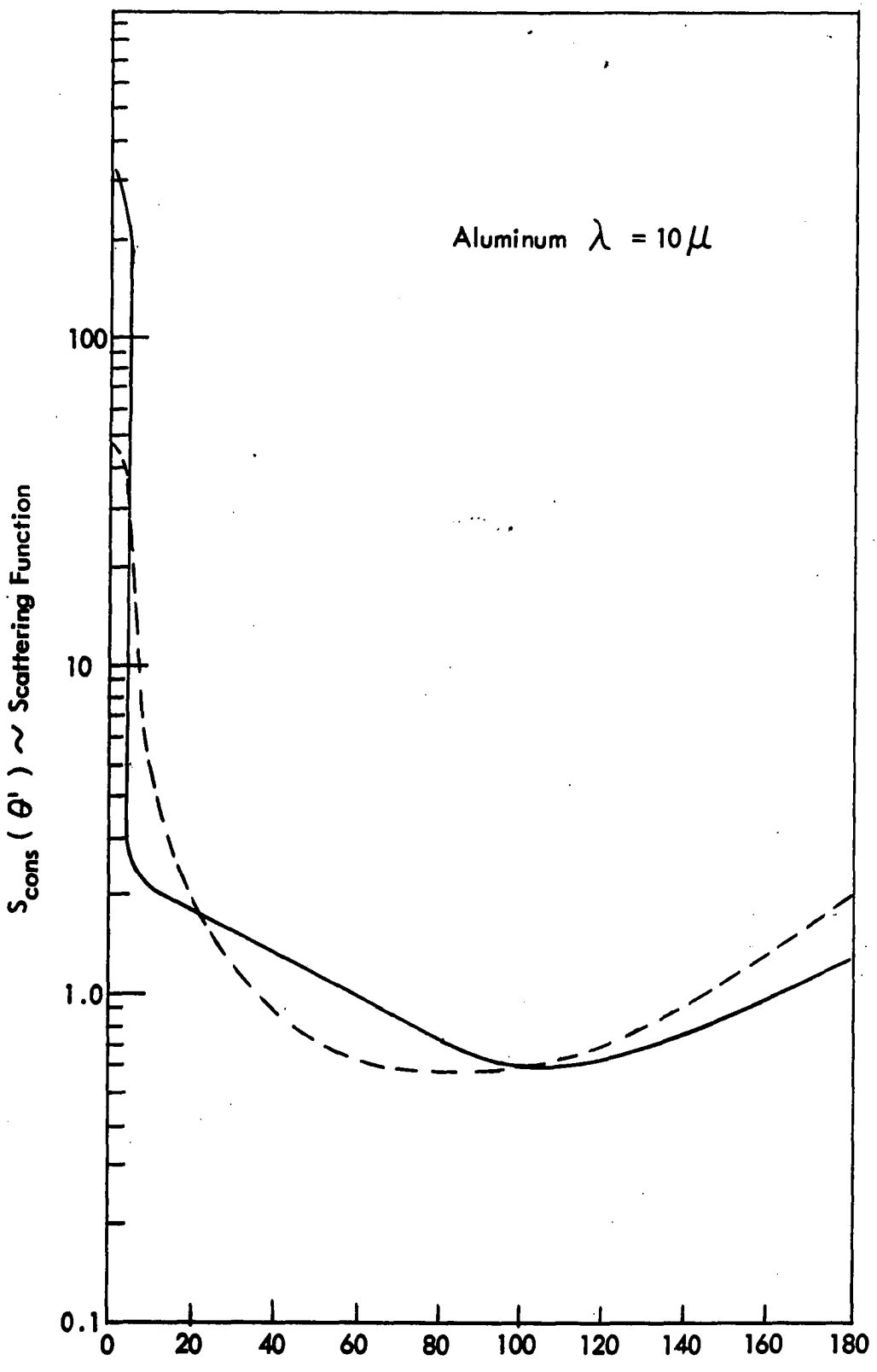

Figure 36
Angular Distribution of Scattering Function -- Experimental Data

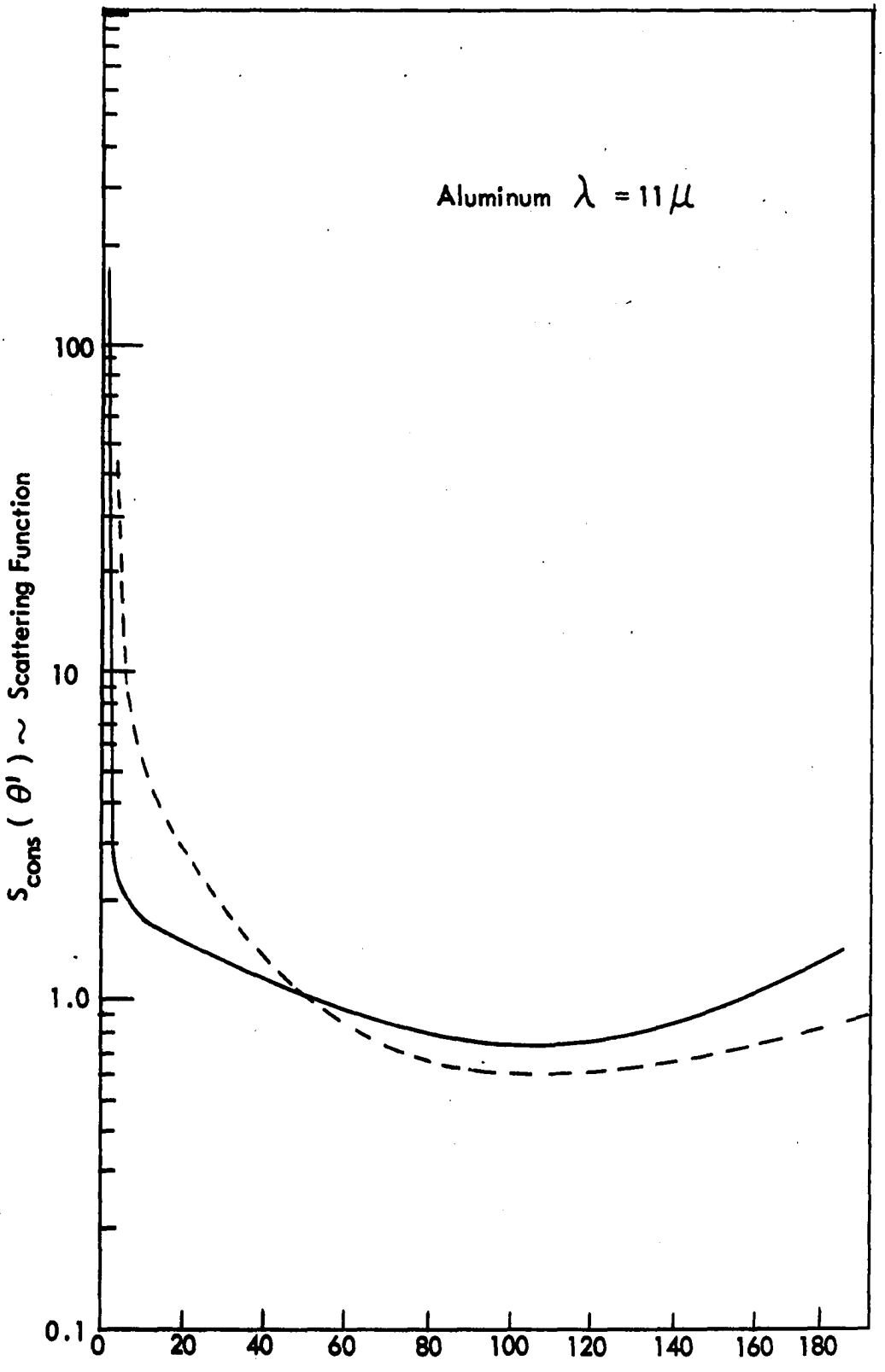

Figure 37
Angular Distribution of Scattering Function -- Experimental Data

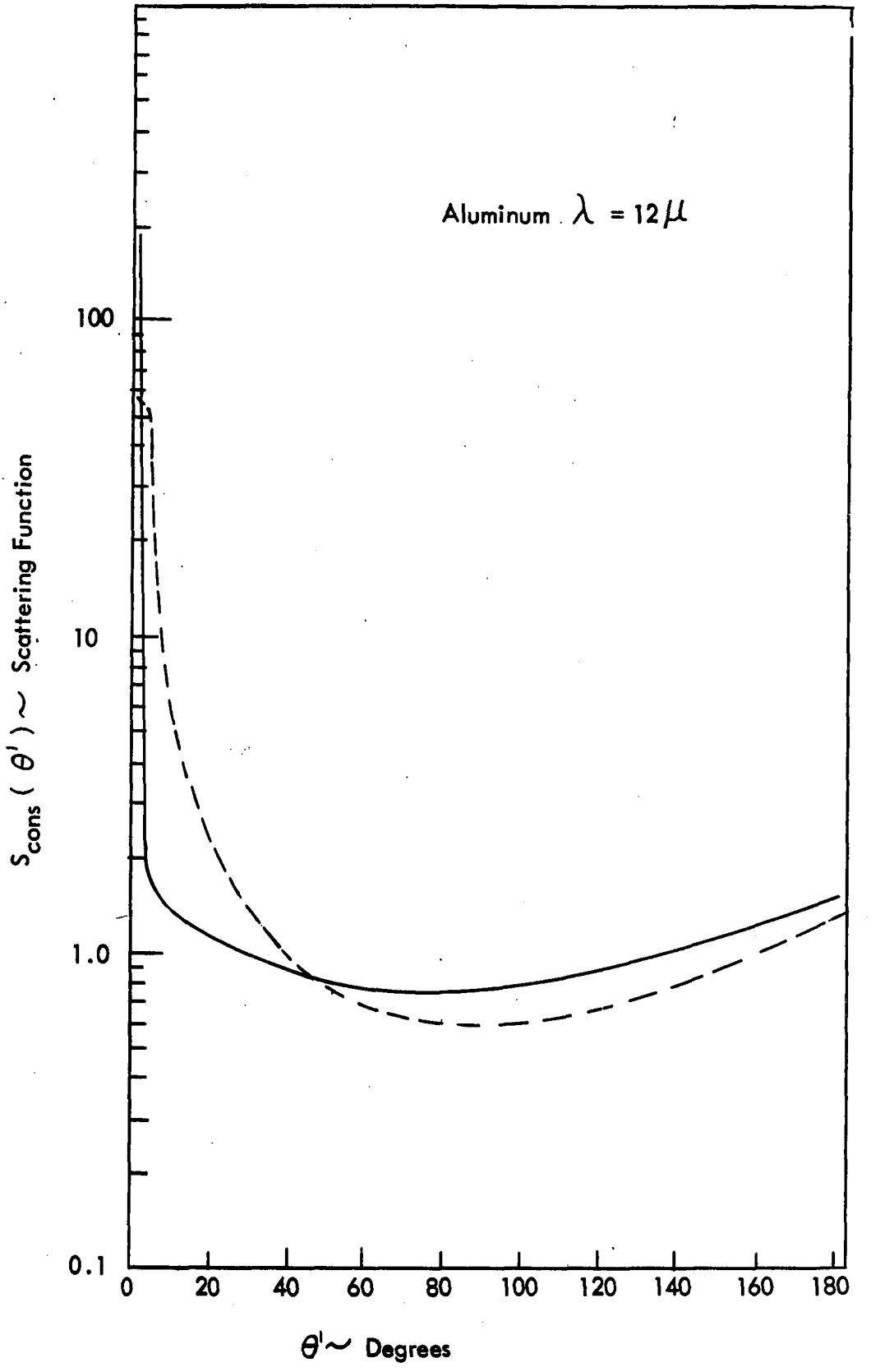

Figure 38
Angular Distribution of Scattering Function -- Experimental Data

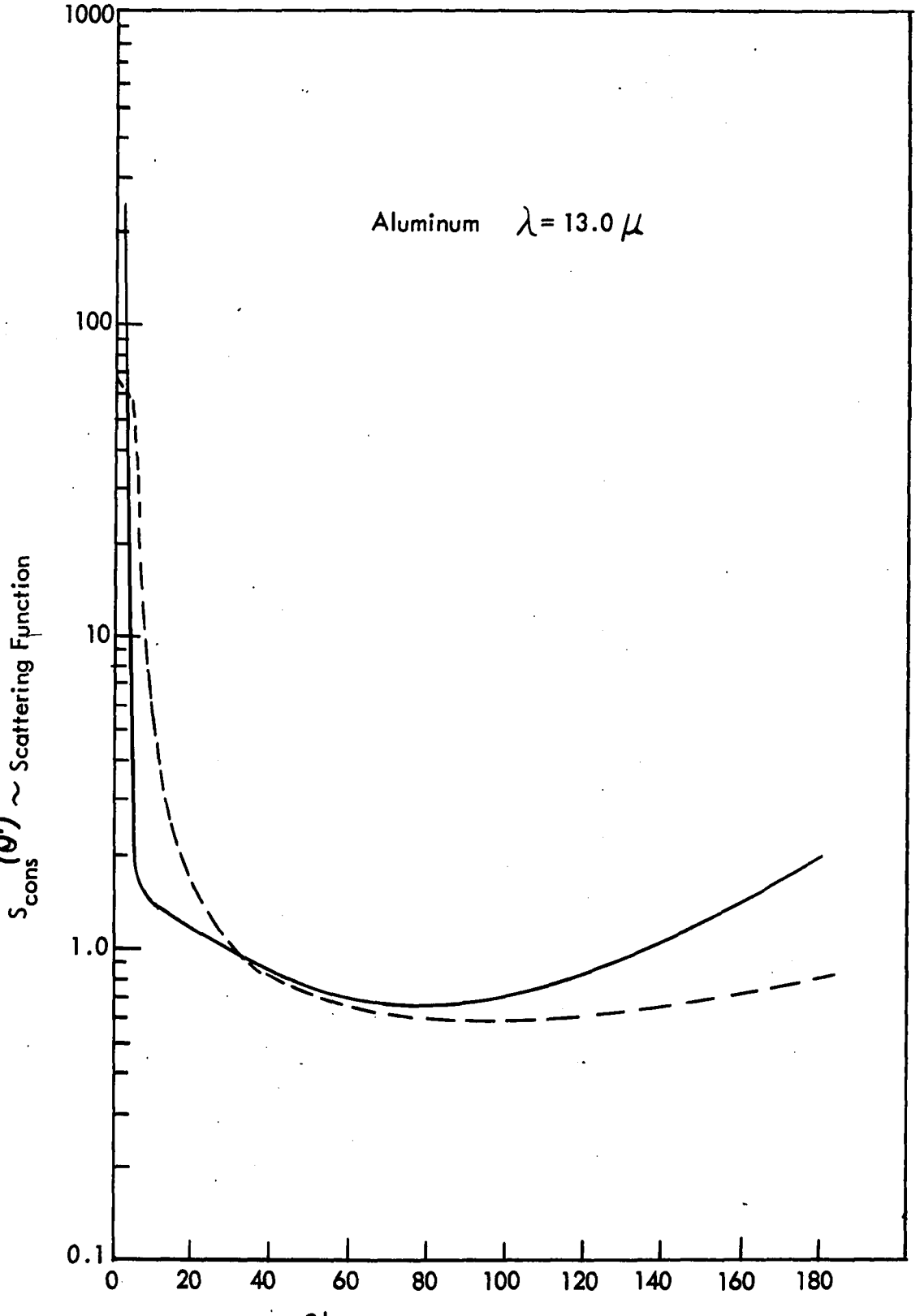

Figure 39
Angular Distribution of Scattering Function -- Experimental Data

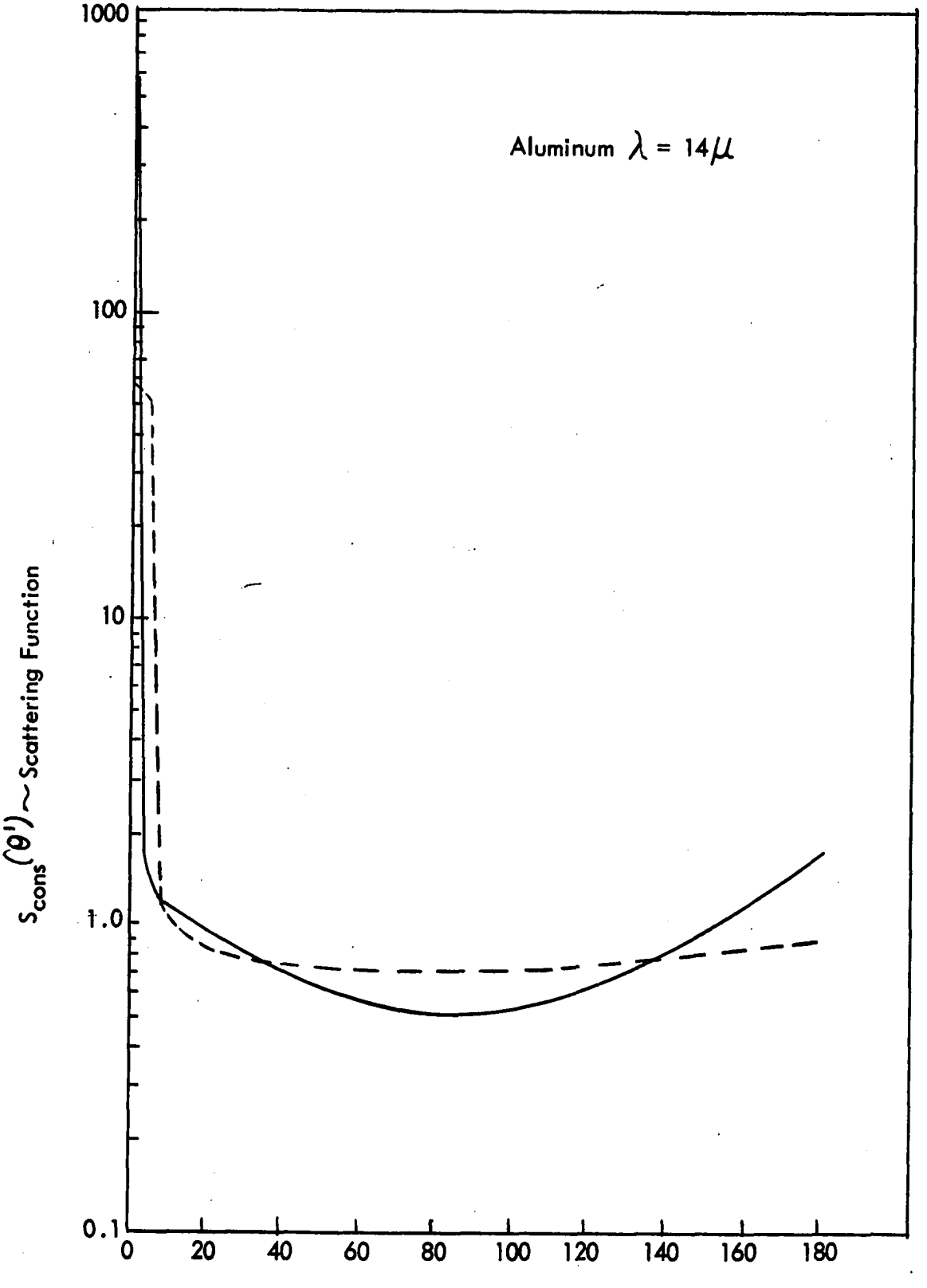

Angular Distribution of Scattering Function -- Experimental Data

Figure 40

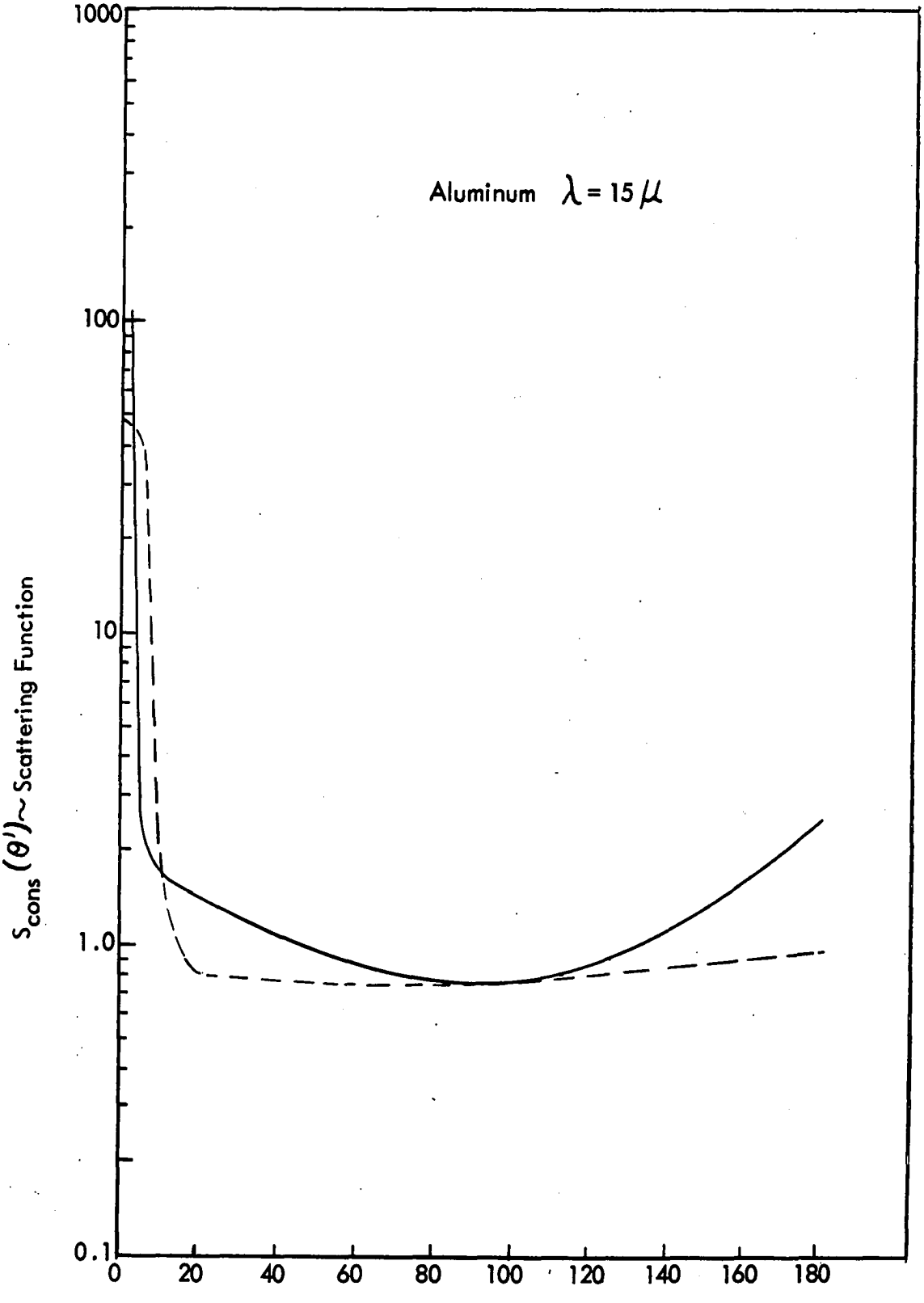

Figure 41
Angular Distribution of Scattering Function -- Experimental Data

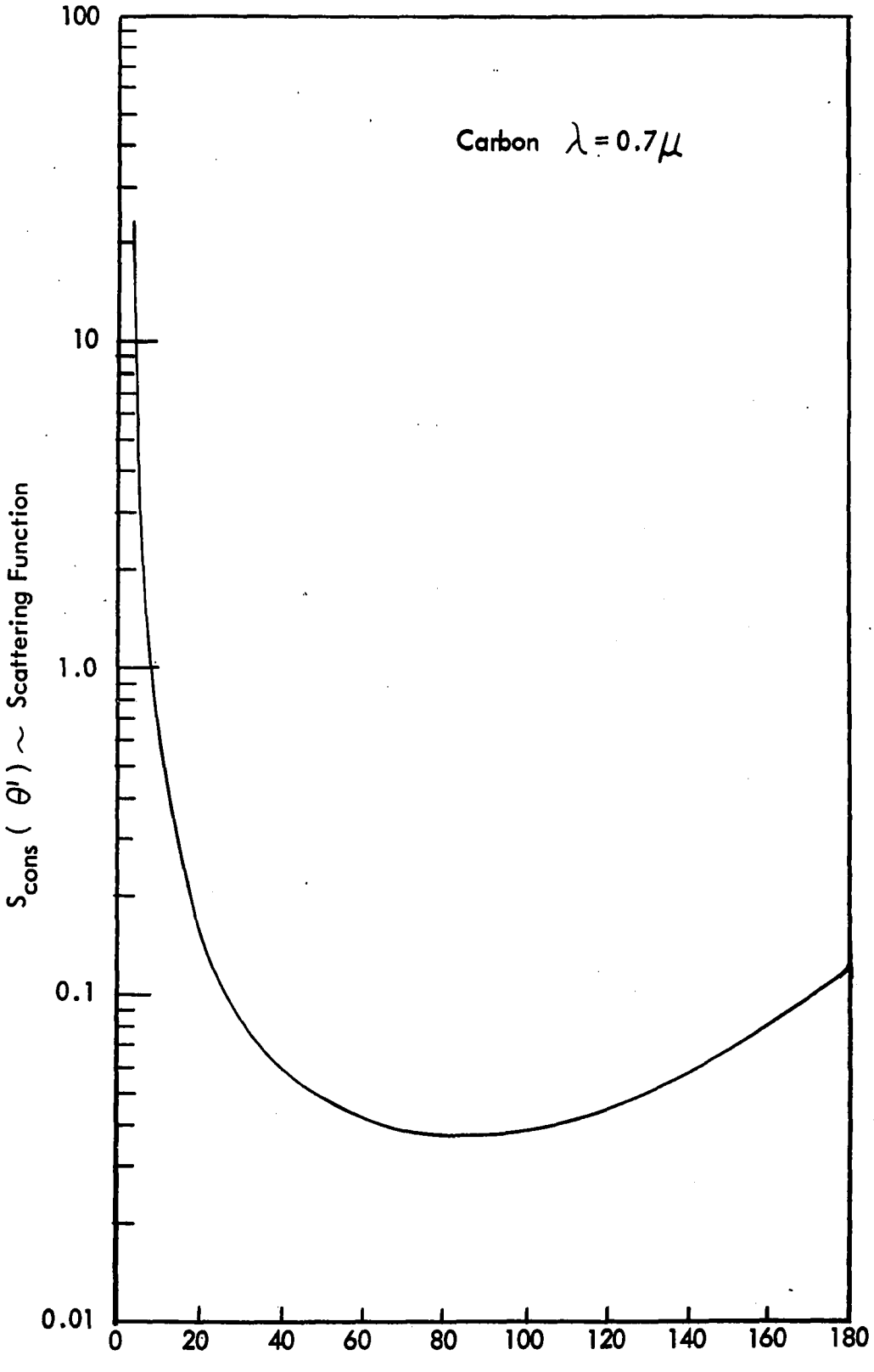

Figure 42

Angular Distribution of Scattering Function -- Experimental Data

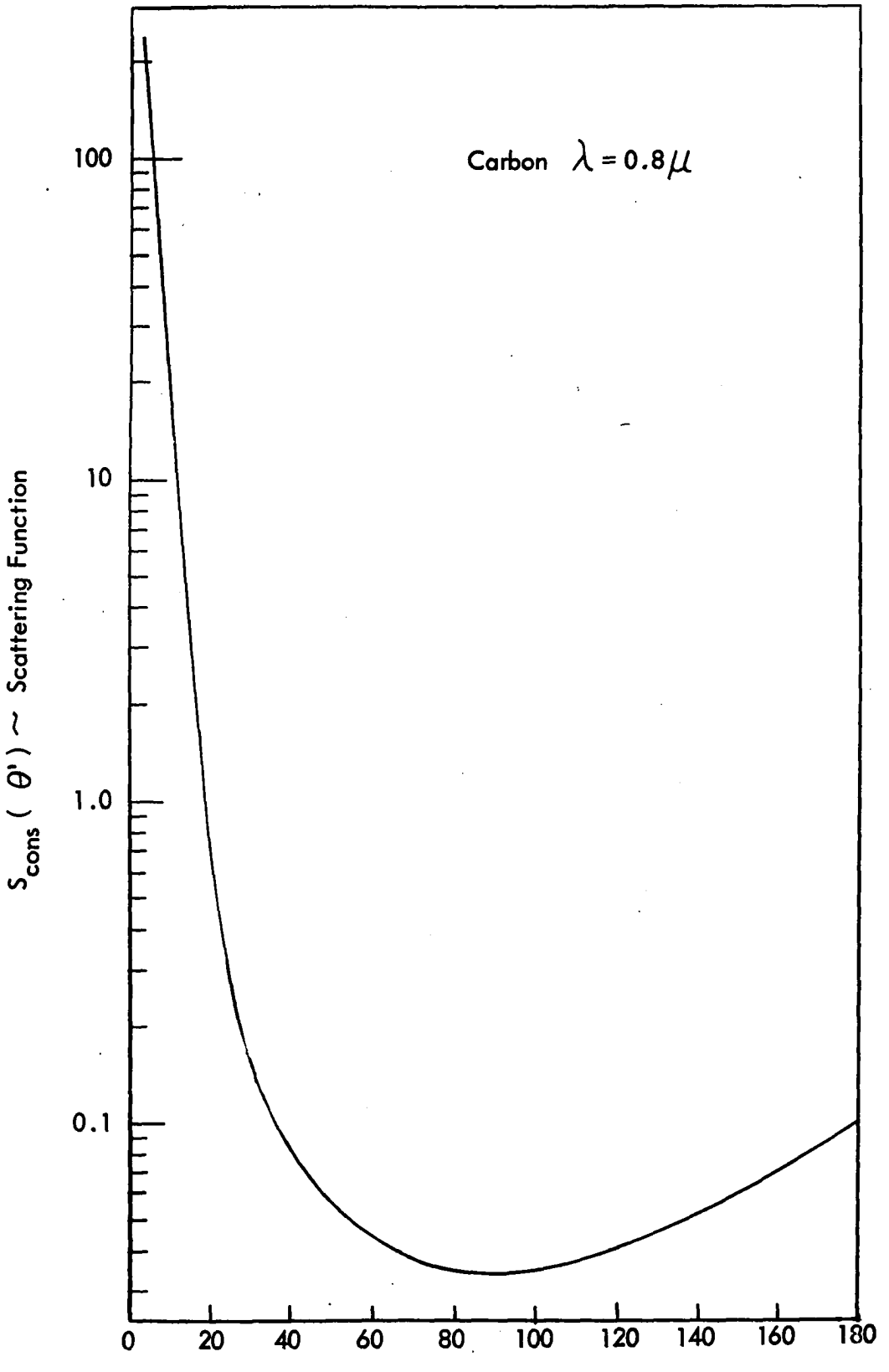

Figure 43
Angular Distribution of Scattering Function -- Experimental Data

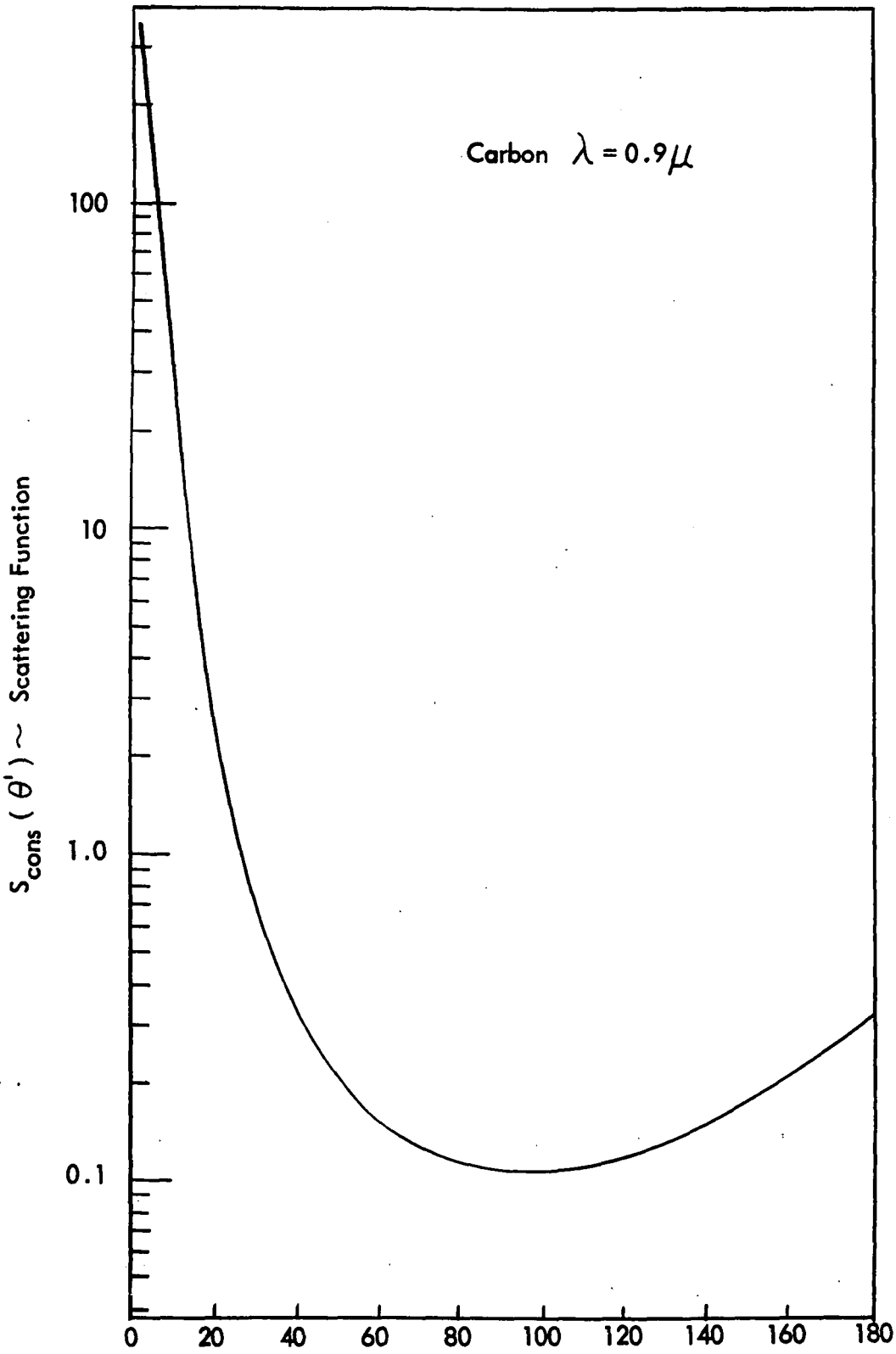

Figure 44
Angular Distribution of Scattering Function -- Experimental Data

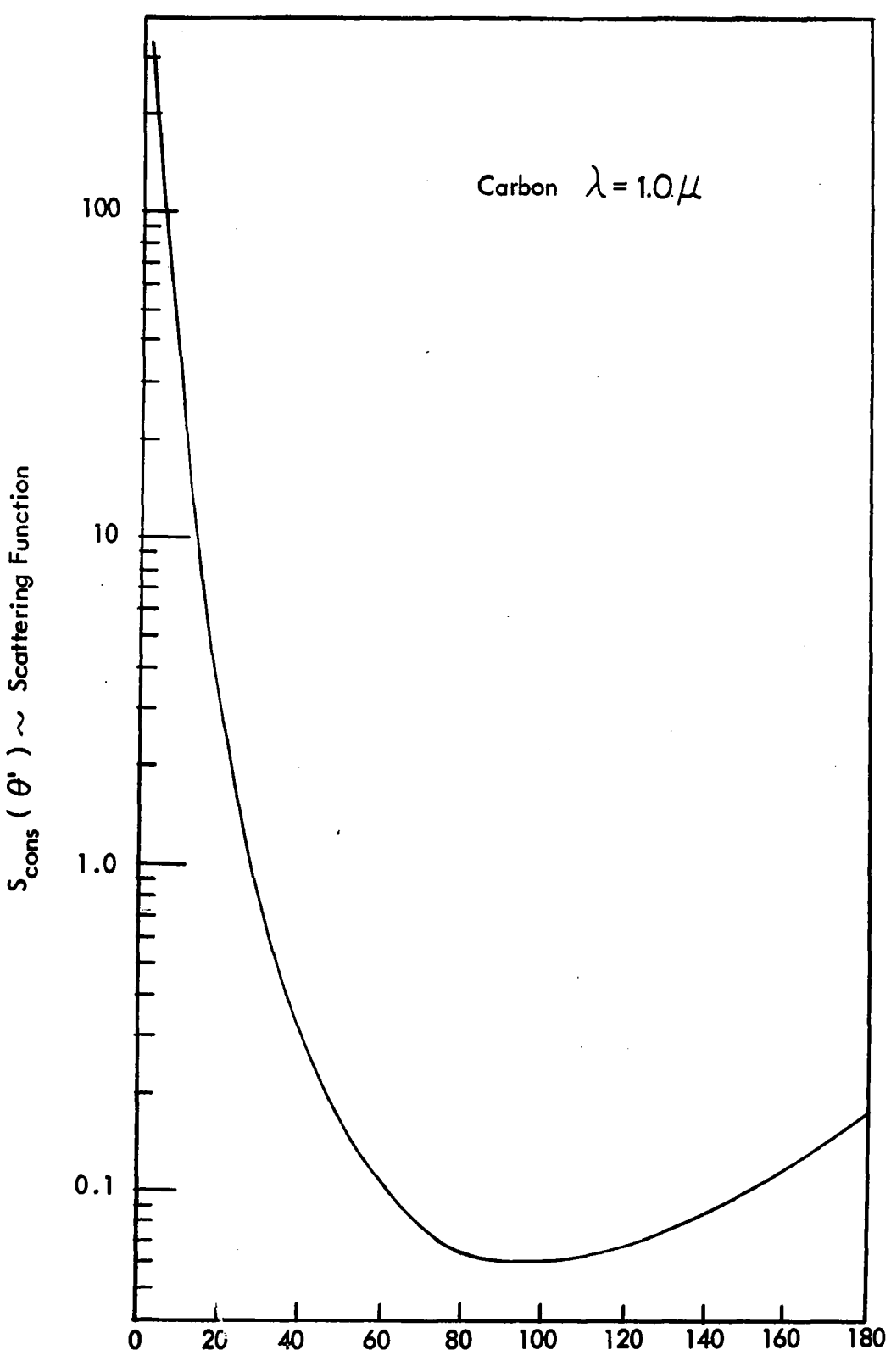

Figure 45
Angular Distribution of Scattering Function -- Experimental Data

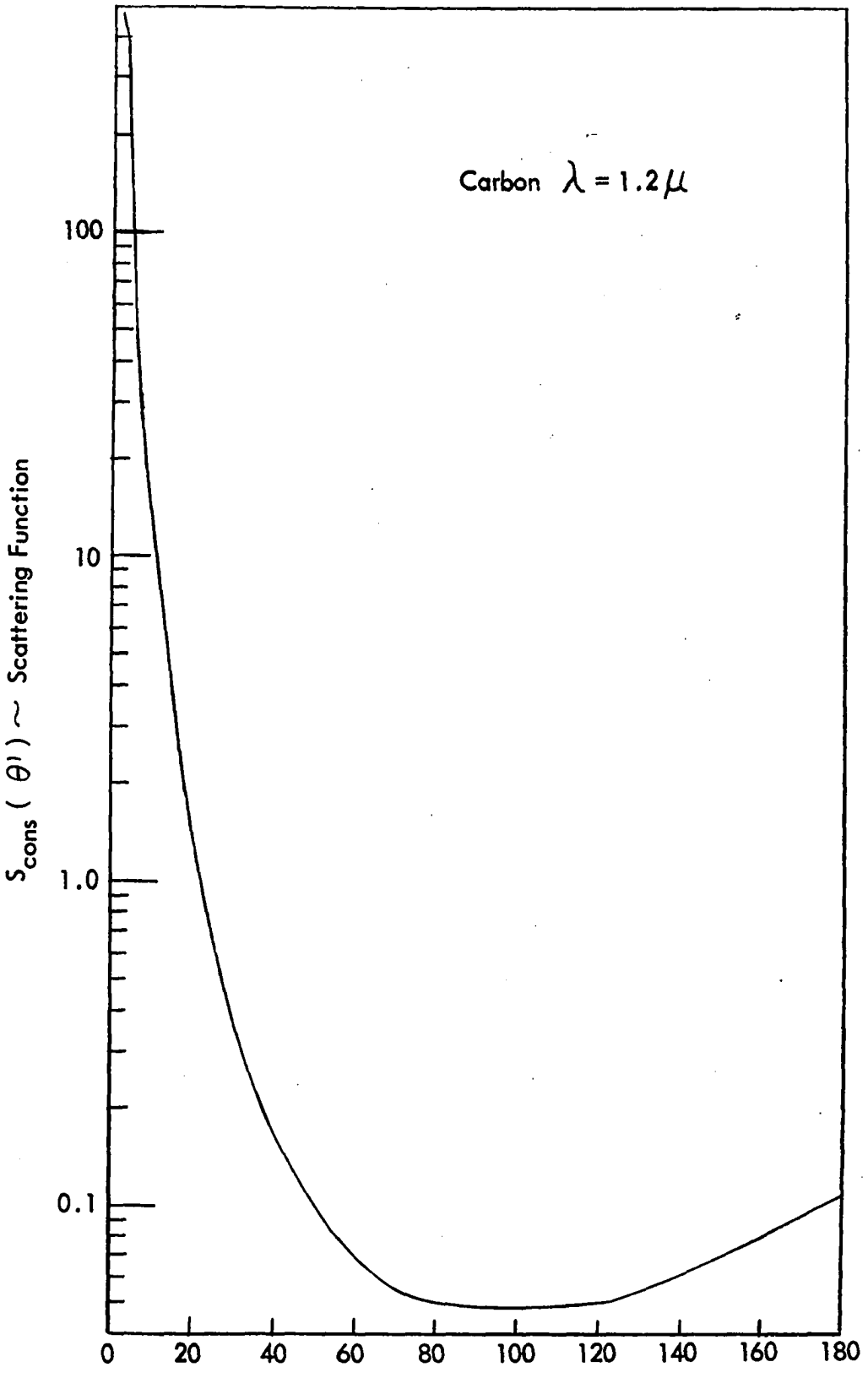

Figure 46
Angular Distribution of Scattering Function -- Experimental Data

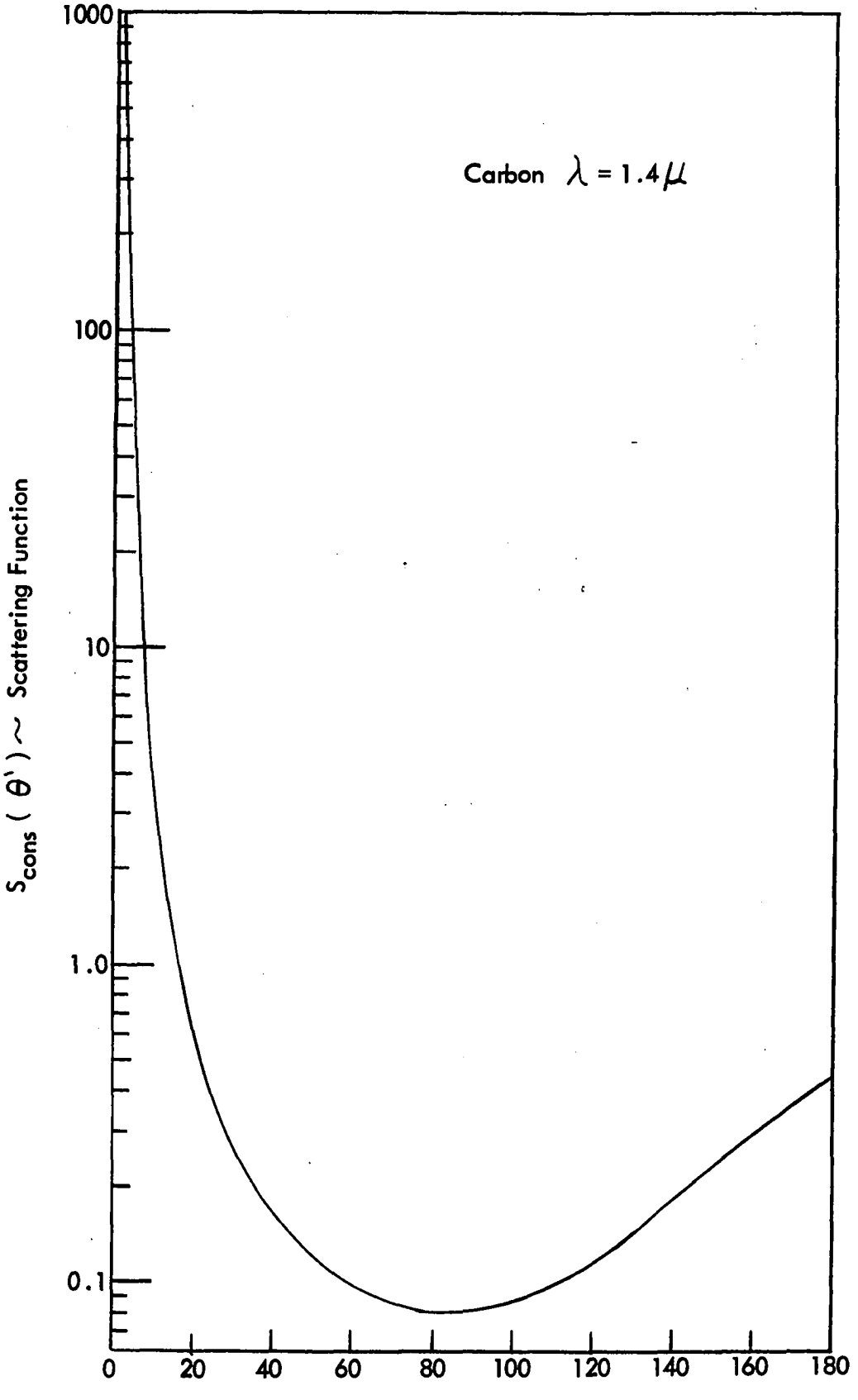

Figure 47
Angular Distribution of Scattering Function -- Experimental Data

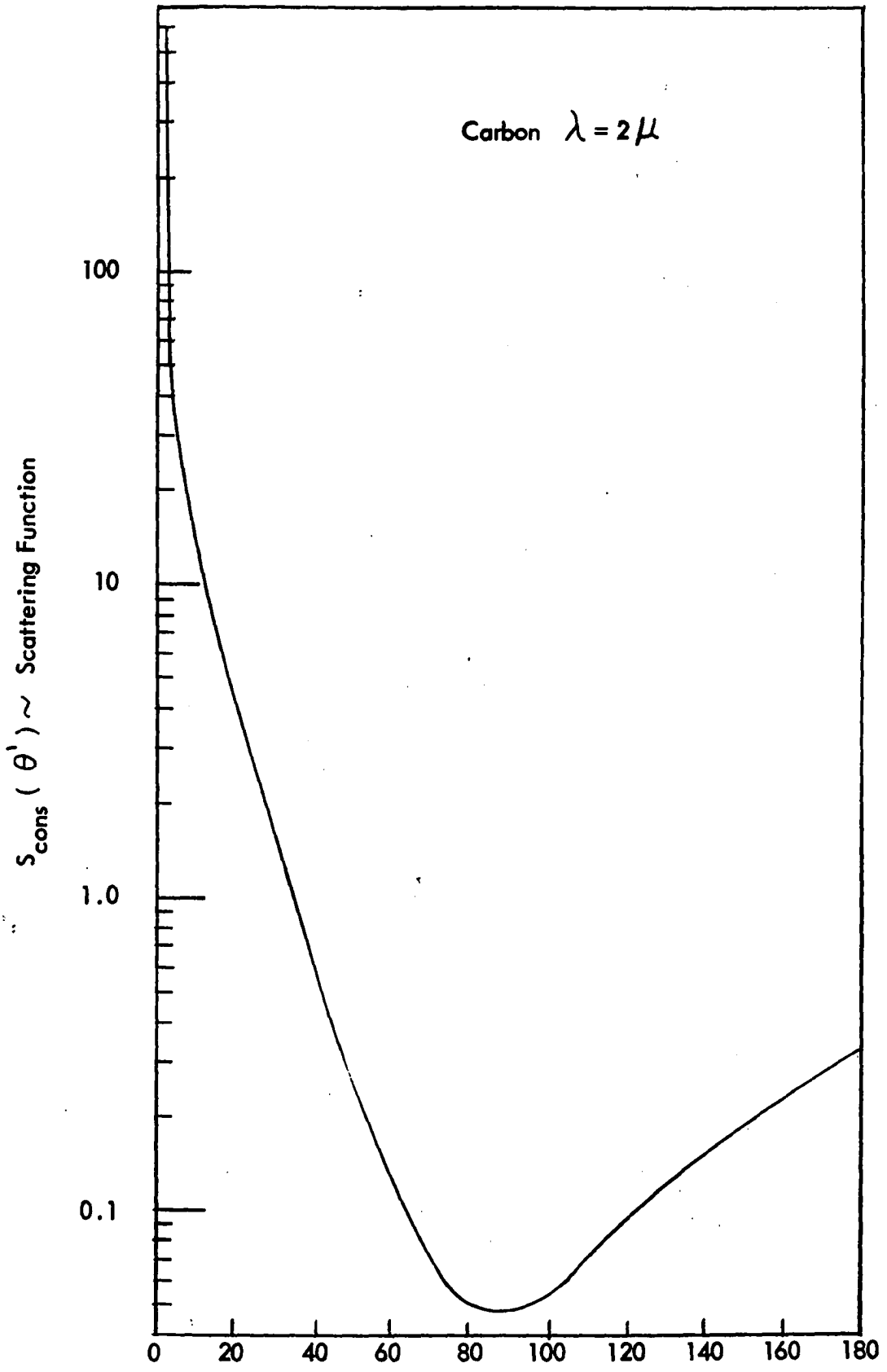

Figure 48
Angular Distribution of Scattering Function -- Experimental Data

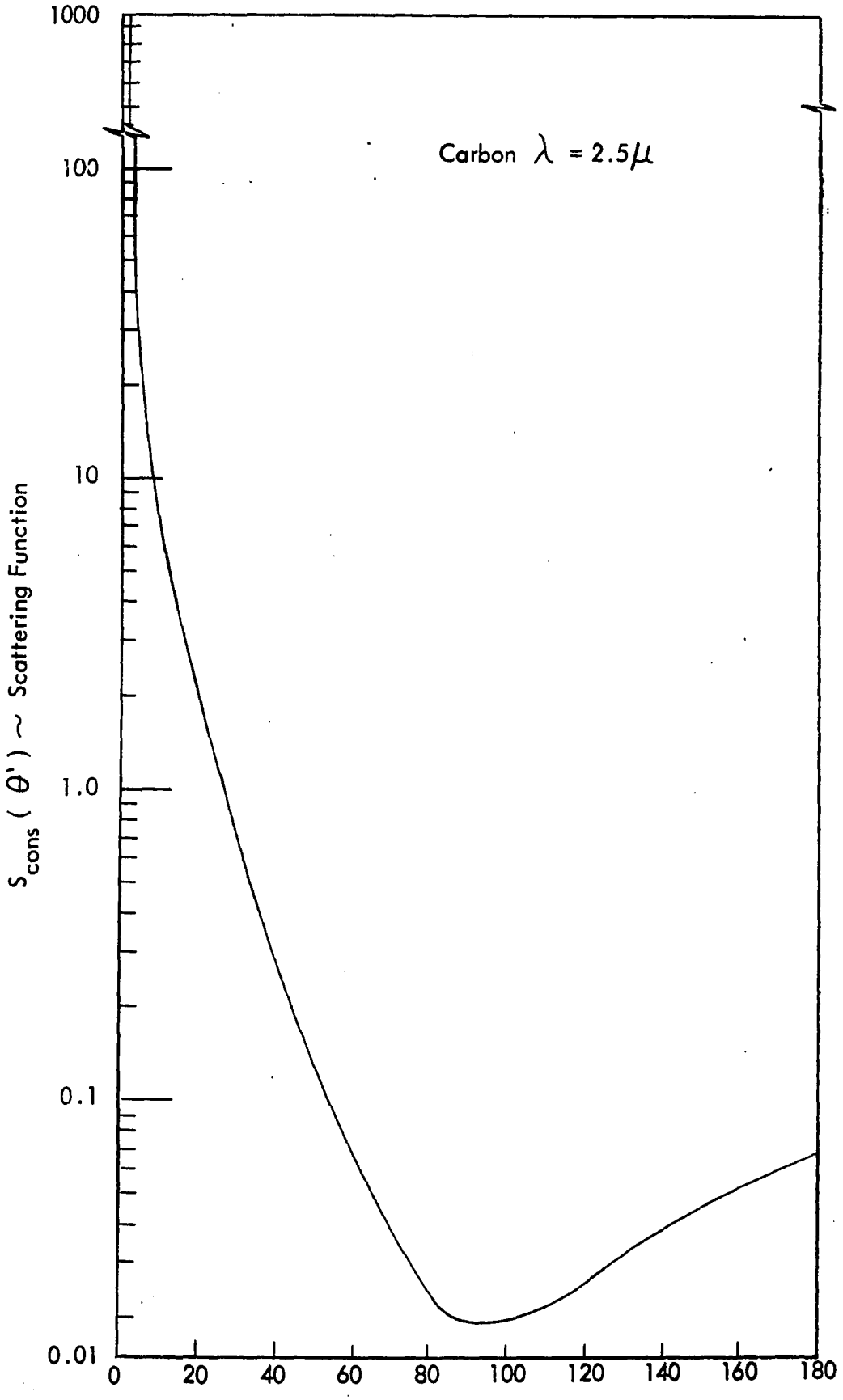

Figure 49
Angular Distribution of Scattering Function -- Experimental Data

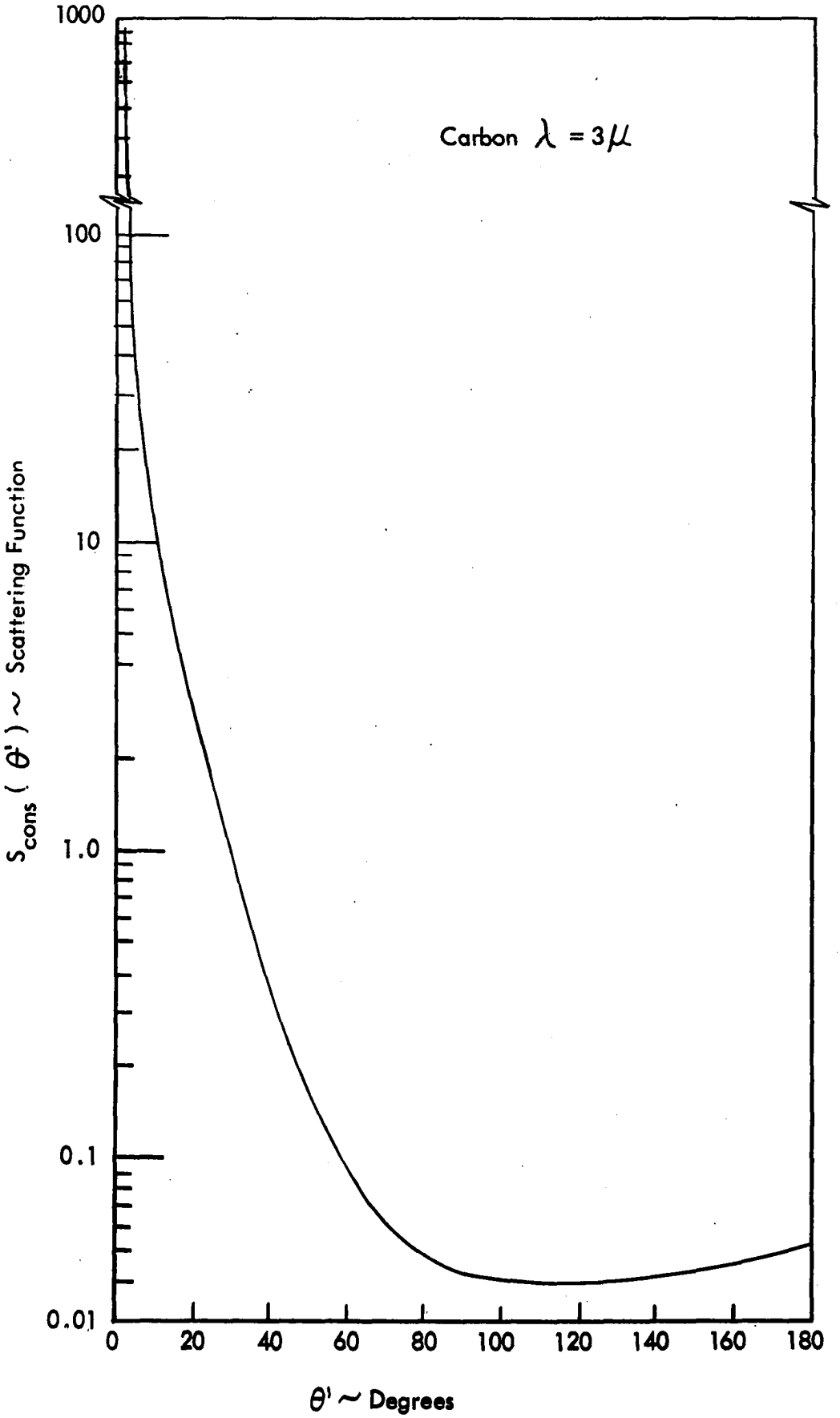

Figure 50
Angular Distribution of Scattering Function -- Experimental Data

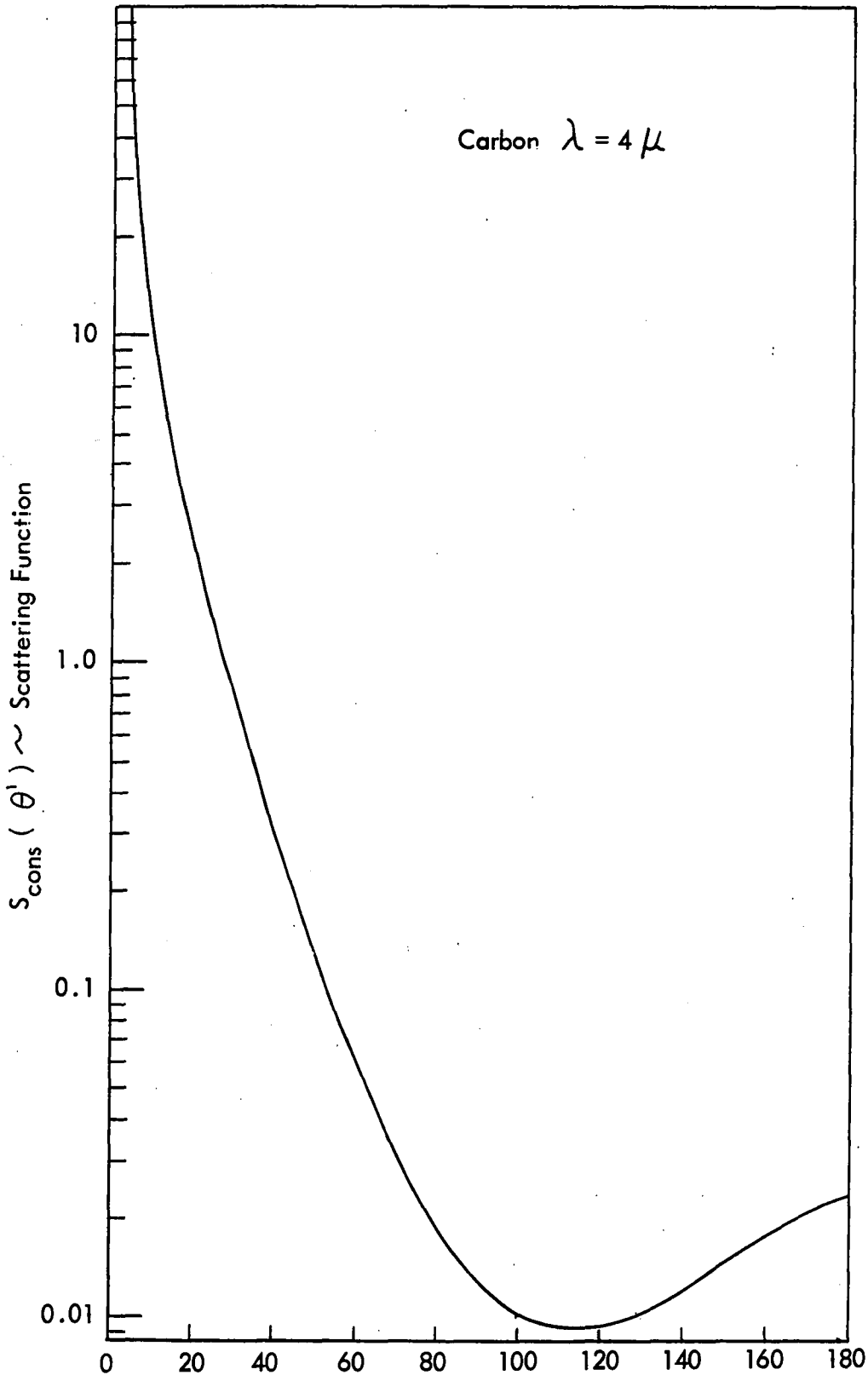

Figure 51

Angular Distribution of Scattering Function -- Experimental Data

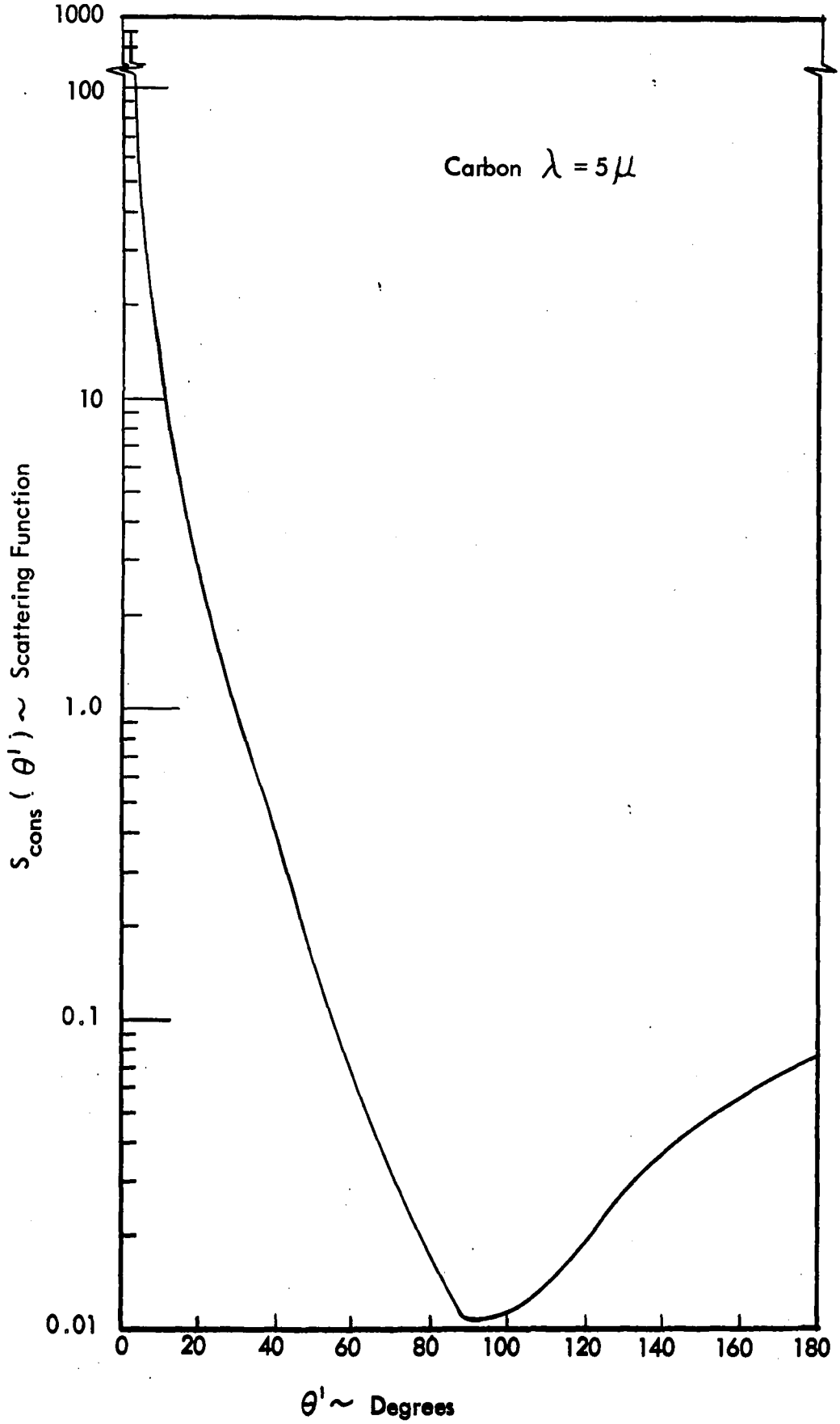

Figure 52
Angular Distribution of Scattering Function -- Experimental Data

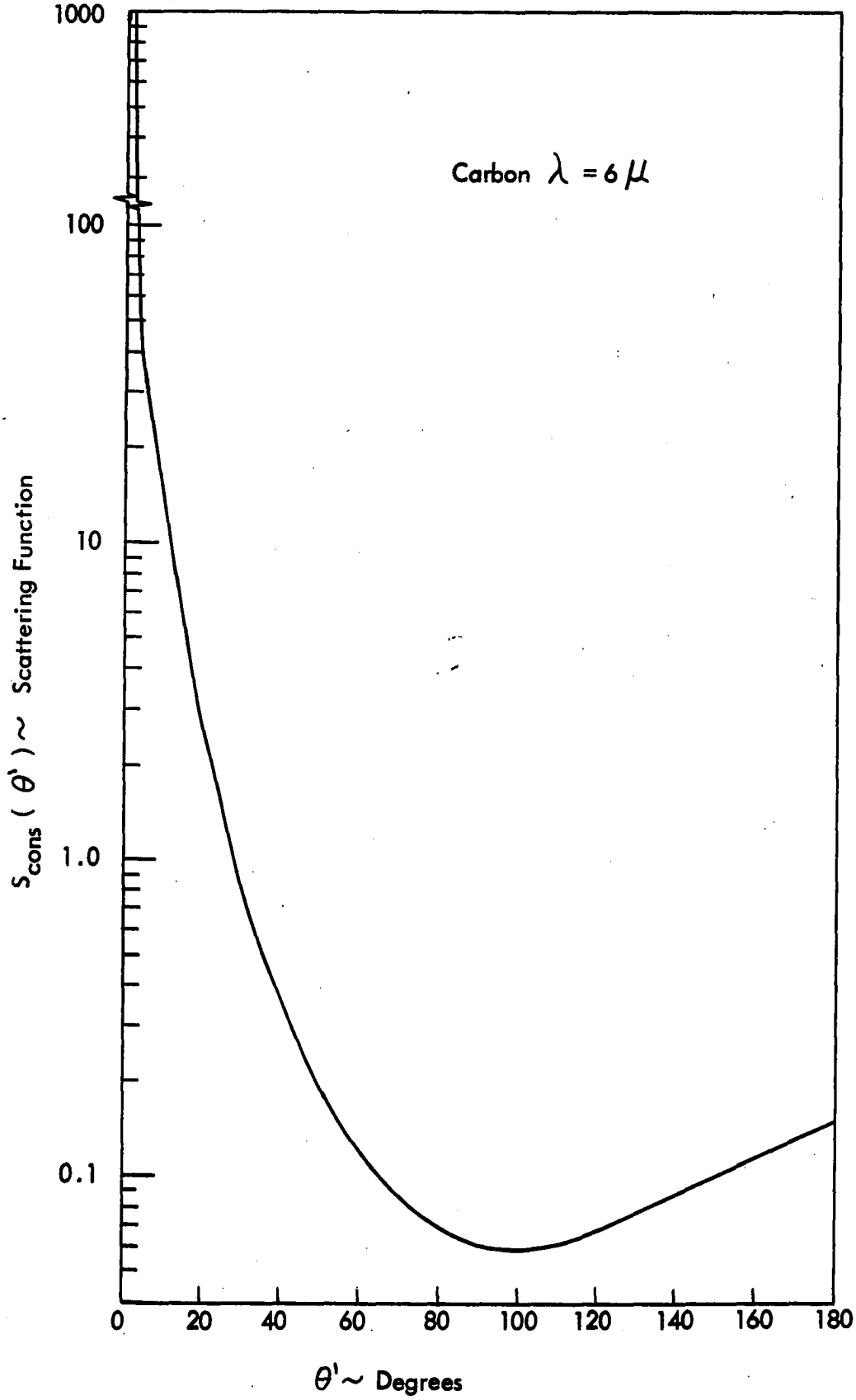

Figure 53
Angular Distribution of Scattering Function -- Experimental Data

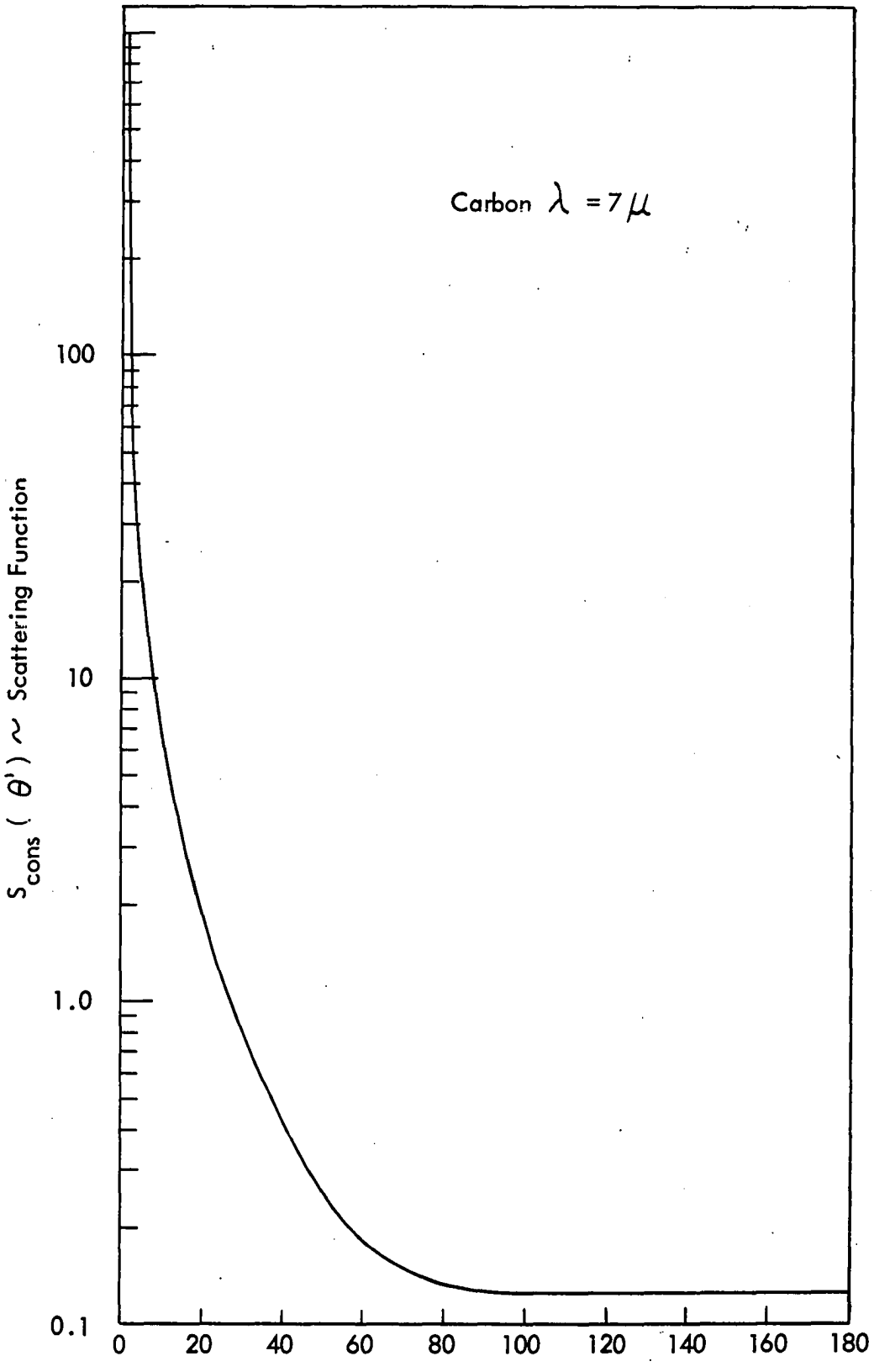

Figure 54
Angular Distribution of Scattering Function -- Experimental Data

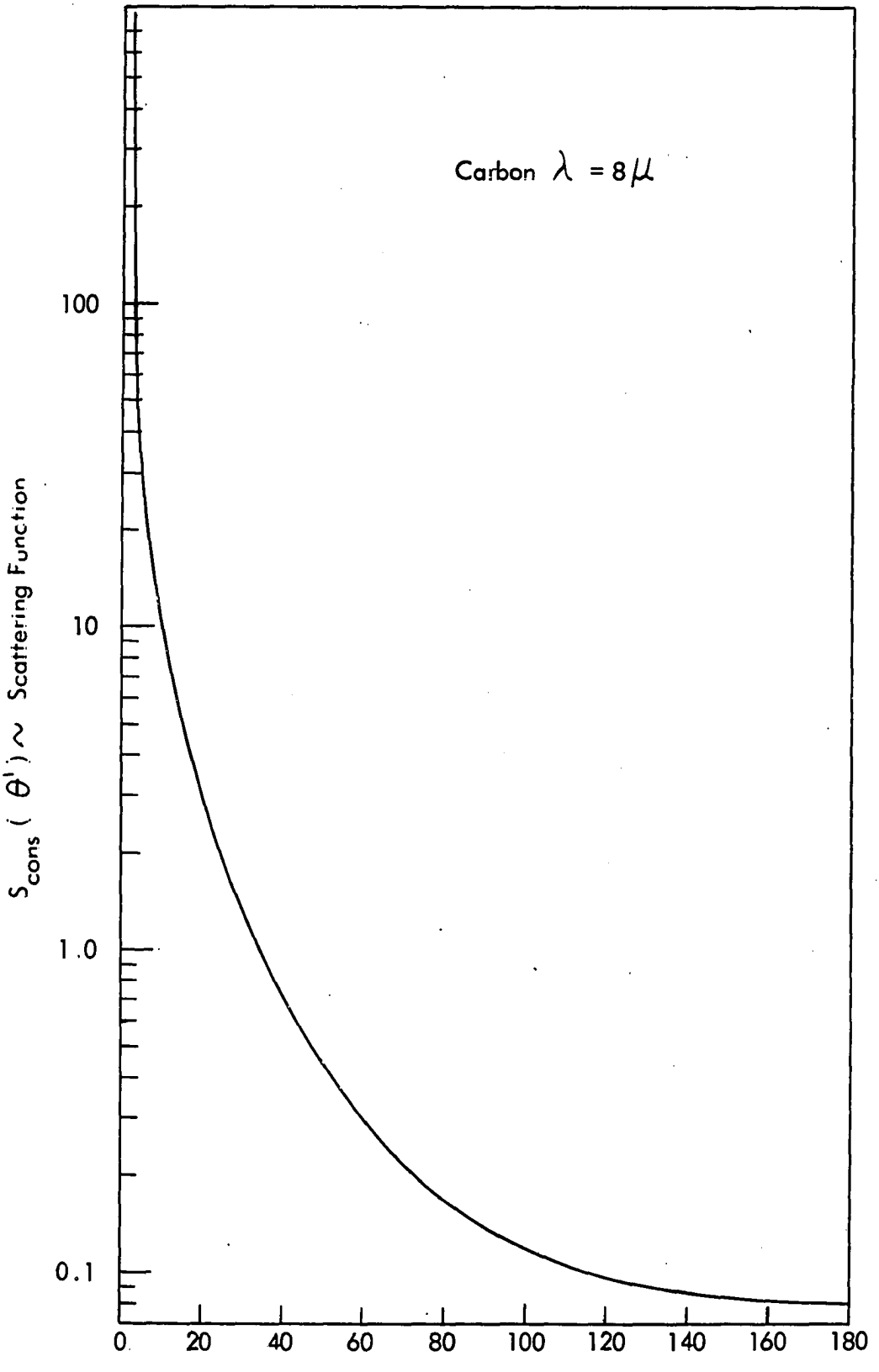

Figure 55
Angular Distribution of Scattering Function -- Experimental Data

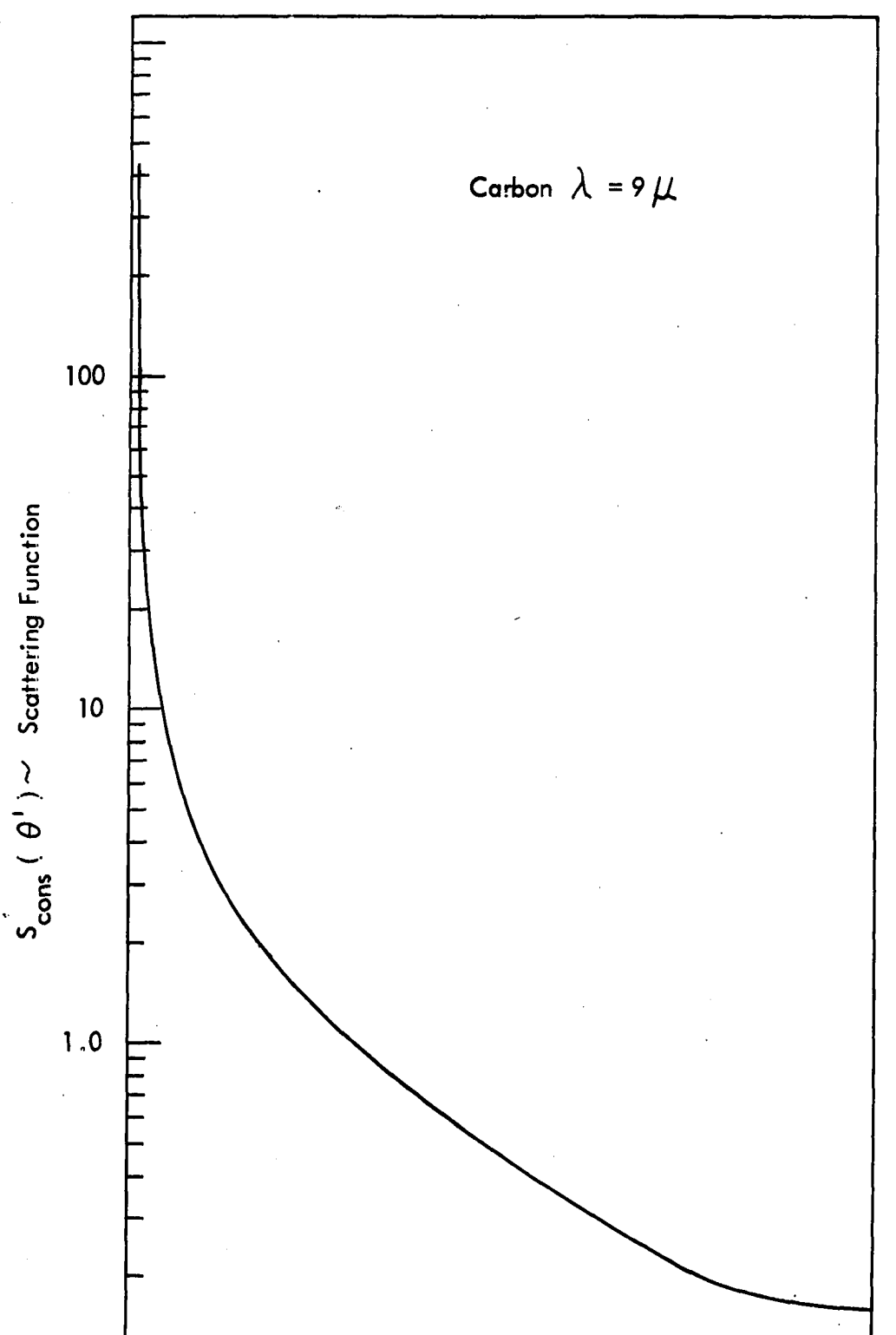

Figure 56
Angular Distribution of Scattering Function -- Experimental Data

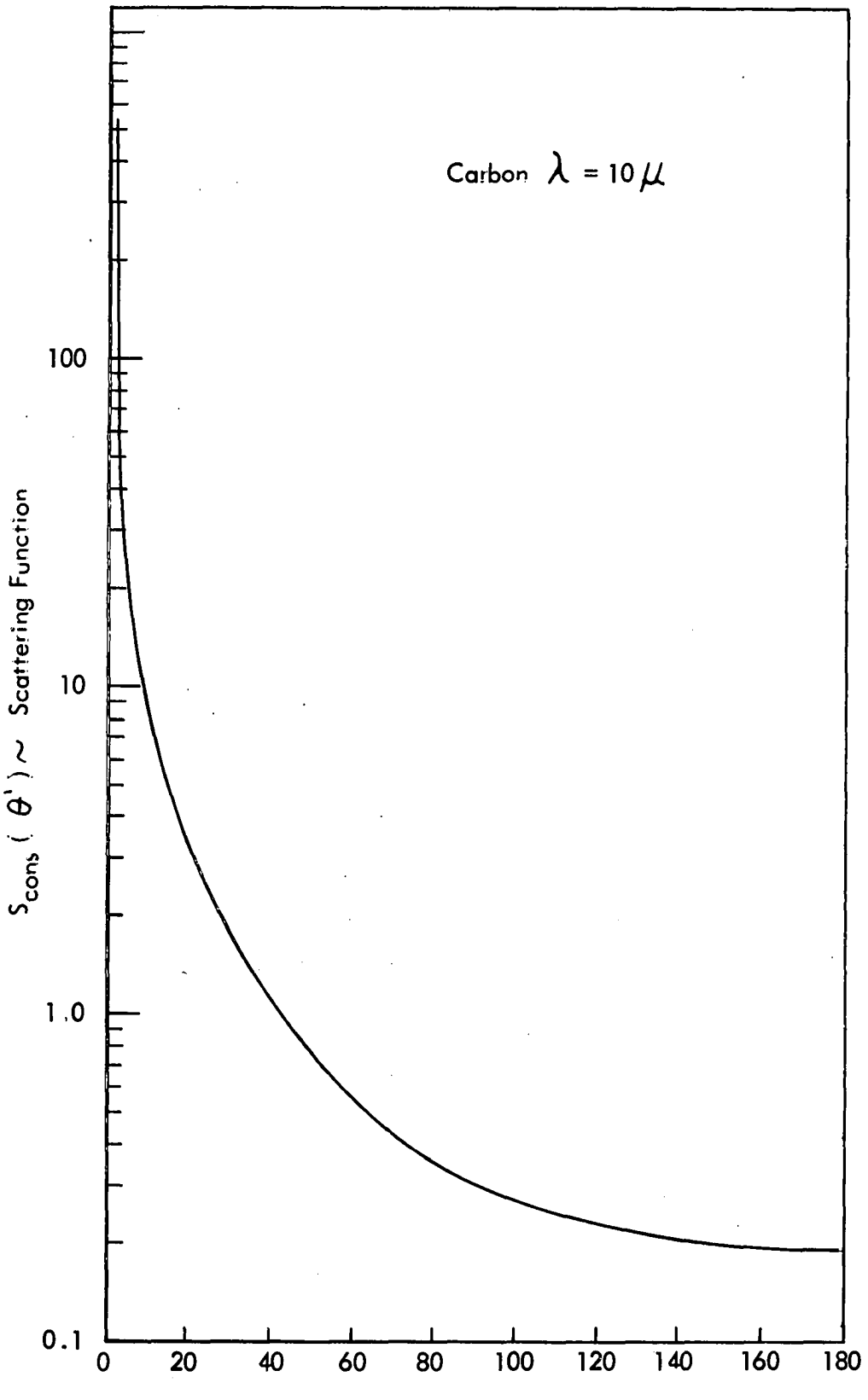

Figure 57
Angular Distribution of Scattering Function -- Experimental Data

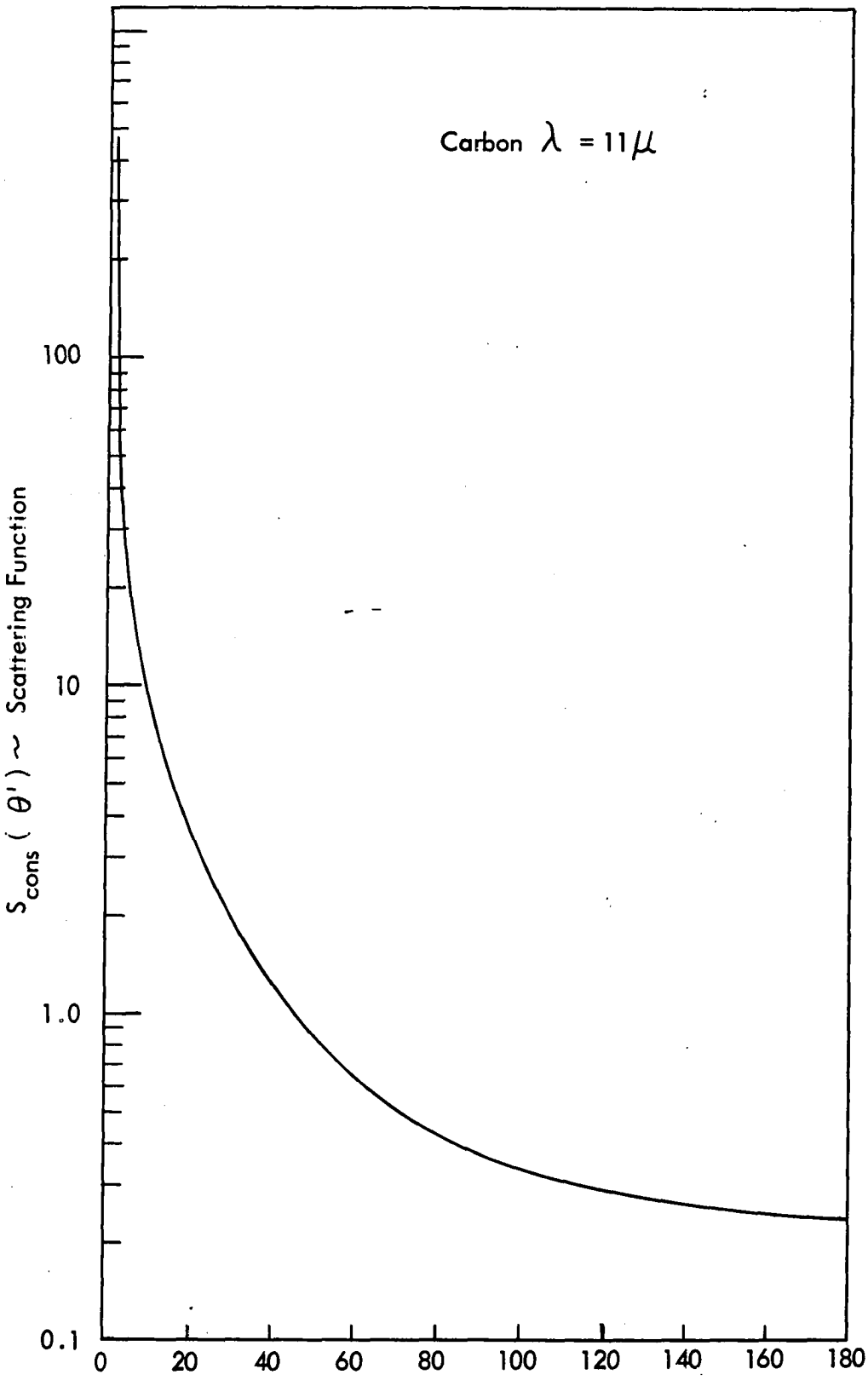

Figure 58
Angular Distribution of Scattering
Function -- Experimental Data

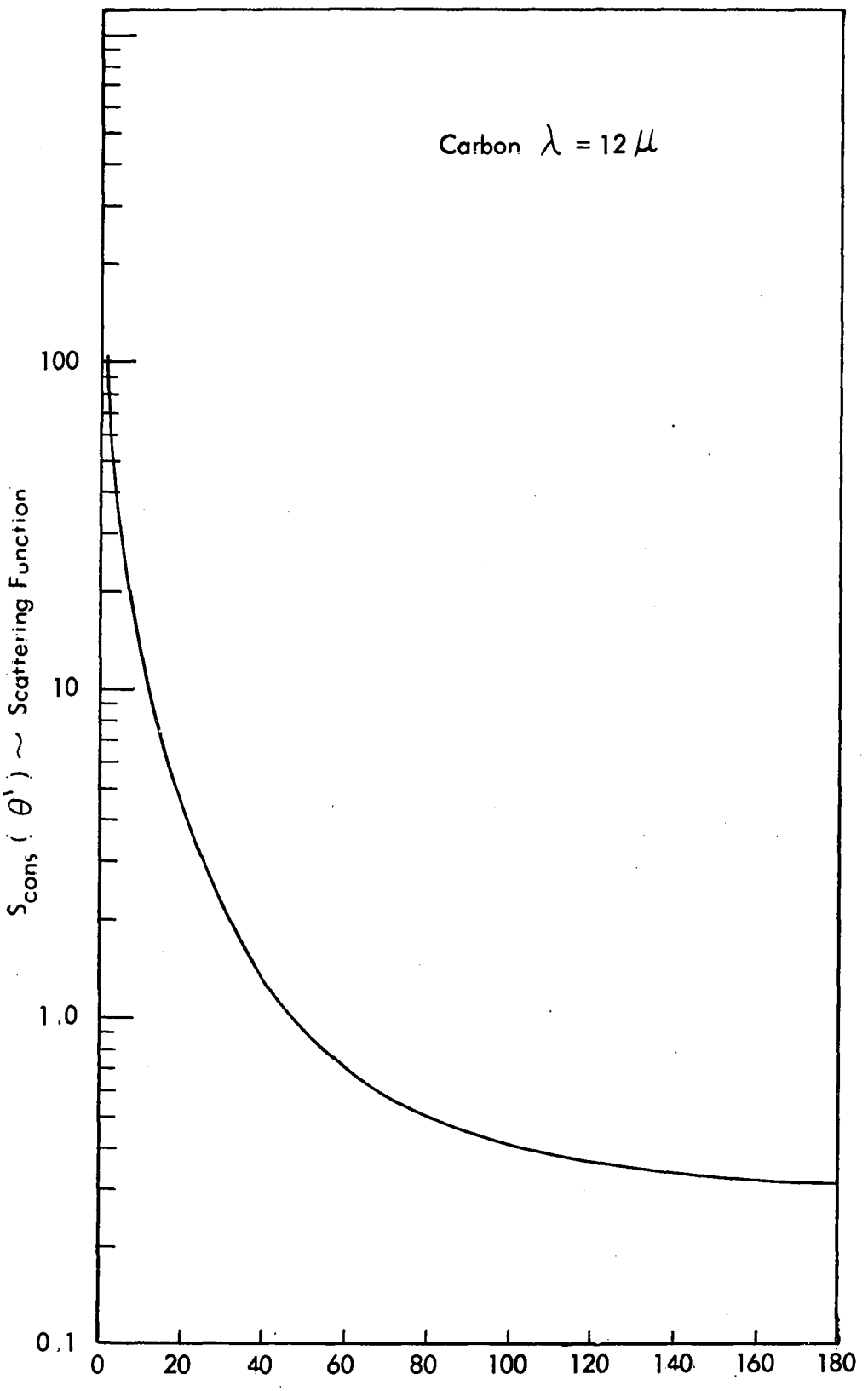

Figure 59
Angular Distribution of Scattering Function -- Experimental Data

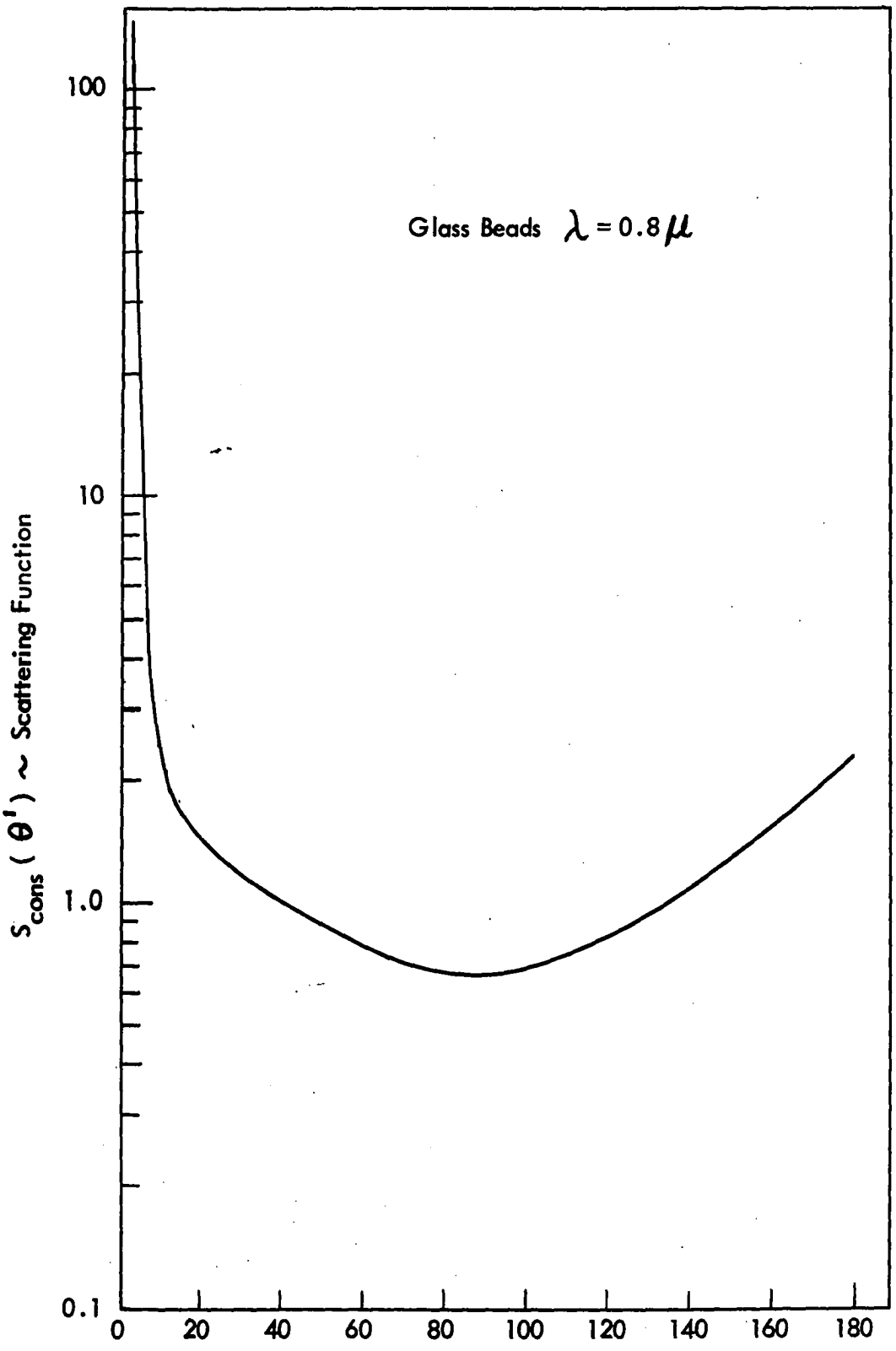

Figure 60
Angular Distribution of Scattering Function -- Experimental Data

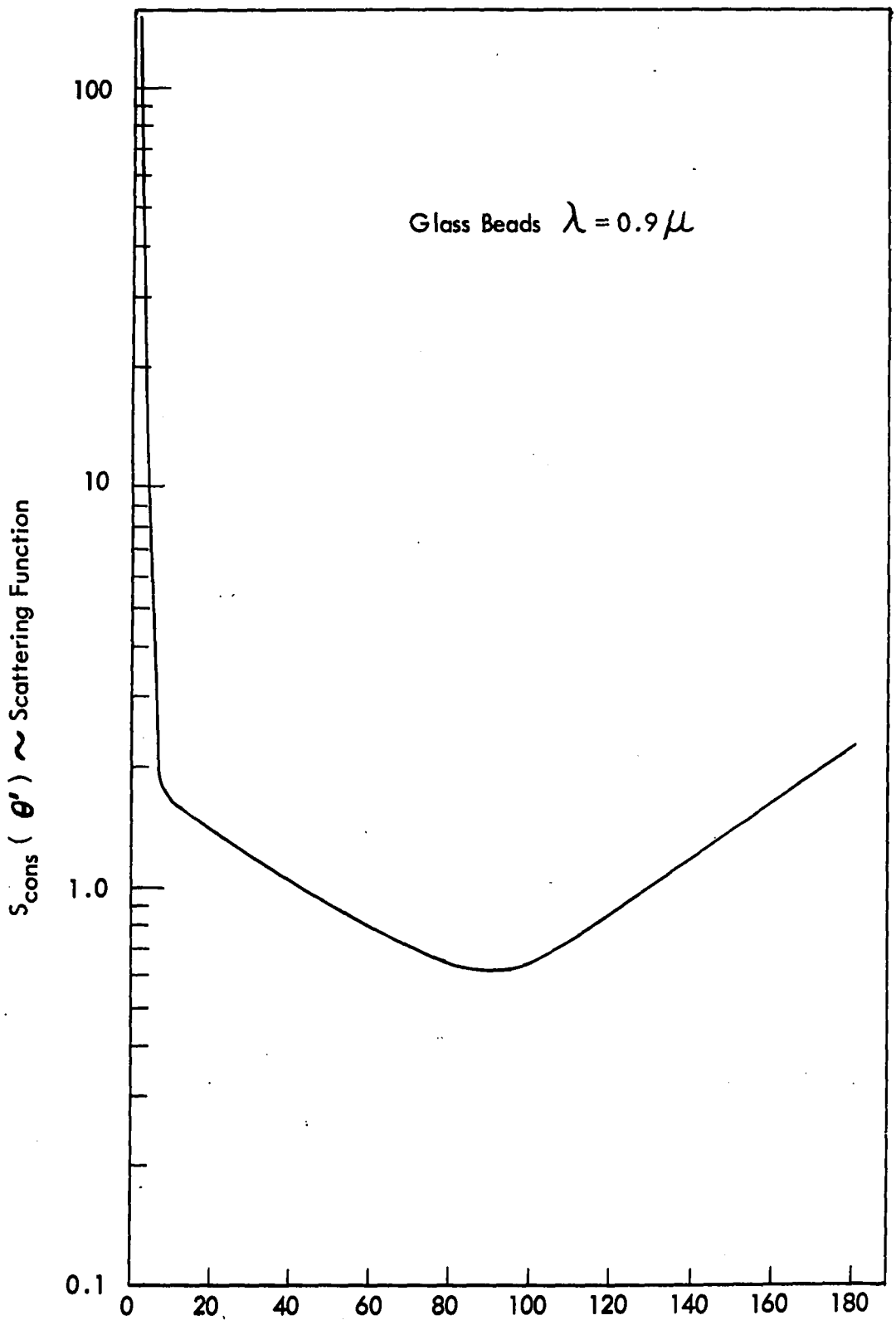

Figure 61
Angular Distribution of Scattering Function -- Experimental Data

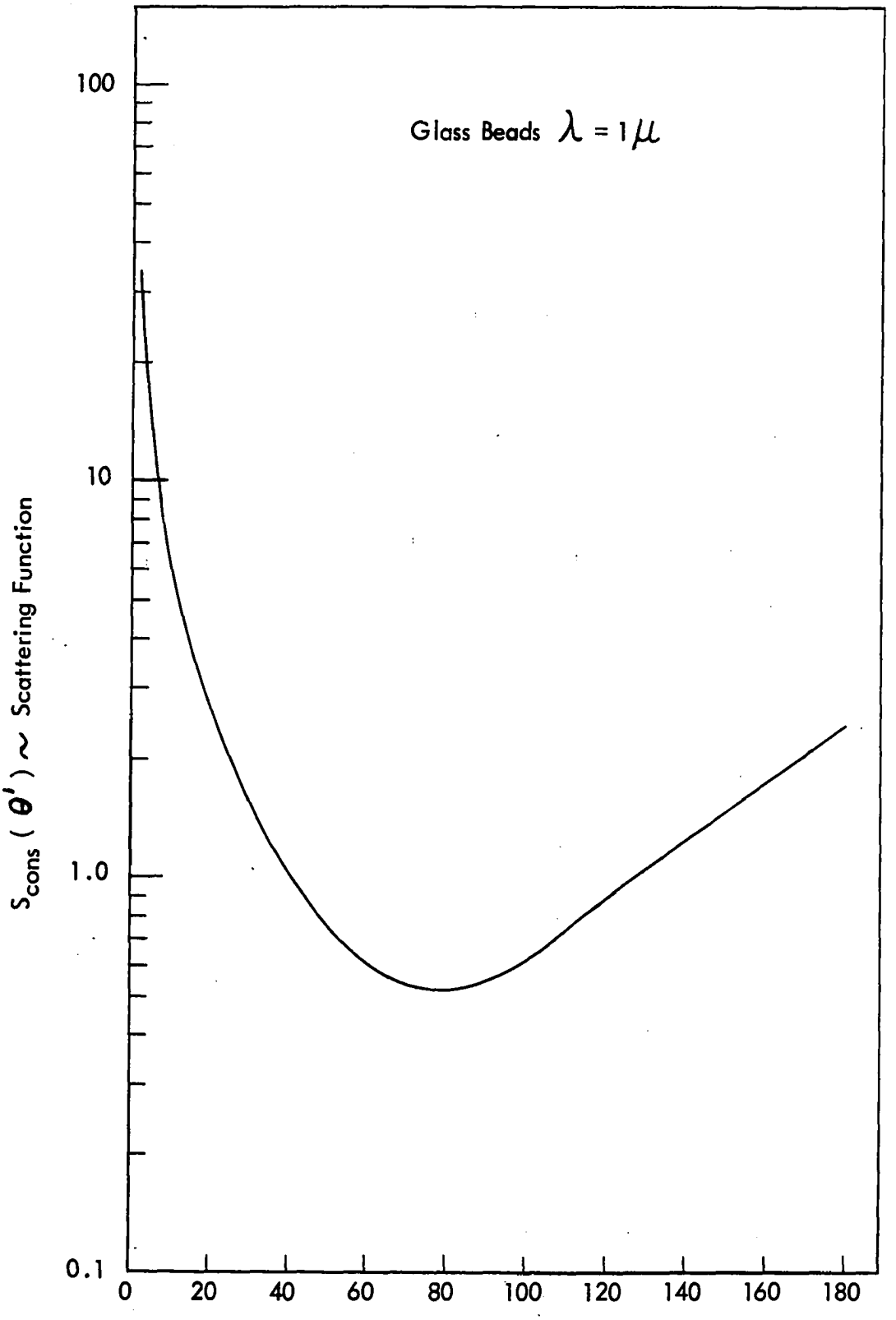

Figure 62
Angular Distribution of Scattering Function -- Experimental Data

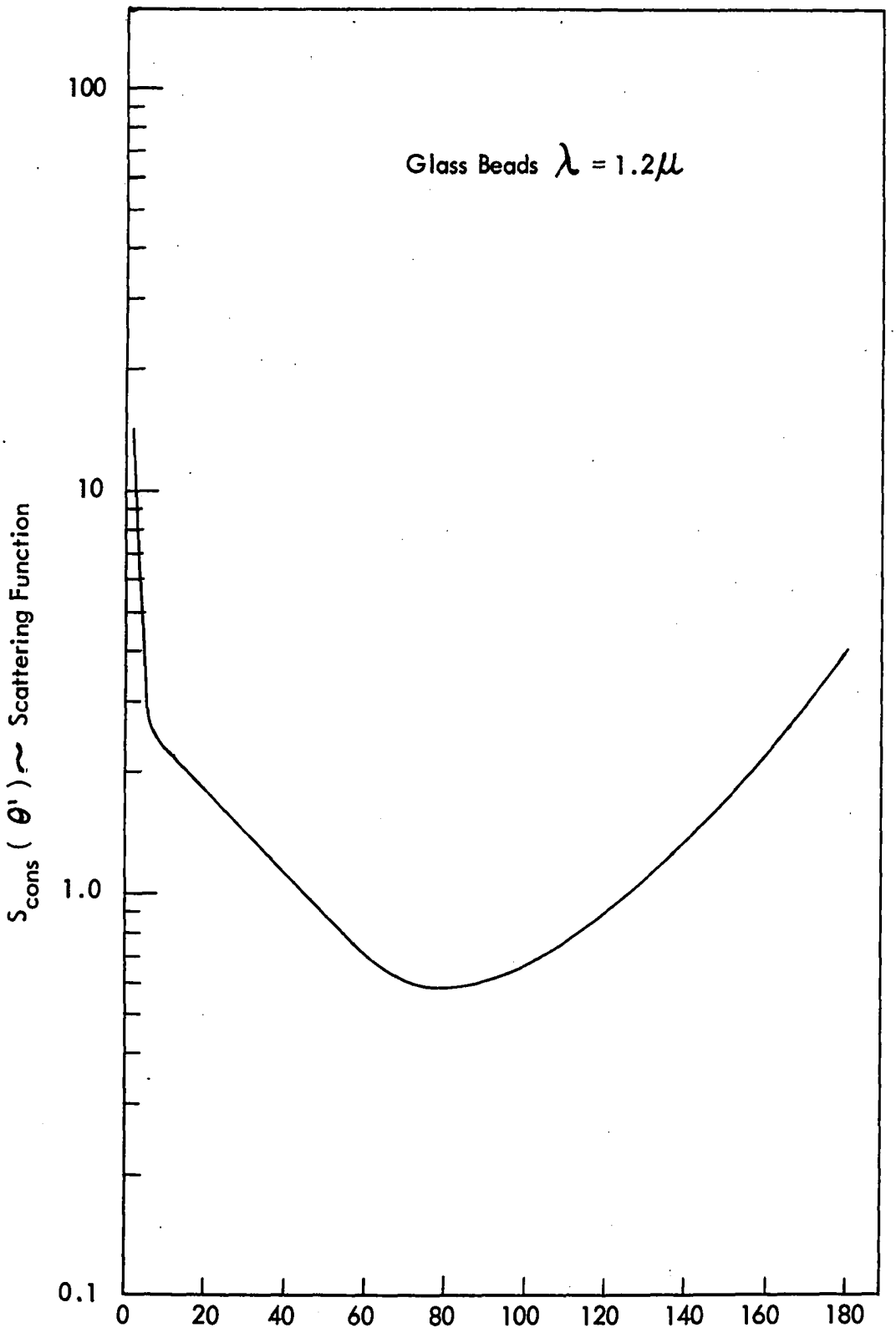

Figure 63
Angular Distribution of Scattering Function -- Experimental Data

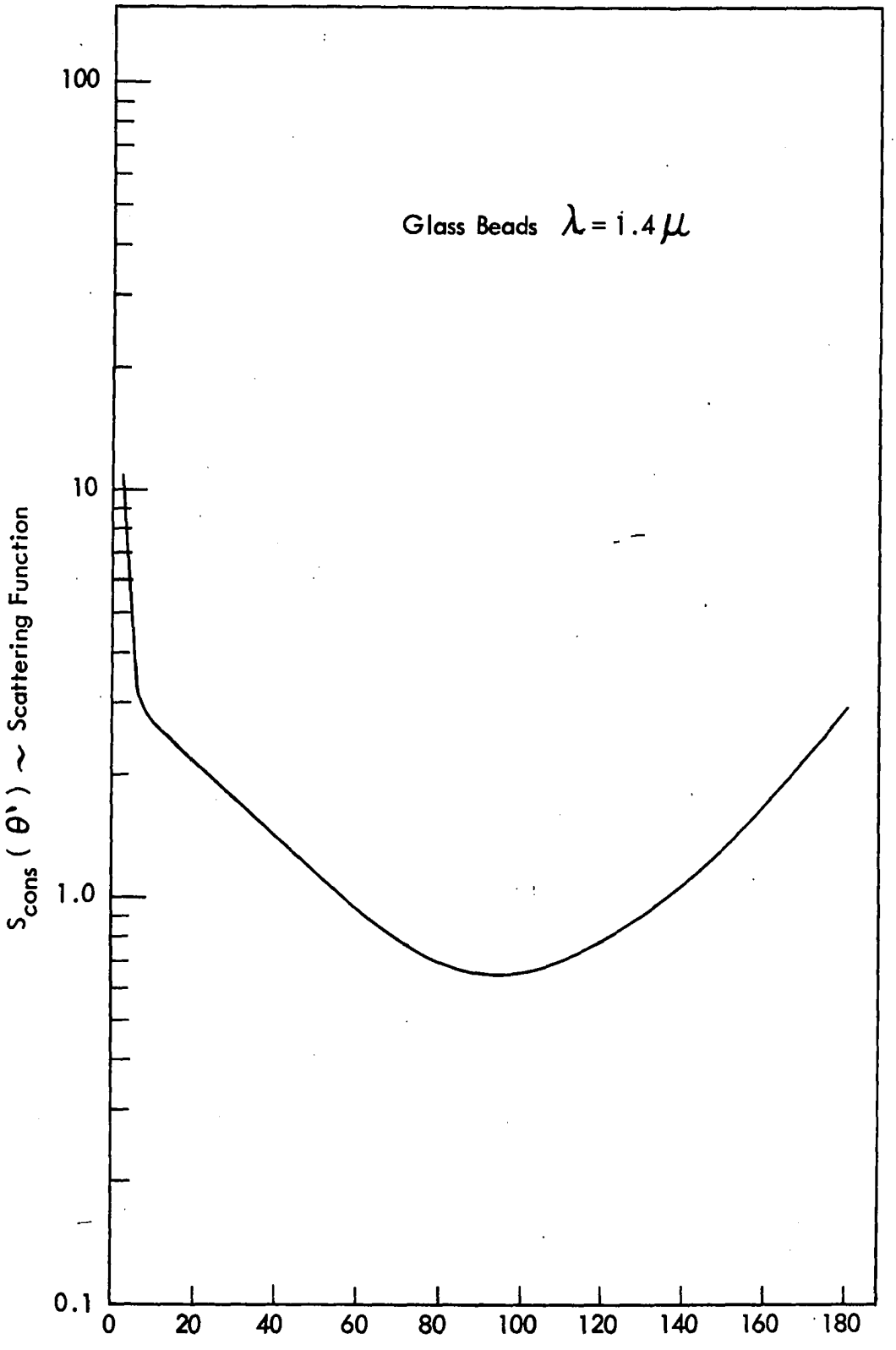

Figure 64
Angular Distribution of Scattering Function -- Experimental Data

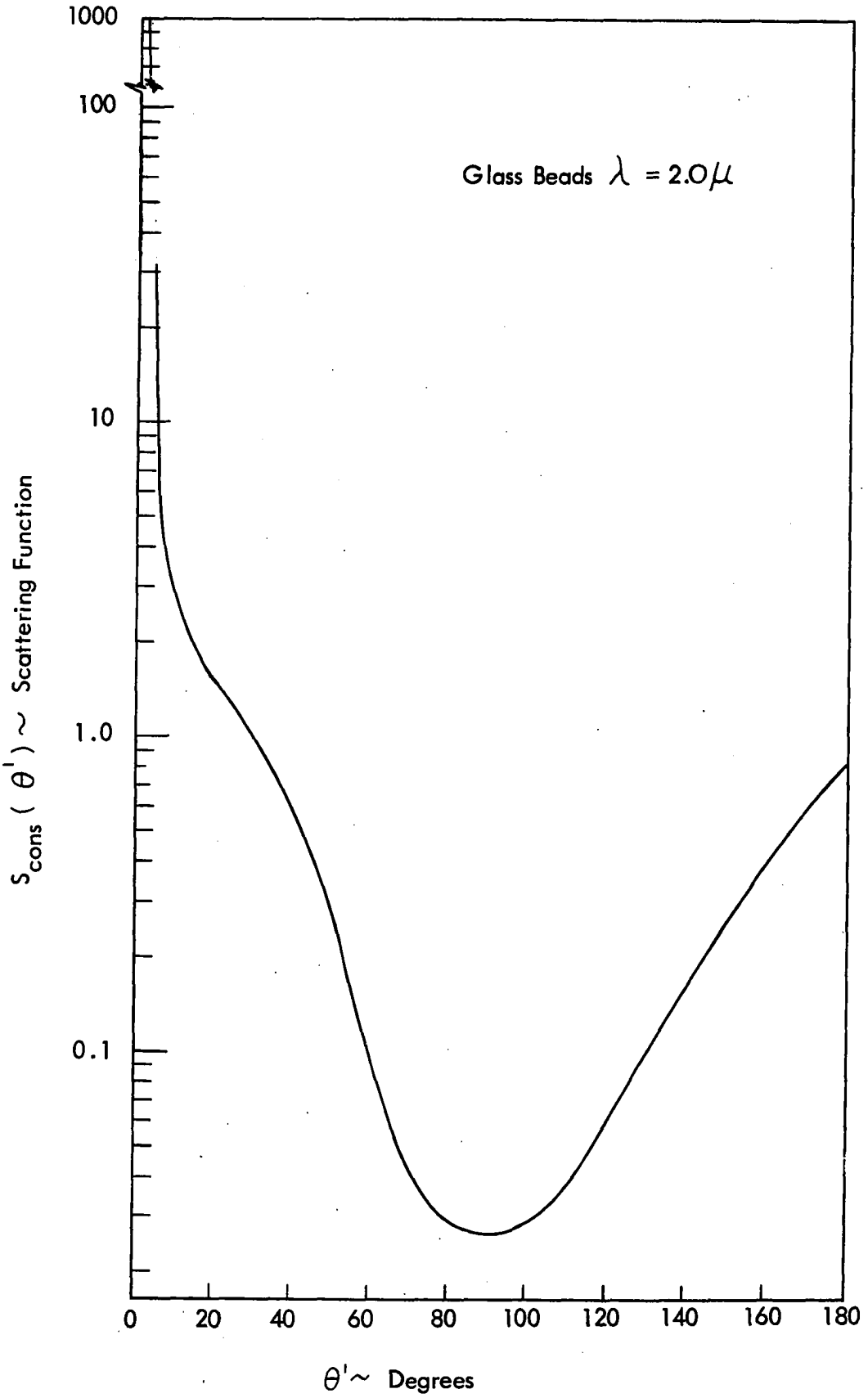

Figure 65
Angular Distribution of Scattering
Function -- Experimental Data

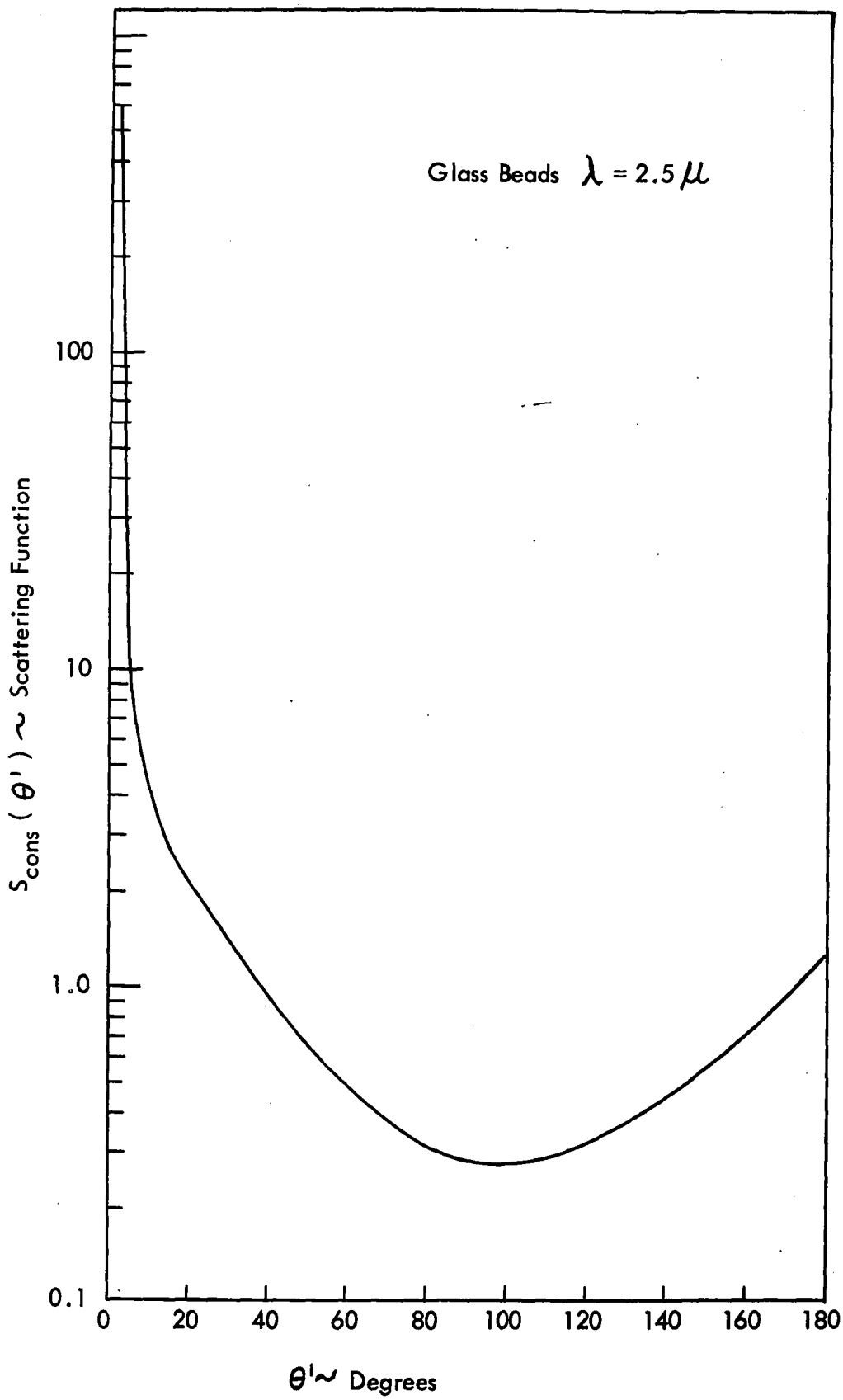

Figure 66
Angular Distribution of Scattering Function -- Experimental Data

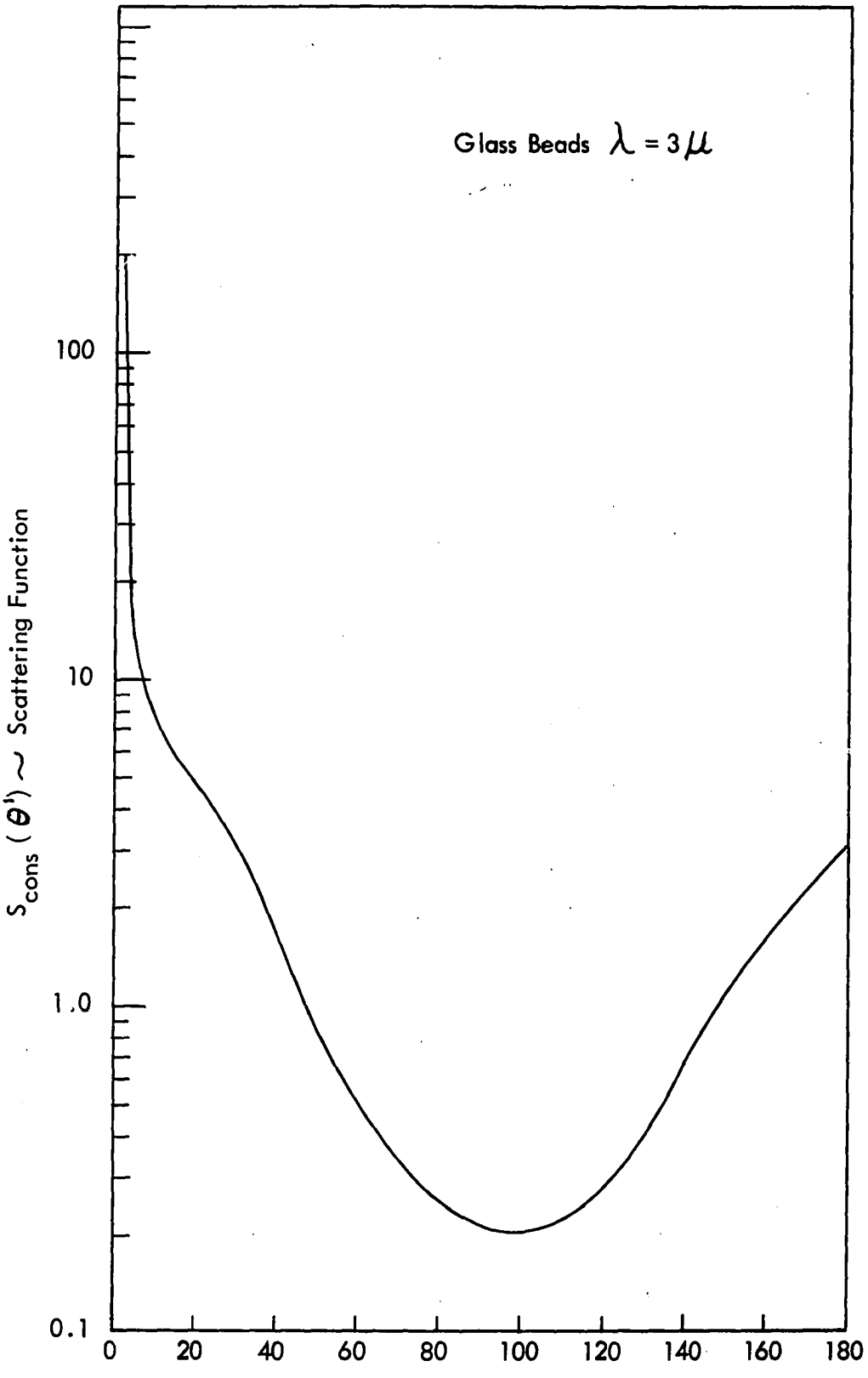

Figure 67
Angular Distribution of Scattering Function -- Experimental Data

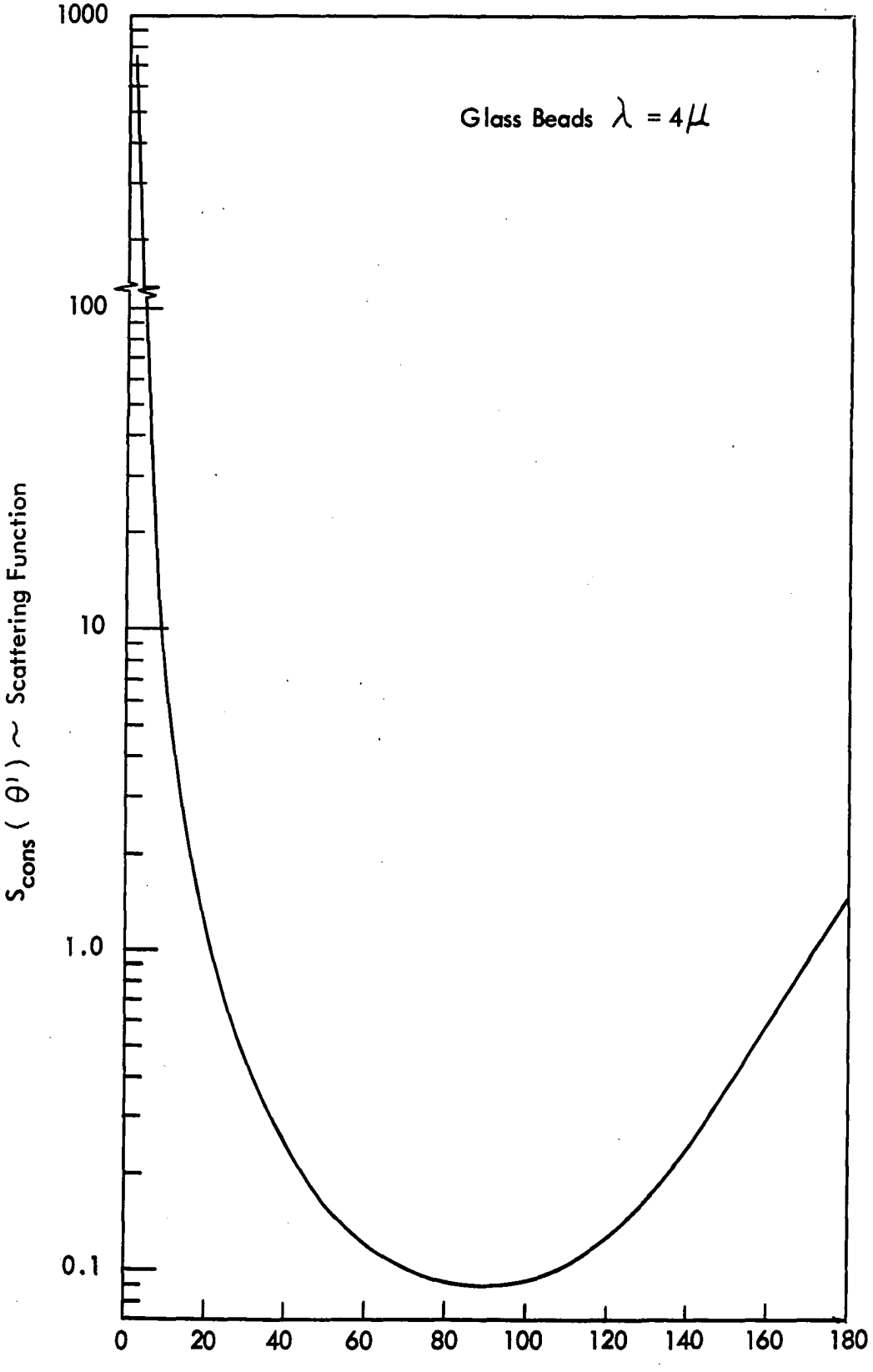

Figure 68
Angular Distribution of Scattering Function -- Experimental Data

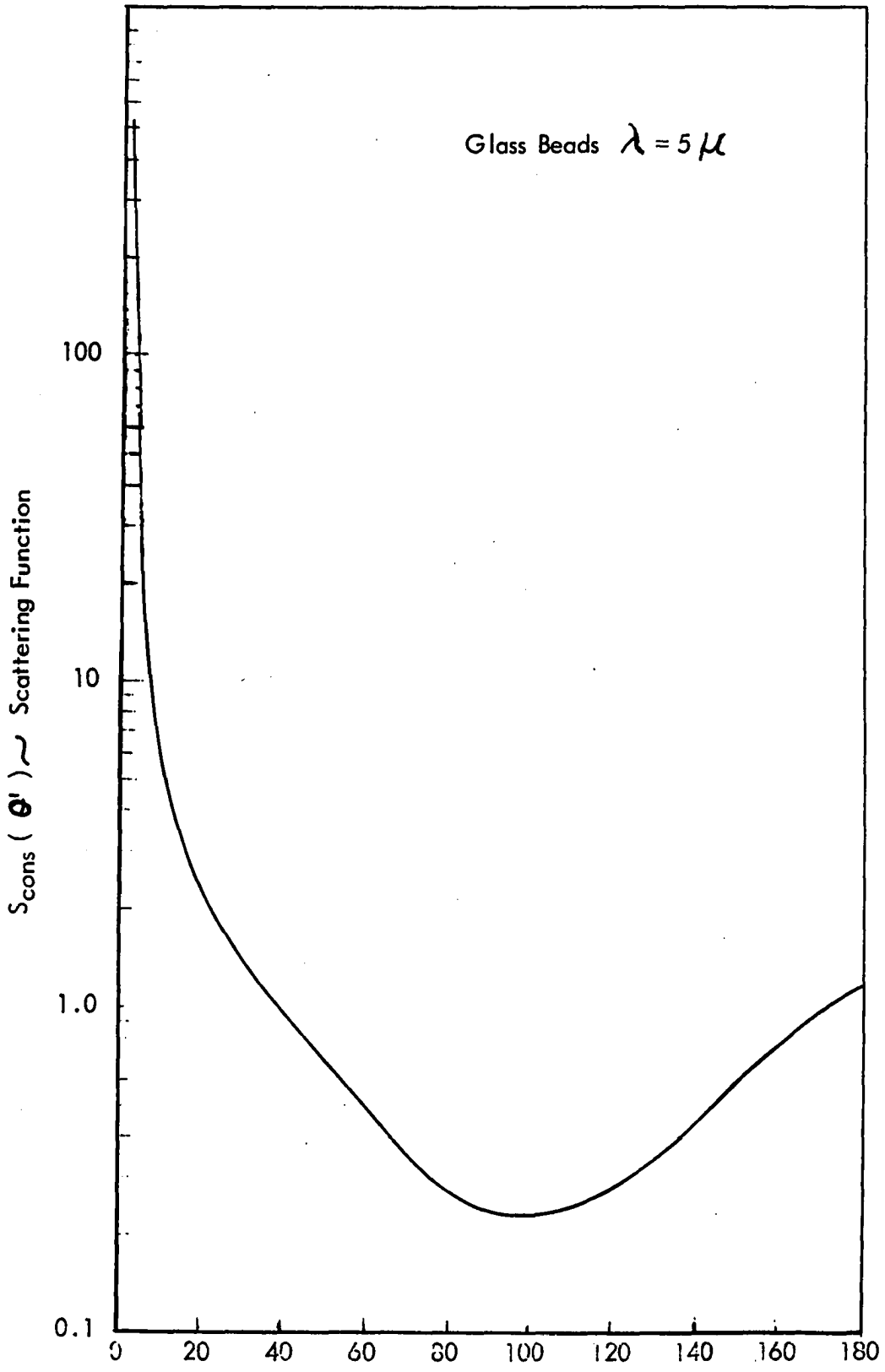

Figure 69
Angular Distribution of Scattering Function -- Experimental Data

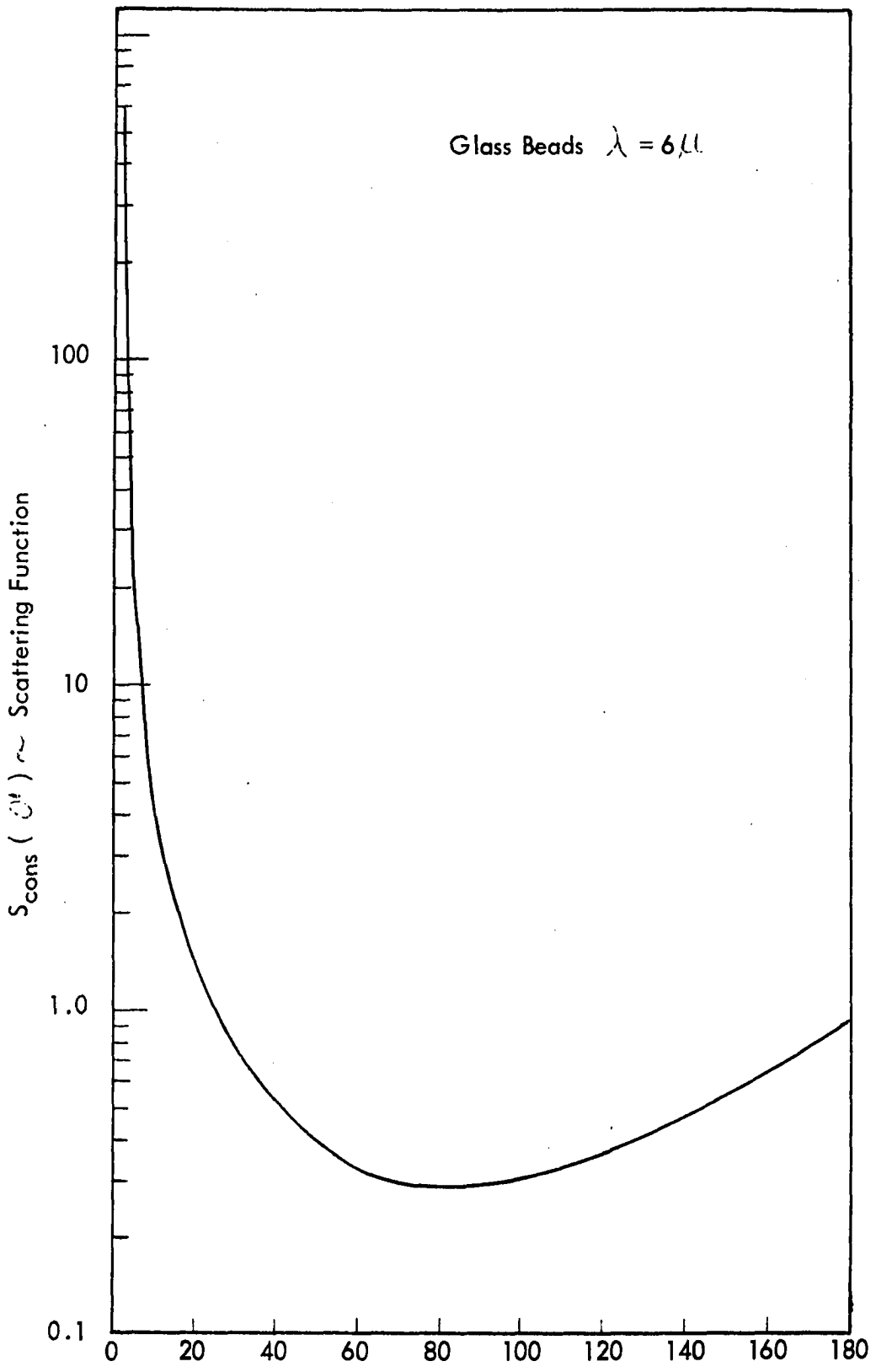

Figure 70
Angular Distribution of Scattering
Function -- Experimental Data

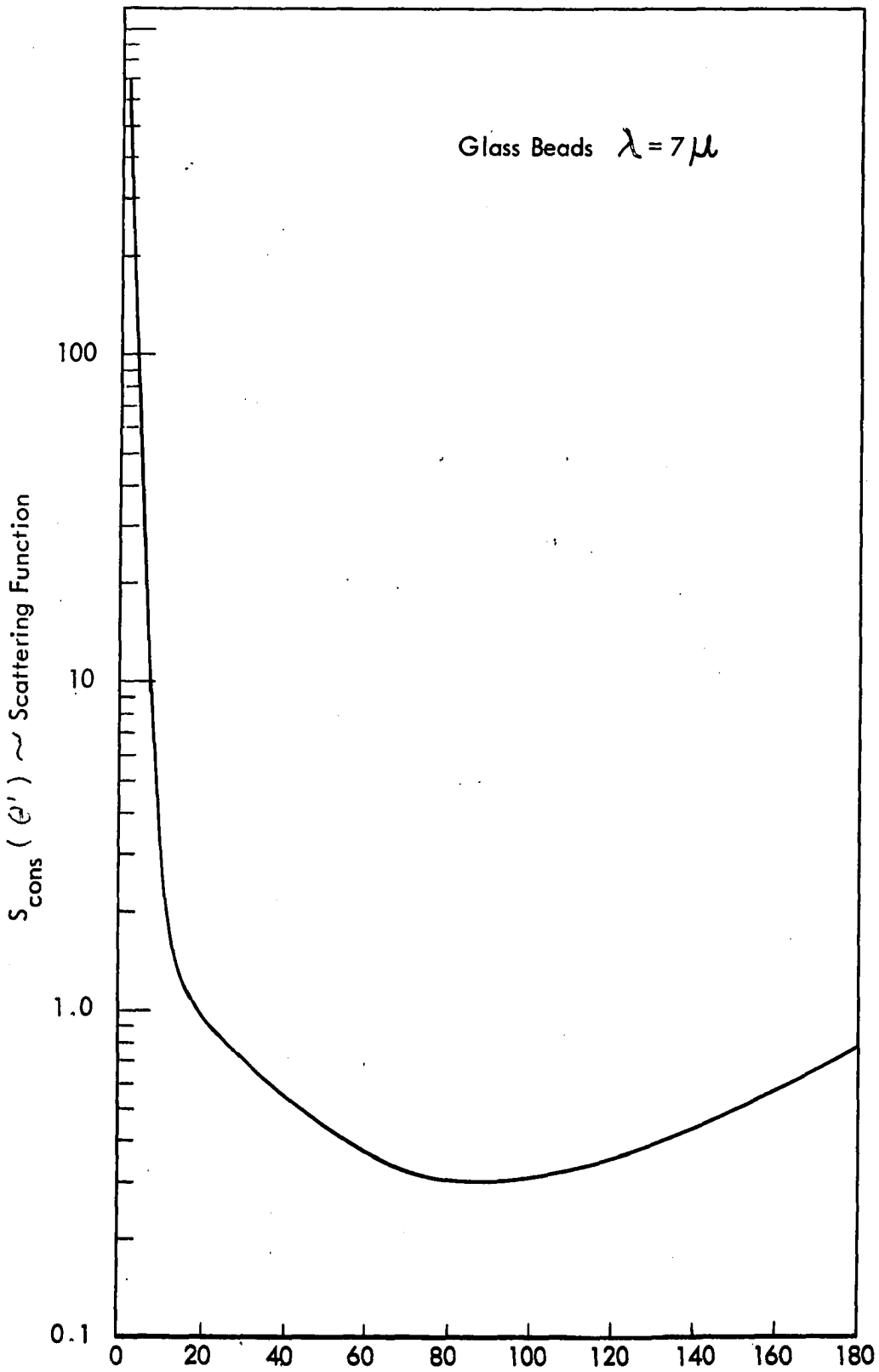

Figure 71
Angular Distribution of Scattering Function -- Experimental Data

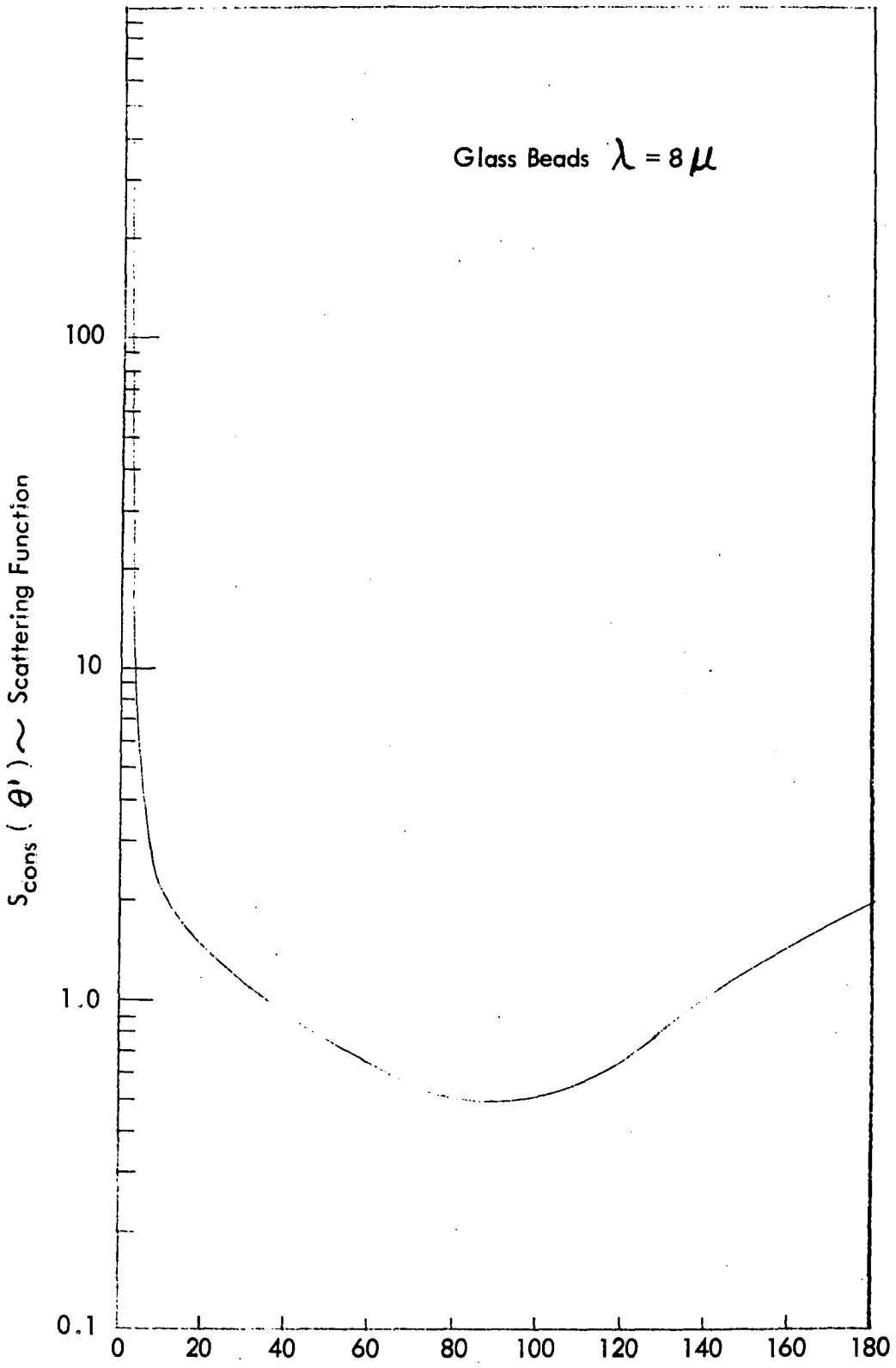

Figure 72
Angular Distribution of Scattering
Function -- Experimental Data

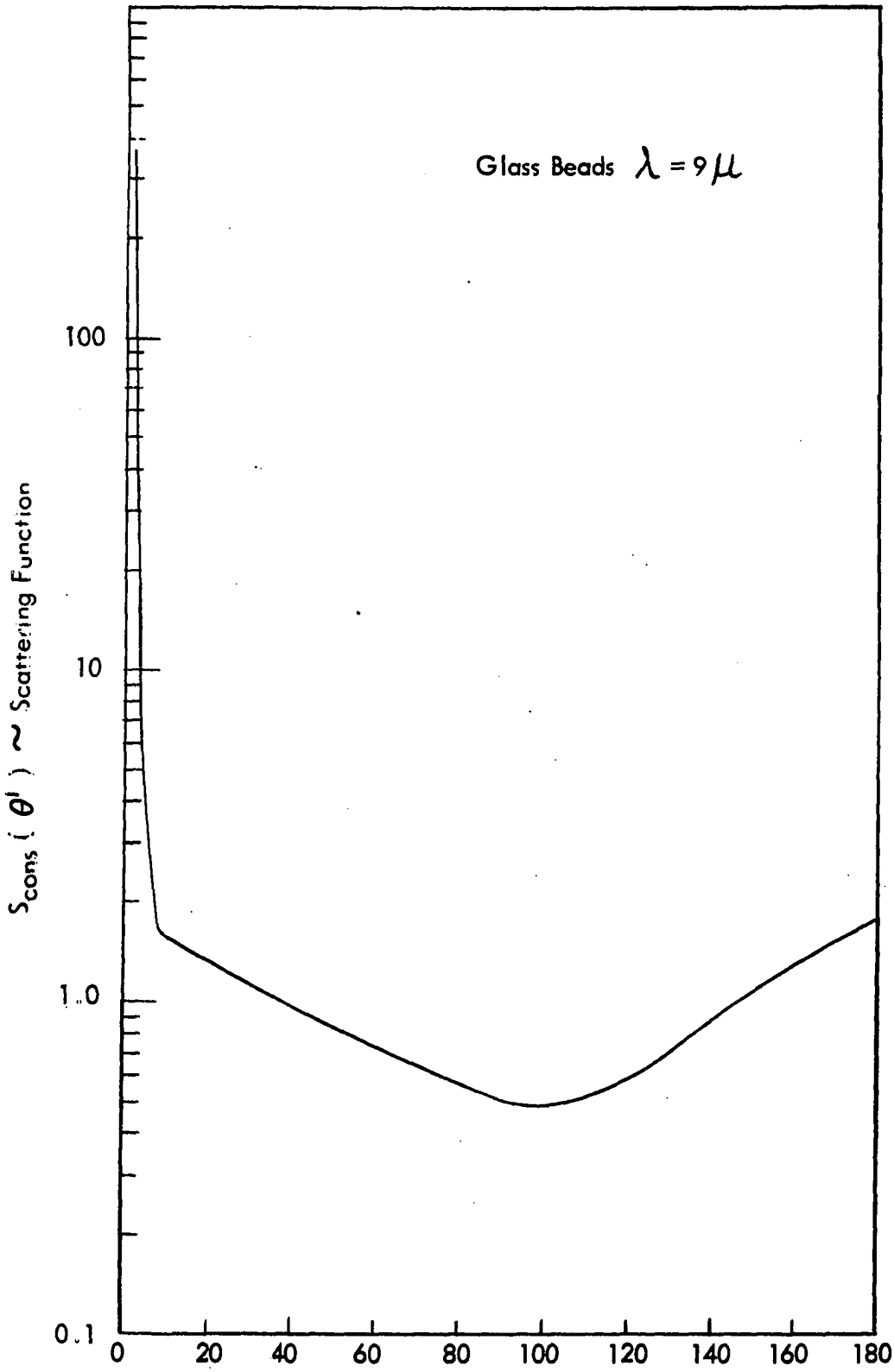

Figure 73
Angular Distribution of Scattering Function -- Experimental Data

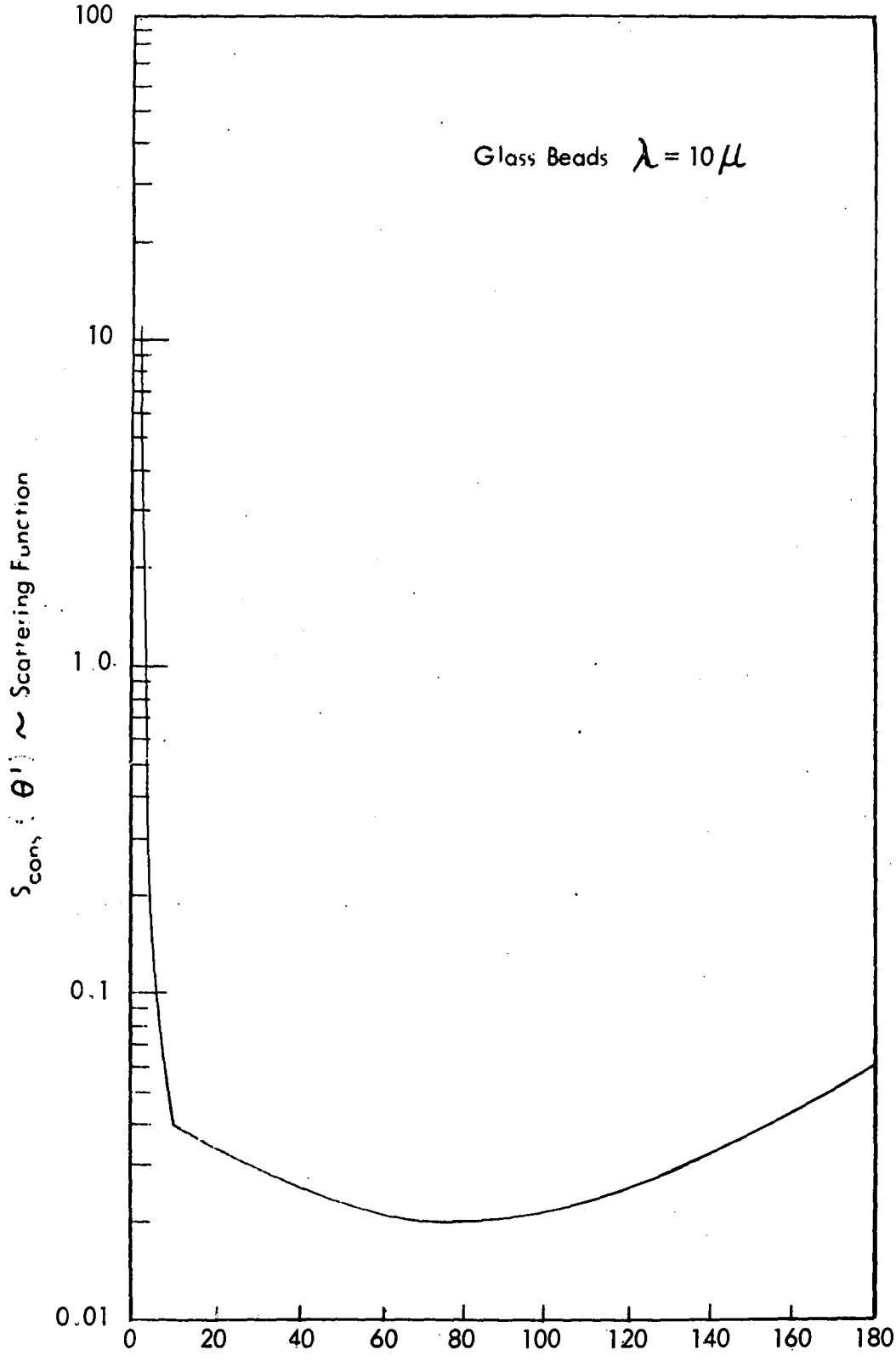

Figure 74
Angular Distribution of Scattering Function -- Experimental Data

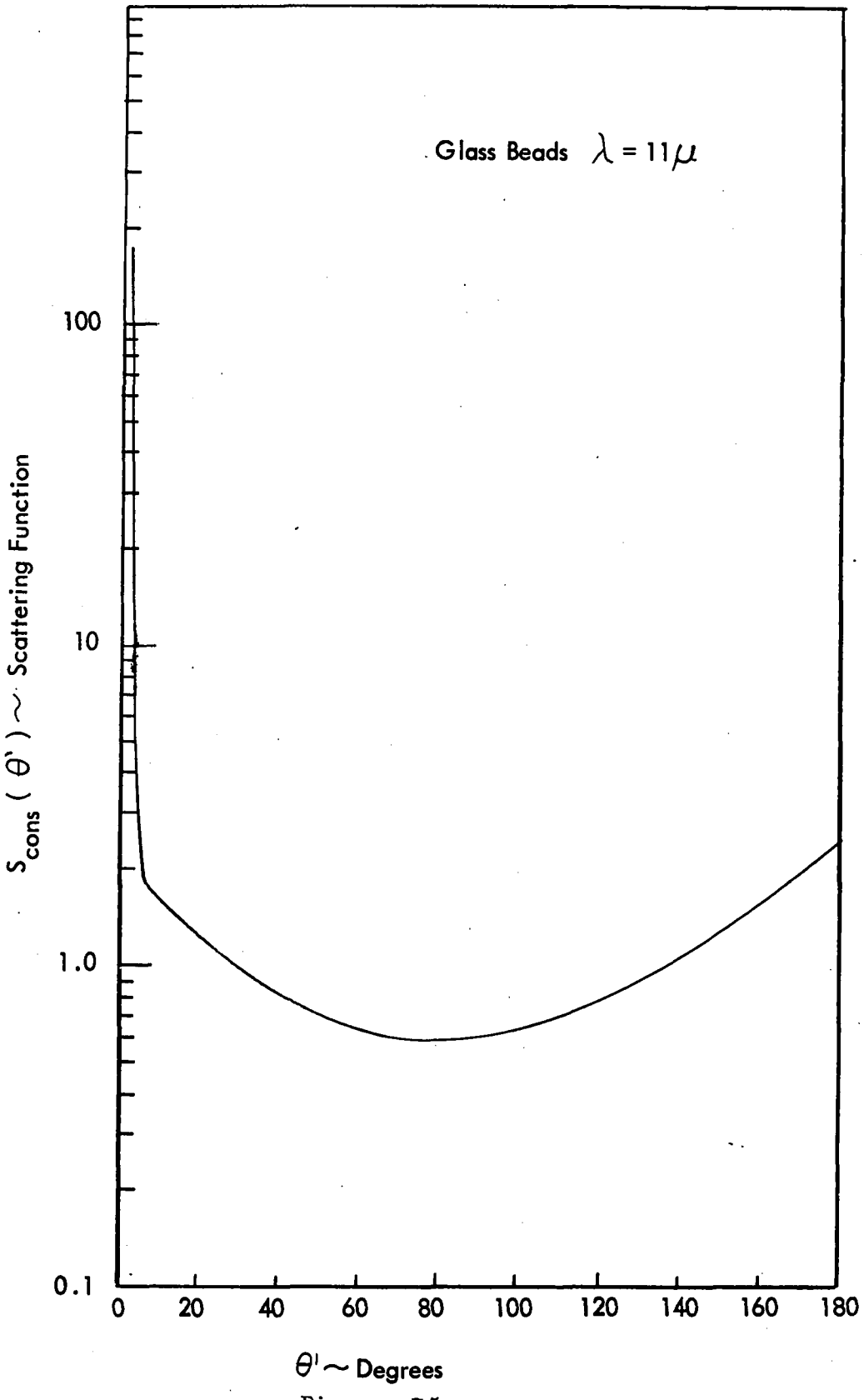

Figure 75
Angular Distribution of Scattering Function -- Experimental Data

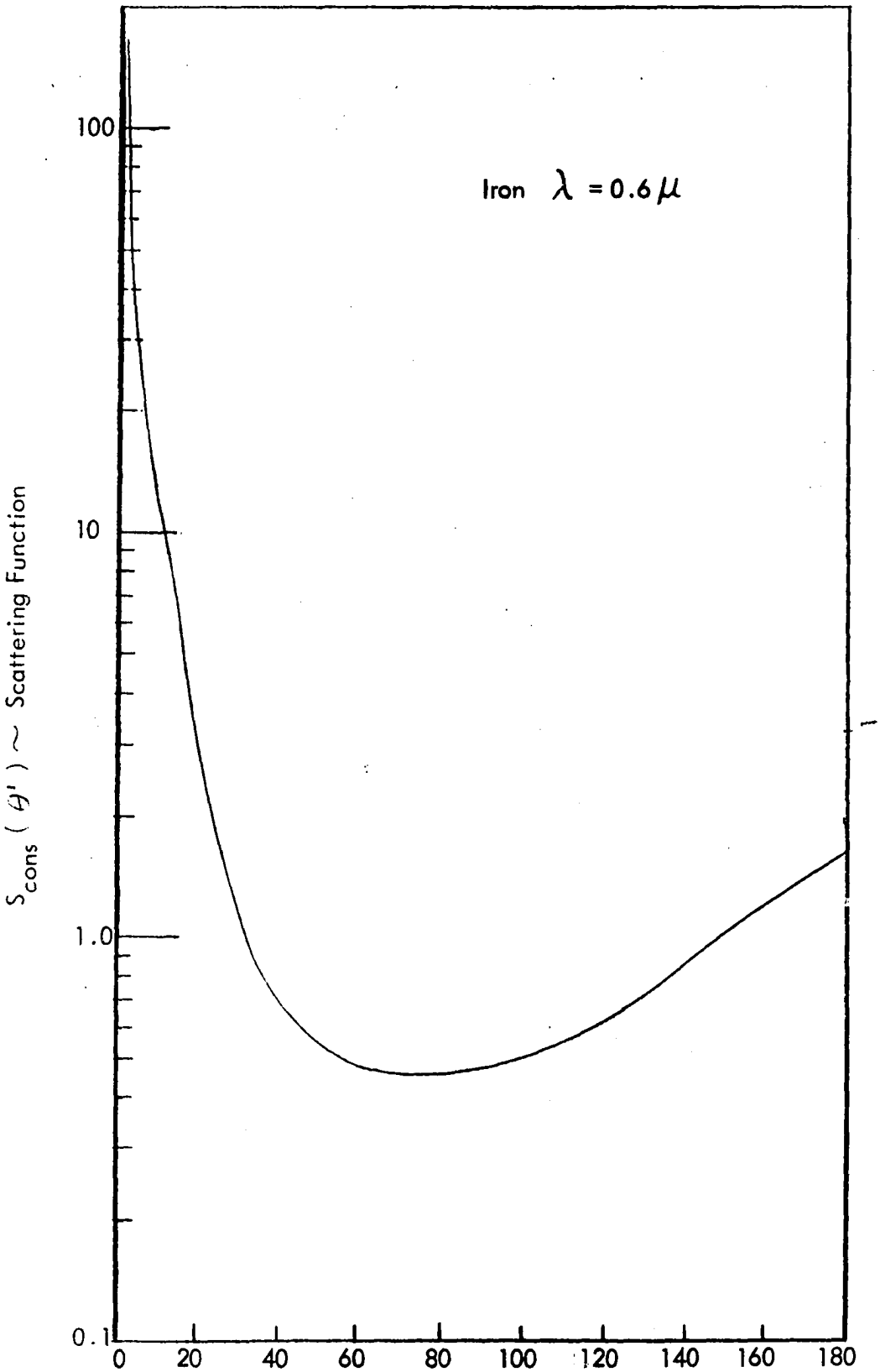

Figure 76
Angular Distribution of Scattering Function -- Experimental Data

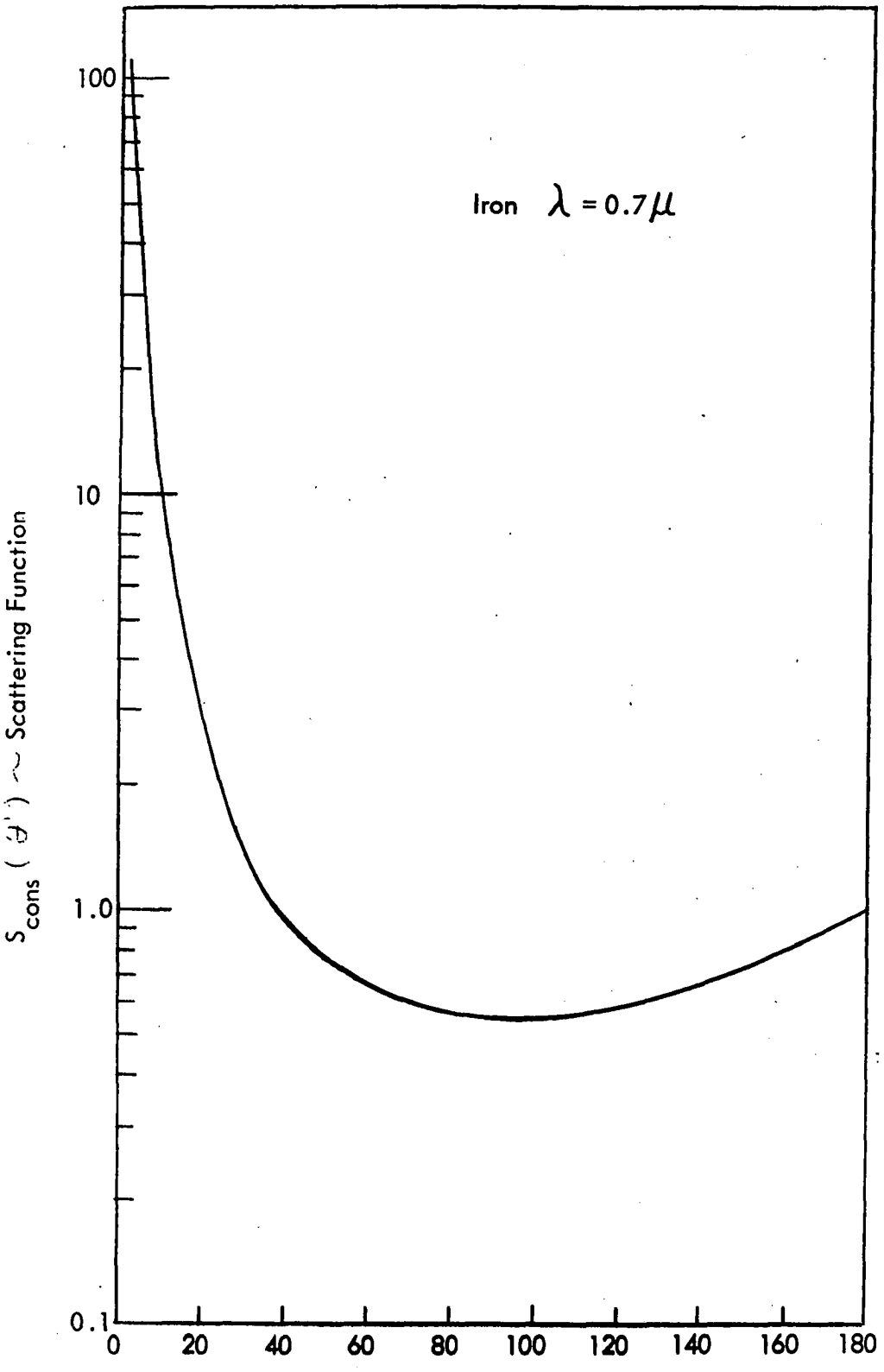

Figure 77
Angular Distribution of Scattering Function -- Experimental Data

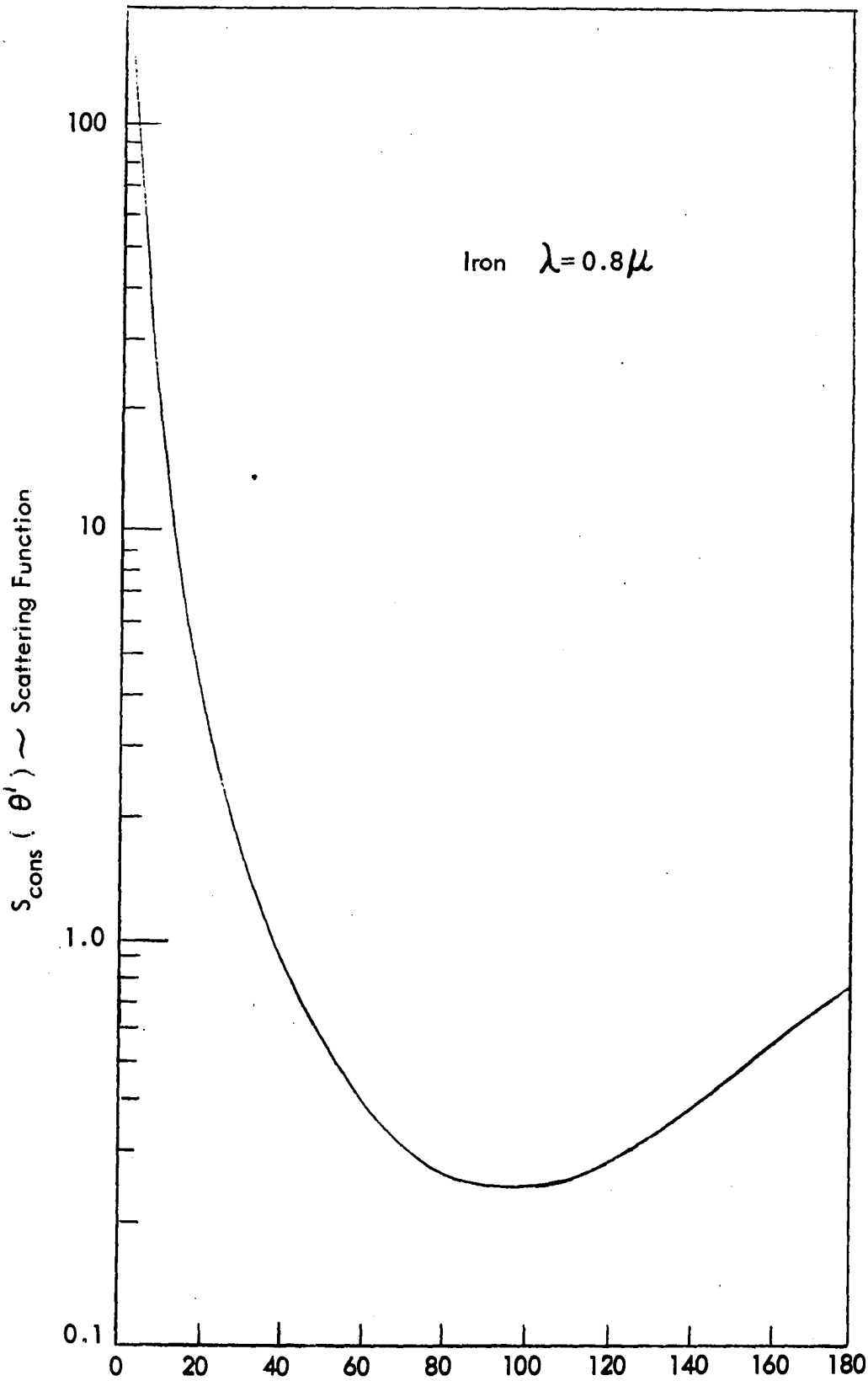

Figure 78
Angular Distribution of Scattering Function -- Experimental Data

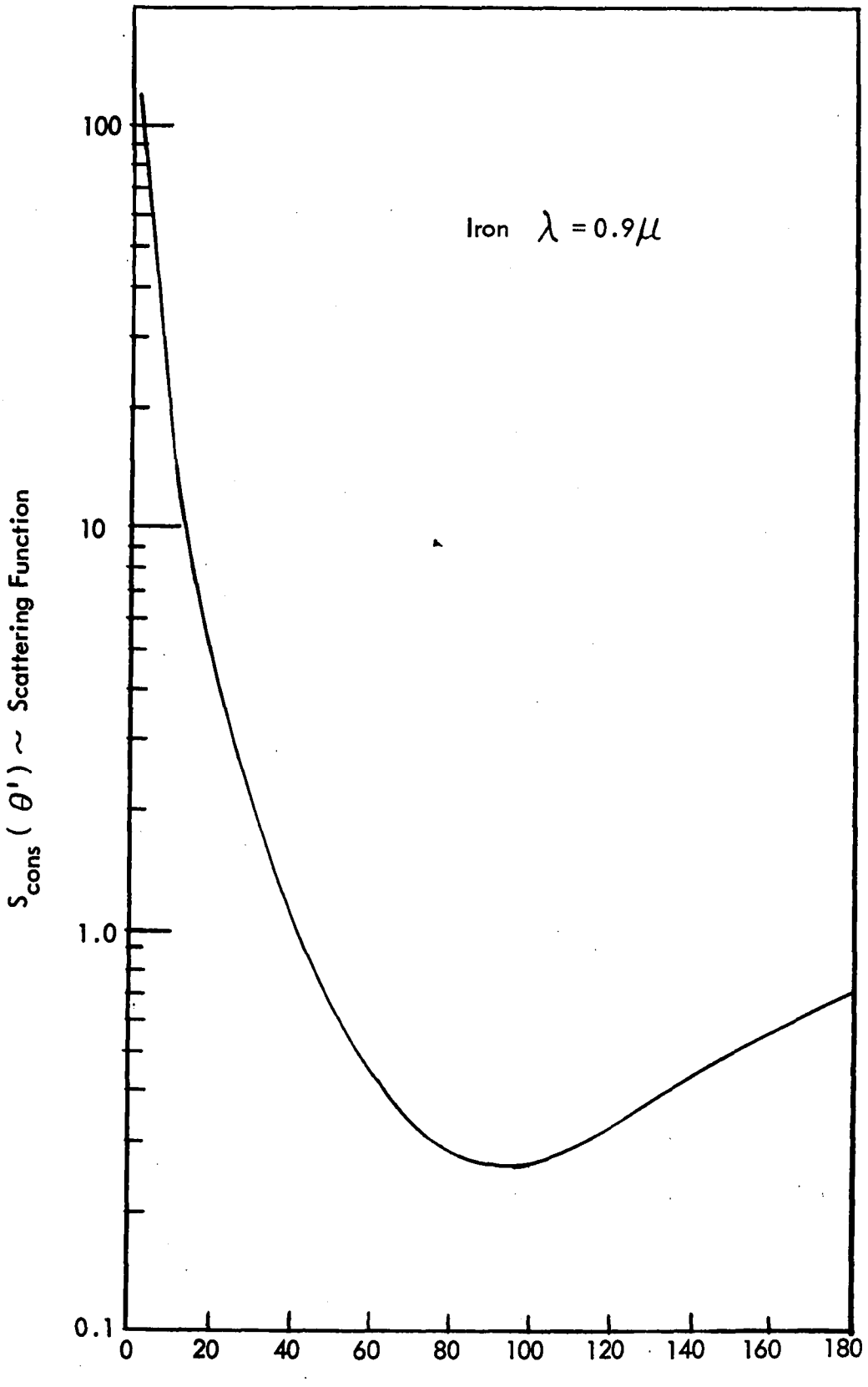

Figure 79
Angular Distribution of Scattering Function -- Experimental Data

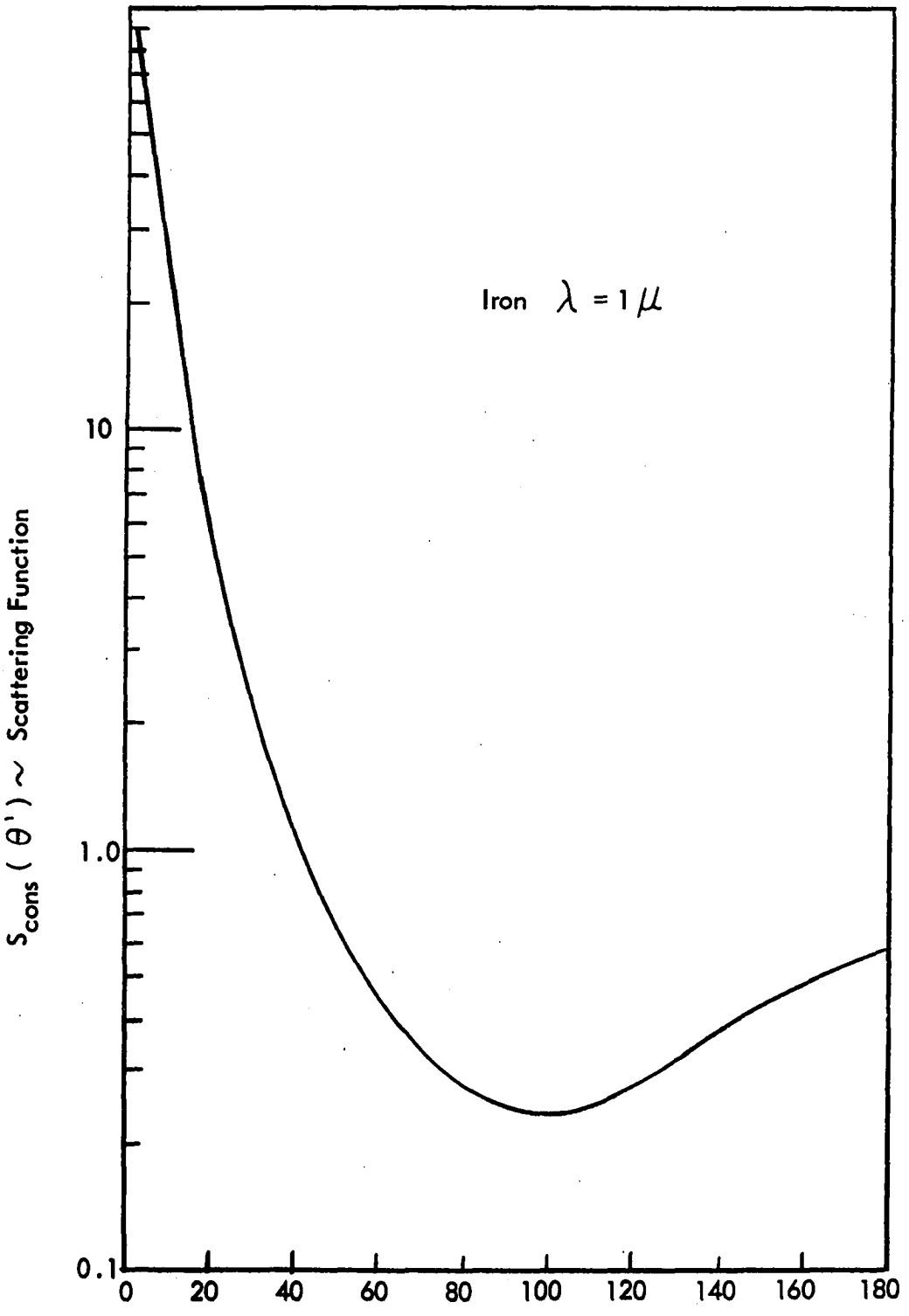

Figure 80
Angular Distribution of Scattering Function -- Experimental Data

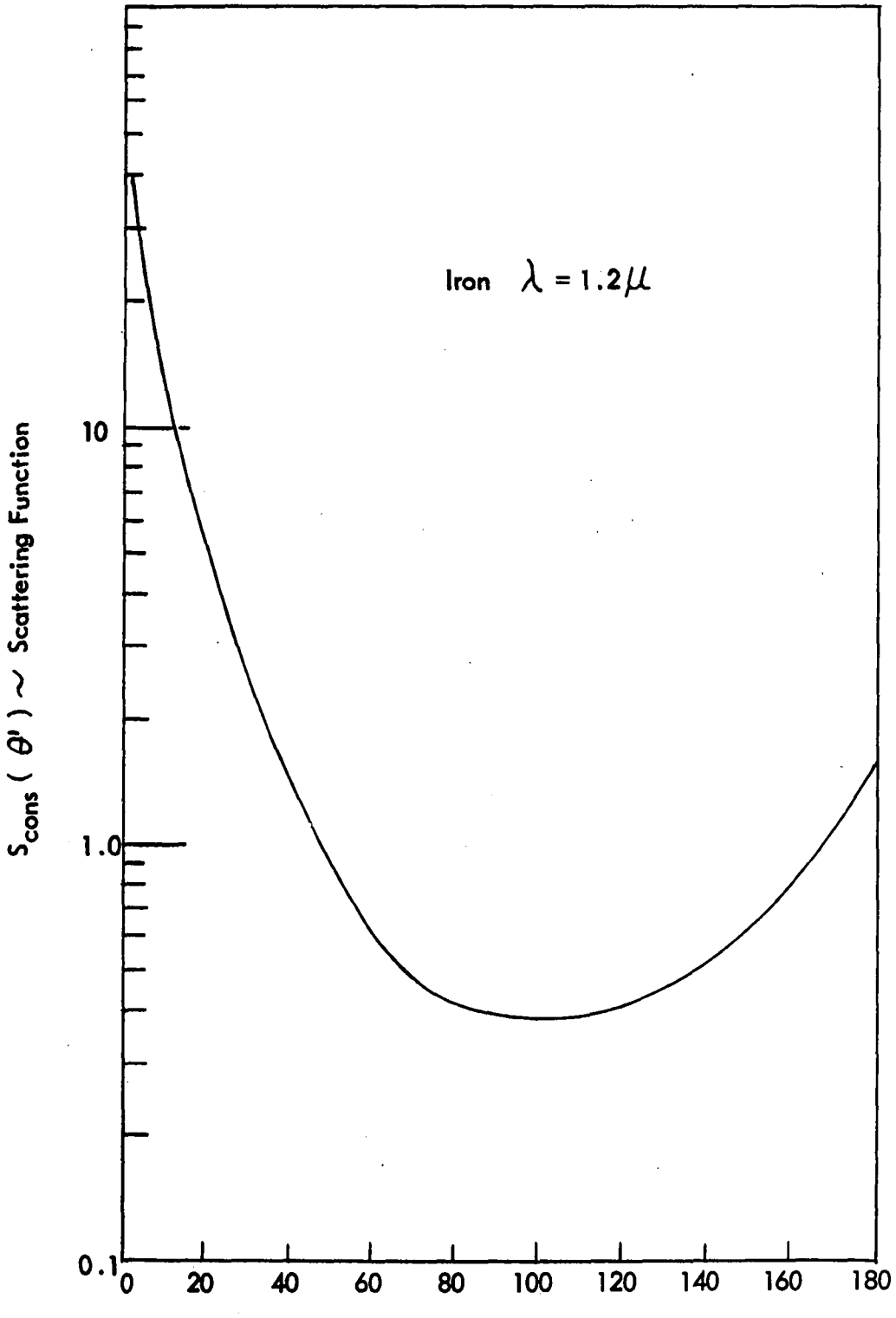

Figure 81
Angular Distribution of Scattering Function -- Experimental Data

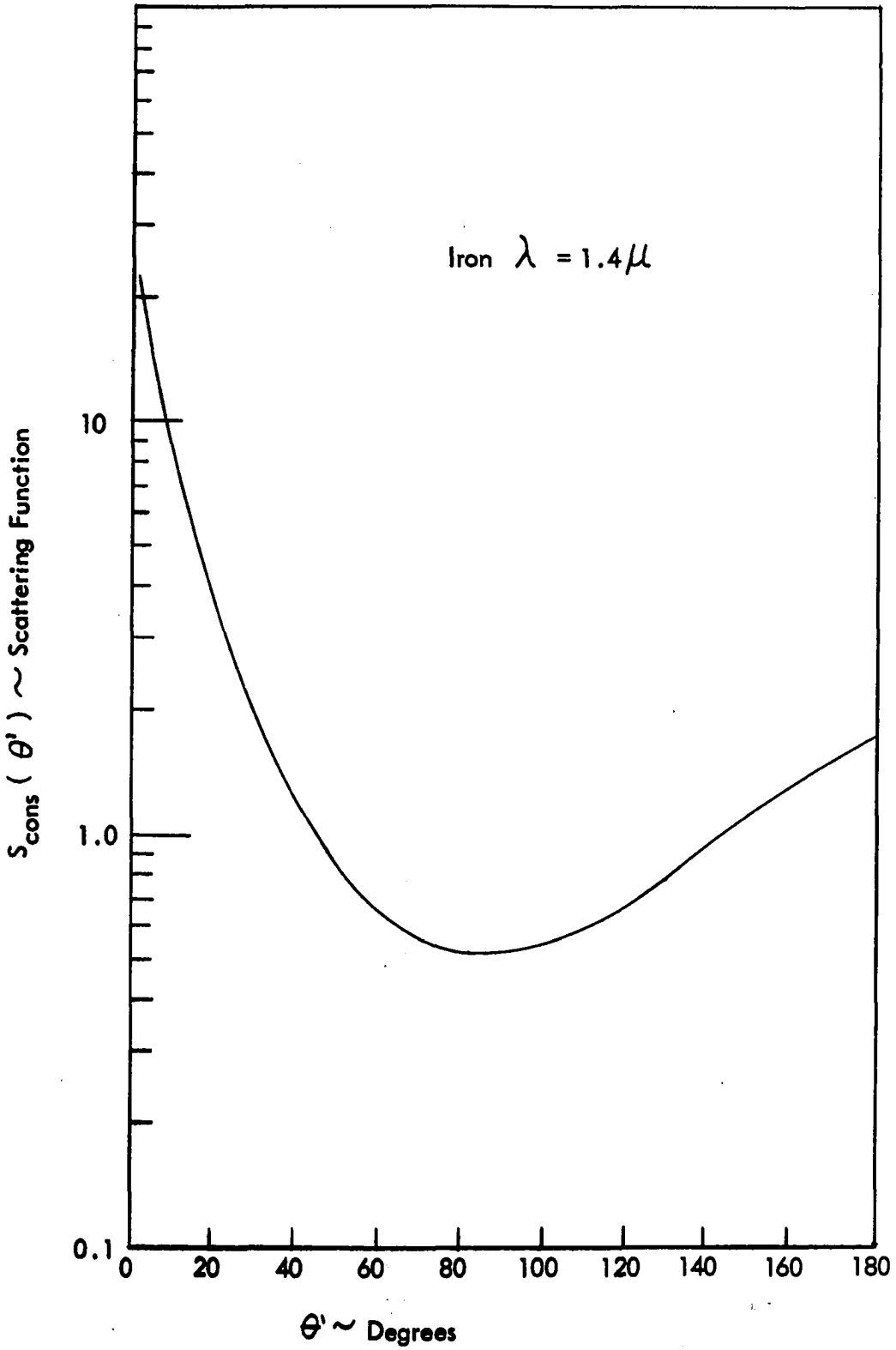

Figure 82
Angular Distribution of Scattering Function -- Experimental Data

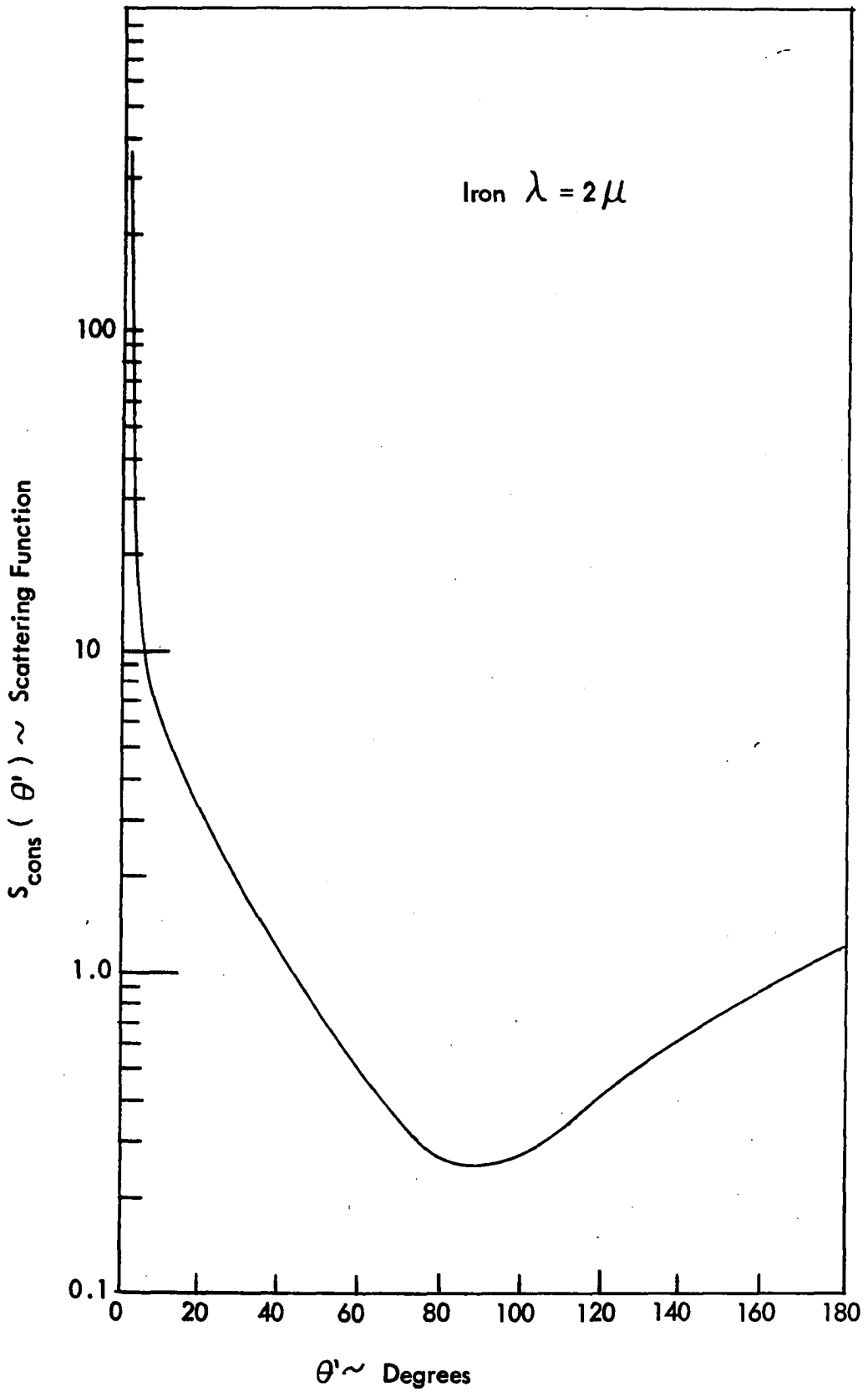

Figure 83
Angular Distribution of Scattering Function -- Experimental Data

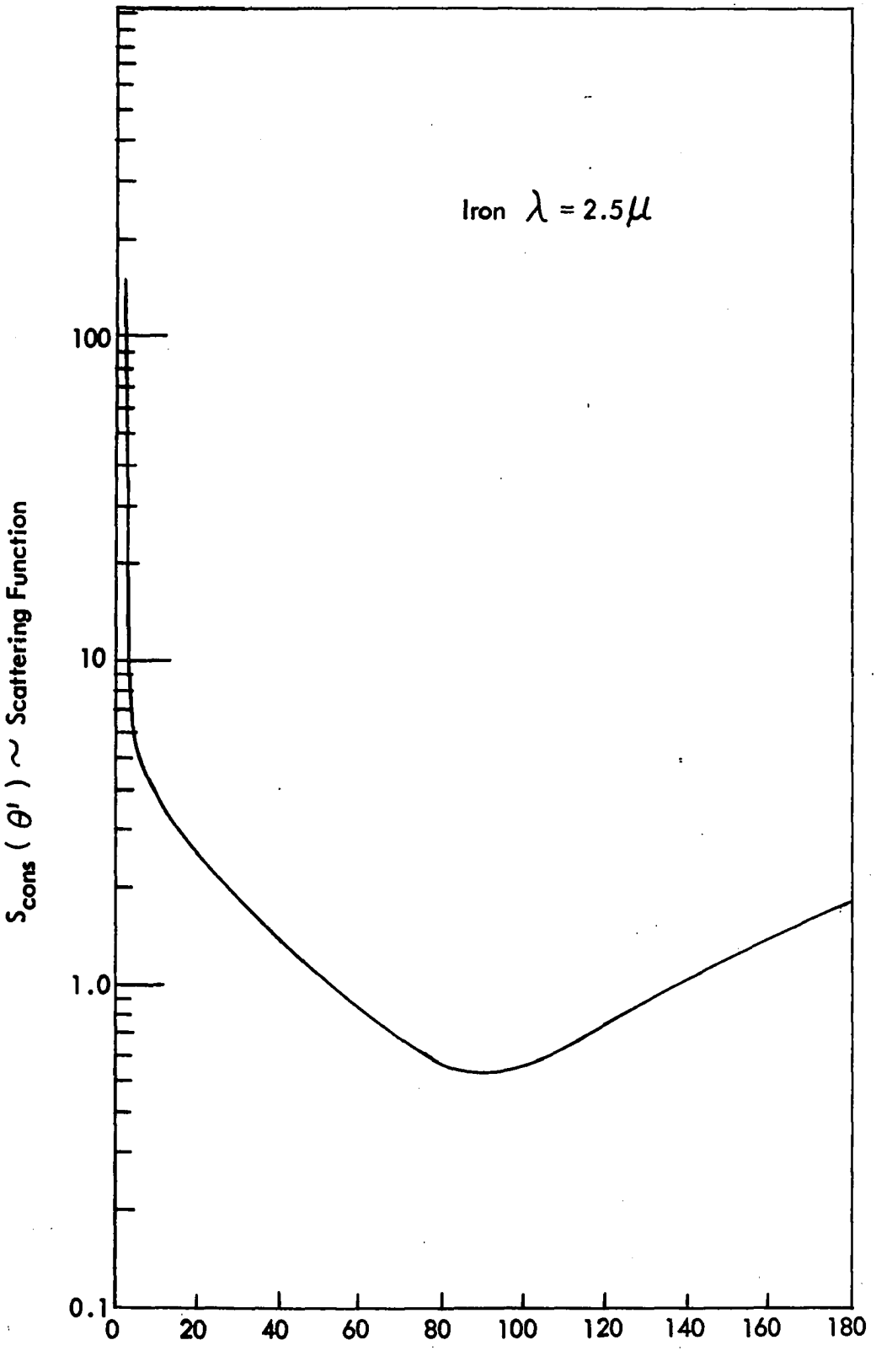

Figure 84
Angular Distribution of Scattering Function -- Experimental Data

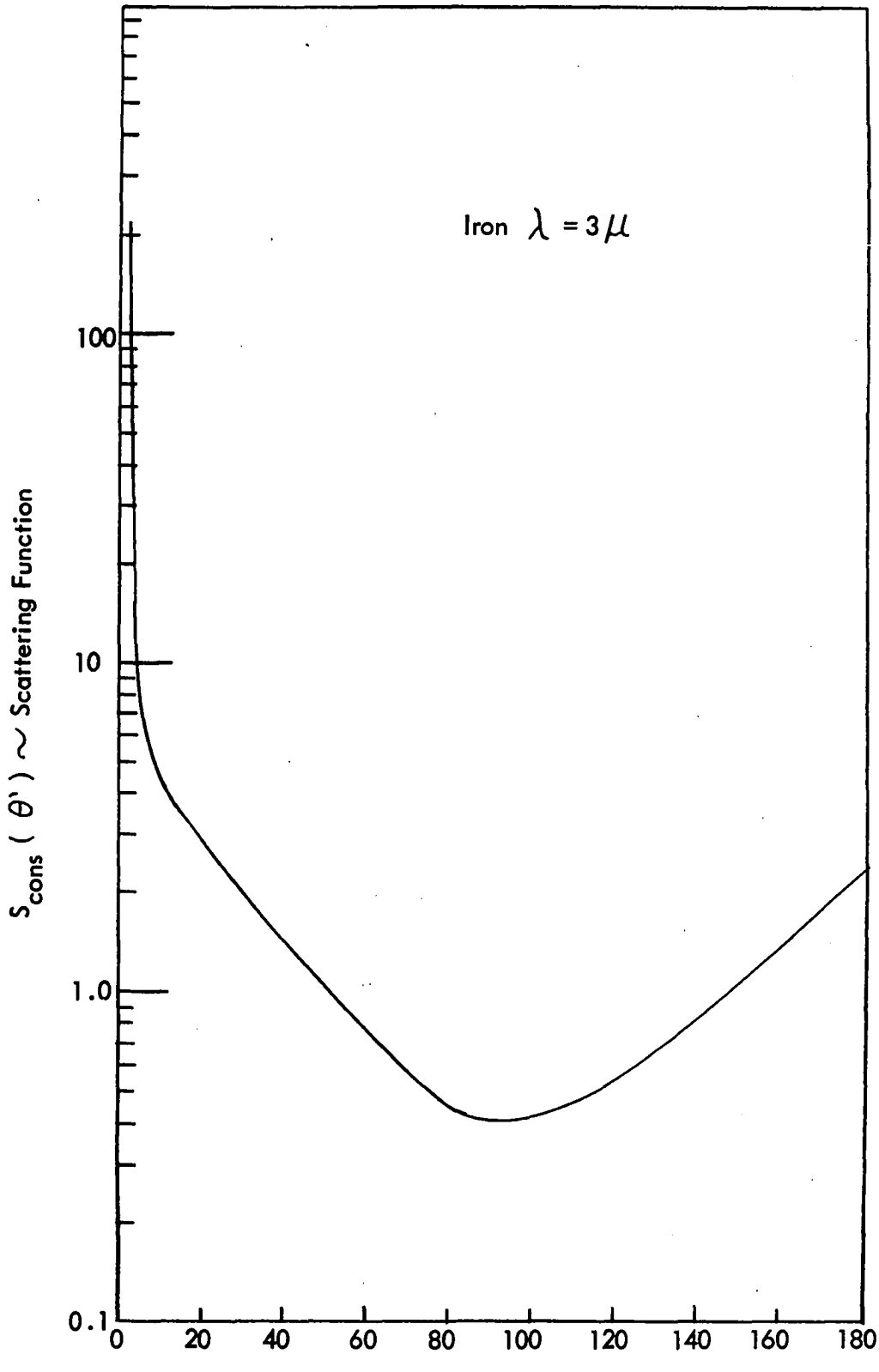

Figure 85
Angular Distribution of Scattering Function -- Experimental Data

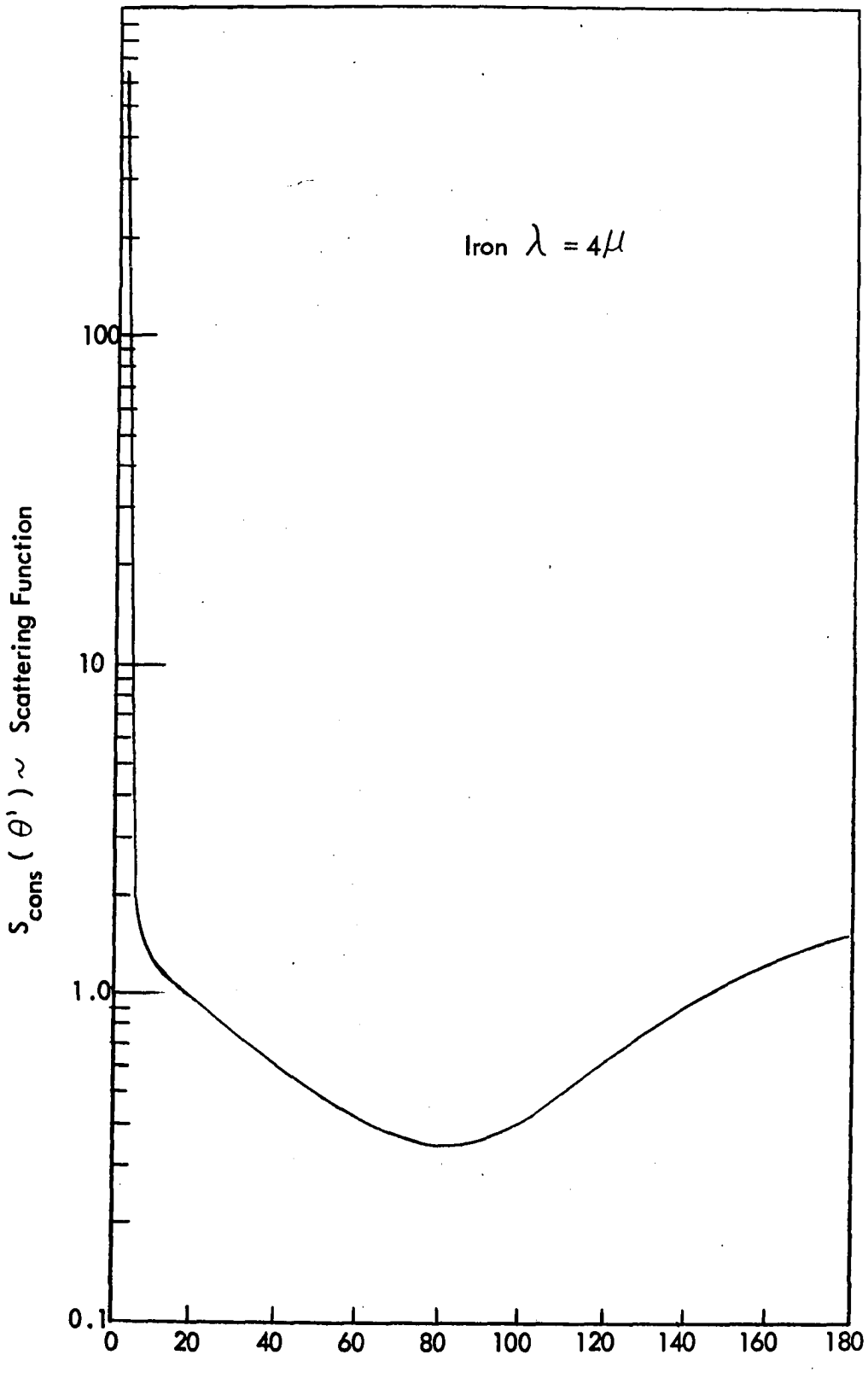

Figure 86
Angular Distribution of Scattering Function -- Experimental Data

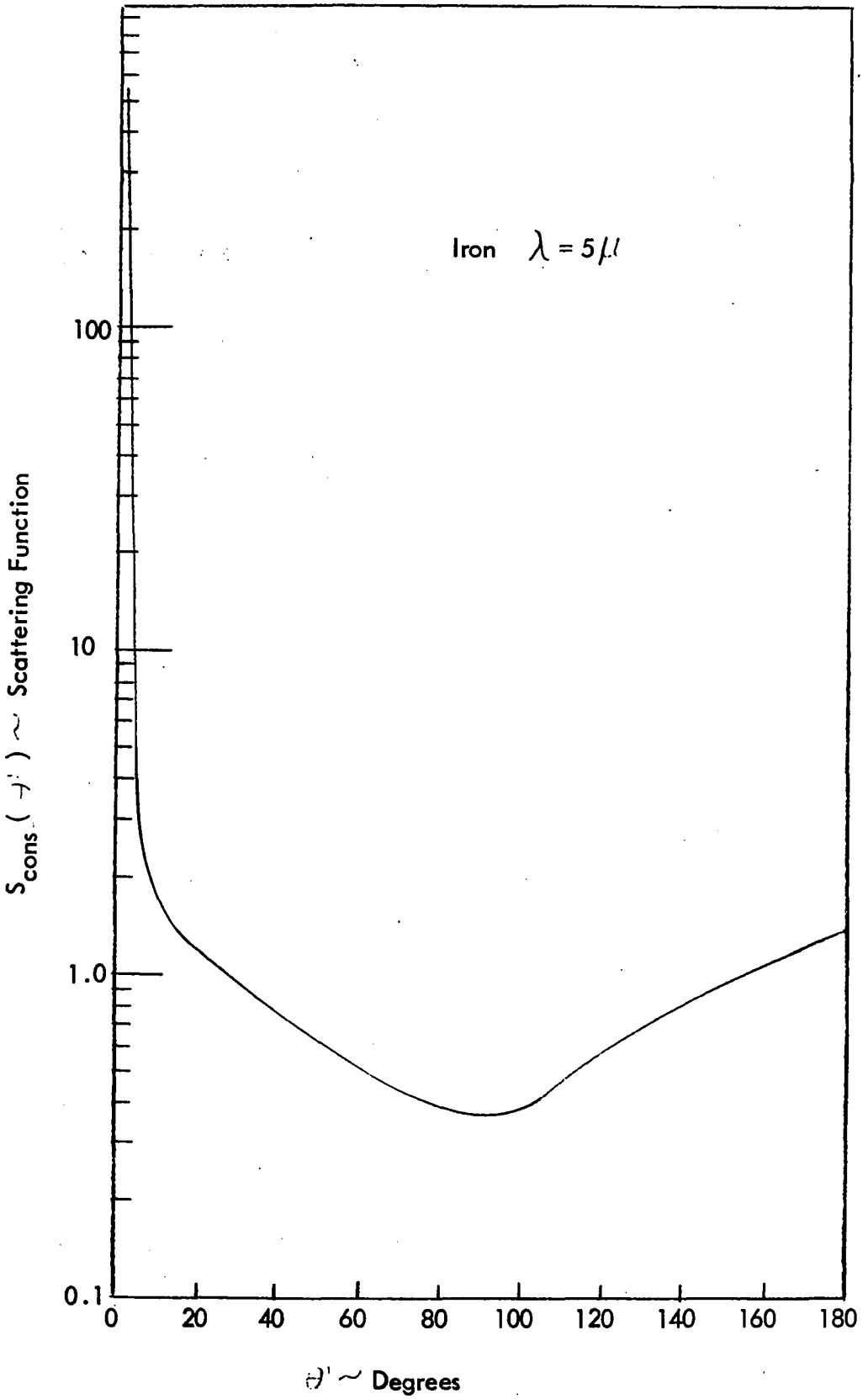

Figure 87
Angular Distribution of Scattering Function -- Experimental Data

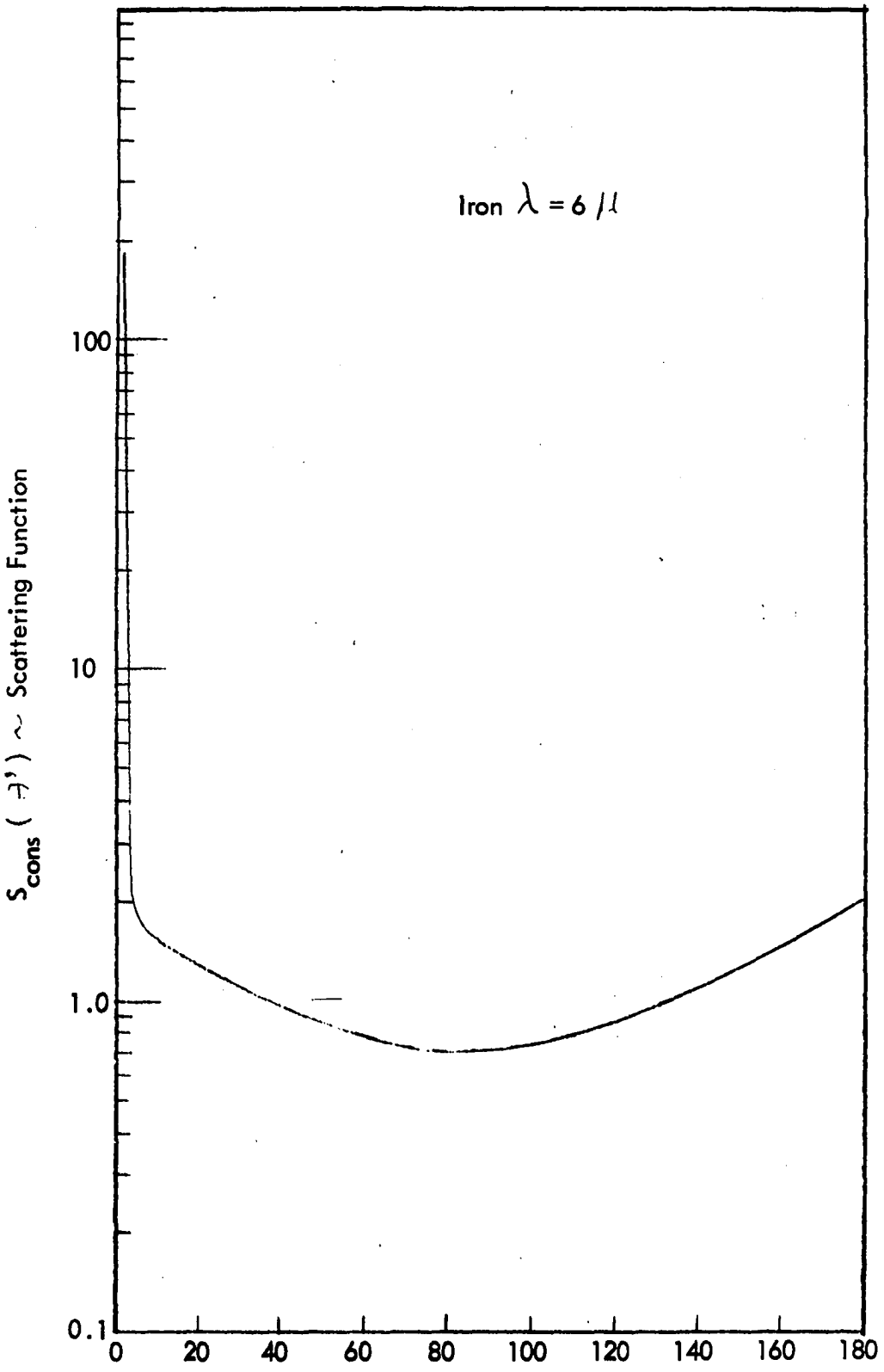

Figure 88
Angular Distribution of Scattering
Functian -- Experimental Data

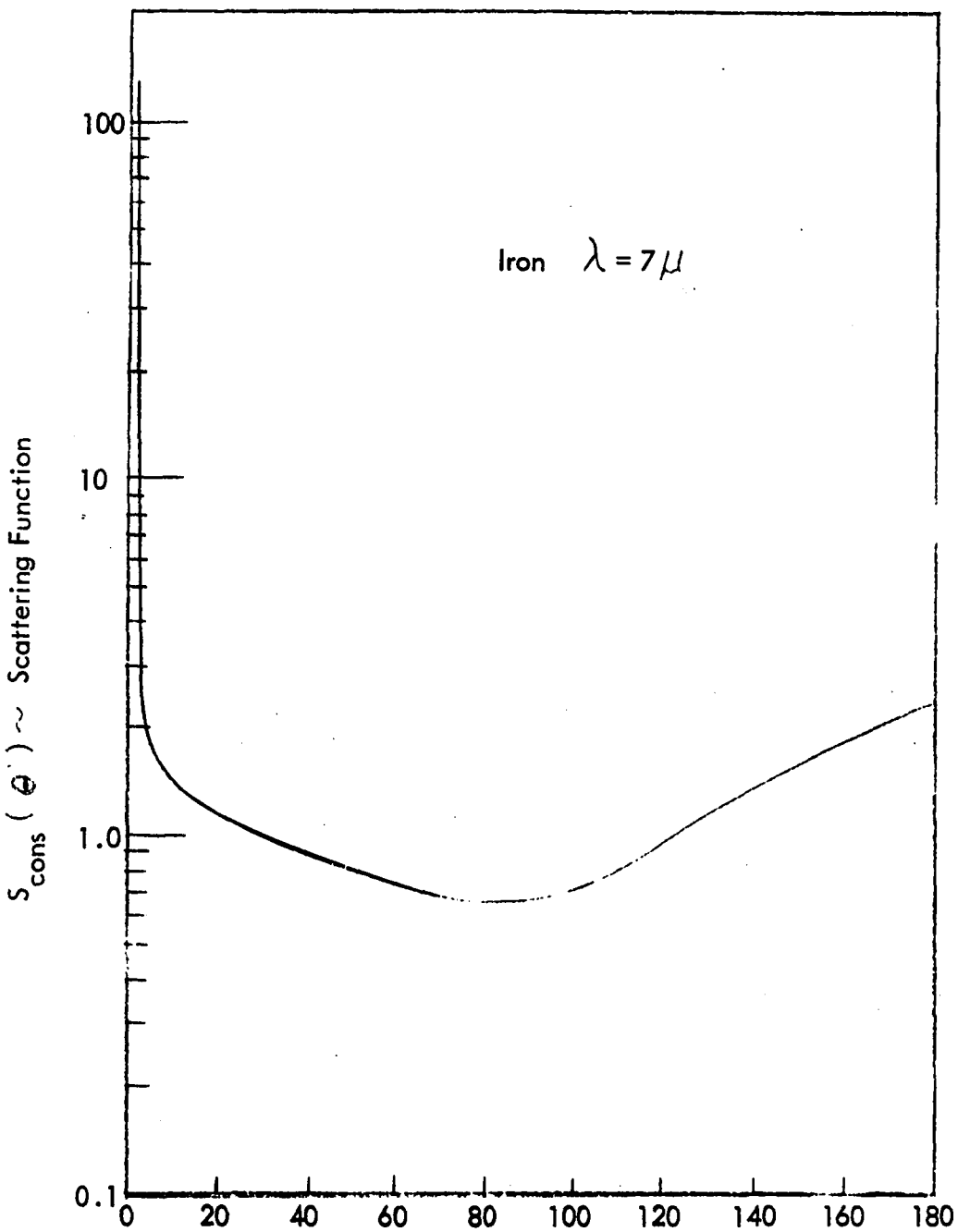

Figure 89
Angular Distribution of Scattering
Function -- Experimental Data

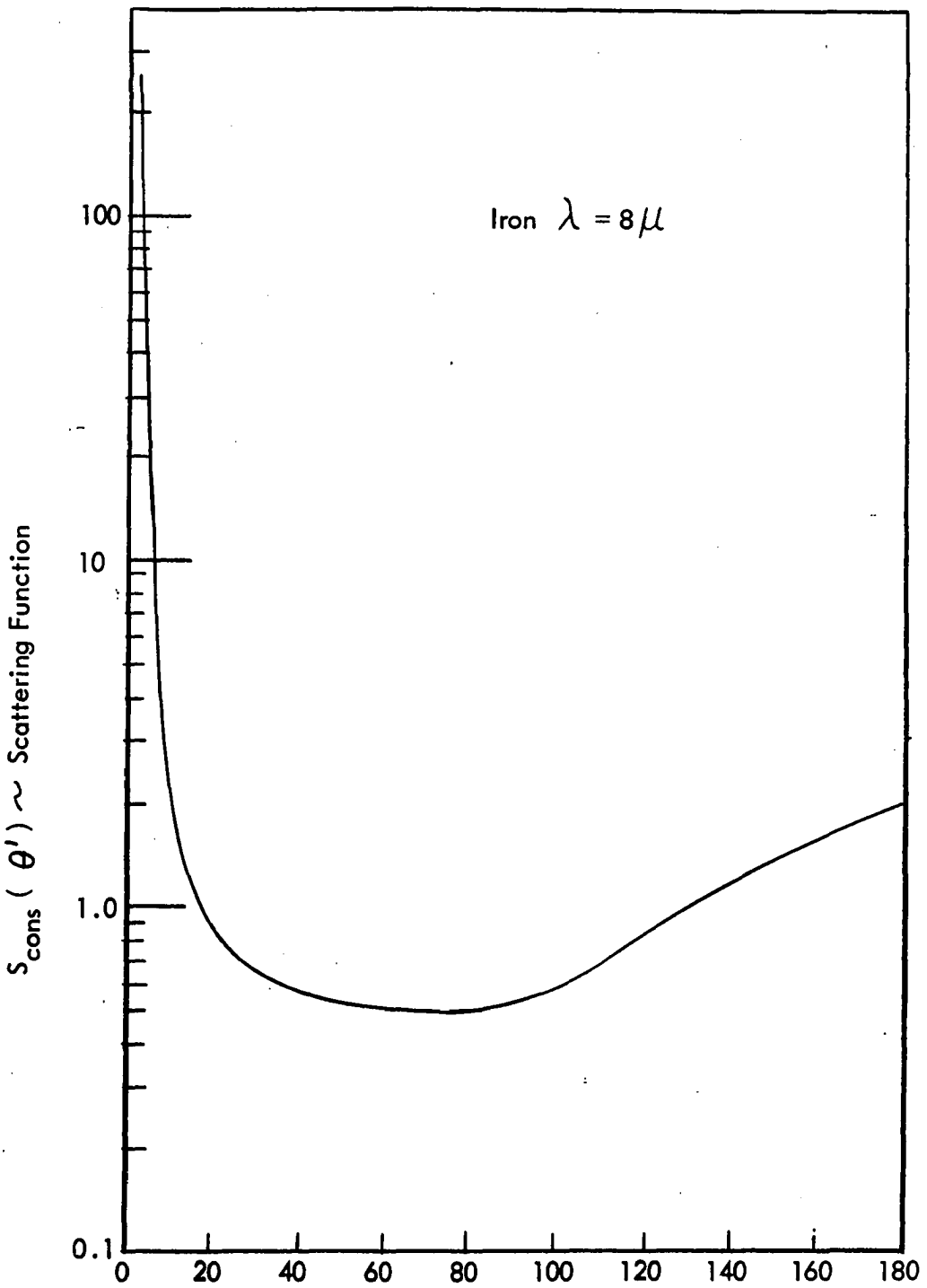

Figure 90

Angular Distribution of Scattering Function -- Experimental Data

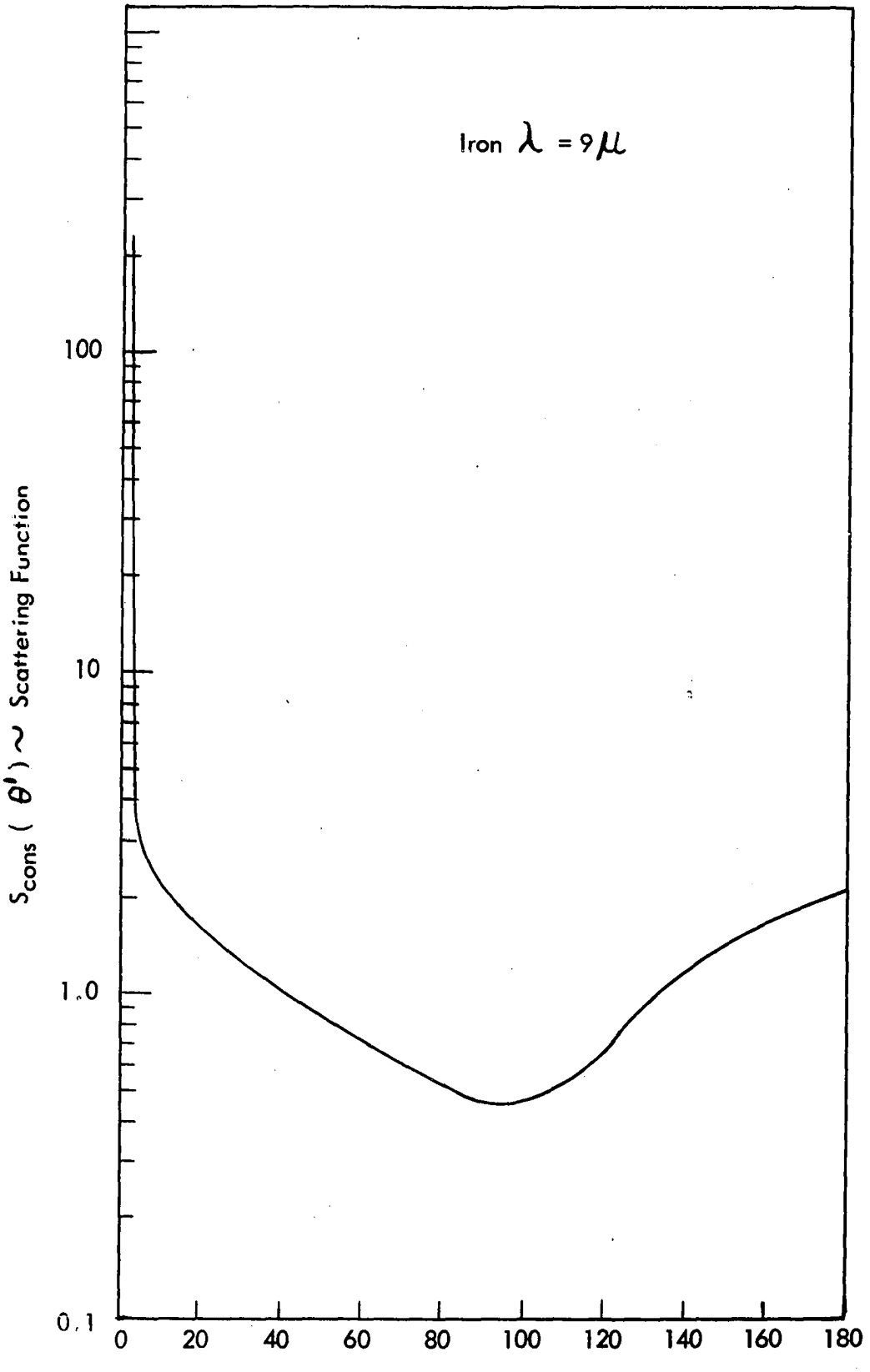

Figure 91
Angular Distribution of Scattering
Function -- Experimental Data

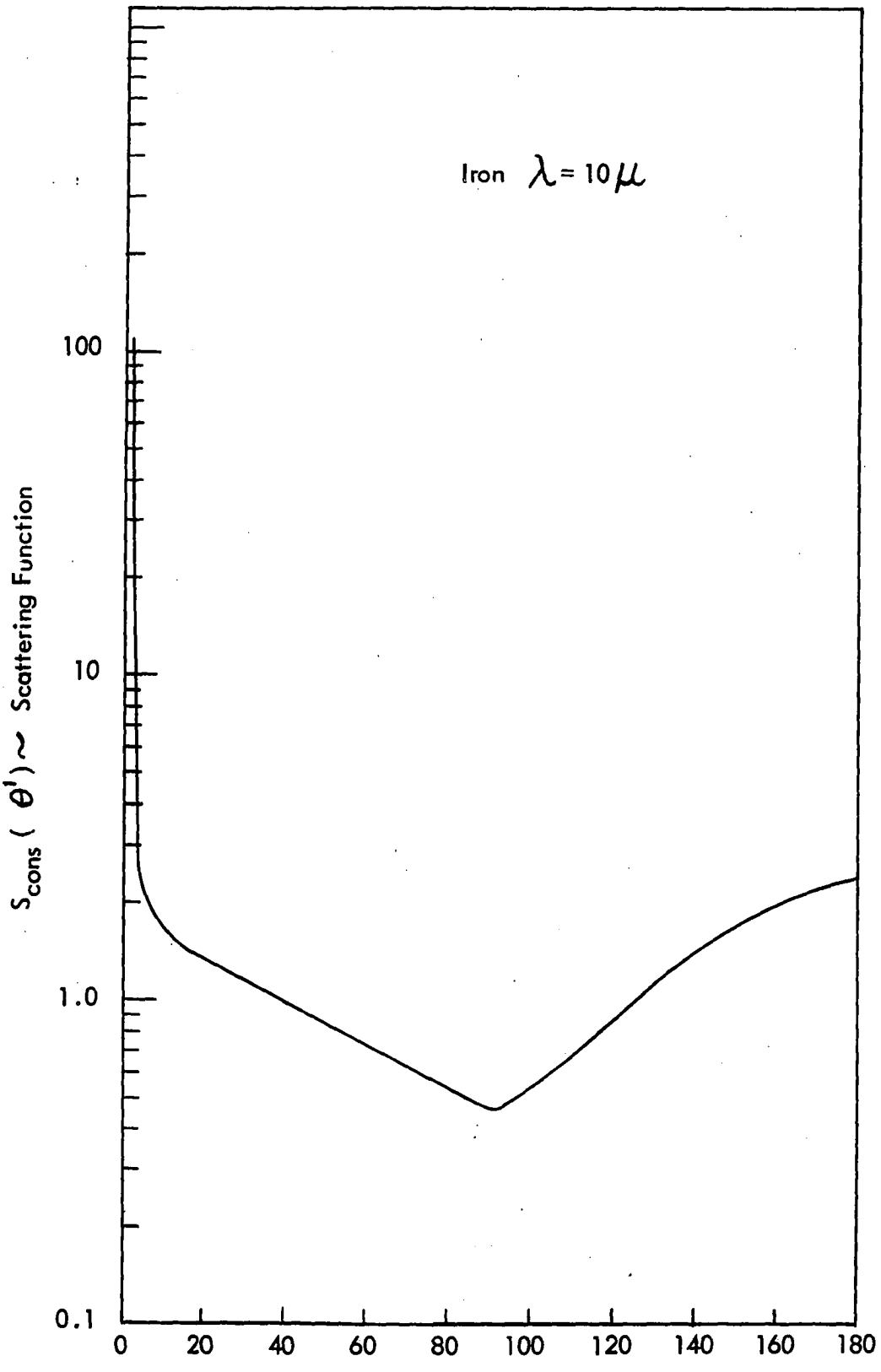

Figure 92
Angular Distribution of Scattering Function -- Experimental Data

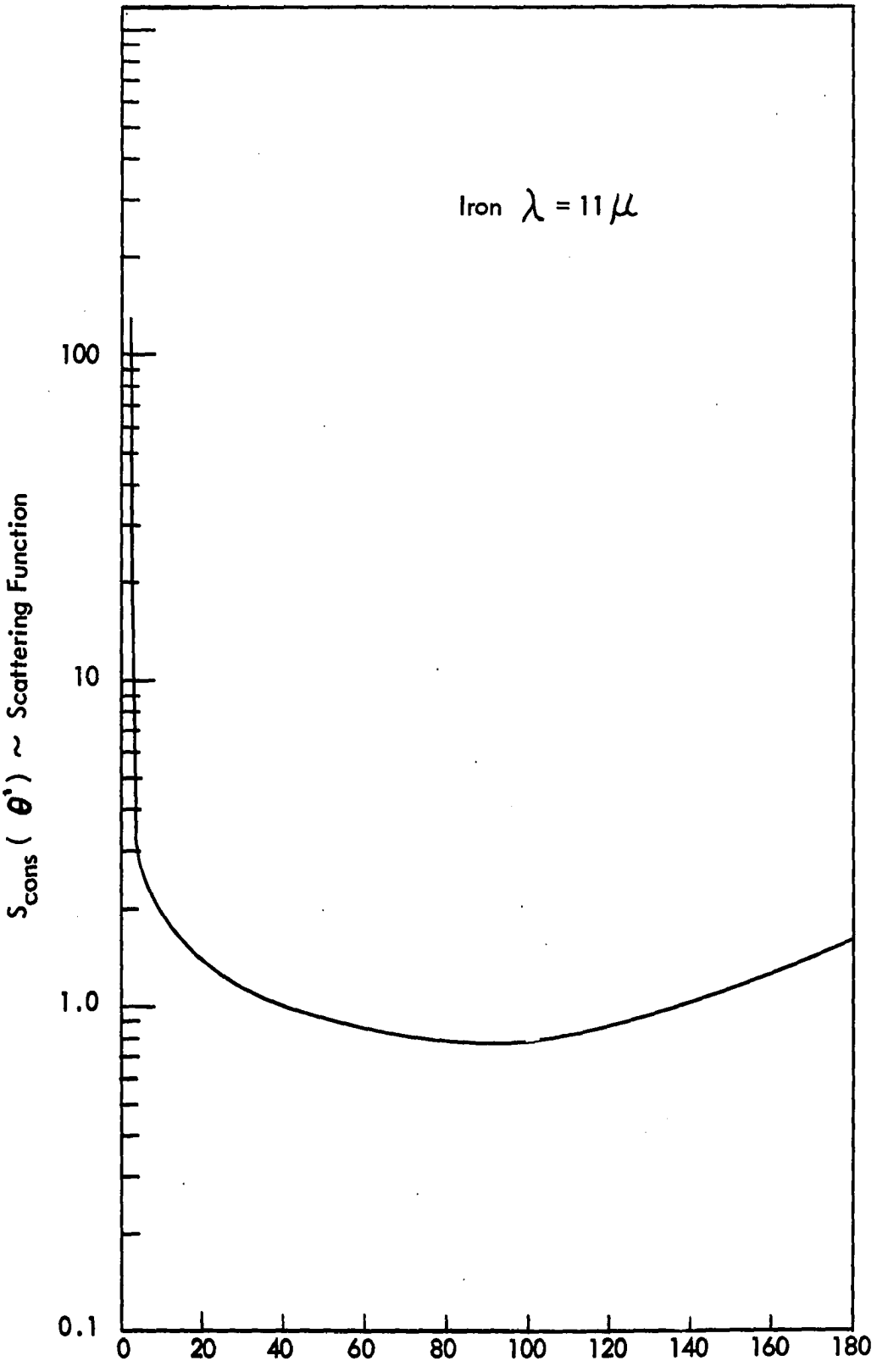

Figure 93
Angular Distribution of Scattering Function -- Experimental Data

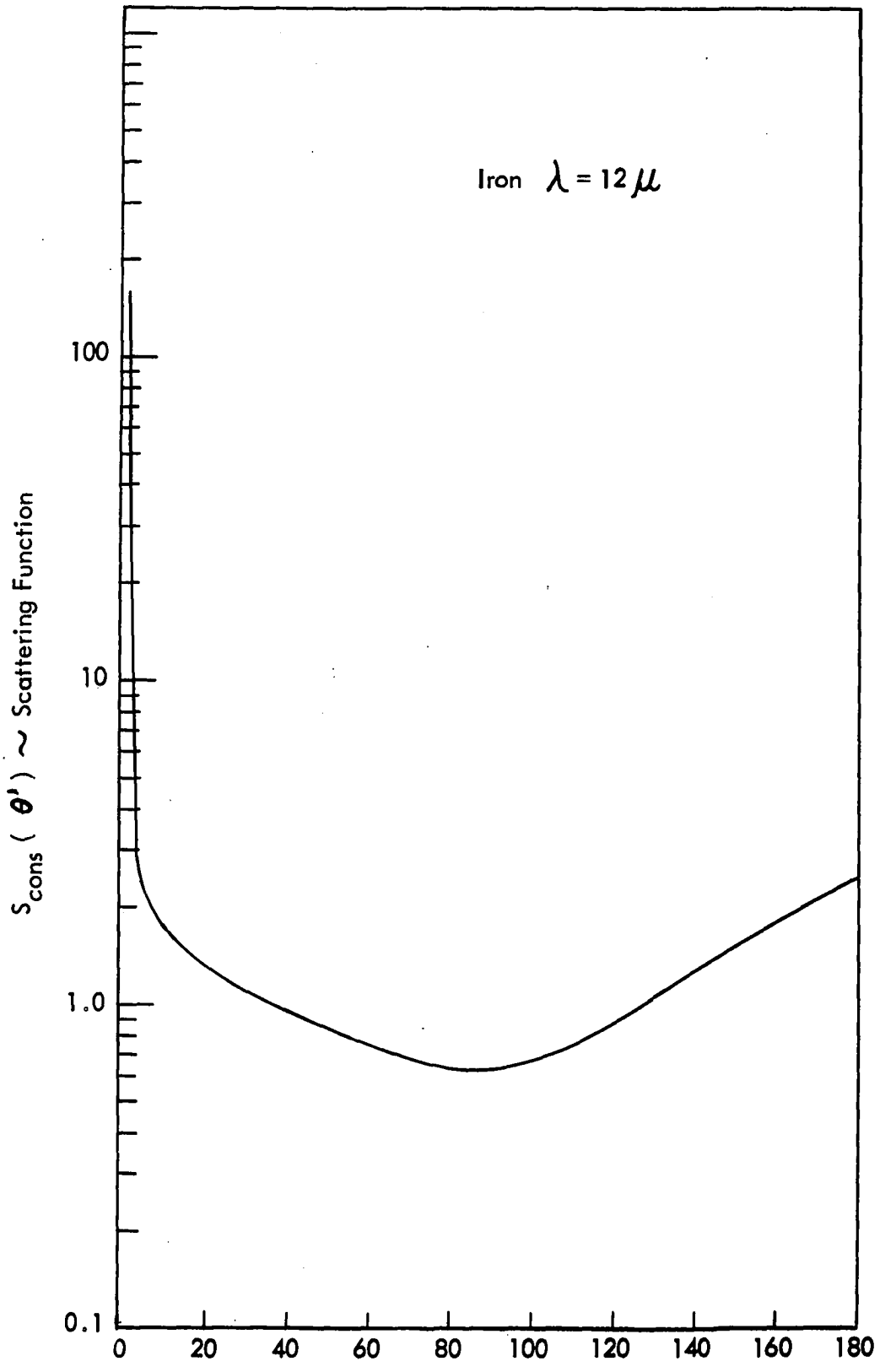

Figure 94
Angular Distribution of Scattering
Function -- Experimental Data

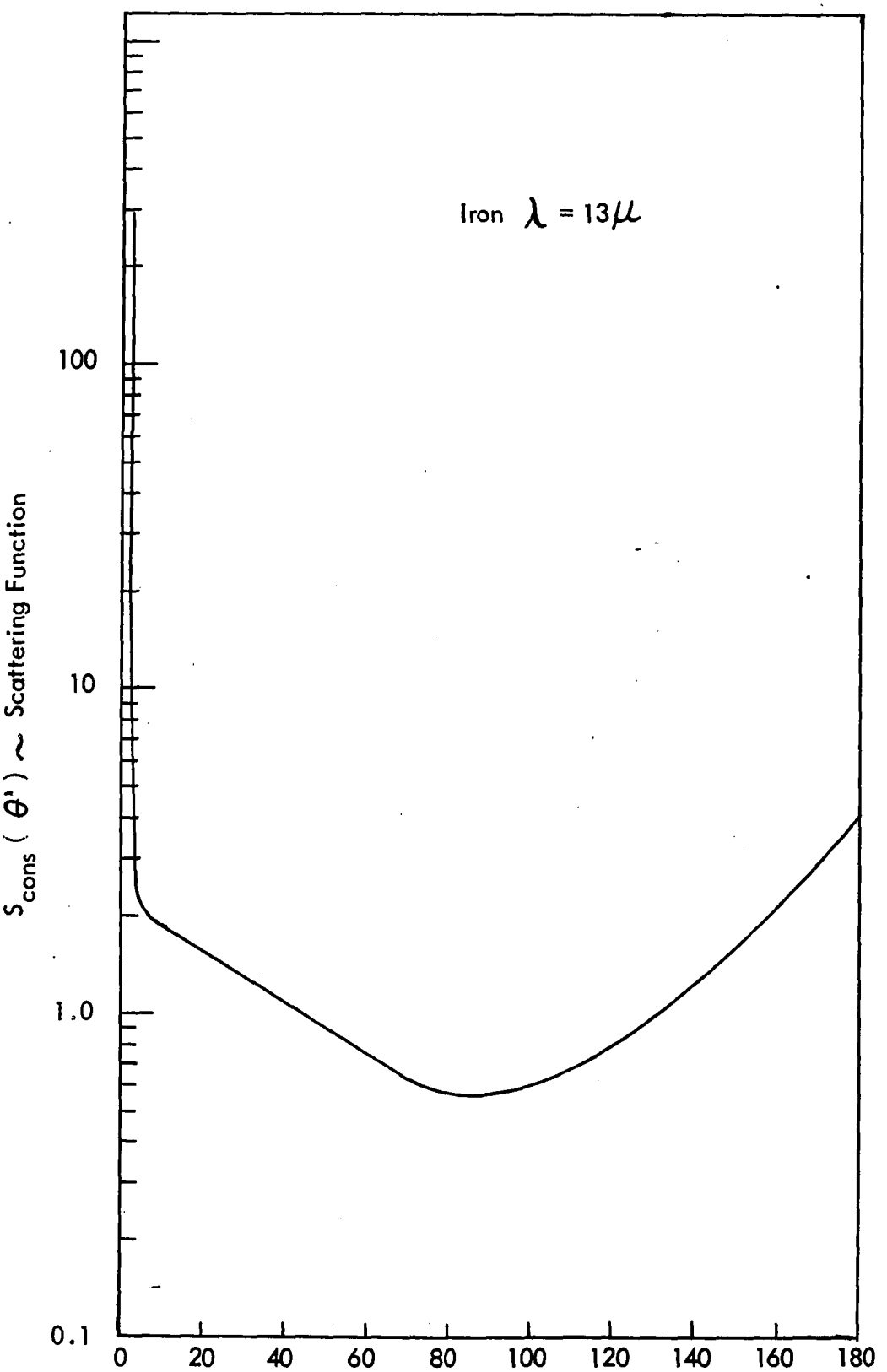

Figure 95
Angular Distribution of Scattering Function -- Experimental Data

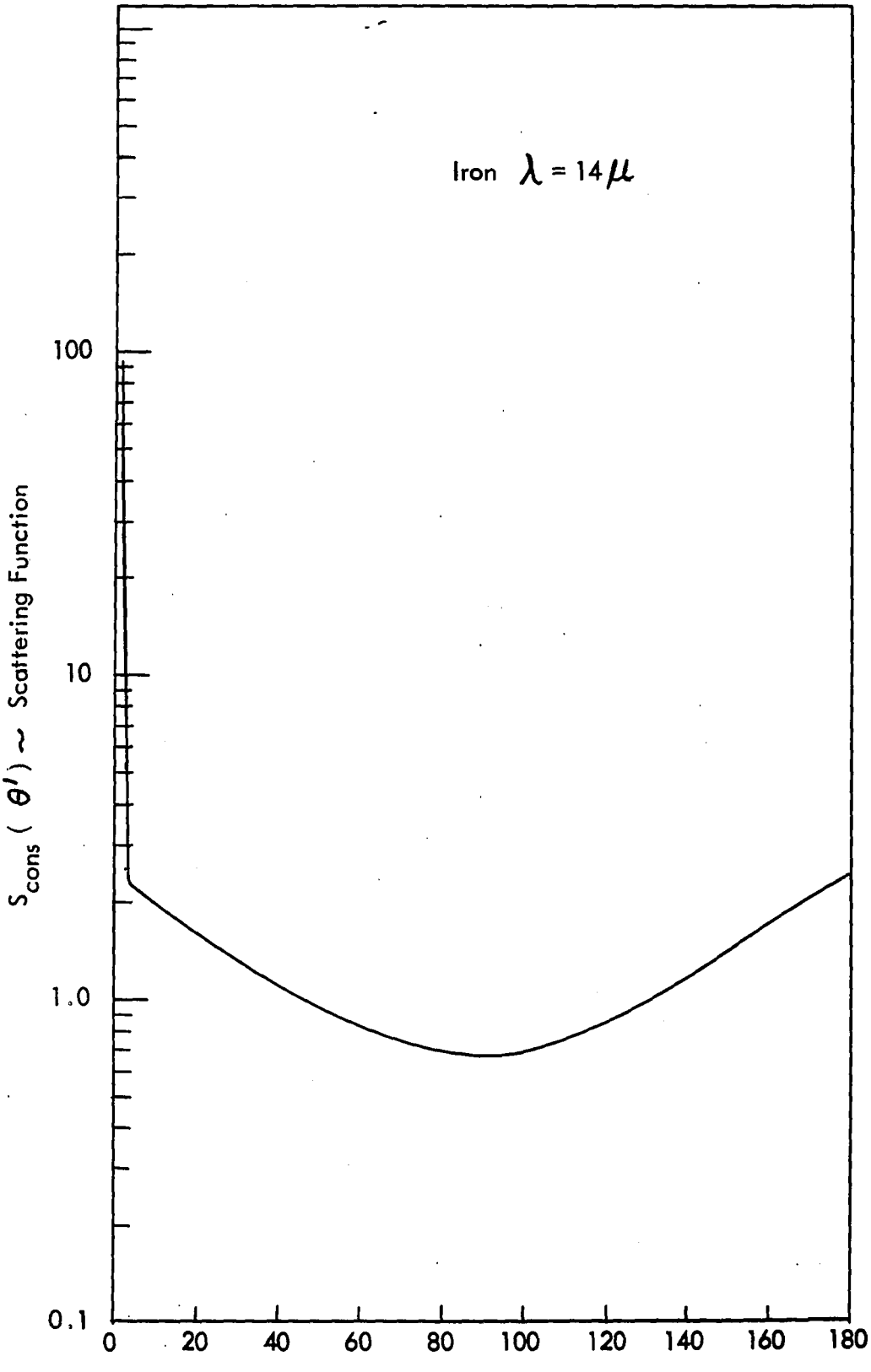

Figure 96
Angular Distribution of Scattering Function -- Experimental Data

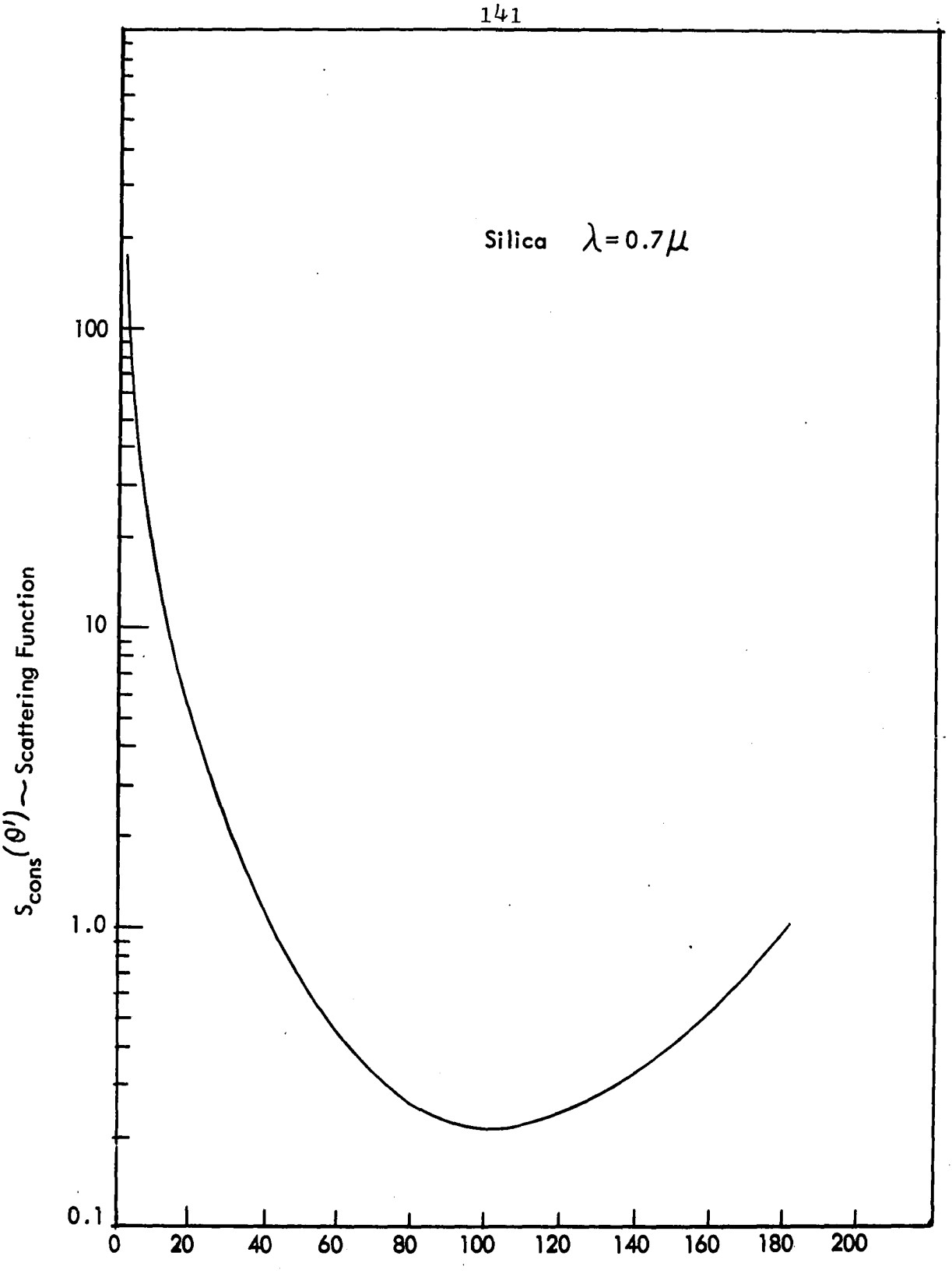

Figure 97
Angular Distribution of Scattering Function -- Experimental Data

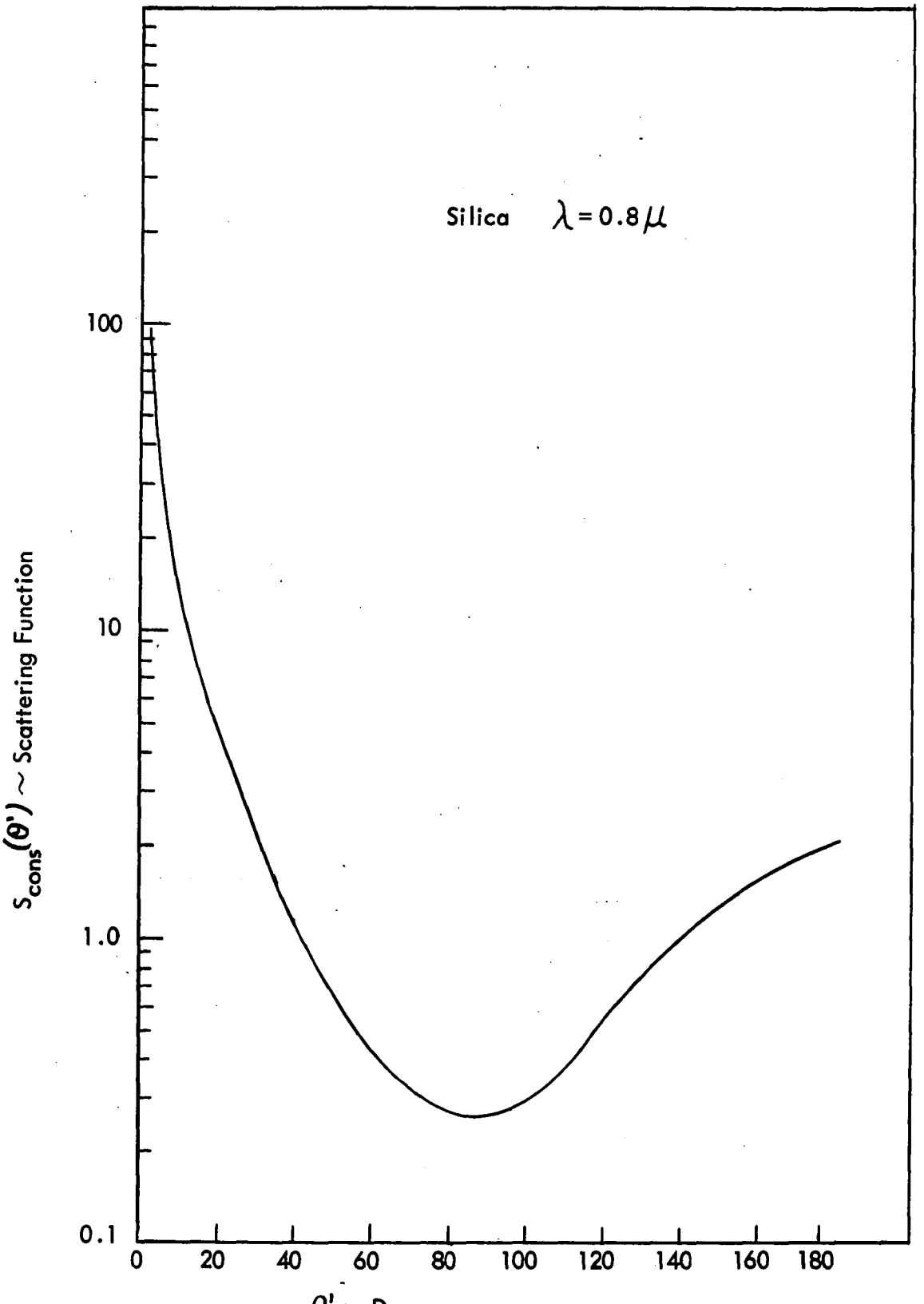

Figure 98
Angular Distribution of Scattering Function -- Experimental Data

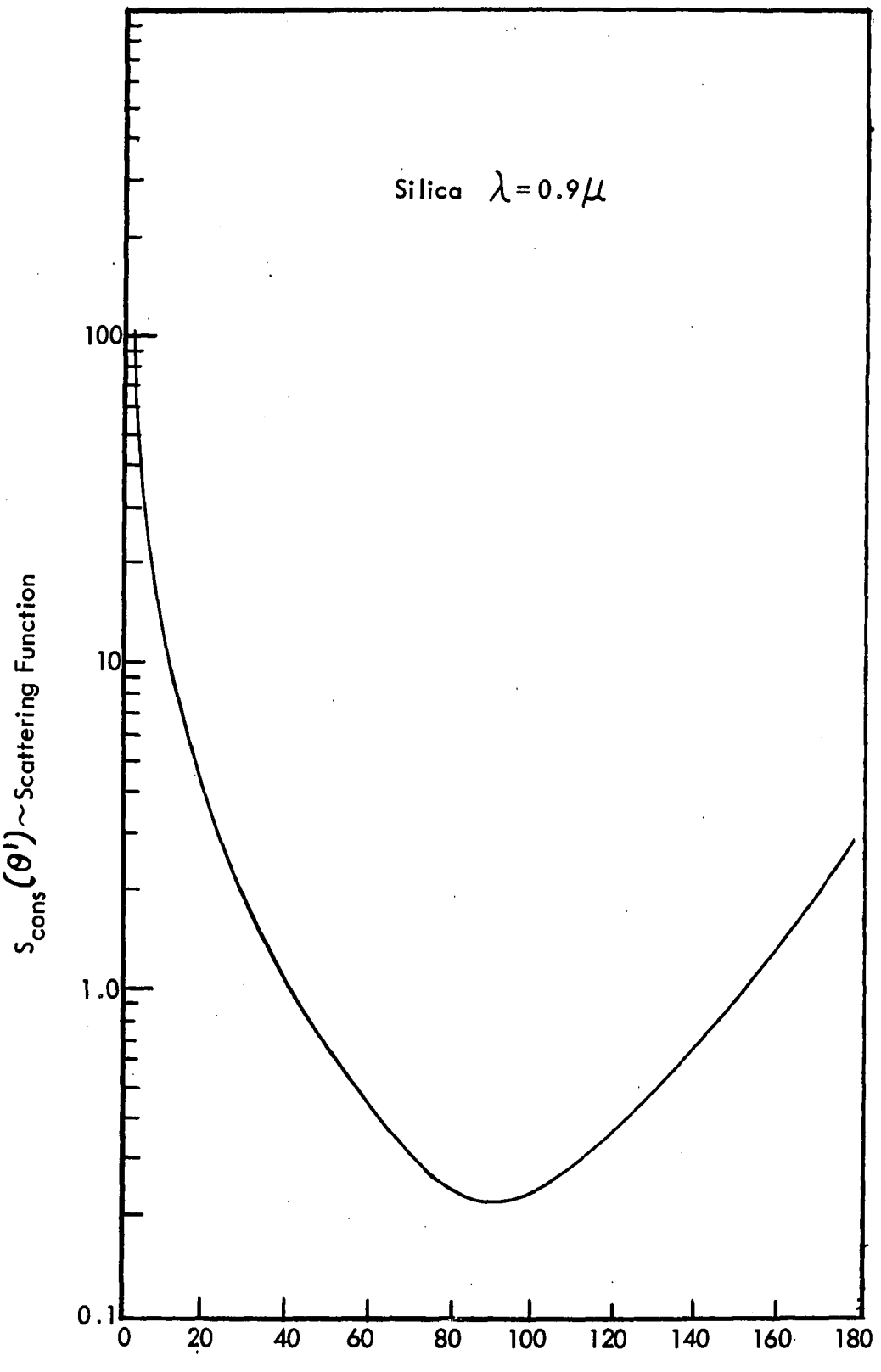

Angular Distribution of Scattering Function -- Experimental Data

Figure 99

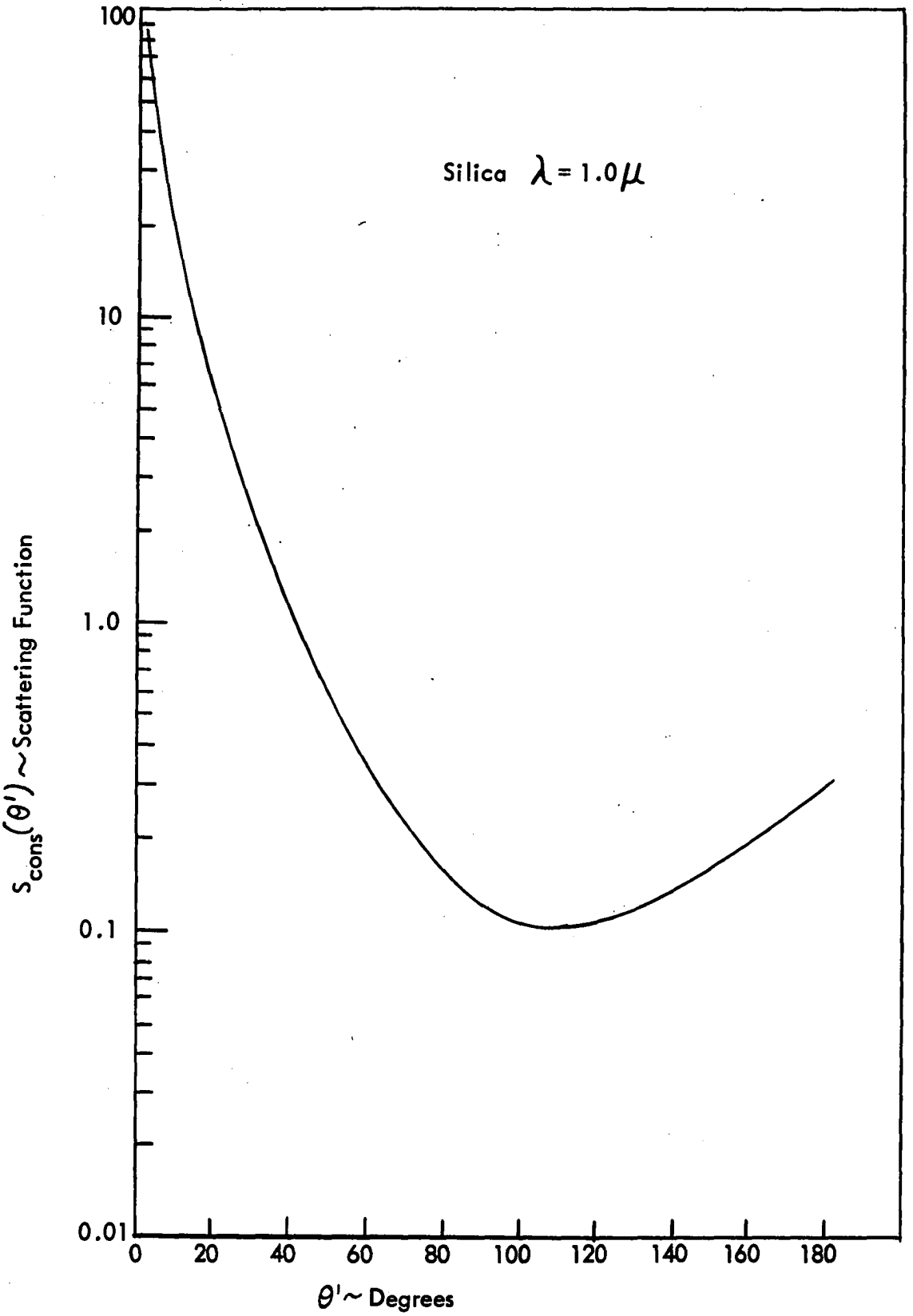

Figure 100
Angular Distribution of Scattering Function -- Experimental Data

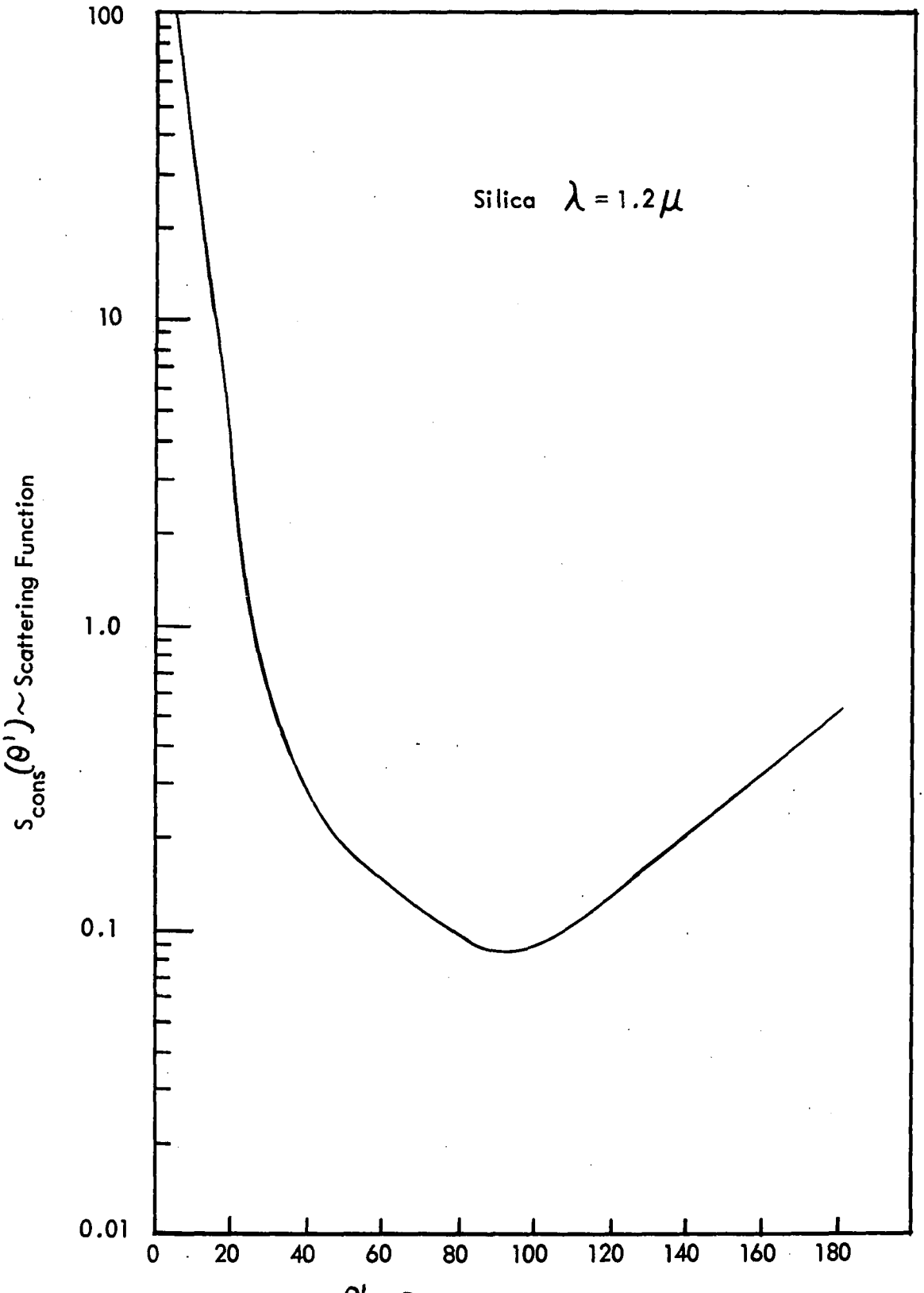

Figure 101
Angular Distribution of Scattering Function -- Experimental Data

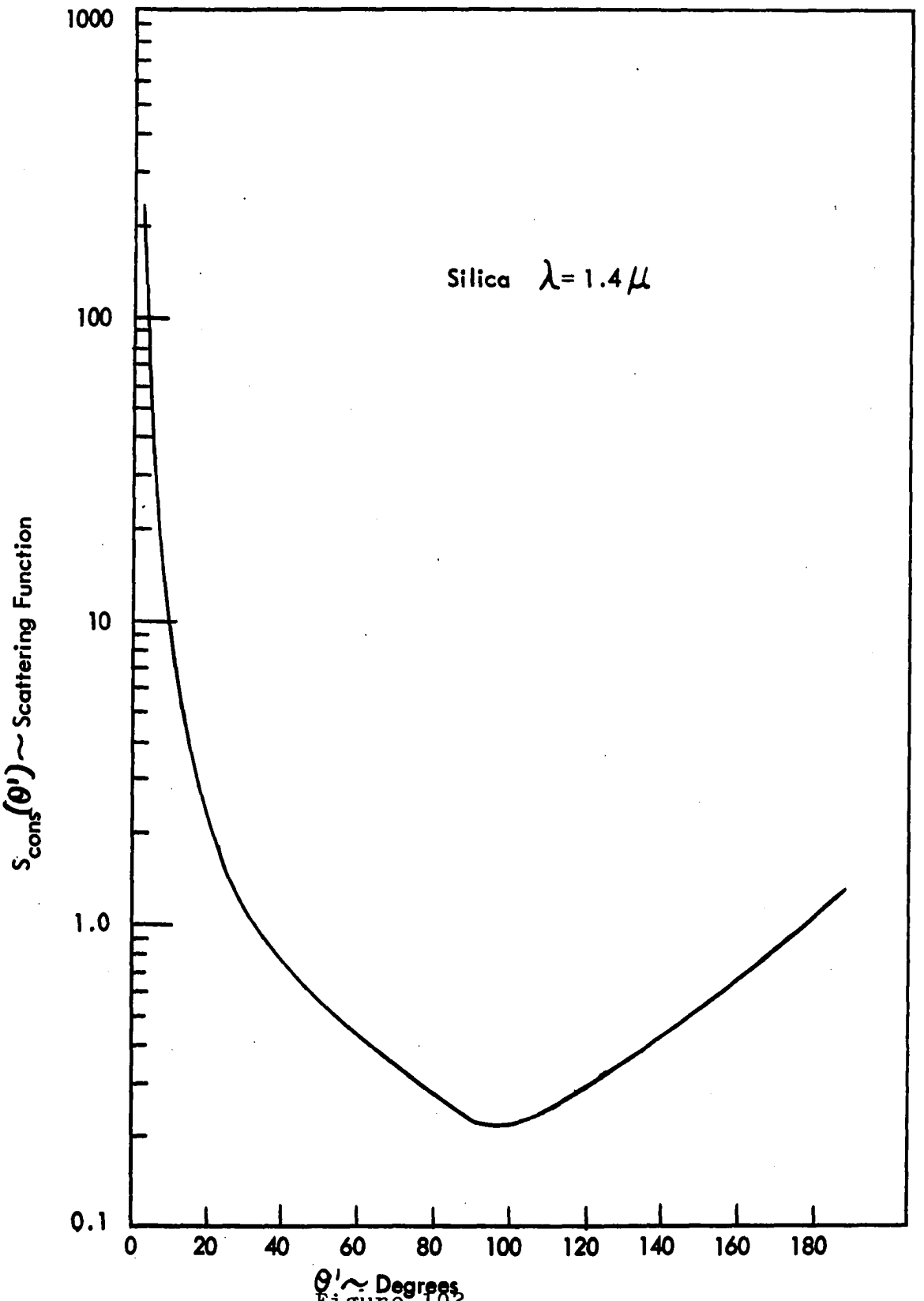

Figure 102
Angular Distribution of Scattering Function -- Experimental Data

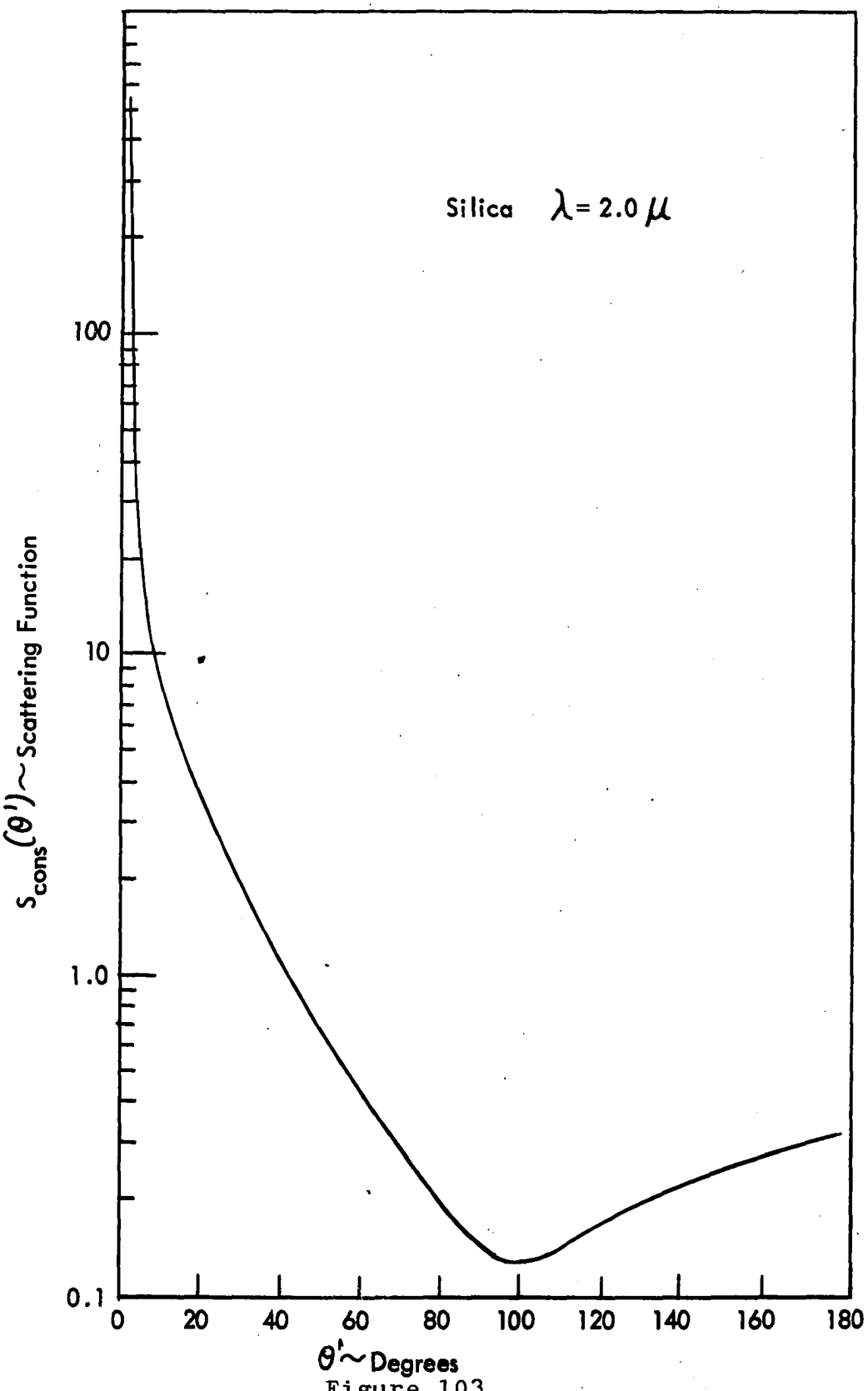

Figure 103
Angular Distribution of Scattering Function -- Experimental Data

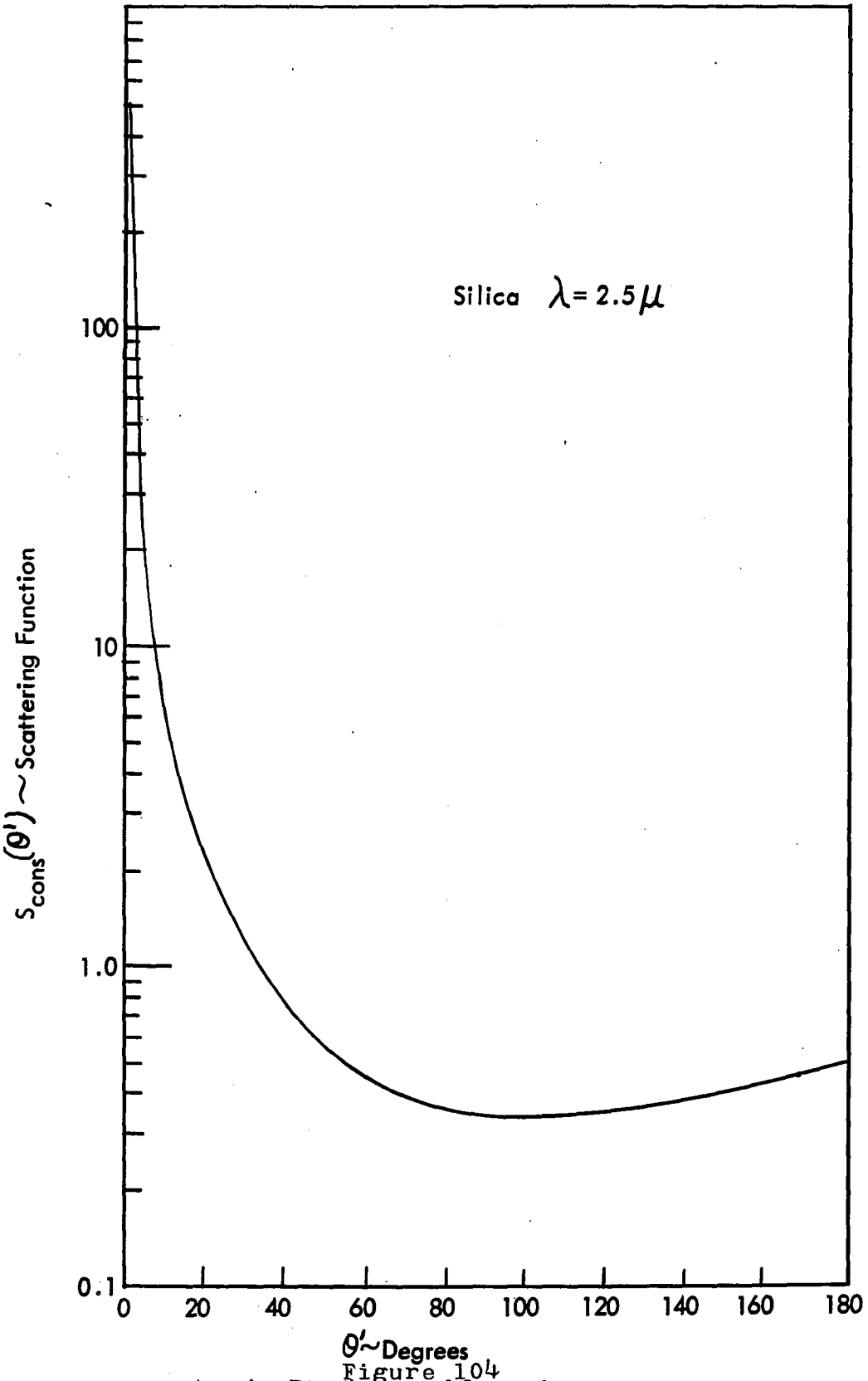

Figure 104
Angular Distribution of Scattering Function -- Experimental Data

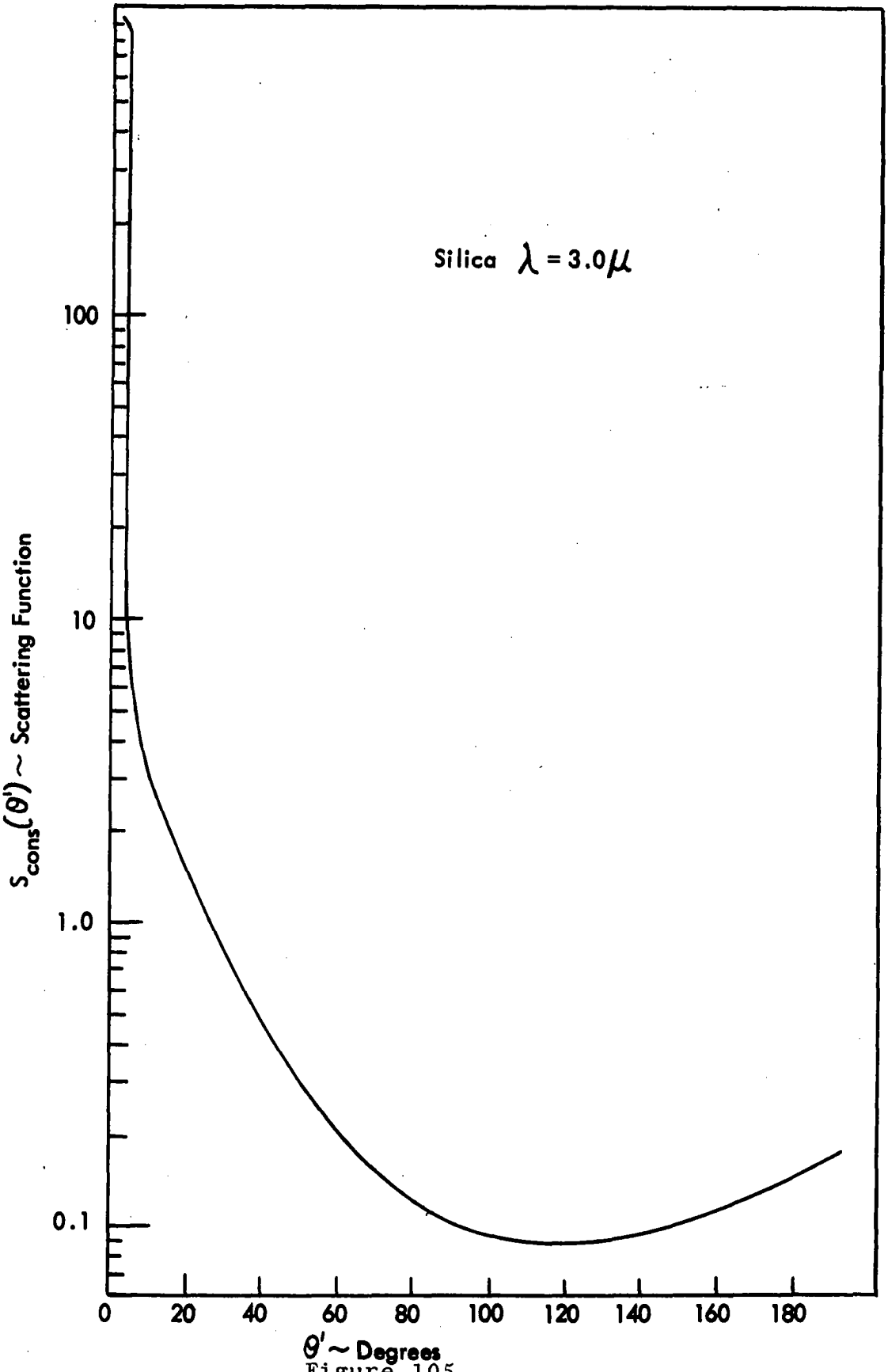

Figure 105
Angular Distribution of Scattering Function -- Experimental Data

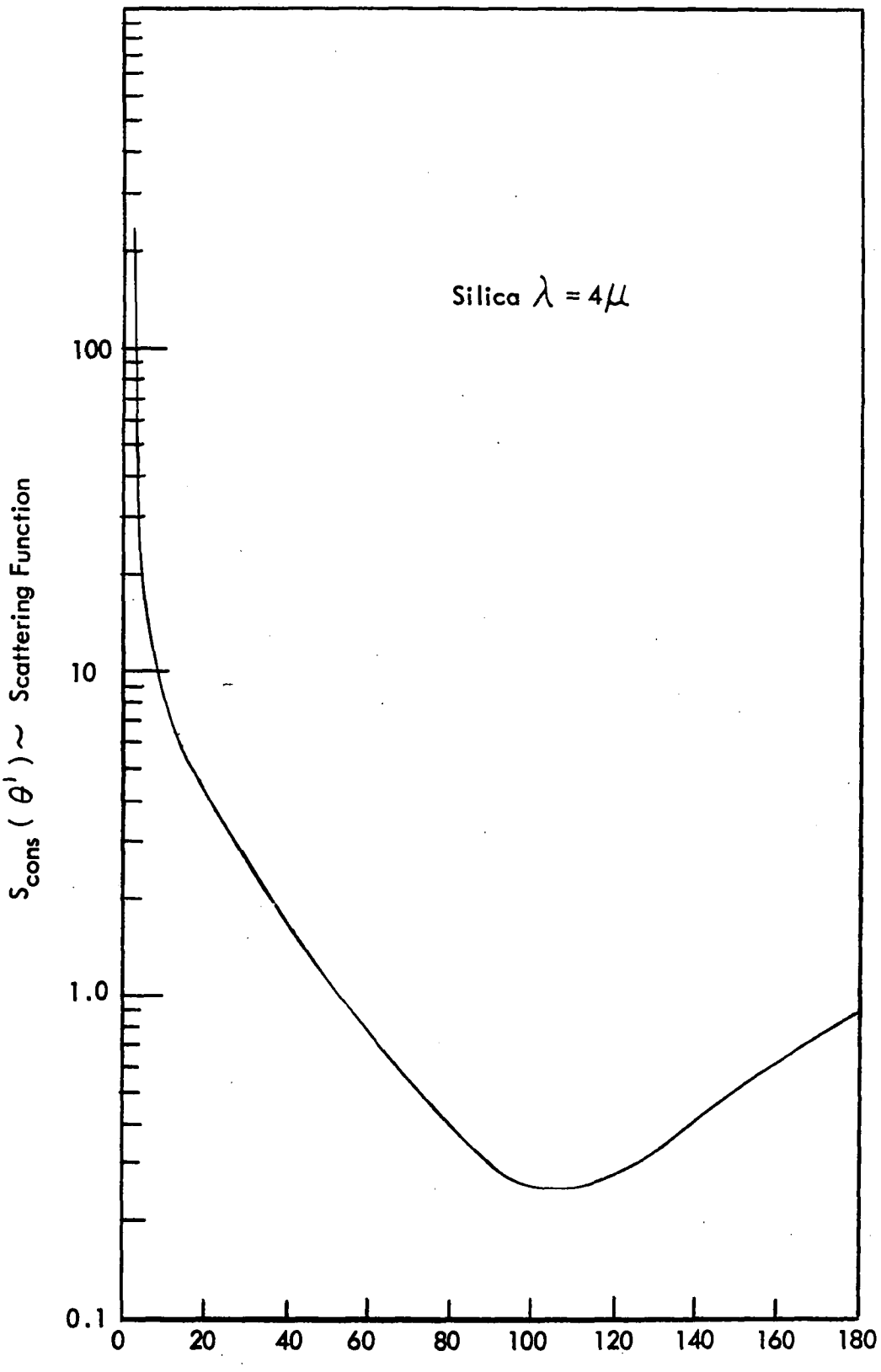

Figure 106
Angular Distribution of Scattering Function -- Experimental Data

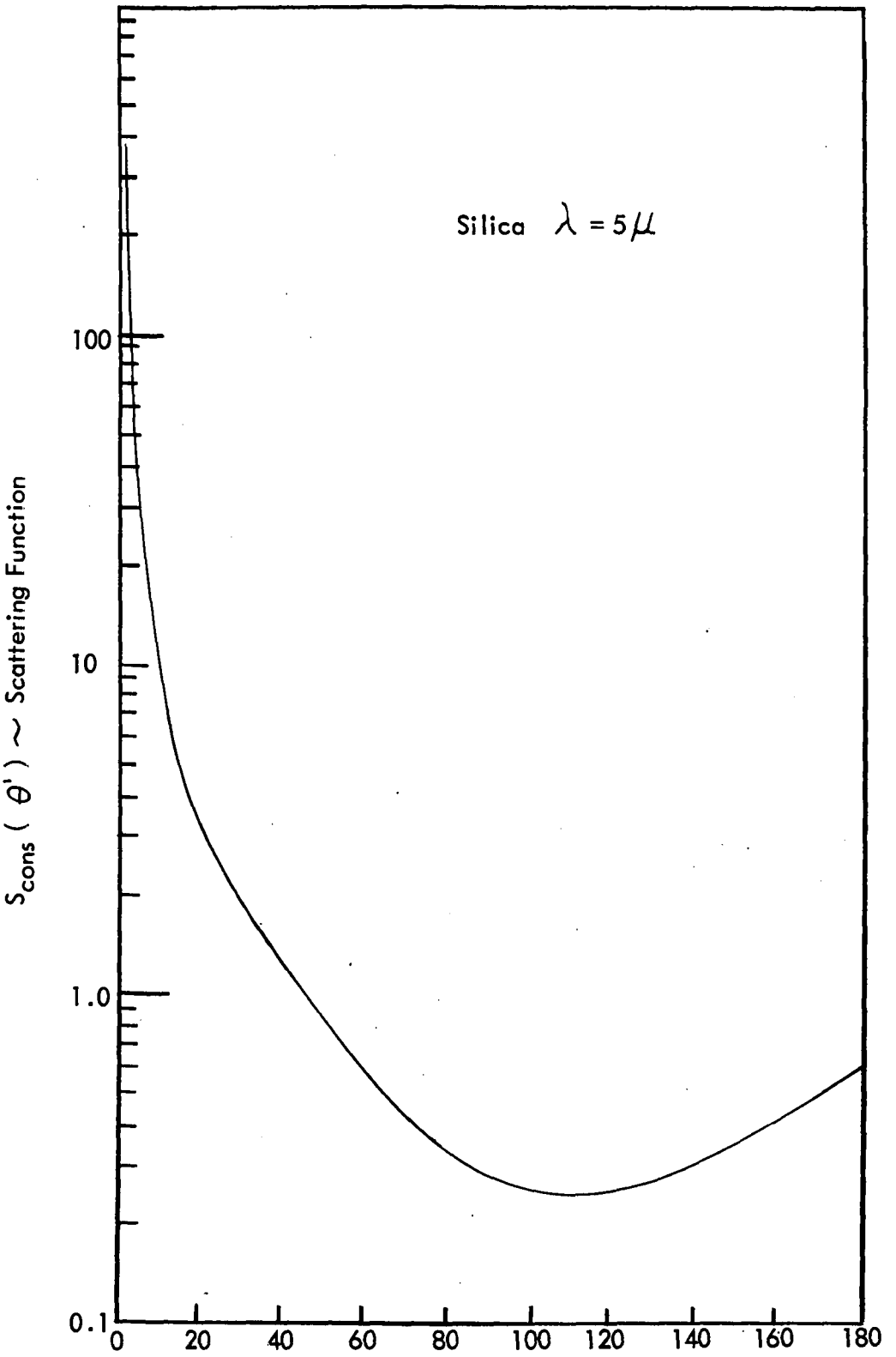

Figure 107
Angular Distribution of Scattering Function -- Experimental Data

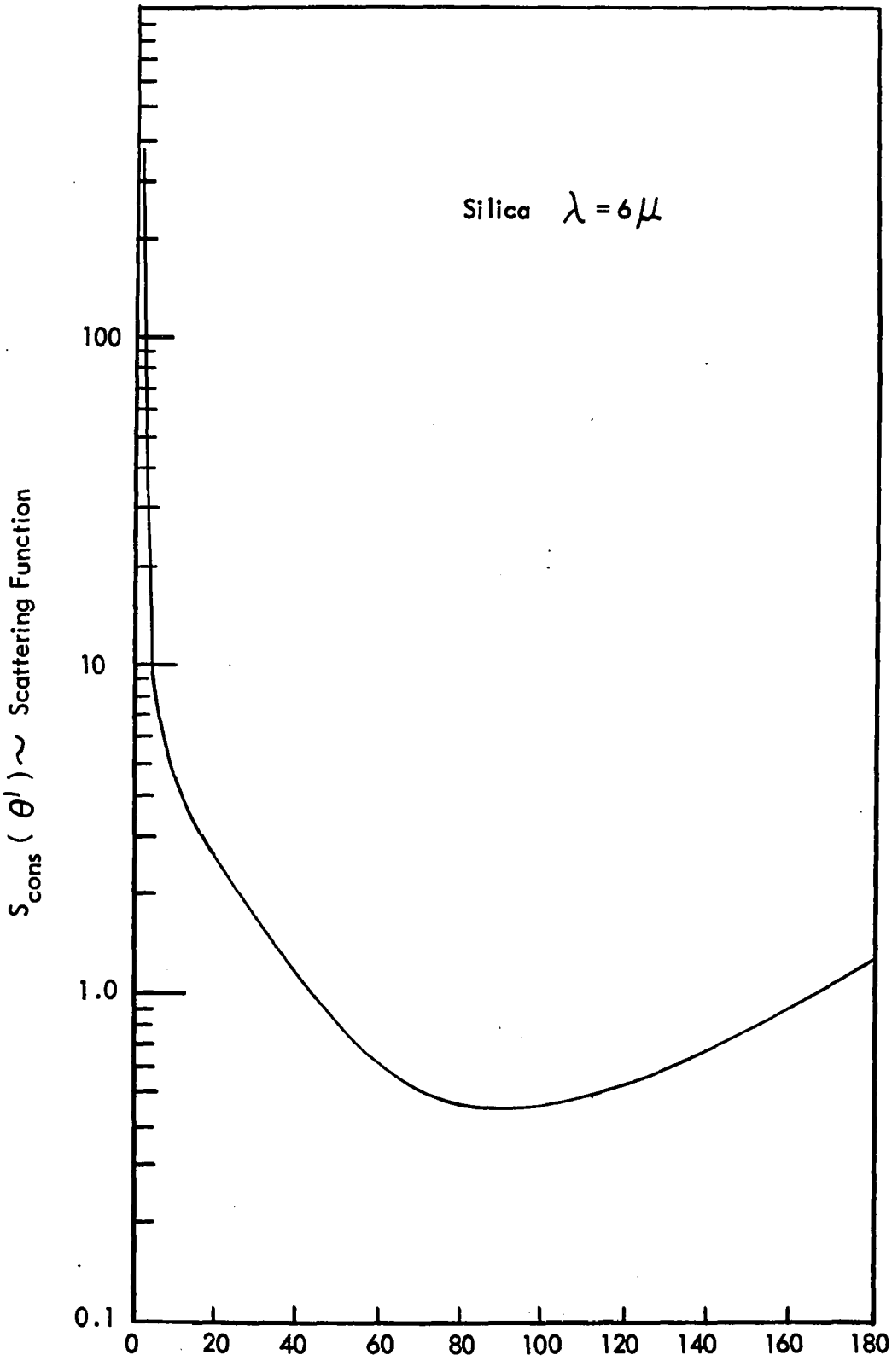

Figure 108
Angular Distribution of Scattering Function -- Experimental Data

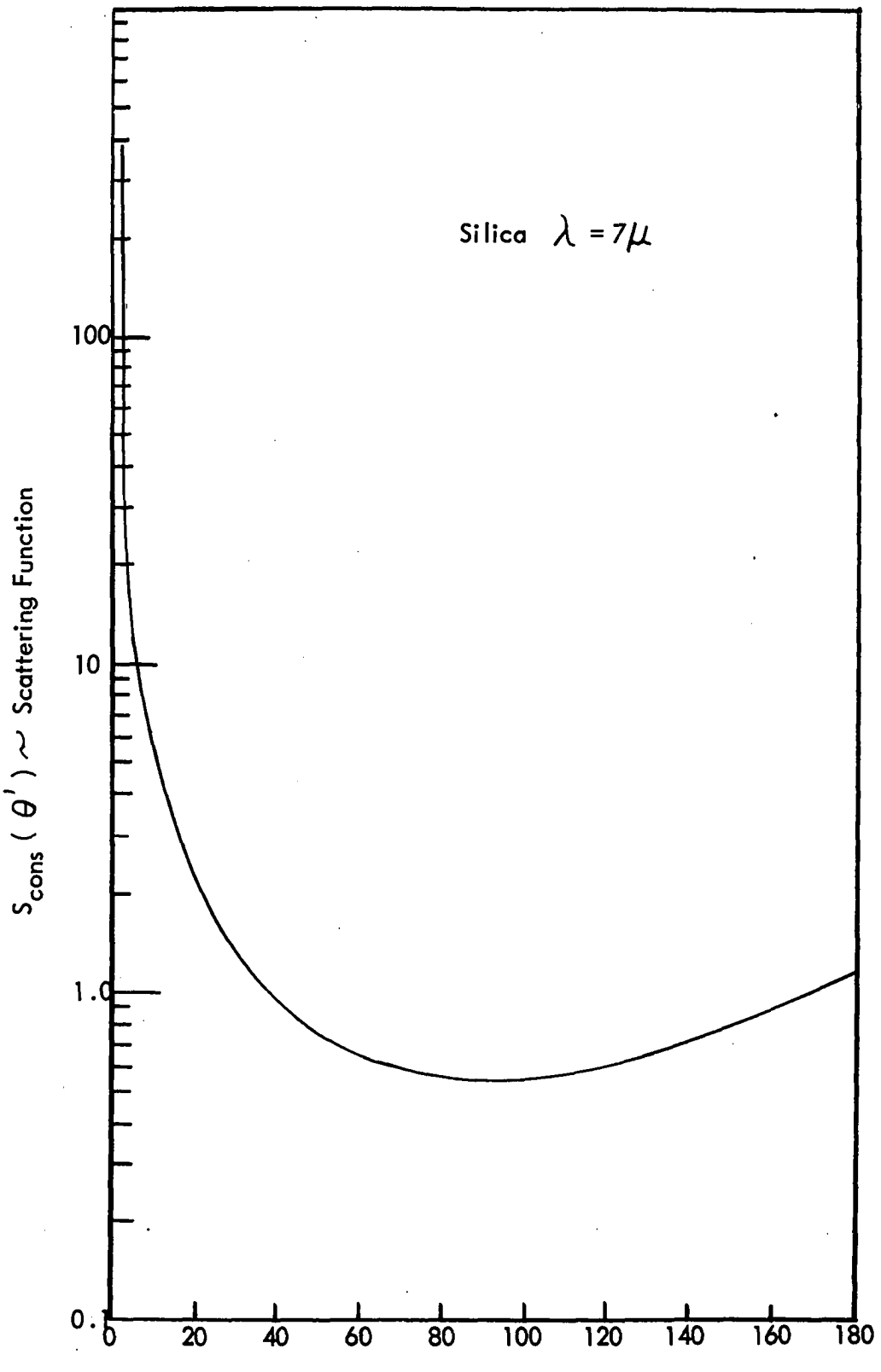

Figure 109
Angular Distribution of Scattering Function -- Experimental Data

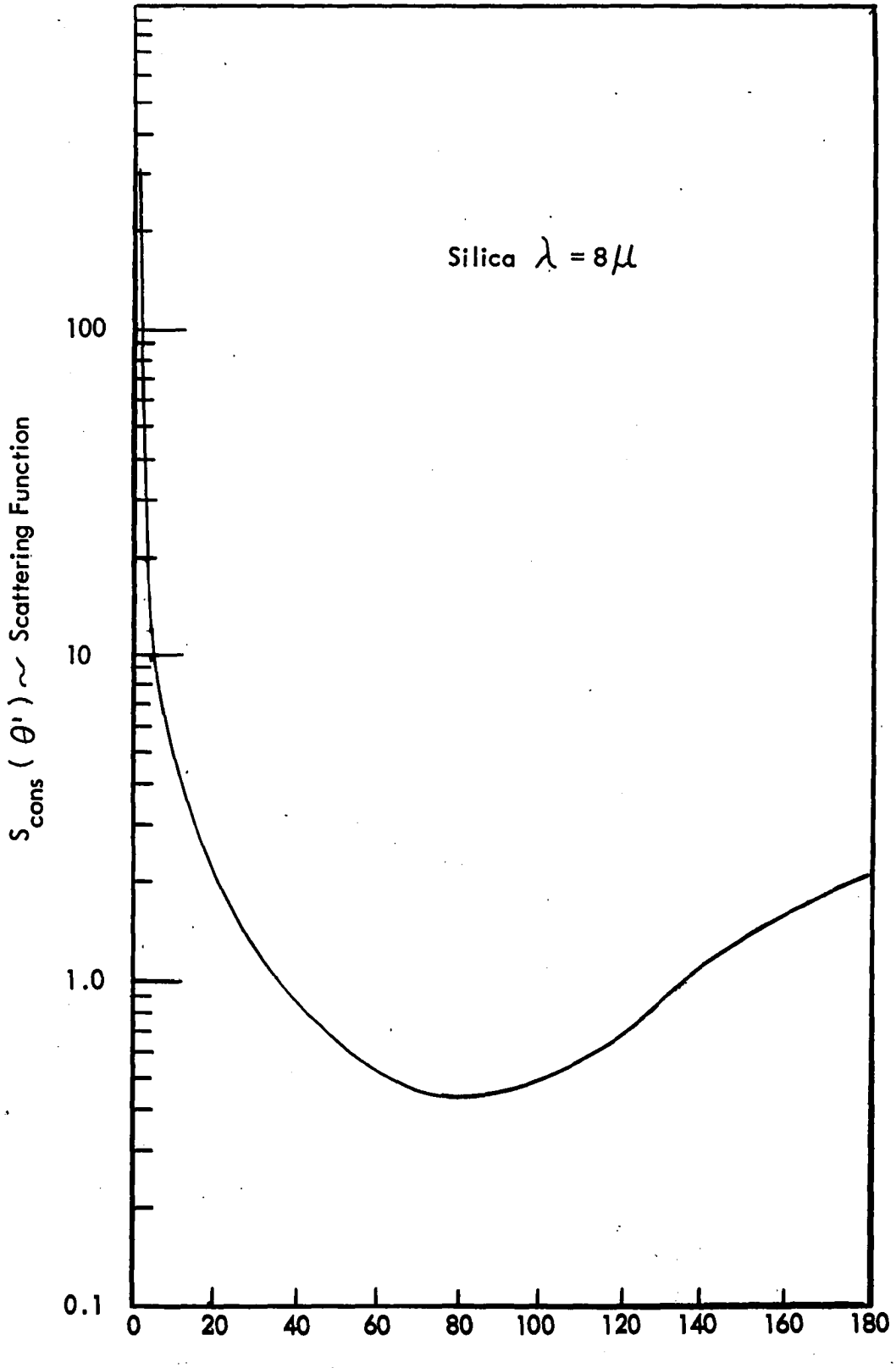

Figure 110
Angular Distribution of Scattering Function -- Experimental Data

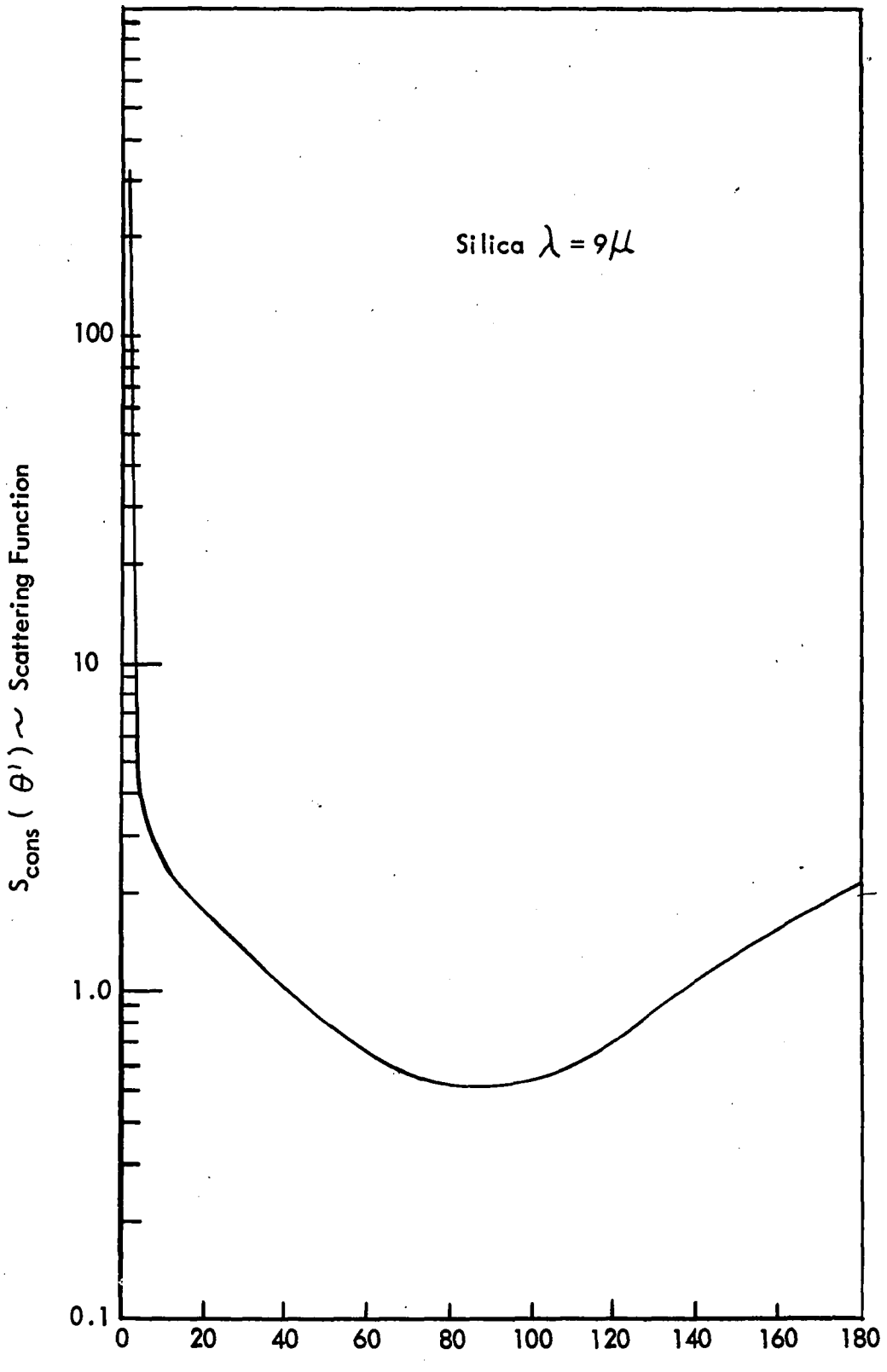

Figure 111
Angular Distribution of Scattering
Function -- Experimental Data

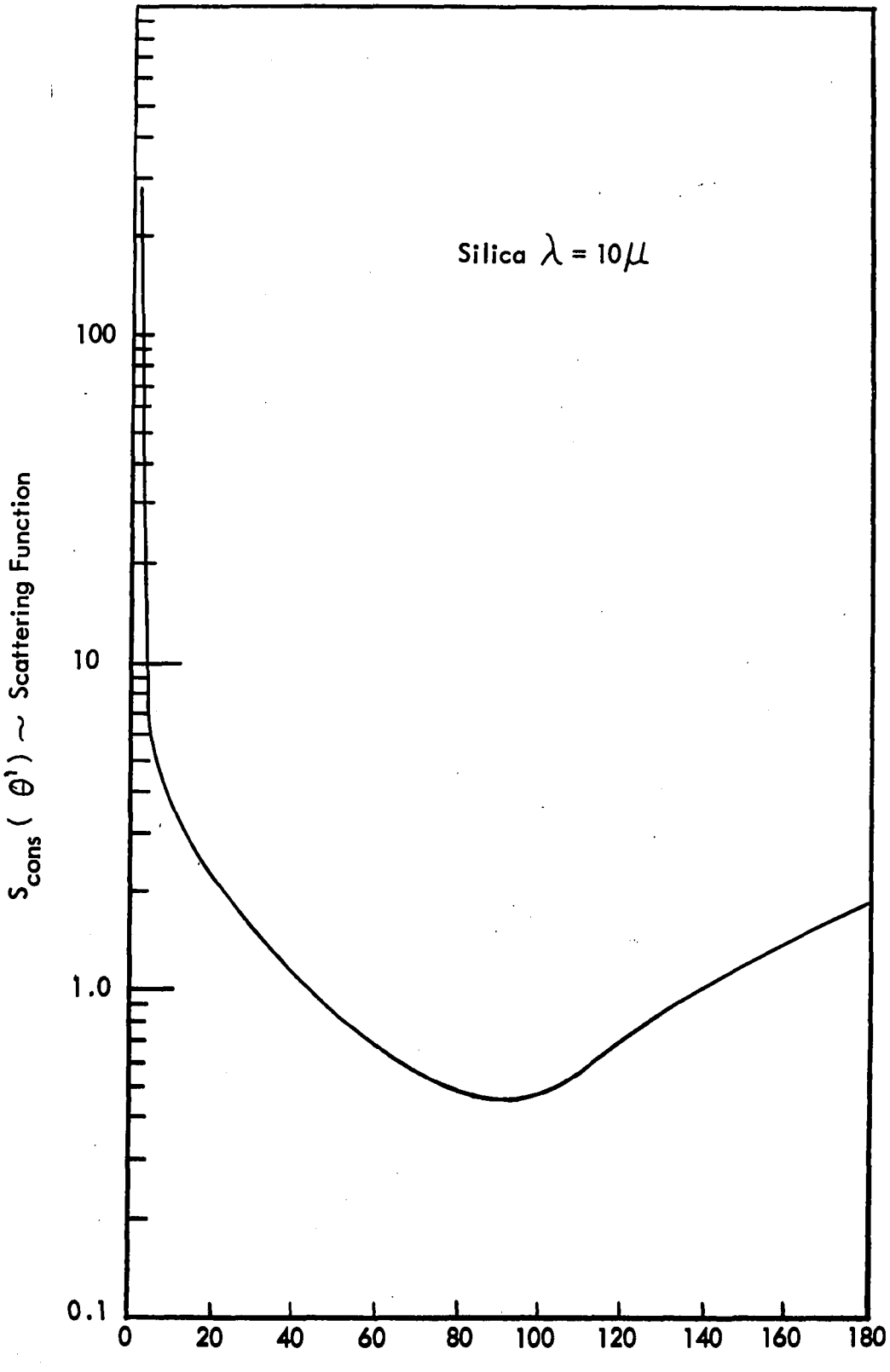

Figure 112

Angular Distribution of Scattering Function -- Experimental Data

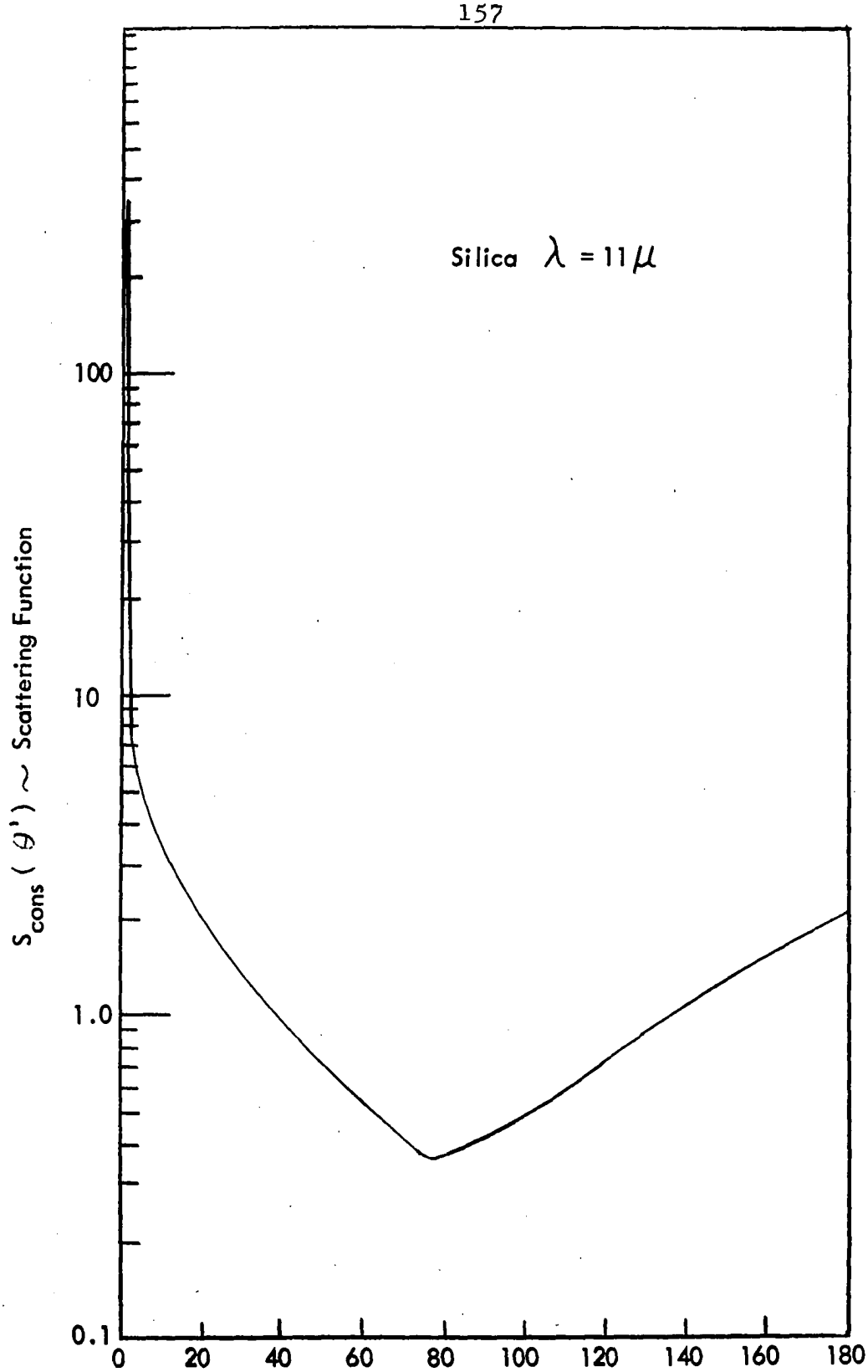

Figure 113
Angular Distribution of Scattering
Function -- Experimental Data

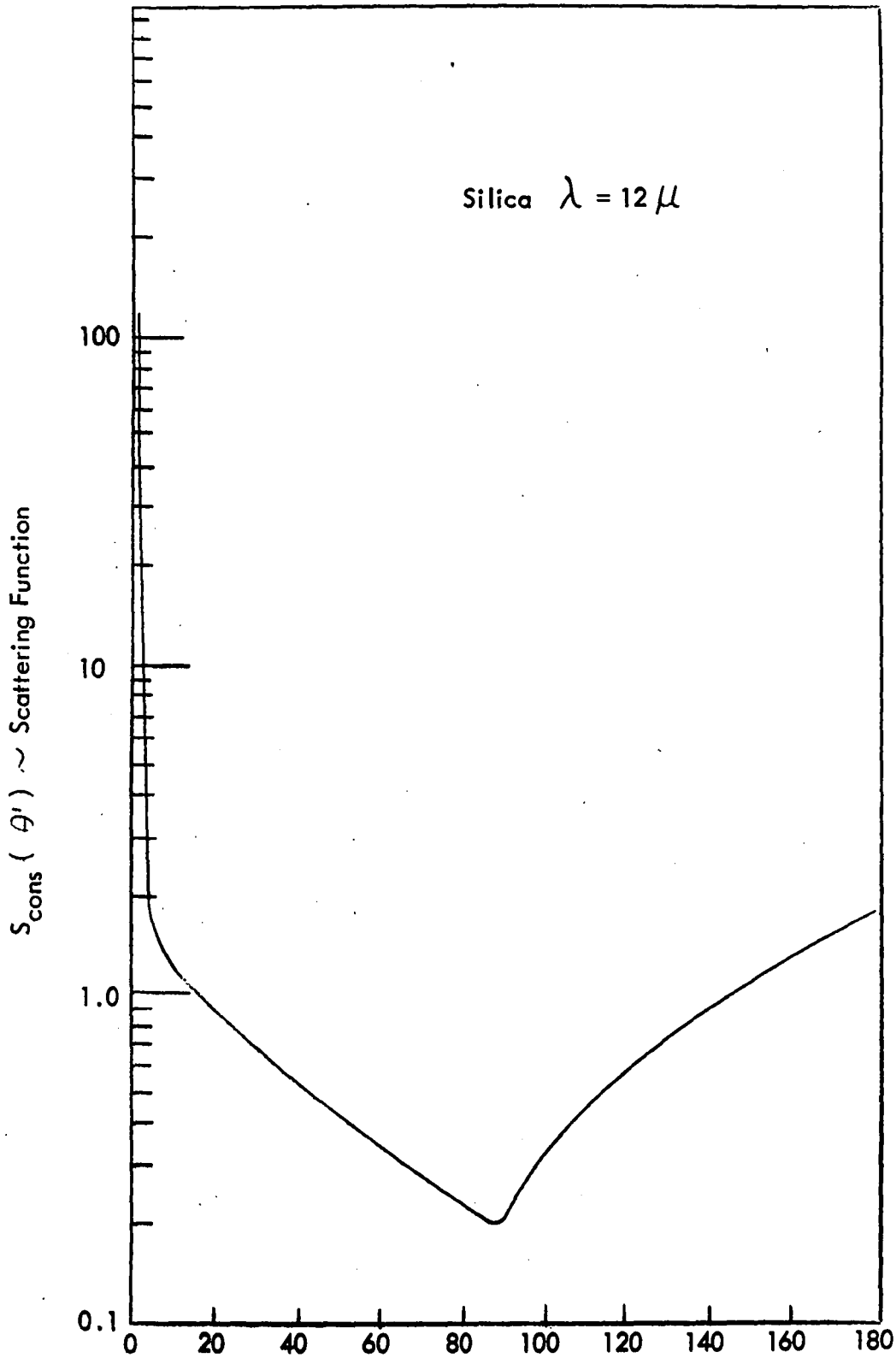

Figure 114
Angular Distribution of Scattering Function -- Experimental Data

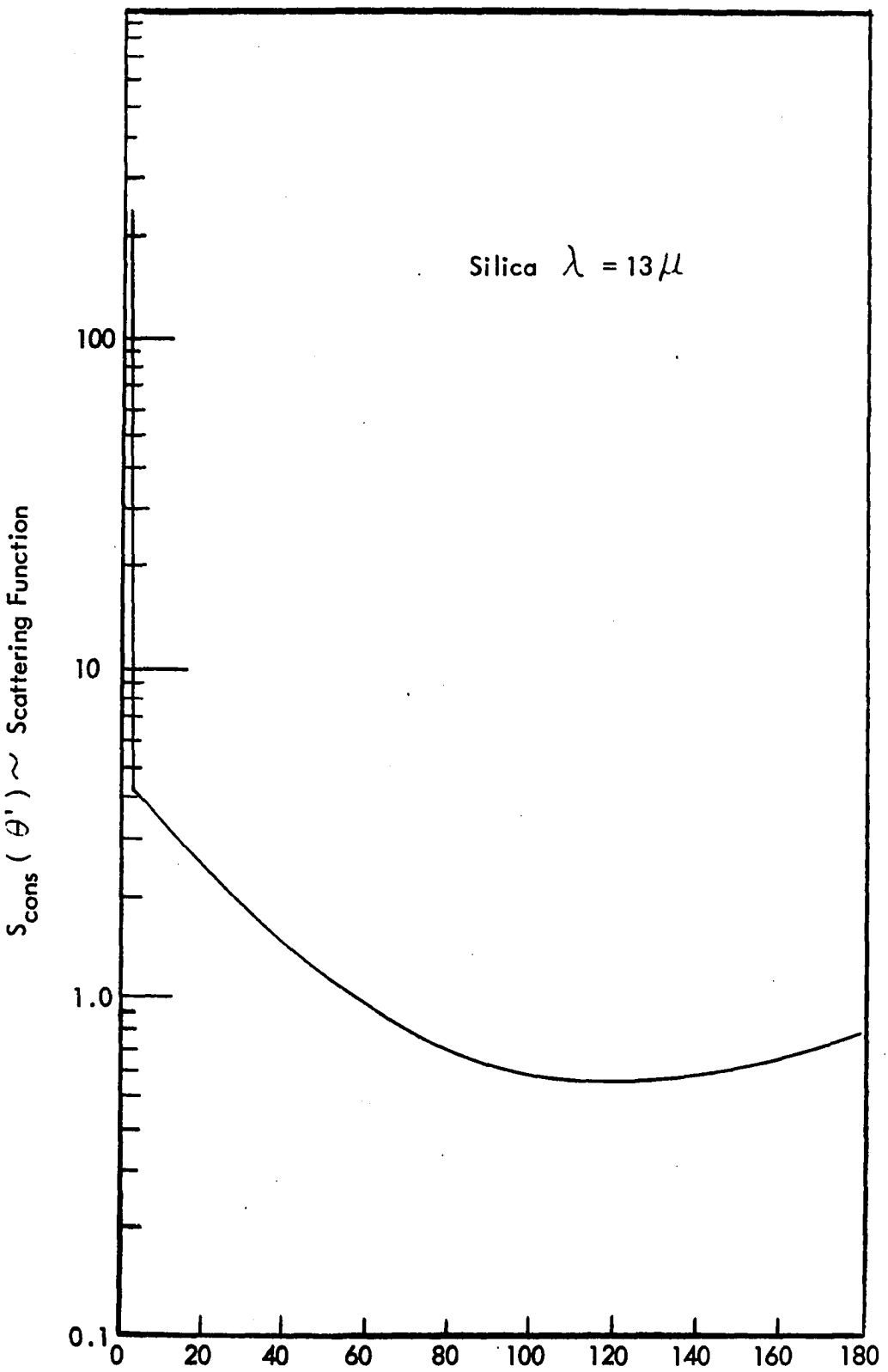

Figure 115
Angular Distribution of Scattering Function -- Experimental Data

CHAPTER VIII

DISCUSSION AND CONCLUSIONS

The mass extinction coefficients were determined by experimental means, and were checked at various times throughout the entire investigation. According to Wheasler (147), for an aluminum powder the mass extinction coefficients should be a constant value of approximately 11,350 ft^2/lbm. This is much higher than the values obtained in this study (see Figure 10). Because of this large difference in the mass extinction coefficients, several runs were made using the exact procedure outlined by Wheasler in an attempt to determine the source of this discrepancy. According to Wheasler a "bell mouth" funnel was used to collect the aerosol powder after it had passed through the ray of incident energy, in order to accurately determine the density of the aerosol. This "bell mouth" funnel was suspended about 10 inches above the aerosol discharge tube. By illuminating the funnel with a high intensity light, one could see that the aerosol had fanned out in such a manner that a large percentage of the aerosol was by-passing the funnel. Using the procedure outlined by Wheasler a mass

extinction coefficient was calculated. The value obtained with this procedure was found to be within 10 per cent of the value reported by Wheasler. It was also found that in removing the filter from the suspended funnel according to Wheasler's procedure, a small portion of the collected powder would fall off of the filter. On account of these sources of error in the density measurements, all density measurements in this investigation were made by placing the filter funnel completely over the aerosol discharge tube, and, after collecting the sample, turning the filter funnel upside down before removing the filter. It should, however, be pointed out that the aluminum powder used throughout this investigation had a different Reynolds batch number than that used by Wheasler.

If a comparison of the experimentally determined mass extinction coefficients is to be made with the Mie theory, one needs to keep in mind that the Mie theory assumes spherical particles having a real index of refraction. If the mass extinction coefficients according to Mie's theory were plotted the curves would show several maxima and minima and these points would decrease in value and eventually become zero as the wave length becomes zero. From Figures 10, 11, it can be seen that the experimental data did not show the maxima and minima predicted by the Mie theory in the longer wave lengths and the following explanation is given. If the refractive index of a scattering medium is

written as a complex number (m = n - ik), the real part (n) of the refractive is the same as m for non-absorbing particles. Then according to Van de Hulst (144), the imaginary component of the refractive index will dampen out the maxima and minima found in plots of the Mie theory for spherical particles having a real index of refraction.

A search of the existing literature yielded only two plots of the Mie theory for absorbing media containing material used in this investigation. These plots showed the extinction cross-section as a function of the particle size parameter for materials having a complex index of refraction of 2.0 - 0.6 i and 1.25 - 1.25 i which according to Love (89), corresponds roughly to carbon and iron respectively. By plotting the Mie curves for the mass extinction coefficients as a function of wave length, a comparison of the experimental mass extinction coefficients with theory was obtained (see Figure 116) for iron and carbon. This plot shows that for iron, the values of the mass extinction coefficients calculated from theory are approximately equal to an average value of the experimental data and, for the wave length region involved, may be represented as a straight line. However, for the carbon, in the wave length region between 3 and 7 microns the experimental data was higher than the values calculated by the Mie theory. It is conceivable that this deviation was caused by the variation in the particle size because, of all the powders used in this

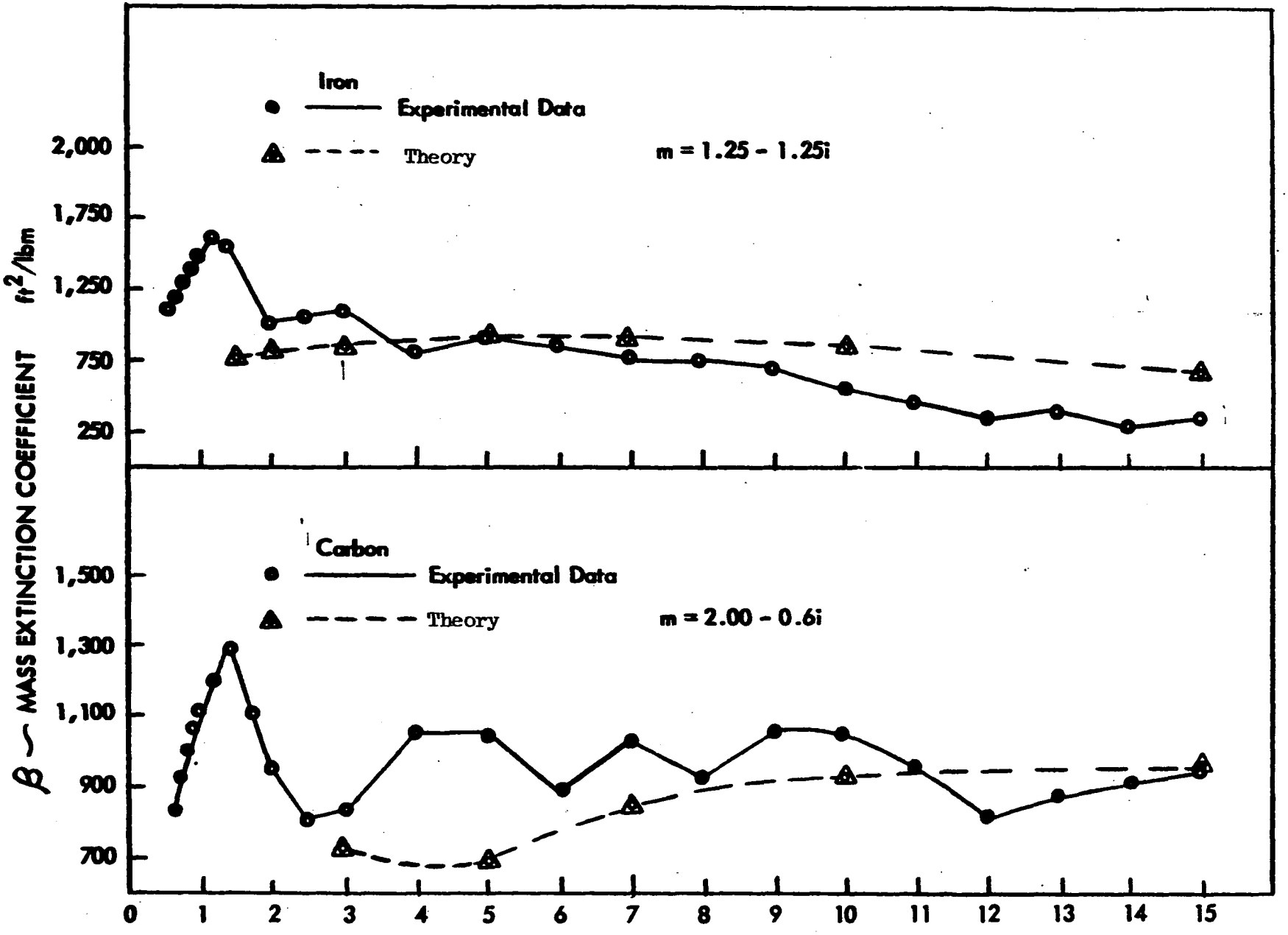
Iron
Experimental Data
Theory
m = 1.25 - 1.25i
2,000
1,750
1,250
750
250
Carbon
Experimental Data
Theory
m = 2.00 - 0.6i
1,500
1,300
1,100
900
700
β — MASS EXTINCTION COEFFICIENT ft²/lbm
0 1 2 3 4 5 6 7 8 9 10 11 12 13 14 15
λ — WAVE LENGTH — MICRONS

Figure 116

investigation, carbon had a greater tendency to pack in the particle generator. This may have caused the average size contained within the aerosol to be larger than the experimentally determined average particle size which was used to calculate the mass extinction coefficients from the Mie theory.

The ratio of the mass scattering coefficient to the mass extinction coefficient indicated that all of the aerosols used in this investigation did contain particles which absorbed energy because the ratio was not equal to unity. The ratio of the mass scattering coefficient to the mass extinction coefficient was essentially a linear function of wave length for all five aerosols within a maximum and minimum deviation of $\pm$ 12 per cent. The function cannot be defined in greater detail because of the experimental precision in the decrease in the incident intensity due scattering.

A plot of the angular distribution of scattered intensity as a function of the scattered angle according to the Mie theory would not be a smooth curve, but would have several maxima and minima, with an increase in the number of maxima and minima as the particle size parameter (α) increased. According to Van de Hulst (144), these maxima and minima do not occur at the same angle for particles of different refractive indicies.

The angular distribution of the scattering functions from the classical Mie theory were calculated for a real

refractive index of 1.6. These results are shown in Figures 117, 118 and for particle size parameter values of 6 and 8, The Mie scattering functions were calculated for angles between 1 and 180 degrees at 5 degree intervals with the aid of tables of the Legendre polynomials (22) and the angular distribution coefficients (17).

A comparison between the angular distribution of the scattering functions plotted from this investigation and the Mie curves shows the same general trends. Also, since the ratio of mass scattering coefficient to the mass extinction coefficient did not equal unity for any of the five powders, the aerosols were absorbers and the index of refraction should be written as a complex number. Van de Hulst (144) states that the imaginary component of the refractive index accounts for the extinction of the incident intensity and will dampen out the maxima and minima found in the Mie theory. Thus, one would intuitively feel that the smooth experimental angular distribution of the scattering functions are a result of the damping component of the index of refraction, and the superposition of changes in the location of the maxima and minima of each individual particle caused by a distribution of particle sizes. In any case, the smooth curves for the conservative scattering functions are consistent with similar work by Hodkinson (67), for the angular distribution of scattered energy from aerosols

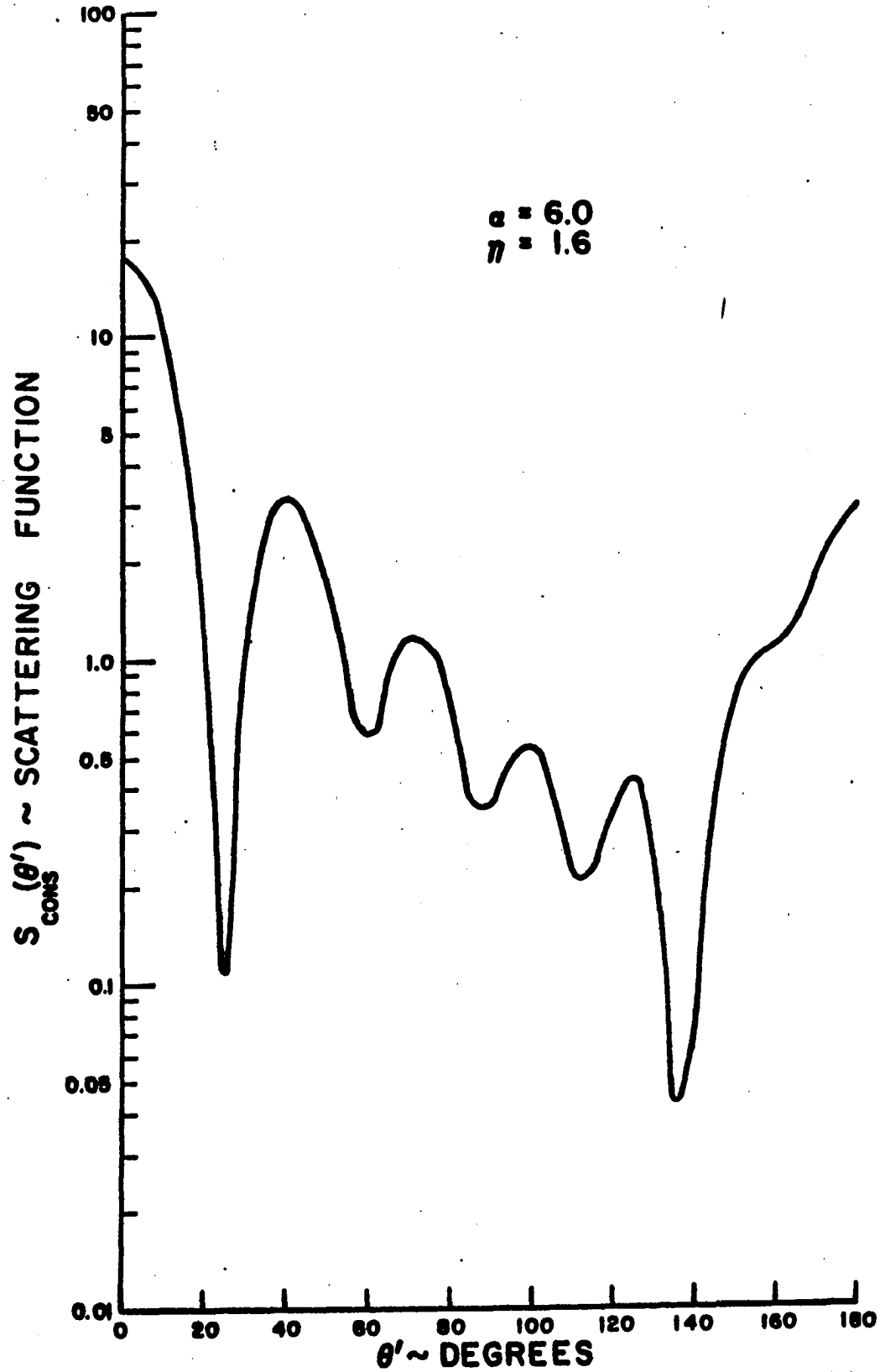

Angular Distribution of Scattering Function-- Theory

Figure 117

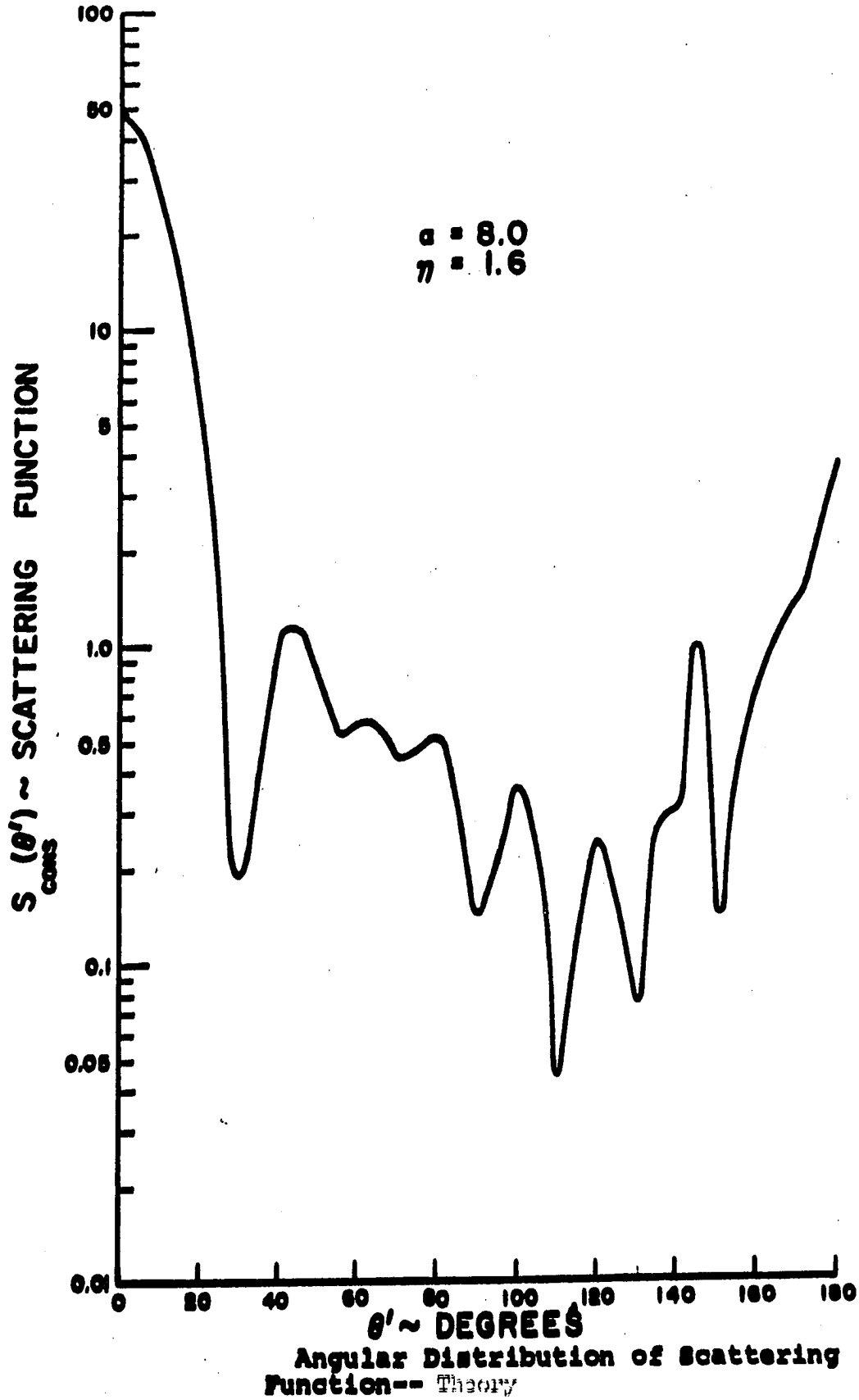

Angular Distribution of Scattering Function-- Theory

Figure 118

of diamond, quartz, and coal dust, all of which have a complex index of refraction.

In figures 24 and 27 through 41 where the solid line represents the experimental data taken in this investigation, and the dashed line that obtained by Wheasler, one can see that the two different sets of data have the same general trends. The scattering functions decrease from a value at $\theta' = 180$ degrees to a minimum value at approximately 90 degrees and then increase to a maximum value at $\theta' = 0$ degrees.

The most significant difference between Wheasler's scattering functions and those obtained in this study was between the scattering angles of 20 and 0 degrees. A portion of this deviation, however, would be caused by the correction procedure required in this region because of the change in gain setting.

The scattering functions calculated from the Mie theory did not change as rapidly in the region for small values of θ as those calculated from the experimental data. The forward scattering was higher for the experiment than predicted by the Mie theory. It is possible that this difference was caused by the use of the fourth order approximation quadrature formula to express the experimental scattering function which may not be adequate in the neighborhood of zero degrees.

In order to make use of the experimental data in

solving the heat transfer equations, there must exist a relationship between $I_s(\mu_i \pm \mu_j)$ and $I_s(\theta')$ in terms of $S(\theta')_{cons}$ or $S(\mu_i \pm \mu_j)_{cons}$ which are known functions ($\mu_i = \cos\theta_i$ and $\mu_j = \cos\theta_j$). The following relationships were developed by Love (89) and were used in calculating the axially-symmetric scattering functions reported by Wheasler (147).

Consider scattering into discrete directions (j) from a particular incident direction (i), then according to Love, the axially-symmetric scattering function is defined as

$$S(\mu_i,\mu_j) = \frac{1}{2}\int_0^{2\pi} S(\Theta_{ij})\, d\phi' \qquad (22)$$

where Θ_{ij} is defined as the angle between the direction of the incident and reflected rays, and from solid geometry

$$\cos\Theta_{ij} = \mu_i\mu_j + (1-\mu_i^2)^{\frac{1}{2}}(1-\mu_j^2)^{\frac{1}{2}}\cos(\phi-\phi'). \qquad (23)$$

Rewriting equation 15 in terms of θ

$$\sigma = \tfrac{1}{4}\int_{-1}^{+1}\int_0^{2\pi} S(\Theta)\, d\phi' d\mu' \qquad (24)$$

but from equation 22, equation 24, now becomes

$$\sigma = \tfrac{1}{2}\int_{-1}^{+1} S(\mu,\mu')\, d\mu' \qquad (25)$$

For the case of conservative scattering, the mass scattering coefficient may be divided out by defining a conservative acially-symmetric scattering function. Thus, equation 25

becomes

$$\tfrac{1}{2}\int_{-1}^{+1} S(\mu,\mu')_{cons}\, d\mu' = 1 \qquad (26)$$

which may be rewritten as

$$\tfrac{1}{2}\left[\int_{o}^{+1} S(\mu,-\mu')_{cons} d\mu' + \int_{o}^{+1} S(\mu,\mu')_{cons} d\mu' = 1.\right. \qquad (27)$$

Now equation 27 may be rewritten in a form suitable for integration by the fourth order approximation method

$$\tfrac{1}{2}\sum_{N=1}^{4} a_j S(\mu_i,\mu_j)_{cons} + \tfrac{1}{2}\sum_{N=1}^{4} a_j S(\mu_i,\mu_j)_{cons} = 1 \qquad (28)$$

where a_j are double Gaussian quadrature weight factors.

Equation 22 was solved using the finite differences where $d\phi = \Delta\phi = 10$ degrees. The values of Φ_{ij} were determined by using values of $\mu_i \pm \mu_j$ as dictated by the fourth order approximation method. The values of $S(\mu_i,\mu_j)_{cons}$ and $S(\mu_i - \mu_j)_{cons}$ for are given in Table 6, while the calculated values of O_{ij} are tabulated in Table 7.

Since $S(\mu_i \pm \mu_j)$ depends upon $S(\Phi_{ij})$, from equation 23 it can be seen that only the positive direction of μ_i need be used since Hemholtz (89) reciprocity law is valid.

$$S(\mu_i,\mu_j) = S(-\mu_i, -\mu_j)$$

$$S(-\mu_i,\mu_j) = S(\mu_i, -\mu_j).$$

The conclusions which may be drawn from this study may be listed as follows:

1. The experimentally determined mass extinction coefficients show a rather different behavior as a function of wave length than the classical Mie theory. The mass extinction coefficients cannot be represented as a straight line as concluded by Wheasler.
2. For the five different powders used in this investigation the ratio of the mass scattering coefficient to the mass extinction coefficient ranged from 0.12 to 0.75 indicating that much of the extinction was caused by absorbtion, which must be included for an accurate energy balance.
3. The experimentally determined axially-symmetric scattering function in contrast to theory was found to be a smooth curve as a function of wave length; the experimental scattering function did not show the maxima or minima predicted by the Mie theory for spherical particles having a real index of refraction. Scattering from irregularly shaped particles having a complex index of refraction will produce smooth curves for the angular distribution of scattered intensity as a function of the scattering angle.
4. For all five powders the extinction of the clouds was linear in cloud density, indicating that single scattering phenomenon exists up to an optical depths of 0.09 for these materials.

TABLE 1

ANGULAR DISTRIBUTION OF SCATTERING FUNCTION, $S_{CONS}(\theta')$
BASED ON EXPERIMENTAL ALUMINUM DATA

θ' (In Degrees) --- λ, Wave Length, (In Microns)				
θ'	λ =0.7	λ =0.8	λ =0.9	λ =1.0
2	232.925	241.501	326.918	368.778
4	93.170	103.500	163.459	138.291
6	37.268	55.200	65.383	64.536
8	19.565	28.980	29.059	32.268
10	10.248	17.250	15.982	18.438
12	6.521	10.350	9.081	11.524
14	4.192	6.900	5.811	6.914
16	2.841	4.416	3.814	4.609
18	2.049	3.174	2.542	3.226
20	1.490	2.208	1.888	2.074
30	.726	.724	.617	.518
40	.586	.434	.355	.336
50	.512	.365	.261	.267
60	.465	.345	.214	.230
70	.465	.345	.196	.212
80	.465	.345	.192	.202
90	.465	.345	.192	.205
100	.465	.345	.199	.214
110	.465	.372	.221	.232
120	.465	.414	.257	.262
130	.503	.469	.312	.318
140	.586	.538	.372	.382
150	.726	.648	.444	.460
160	.913	.776	.526	.553
170	1.094	.966	.635	.668
180	1.281	1.207	.744	.806

ALUMINUM TABLE - Continued

θ'	λ =1.2	λ =1.4	λ =2.0	λ =2.5
2	387.224	83.390	701.276	504.180
4	145.209	50.034	35.063	37.813
6	62.923	31.688	17.142	23.528
8	29.041	20.013	10.908	16.806
10	15.488	12.675	7.791	11.764
12	9.196	7.505	4.908	7.730
14	6.389	5.003	3.506	5.714
16	4.549	3.335	2.610	4.033
18	3.291	2.418	2.025	3.109
20	2.323	1.667	1.558	2.352
30	.677	.450	.716	1.008
40	.324	.195	.467	.613
50	.232	.131	.358	.462
60	.193	.101	.307	.386
70	.167	.088	.280	.348
80	.162	.083	.268	.348
90	.164	.083	.268	.365
100	.171	.083	.288	.399
110	.183	.097	.327	.453
120	.208	.125	.389	.520
130	.246	.153	.483	.621
140	.300	.183	.638	.731
150	.387	.216	.857	.861
160	.503	.258	1.168	.987
170	.687	.308	1.402	1.113
180	.948	.366	1.558	1.218

ALUMINUM TABLE - Continued

θ'	λ =3.0	λ =4.0	λ =5.0	λ =6.0
2	651.382	601.421	494.550	77.356
4	45.596	14.677	34.618	18.640
6	26.055	11.169	23.079	10.252
8	19.541	9.737	16.485	7.456
10	14.330	8.305	11.209	5.592
12	11.073	6.586	8.407	4.660
14	8.467	5.298	6.429	3.728
16	6.513	4.295	4.945	3.262
18	5.080	3.293	4.121	2.796
20	3.582	2.577	3.461	2.423
30	.960	.887	1.681	1.399
40	.462	.515	.857	1.048
50	.312	.408	.494	.866
60	.244	.365	.329	.782
70	.214	.350	.260	.726
80	.198	.340	.224	.685
90	.195	.340	.207	.671
100	.205	.357	.211	.689
110	.231	.400	.263	.717
120	.270	.465	.329	.773
130	.323	.536	.403	.838
140	.384	.615	.494	.932
150	.455	.694	.593	1.025
160	.534	.787	.692	1.165
170	.612	.873	.791	1.328
180	.683	.945	.857	1.537

ALUMINUM TABLE - Continued

θ'	λ =7.0	λ =8.0	λ =9.0	λ =10.0
2	387.081	653.858	307.285	224.161
4	9.677	23.776	8.380	7.472
6	6.128	4.279	2.793	2.391
8	4.946	3.150	2.304	2.204
10	4.085	2.615	2.060	2.129
12	3.440	2.258	1.850	2.054
14	3.010	2.021	1.711	2.017
16	2.580	1.812	1.606	1.942
18	2.257	1.664	1.536	1.868
20	2.042	1.486	1.431	1.830
30	1.344	1.010	1.145	1.550
40	1.021	.772	.949	1.344
50	.806	.624	.824	1.154
60	.677	.534	.726	.971
70	.591	.469	.670	.840
80	.537	.430	.628	.724
90	.516	.407	.607	.642
100	.516	.404	.614	.612
110	.521	.416	.649	.620
120	.537	.445	.698	.650
130	.585	.487	.796	.694
140	.677	.540	.921	.765
150	.860	.612	1.075	.859
160	1.075	.698	1.271	.971
170	1.290	.817	1.536	1.120
180	1.478	.921	1.920	1.307

ALUMINUM TABLE - Continued

θ'	λ =11.0	λ =12.0	λ =13.0	λ =14.0	λ =15.0
2	169.214	182.646	230.293	557.598	103.442
4	3.384	6.088	11.514	7.806	9.309
6	2.115	1.715	1.784	1.463	2.224
8	1.861	1.522	1.554	1.254	1.861
10	1.692	1.439	1.439	1.157	1.717
12	1.649	1.397	1.381	1.115	1.634
14	1.607	1.356	1.324	1.073	1.572
16	1.565	1.300	1.266	1.031	1.510
18	1.544	1.245	1.237	1.003	1.448
20	1.501	1.106	1.180	.961	1.406
30	1.311	1.023	.990	.808	1.199
40	1.184	.913	.852	.696	1.034
50	1.057	.816	.765	.606	.918
60	.930	.761	.713	.550	.848
70	.846	.752	.690	.529	.796
80	.786	.761	.685	.515	.765
90	.744	.774	.690	.515	.755
100	.719	.808	.725	.522	.765
110	.723	.844	.771	.557	.786
120	.744	.899	.840	.620	.837
130	.786	.968	.932	.696	.930
140	.846	1.037	1.059	.808	1.055
150	1.057	1.134	1.209	.961	1.230
160	1.078	1.245	1.439	1.157	1.510
170	1.269	1.369	1.669	1.428	1.924
180	1.480	1.522	2.015	1.742	2.586

TABLE 2

ANGULAR DISTRIBUTION OF SCATTERING FUNCTION, $S_{CONS}(\theta')$
BASED ON EXPERIMENTAL CARBON DATA

θ' (In Degrees) --- λ Wave Length, (In Microns)						
θ'	λ =0.7	λ =0.8	λ =0.9	λ =1.0	λ =1.2	λ =1.4
2	1477.120	764.542	339.463	324.651	479.194	114.892
4	23.633	237.271	175.584	146.093	305.868	68.935
6	5.908	39.545	70.233	71.423	61.173	18.382
8	2.363	15.818	30.434	44.369	20.391	7.353
10	1.033	8.436	23.411	27.054	10.195	3.676
12	.590	6.063	12.876	18.396	5.913	2.343
14	.398	3.585	8.193	12.444	3.874	1.608
16	.276	2.109	5.150	8.224	2.650	1.194
18	.214	1.405	3.628	5.627	1.937	.873
20	.166	.817	2.458	4.058	1.427	.689
30	.077	.168	.702	.714	.377	.252
40	.055	.081	.339	.297	.152	.165
50	.045	.055	.210	.156	.088	.126
60	.039	.043	.152	.102	.064	.101
70	.036	.037	.122	.077	.054	.086
80	.035	.034	.110	.064	.050	.079
90	.035	.034	.104	.058	.050	.077
100	.036	.035	.104	.059	.050	.082
110	.039	.037	.108	.062	.050	.096
120	.042	.041	.117	.068	.050	.114
130	.048	.046	.131	.076	.050	.142
140	.056	.052	.152	.087	.054	.179
150	.066	.061	.177	.101	.061	.222
160	.079	.072	.213	.121	.072	.280
170	.096	.085	.263	.144	.089	.353
180	.120	.100	.321	.178	.114	.459

CARBON TABLE - Continued

θ'	λ =2.0	λ =2.5	λ =3.0	λ =4.0	λ =5.0	λ=6.0
2	595.777	1216.240	947.603	956.939	881.817	976.943
4	79.436	27.641	44.819	117.777	77.159	44.120
6	24.824	14.373	25.610	25.027	28.659	23.950
8	17.376	9.729	18.567	14.722	19.840	15.757
10	12.412	7.186	12.805	8.980	12.786	11.345
12	9.631	5.417	8.963	6.624	9.259	8.193
14	7.745	4.201	6.658	4.858	6.834	6.176
16	6.156	3.261	4.994	3.754	5.290	4.538
18	5.163	2.598	3.841	3.018	4.188	3.403
20	4.269	2.045	2.945	2.429	3.306	2.584
30	1.638	.729	.960	.883	1.036	.756
40	.714	.298	.396	.360	.363	.321
50	.317	.129	.185	.154	.154	.176
60	.142	.058	.092	.069	.072	.109
70	.068	.033	.059	.033	.037	.078
80	.050	.023	.046	.016	.018	.064
90	.047	.019	.040	.011	.010	.059
100	.051	.019	.038	.010	.011	.055
110	.075	.022	.039	.009	.014	.061
120	.099	.026	.039	.009	.020	.069
130	.126	.031	.040	.010	.027	.078
140	.158	.038	.042	.012	.035	.088
150	.193	.045	.044	.014	.047	.102
160	.233	.052	.046	.018	.058	.116
170	.278	.059	.048	.020	.069	.132
180	.332	.066	.051	.023	.077	.148

CARBON TABLE - Continued

θ'	λ =7.0	λ =8.0	λ =9.0	λ =10.0	λ =11.0	λ =12.0
2	999.318	792.037	428.655	543.832	475.885	107.766
4	34.976	51.099	37.822	39.276	29.327	41.204
6	17.987	22.994	16.137	16.919	17.707	25.356
8	11.492	14.052	11.598	10.574	13.003	17.115
10	7.994	10.219	8.825	8.157	9.960	12.551
12	5.995	7.409	7.060	6.646	8.023	10.142
14	4.496	5.748	5.799	5.438	6.363	7.860
16	3.397	4.471	4.790	4.531	5.256	6.719
18	2.698	3.704	4.160	3.927	4.316	5.705
20	2.048	2.938	3.656	3.398	3.652	4.817
30	.799	1.277	2.118	1.812	1.743	2.377
40	.424	.728	1.412	1.087	1.106	1.445
50	.269	.447	1.071	.755	.802	.938
60	.179	.300	.844	.558	.622	.709
70	.134	.217	.680	.438	.509	.583
80	.124	.169	.554	.355	.431	.507
90	.124	.140	.460	.302	.376	.450
100	.124	.120	.390	.268	.337	.412
110	.124	.106	.327	.241	.309	.380
120	.124	.095	.282	.226	.287	.361
130	.124	.089	.231	.214	.271	.348
140	.124	.085	.191	.208	.260	.335
150	.124	.083	.179	.200	.249	.327
160	.124	.080	.171	.196	.243	.316
170	.124	.079	.163	.193	.240	.316
180	.124	.078	.156	.191	.237	.316

TABLE 3

ANGULAR DISTRIBUTION OF SCATTERING FUNCTION, $S_{CONS}(\theta')$
BASED ON EXPERIMENTAL GLASS BEAD DATA

θ' (In Degrees) --- λ, Wave Length, (In Microns)				
θ'	λ =0.8	λ =0.9	λ =1.0	λ =1.2
2	146.013	150.383	33.027	14.633
4	9.990	15.038	21.423	4.572
6	4.918	3.508	14.282	2.743
8	3.073	1.754	9.818	2.423
10	2.305	1.679	7.141	2.286
12	1.882	1.604	5.355	2.194
14	1.729	1.553	4.016	2.057
16	1.575	1.493	3.481	1.966
18	1.490	1.453	3.124	1.874
20	1.414	1.383	2.633	1.755
30	1.152	1.178	1.472	1.371
40	.968	1.002	.959	1.088
50	.853	.862	.723	.868
60	.768	.761	.598	.704
70	.707	.681	.535	.585
80	.676	.621	.517	.567
90	.668	.601	.544	.606
100	.683	.631	.624	.667
110	.737	.741	.740	.786
120	.829	.872	.892	.932
130	.952	1.002	1.048	1.134
140	1.121	1.178	1.249	1.408
150	1.337	1.403	1.495	1.792
160	1.575	1.654	1.785	2.286
170	1.921	1.929	2.097	3.018
180	2.305	2.255	2.454	4.115

GLASS BEAD TABLE - Continued

θ'	λ =1.4	λ =2.0	λ =2.5	λ =3.0
2	10.976	1013.120	612.684	200.405
4	4.077	112.569	61.268	17.368
6	3.214	56.284	8.169	12.024
8	2.822	3.489	5.003	9.352
10	2.665	2.814	4.084	7.682
12	2.587	2.363	3.369	6.847
14	2.469	2.026	2.961	6.145
16	2.352	1.834	2.654	5.544
18	2.234	1.688	2.450	5.210
20	2.116	1.575	2.195	4.809
30	1.685	1.103	1.347	3.340
40	1.379	.585	.898	1.736
50	1.113	.247	.622	.835
60	.925	.099	.469	.487
70	.784	.041	.372	.327
80	.689	.027	.316	.252
90	.650	.026	.285	.217
100	.658	.028	.275	.207
110	.697	.039	.285	.227
120	.784	.064	.316	.283
130	.901	.105	.362	.414
140	1.082	.168	.439	.661
150	1.332	.270	.551	1.035
160	1.693	.422	.717	1.603
170	2.195	.630	.959	2.338
180	2.901	.844	1.286	3.006

GLASS BEAD TABLE - Continued

θ'	λ =4.0	λ =5.0	λ =6.0	λ =7.0
2	734.447	524.173	600.530	698.187
4	128.528	62.900	112.599	89.766
6	47.739	22.015	26.273	12.966
8	2.033	10.483	6.001	6.383
10	9.180	6.080	4.203	3.989
12	4.039	4.507	3.115	2.094
14	2.717	3.564	2.477	1.496
16	2.019	2.987	2.026	1.196
18	1.579	2.516	1.688	1.017
20	1.230	2.253	1.426	.927
30	.495	1.441	.750	.698
40	.246	.985	.495	.553
50	.150	.702	.382	.448
60	.115	.492	.322	.379
70	.099	.351	.296	.334
80	.089	.267	.285	.309
90	.088	.235	.289	.299
100	.091	.225	.300	.309
110	.102	.235	.326	.329
120	.124	.262	.360	.359
130	.157	.340	.405	.398
140	.227	.456	.465	.448
150	.367	.608	.547	.523
160	.605	.796	.645	.598
170	.991	.995	.788	.658
180	1.468	1.153	.938	.678

GLASS BEAD TABLE - Continued

θ'	λ =8.0	λ =9.0	λ =10.0	λ =11.0
2	398.175	357.801	11.757	169.532
4	14.220	32.955	7.944	8.476
6	4.834	4.237	.111	1.864
8	2.730	1.600	.044	1.661
10	2.218	1.553	.039	1.576
12	1.933	1.506	.037	1.508
14	1.763	1.459	.036	1.432
16	1.649	1.388	.034	1.373
18	1.535	1.365	.034	1.305
20	1.422	1.294	.033	1.254
30	1.023	1.106	.029	1.017
40	.839	.941	.025	.847
50	.696	.838	.023	.720
60	.597	.725	.021	.644
70	.540	.640	.020	.601
80	.500	.574	.020	.584
90	.489	.508	.020	.601
100	.500	.499	.021	.635
110	.551	.517	.023	.703
120	.639	.580	.026	.805
130	.796	.706	.028	.932
140	.981	.866	.032	1.101
150	.011	1.082	.037	1.339
160	.014	1.294	.042	1.644
170	.017	1.530	.050	2.034
180	.019	1.765	.060	2.542

TABLE 4

ANGULAR DISTRIBUTION OF SCATTERING FUNCTION, $S_{CONS}(\theta')$
BASED ON EXPERIMENTAL IRON DATA

θ' (In Degrees) ---λ, Wave Length, (In Microns)						
θ'	λ =0.6	λ =0.7	λ =0.8	λ =0.9	λ =1.0	λ =1.2
2	157.455	111.474	160.857	119.622	87.859	39.151
4	31.491	44.589	80.428	69.013	61.501	29.879
6	19.524	25.267	46.648	41.407	41.001	22.666
8	15.115	15.606	29.758	27.605	27.822	16.897
10	11.966	10.775	19.302	17.943	19.768	13.600
12	9.132	8.174	13.270	12.882	15.375	10.715
14	7.557	6.131	9.651	9.201	11.714	8.860
16	5.668	4.830	7.238	7.131	9.152	7.418
18	4.408	4.087	5.308	5.751	7.321	6.181
20	3.401	3.344	4.182	4.600	5.857	5.151
30	1.259	1.412	1.648	1.978	2.123	2.575
40	.677	.928	.884	1.081	1.006	1.442
50	.535	.743	.554	.667	.658	.927
60	.478	.650	.390	.460	.453	.638
70	.459	.603	.309	.345	.336	.484
80	.459	.566	.269	.280	.270	.412
90	.478	.557	.249	.257	.241	.412
100	.510	.549	.249	.262	.234	.412
110	.566	.557	.261	.285	.248	.412
120	.629	.575	.285	.326	.278	.412
130	.724	.613	.321	.372	.325	.453
140	.850	.622	.373	.427	.373	.463
150	1.007	.724	.442	.483	.431	.618
160	1.228	.789	.538	.552	.490	.824
170	1.464	.882	.667	.621	.549	1.133
180	1.637	1.021	.844	.706	.593	1.545

IRON TABLE - Continued

θ'	λ =1.4	λ =2.0	λ =2.5	λ =3.0	λ =4.0
2	21.907	343.625	148.013	213.148	625.119
4	17.170	27.490	11.841	10.657	25.004
6	13.617	11.454	5 180	7.389	2.083
8	10.953	8.476	4.440	5.683	1.458
10	8.881	6.872	3.996	4.547	1.250
12	7.401	5.612	3.515	4.120	1.187
14	6.216	4.810	3.256	3.765	1.125
16	5.328	4.352	2.960	3.339	1.083
18	4.618	3.951	2.738	3.126	1.021
20	3.907	3.665	2.516	2.913	.968
30	2.072	2.176	1.776	2.060	.729
40	1.243	1.259	1.332	1.492	.583
50	.858	.755	1.036	1.094	.487
60	.651	.486	.814	.781	.416
70	.556	.349	.658	.596	.375
80	.526	.263	.562	.461	.451
90	.521	.263	.518	.390	.343
100	.532	.263	.540	.412	.406
110	.580	.326	.636	.476	.500
120	.666	.412	.740	.568	.614
130	.799	.509	.858	.696	.739
140	.932	.618	1.006	.881	.885
150	1.095	.744	1.169	1.108	1.041
160	1.272	.881	1.346	1.406	1.208
170	1.450	1.030	1.554	1.776	1.375
180	1.628	1.202	1.739	2.273	1.521

IRON TABLE - Continued

θ'	λ =5.0	λ =6.0	λ =7.0	λ =8.0	λ =9.0
2	560.298	172.555	125.651	247.379	232.318
4	42.022	1.984	1.884	76.962	7.494
6	3.501	1.725	1.633	13.193	2.697
8	2.241	1.617	1.507	2.968	2.360
10	1.848	1.531	1.429	1.924	2.135
12	1.624	1.488	1.350	1.484	2.023
14	1.512	1.445	1.319	1.264	1.985
16	1.358	1.380	1.256	1.044	1.873
18	1.302	1.337	1.209	.934	1.798
20	1.232	1.294	1.162	.852	1.761
30	.966	1.100	1.036	.659	1.438
40	.784	.959	.910	.577	1.199
50	.630	.851	.816	.533	.974
60	.532	.776	.722	.511	.794
70	.448	.722	.678	.511	.637
80	.385	.701	.628	.511	.502
90	.350	.701	.628	.522	.457
100	.378	.733	.706	.549	.464
110	.462	.793	.841	.687	.509
120	.546	.862	.973	.824	.659
130	.658	.981	1.162	.989	.936
140	.770	1.121	1.350	1.154	1.180
150	.903	1.294	1.570	1.319	1.386
160	1.050	1.509	1.790	1.511	1.611
170	1.204	1.725	2.073	1.731	1.836
180	1.344	1.941	2.355	1.979	2.135

IRON TABLE - Continued

θ'	λ =10.0	λ =11.0	λ =12.0	λ =13.0	λ =14.0
2	109.072	129.193	160.754	129.635	96.759
4	2.545	3.229	2.592	2.592	2.287
6	1.963	2.390	2.160	2.074	2.199
8	1.745	2.099	1.901	1.944	2.067
10	1.636	1.873	1.771	1.851	1.979
12	1.563	1.744	1.642	1.780	1.891
14	1.490	1.614	1.555	1.728	1.803
16	1.439	1.518	1.477	1.685	1.741
18	1.388	1.453	1.417	1.598	1.671
20	1.345	1.388	1.348	1.555	1.583
30	1.181	1.149	1.106	1.296	1.319
40	.981	1.001	.924	1.080	1.090
50	.836	.904	.812	.907	.932
60	.727	.839	.734	.743	.818
70	.618	.807	.682	.622	.747
80	.530	.791	.648	.544	.694
90	.465	.775	.630	.553	.677
100	.545	.794	.656	.596	.694
110	.676	.826	.717	.682	.756
120	.872	.888	.864	.812	.844
130	1.145	.952	1.071	.993	.967
140	1.454	1.033	1.296	1.296	1.143
150	1.654	1.130	1.503	1.685	1.389
160	1.817	1.259	1.728	1.944	1.759
170	2.072	1.434	2.031	2.938	2.067
180	2.363	1.614	2.376	4.148	2.418

TABLE 5

ANGULAR DISTRIBUTION OF SCATTERING FUNCTION, $S_{CONS}(\theta')$
BASED ON EXPERIMENTAL SILICA DATA

θ' (In Degrees) --- λ, Wave Length, (In Microns)					
θ'	λ =0.7	λ =0.8	λ =0.9	λ =1.0	λ =1.2
2	167.145	91.492	101.002	83.354	196.542
4	88.488	36.596	45.450	55.141	123.907
6	44.244	23.003	25.250	39.753	74.771
8	25.563	15.161	16.917	30.456	46.999
10	17.206	11.763	12.625	23.723	29.908
12	11.798	9.149	9.216	18.594	19.227
14	8.848	7.319	7.322	14.747	12.818
16	6.882	6.012	5.933	11.861	8.545
18	5.505	5.228	5.050	9.938	5.981
20	4.424	4.443	4.418	7.694	4.272
30	2.064	2.169	2.525	2.885	.608
40	1.106	1.150	1.590	1.346	.293
50	.629	.653	.883	.705	.187
60	.417	.437	.492	.378	.138
70	.309	.333	.315	.227	.111
80	.250	.282	.244	.157	.092
90	.226	.261	.220	.121	.081
100	.216	.294	.242	.105	.082
110	.221	.379	.277	.105	.102
120	.240	.535	.334	.110	.132
130	.270	.731	.441	.118	.166
140	.319	.980	.631	.131	.207
150	.393	1.241	.959	.153	.256
160	.506	1.516	1.439	.189	.320
170	.688	1.777	2.020	.237	.405
180	.983	2.012	2.840	.304	.512

SILICA TABLE - Continued

θ'	λ =1.4	λ =2.0	λ =2.5	λ =3.0	λ =4.0
2	223.741	528.698	490.171	956.858	206.143
4	80.547	110.145	53.918	150.363	38.480
6	34.008	14.979	29.410	4.647	16.491
8	17.004	9.692	14.705	3.349	11.406
10	10.739	7.489	8.332	2.870	9.070
12	7.159	6.168	5.391	2.460	7.558
14	5.011	5.507	4.166	2.050	6.596
16	3.579	4.736	3.284	1.777	5.772
18	2.774	4.317	2.744	1.571	5.084
20	2.192	3.700	2.377	1.366	4.466
30	1.073	1.894	1.323	.738	2.611
40	.733	1.101	.833	.444	1.717
50	.554	.682	.588	.293	1.126
60	.434	.436	.460	.201	.755
70	.340	.273	.392	.150	.535
80	.272	.185	.357	.118	.391
90	.228	.140	.343	.100	.302
100	.223	.127	.340	.090	.257
110	.259	.143	.343	.086	.250
120	.313	.165	.352	.086	.274
130	.371	.187	.367	.090	.308
140	.456	.213	.382	.095	.412
150	.563	.240	.406	.103	.501
160	.698	.270	.431	.114	.611
170	.886	.299	.460	.128	.728
180	1.118	.326	.502	.143	.852

SILICA TABLE - Continued

θ'	λ =5.0	λ =6.0	λ =7.0	λ =8.0	λ =9.0
2	336.216	370.589	376.234	294.862	325.272
4	73.090	9.264	11.287	10.952	5.322
6	22.219	6.882	8.230	8.087	3.548
8	15.495	5.558	6.584	6.571	2.907
10	10.817	4.764	5.173	5.223	2.562
12	7.747	4.076	4.279	4.296	2.267
14	5.847	3.600	3.527	3.538	2.119
16	4.677	3.229	3.009	2.948	1.971
18	3.946	2.911	2.633	2.527	1.823
20	3.289	2.647	2.257	2.148	1.700
30	1.988	1.852	1.269	1.179	1.232
40	1.315	1.217	.893	.791	.936
50	.803	.820	.719	.606	.749
60	.555	.608	.623	.513	.620
70	.409	.497	.590	.459	.551
80	.321	.463	.552	.433	.512
90	.277	.444	.540	.438	.502
100	.254	.463	.550	.480	.522
110	.248	.497	.564	.589	.581
120	.257	.529	.587	.732	.719
130	.289	.595	.634	.884	.867
140	.336	.675	.691	1.095	1.059
150	.380	.780	.775	1.347	1.256
160	.438	.910	.870	1.600	1.503
170	.511	1.085	.987	1.895	1.774
180	.584	1.270	1.128	2.106	2.094

SILICA TABLE - Continued

θ'	λ =10.0	λ =11.0	λ =12.0	λ =13.0
2	270.543	326.615	114.769	236.052
4	6.550	6.124	1.809	4.248
6	4.983	4.593	1.456	3.855
8	4.200	3.827	1.324	3.619
10	3.559	3.470	1.191	3.344
12	3.168	3.215	1.147	3.147
14	2.847	2.908	1.081	2.950
16	2.598	2.653	1.015	2.753
18	2.349	2.449	.957	2.596
20	2.135	2.245	.904	2.439
30	1.459	1.428	.670	1.849
40	1.103	.949	.520	1.416
50	.854	.673	.406	1.140
60	.684	.520	.326	.944
70	.569	.428	.269	.806
80	.498	.382	.225	.692
90	.455	.428	.216	.633
100	.469	.500	.308	.597
110	.583	.612	.459	.578
120	.711	.734	.600	.566
130	.854	.887	.732	.574
140	.996	1.071	.882	.590
150	1.174	1.275	1.059	.621
160	1.388	1.531	1.280	.660
170	1.601	1.786	1.500	.708
180	1.868	2.041	1.765	.786

TABLE 6

INTEGRATED AXIALLY-SYMMETRIC SCATTERING FUNCTIONS
FOR DISCRETE POSITIONS AND WAVE LENGTHS (λ)
BASED ON EXPERIMENTAL ALUMINUM DATA

Wave Length	Integrated Functions			
λ	$s(\mu_1, \mu_1,)$	$s(\mu_1, \mu_2,)$	$s(\mu_1, \mu_3,)$	$s(\mu_1,, \mu_4,)$
0.6	13.250	0.802	0.537	0.479
0.7	14.200	0.746	0.510	0.455
0.8	14.050	0.770	0.405	0.342
0.9	23.450	0.653	0.269	0.203
1.0	25.350	0.695	0.264	0.217
1.2	24.800	0.655	0.279	0.174
1.4	6.660	0.458	0.134	0.089
2.0	37.700	0.713	0.390	0.288
2.5	27.500	0.982	0.500	0.376
3.0	35.500	0.982	0.302	0.209
4.0	32.600	0.947	0.461	0.356
5.0	27.550	1.073	0.418	0.243
6.0	5.740	1.060	0.800	0.700
7.0	20.950	0.952	0.667	0.545
8.0	35.400	0.721	0.528	0.431
9.0	17.200	0.927	0.744	0.628
10.0	17.800	1.015	0.909	0.725
11.0	9.900	0.992	0.924	0.778
12.0	10.625	0.941	0.844	0.778
13.0	13.550	0.940	0.797	0.703
14.0	30.150	0.737	0.613	0.530
15.0	6.550	1.054	0.892	0.787

TABLE 6 --- Continued

Wave Length	Integrated Functions			
λ	$s(\mu_1,-\mu_1')$	$s(\mu_1,-\mu_2')$	$s(\mu_1,-\mu_3')$	$s(\mu_1,-\mu_4')$
0.6	1.345	0.662	0.553	0.486
0.7	1.253	0.629	0.502	0.454
0.8	2.255	0.572	0.402	0.354
0.9	2.005	0.368	0.257	0.219
1.0	2.325	0.382	0.262	0.220
1.2	1.530	0.382	0.220	0.173
1.4	1.088	0.239	0.127	0.091
2.0	1.032	0.598	0.352	0.302
2.5	1.351	0.733	0.496	0.396
3.0	1.495	0.511	0.275	0.202
4.0	1.125	0.644	0.457	0.369
5.0	1.105	0.729	0.372	0.249
6.0	1.295	0.975	0.798	0.697
7.0	1.075	0.842	0.637	0.527
8.0	0.781	0.652	0.505	0.420
9.0	1.015	0.807	0.741	0.625
10.0	1.032	0.990	0.817	0.683
11.0	1.022	0.974	0.848	0.653
12.0	0.985	0.945	0.842	0.792
13.0	1.005	0.937	0.811	0.720
14.0	0.813	0.746	0.621	0.539
15.0	1.163	1.055	0.895	0.787

TABLE 6 --- Continued

Wave Length	Integrated Functions			
λ	$s(\mu_2,\mu_1)$	$s(\mu_2,\mu_2)$	$s(\mu_2,\mu_3)$	$s(\mu_2,\mu_4)$
0.6	0.802	13.200	0.600	0.492
0.7	0.746	13.520	0.584	0.471
0.8	0.770	14.030	0.453	0.347
0.9	0.653	18.580	0.387	0.213
1.0	0.695	20.750	0.342	0.228
1.2	0.655	21.650	0.342	0.186
1.4	0.458	5.300	0.219	0.100
2.0	0.713	37.550	0.443	0.345
2.5	0.982	27.500	0.620	0.383
3.0	0.982	35.450	0.489	0.234
4.0	0.947	32.550	0.572	0.391
5.0	1.073	27.550	0.684	0.311
6.0	1.060	5.230	0.916	0.739
7.0	0.952	21.550	0.802	0.623
8.0	0.721	35.450	0.624	0.488
9.0	0.927	17.150	0.781	0.674
10.0	1.015	18.250	0.921	0.854
11.0	0.992	9.860	0.934	0.855
12.0	0.941	10.600	0.821	0.774
13.0	0.940	12.950	0.807	0.714
14.0	0.737	30.100	0.633	0.546
15.0	1.054	6.480	0.926	0.830

TABLE 6 --- Continued

Wave Length	Integrated Functions			
λ	$s(\mu_2,-\mu_1)$	$s(\mu_2,-\mu_2)$	$s(\mu_2,-\mu_3)$	$s(\mu_2,-\mu_4)$
0.6	0.662	0.632	0.563	0.512
0.7	0.629	0.597	0.516	0.476
0.8	0.572	0.498	0.434	0.383
0.9	0.368	0.332	0.271	0.235
1.0	0.382	0.337	0.299	0.241
1.2	0.382	0.319	0.239	0.196
1.4	0.239	0.169	0.134	0.109
2.0	0.598	0.566	0.475	0.369
2.5	0.733	0.614	0.448	0.469
3.0	0.511	0.363	0.289	0.243
4.0	0.644	0.538	0.474	0.421
5.0	0.729	0.495	0.366	0.283
6.0	0.975	0.903	0.799	0.729
7.0	0.842	0.771	0.627	0.531
8.0	0.652	0.587	0.492	0.429
9.0	0.807	0.898	0.762	0.660
10.0	0.990	0.929	0.786	0.645
11.0	0.974	0.957	0.810	0.747
12.0	0.945	0.945	0.886	0.821
13.0	0.937	0.966	0.874	0.783
14.0	0.746	0.764	0.662	0.584
15.0	1.055	1.092	0.935	0.819

TABLE 6 --- Continued

Wave Length	Integrated Functions			
λ	$s(\mu_3, \mu_1)$	$s(\mu_3, \mu_2)$	$s(\mu_3, \mu_3)$	$s(\mu_3, \mu_4)$
0.6	0.537	0.600	13.800	0.615
0.7	0.510	0.584	14.300	0.599
0.8	0.405	0.453	15.900	0.465
0.9	0.269	0.387	21.000	0.401
1.0	0.264	0.342	23.650	0.356
1.2	0.279	0.342	23.100	0.377
1.4	0.134	0.219	6.080	0.228
2.0	0.390	0.443	37.900	0.461
2.5	0.500	0.620	28.000	0.655
3.0	0.302	0.489	36.200	0.507
4.0	0.461	0.572	32.800	0.586
5.0	0.418	0.684	28.100	0.701
6.0	0.800	0.916	5.430	0.971
7.0	0.667	0.802	21.300	0.821
8.0	0.528	0.624	35.500	0.646
9.0	0.744	0.781	17.200	0.809
10.0	0.909	0.921	19.450	1.178
11.0	0.924	0.934	9.900	1.067
12.0	0.844	0.821	10.530	0.850
13.0	0.797	0.807	13.420	0.835
14.0	0.613	0.633	30.100	0.650
15.0	0.892	0.926	6.480	0.960

TABLE 6 --- Continued

Wave Length	Integrated Functions			
λ	$s(\mu_3,-\mu_1)$	$s(\mu_3,-\mu_2)$	$s(\mu_3,-\mu_3)$	$s(\mu_3,-\mu_4)$
0.6	0.553	0.563	0.690	0.605
0.7	0.502	0.516	0.609	0.550
0.8	0.402	0.434	0.517	0.448
0.9	0.257	0.271	0.332	0.296
1.0	0.262	0.299	0.381	0.311
1.2	0.220	0.239	0.308	0.268
1.4	0.127	0.134	0.171	0.159
2.0	0.352	0.475	0.602	0.451
2.5	0.496	0.448	0.538	0.645
3.0	0.275	0.289	0.331	0.335
4.0	0.457	0.474	0.531	0.532
5.0	0.372	0.366	0.403	0.416
6.0	0.798	0.799	0.860	0.792
7.0	0.637	0.627	0.678	0.625
8.0	0.505	0.492	0.534	0.500
9.0	0.741	0.762	0.827	0.810
10.0	0.817	0.786	0.854	0.720
11.0	0.848	0.810	0.879	0.816
12.0	0.842	0.886	0.965	0.965
13.0	0.811	0.874	0.944	0.929
14.0	0.621	0.662	0.716	0.681
15.0	0.895	0.935	1.008	0.980

Table 6 --- Continued

Wave Length	Integrated Functions			
λ	$s(\mu_4, \mu_1,)$	$s(\mu_4, \mu_2,)$	$s(\mu_4, \mu_3,)$	$s(\mu_4, \mu_4,)$
0.6	0.479	0.492	0.615	20.000
0.7	0.455	0.471	0.599	21.450
0.8	0.342	0.347	0.465	21.050
0.9	0.203	0.213	0.401	35.000
1.0	0.217	0.228	0.356	37.600
1.2	0.174	0.186	0.377	33.900
1.4	0.089	0.100	0.228	8.530
2.0	0.288	0.345	0.461	45.200
2.5	0.376	0.383	0.655	30.750
3.0	0.209	0.234	0.507	39.800
4.0	0.356	0.391	0.586	36.400
5.0	0.243	0.311	0.701	30.550
6.0	0.700	0.739	0.971	6.300
7.0	0.545	0.623	0.821	22.800
8.0	0.431	0.488	0.646	38.100
9.0	0.628	0.674	0.809	18.300
10.0	0.725	0.854	1.178	18.720
11.0	0.778	0.855	1.067	10.300
12.0	0.778	0.774	0.850	11.000
13.00	0.703	0.714	0.835	13.950
14.0	0.530	0.546	0.650	30.650
15.0	0.787	0.830	0.960	7.180

TABLE 6 --- Continued

Wave Length	Integrated Functions			
λ	$s(\mu_4,-\mu_1)$	$s(\mu_4,-\mu_2)$	$s(\mu_4,-\mu_3)$	$s(\mu_4,-\mu_4)$
0.6	0.486	0.512	0.605	0.807
0.7	0.454	0.476	0.550	0.768
0.8	0.354	0.383	0.448	0.661
0.9	0.219	0.235	0.296	0.456
1.0	0.220	0.241	0.311	0.503
1.2	0.173	0.196	0.268	0.458
1.4	0.091	0.109	0.159	0.266
2.0	0.302	0.369	0.451	0.704
2.5	0.396	0.469	0.645	0.965
3.0	0.202	0.243	0.335	0.480
4.0	0.369	0.421	0.532	0.734
5.0	0.249	0.283	0.416	0.574
6.0	0.697	0.729	0.792	1.102
7.0	0.527	0.531	0.625	0.875
8.0	0.420	0.429	0.500	0.704
9.0	0.625	0.660	0.810	1.145
10.0	0.683	0.645	0.720	0.918
11.0	0.653	0.747	0.816	1.145
12.0	0.792	0.821	0.965	1.370
13.0	0.720	0.783	0.929	1.325
14.0	0.539	0.584	0.681	0.980
15.0	0.787	0.819	0.980	1.423

TABLE 7

Φ_{ij} (BASED ON $\Delta\theta = 10^{o}$) FOR DISCRETE POSITIONS OF INCIDENT RAY AND WAY LENGTH

Values of Φ in Degrees									
$\Phi_{1,1}$	$\Phi_{1,-1}$	$\Phi_{1,2}$	$\Phi_{1,-2}$	$\Phi_{1,3}$	$\Phi_{1,-3}$	$\Phi_{1,4}$	$\Phi_{1,-4}$	$\Phi_{2,2}$	$\Phi_{2,-2}$
0	9	15	23	38	46	64	72	0	39
10	19	18	26	39	47	65	73	10	40
20	29	25	30	42	50	66	74	19	43
30	39	33	38	46	53	67	75	28	48
40	49	42	46	52	59	70	78	38	55
50	59	51	54	60	65	73	80	47	62
60	69	60	64	65	71	76	83	57	70
70	77	70	73	73	78	79	86	66	79
80	82	80	82	80	85	83	90	75	88
90	90	89	91	88	92	86	94	84	96
98	100	98	100	95	100	90	97	92	105
103	110	107	110	102	107	94	101	101	114
111	120	116	120	109	115	97	104	110	123
121	130	126	129	115	120	100	107	118	133
131	140	134	138	121	128	102	110	125	142
141	150	142	147	127	134	105	113	132	152
151	160	150	155	130	138	106	114	137	161
161	170	154	162	133	141	107	115	140	170
171	180	157	165	134	142	108	116	141	180

TABLE 7--Continued

Values of Θ in Degrees									
$\Theta_{1,2}$	$\Theta_{2,-3}$	$\Theta_{2,4}$	$\Theta_{2,-4}$	$\Theta_{3,3}$	$\Theta_{3,-3}$	$\Theta_{3,4}$	$\Theta_{3,-4}$	$\Theta_{4,4}$	$\Theta_{4,-4}$
23	55	49	88	0	84	26	110	0	137
24	62	49	88	7	85	27	111	3	137
29	64	51	90	15	86	29	112	7	138
34	68	53	90	22	89	31	113	11	139
41	72	55	93	30	91	34	114	15	140
48	77	58	95	37	96	37	117	18	141
57	83	61	98	44	100	40	119	21	143
63	89	65	101	50	105	44	122	24	145
70	96	68	104	57	111	47	125	27	147
77	103	72	108	63	117	51	129	30	150
84	110	76	112	69	123	55	133	33	153
91	117	79	115	75	130	58	136	35	156
97	123	82	119	80	136	61	140	37	159
103	132	85	122	84	143	63	143	39	162
108	139	87	125	89	150	66	146	40	165
112	146	90	127	91	158	67	149	41	169
116	151	90	129	94	165	68	151	42	173
118	156	92	131	95	173	69	153	43	177
125	157	92	131	96	180	70	154	43	180

TABLE 8

PARTICLE COUNT DATA AND SIZE DATA

ALUMINUM

75 ml. of 95 Per Cent Ethanol
0.1345 gms. Powder

Count of Particles in 16 Squares Section				
40	36	43	39	37
38	38	39	42	38
45	35	35	36	44
32	38	36	33	42
41	49	37	37	43

$$\frac{\text{Average Particles}}{\text{16 Squares}} = 39$$

36	37	37	34	29
34	38	32	32	35
33	38	31	30	38
36	32	34	27	32
40	40	33	31	30

$$\frac{\text{Average Particles}}{\text{16 Squares}} = 34$$

TABLE 8 --- Continued

PARTICLE COUNT DATA AND SIZE DATA

ALUMINUM

108	103	96	120	97
123	140	102	116	87
102	110	110	102	109
93	92	112	98	110
130	93	119	93	113

$$\frac{\text{Average Particles}}{\text{16 Squares}} = 107$$

19	28	12	13	24
16	29	17	21	22
23	16	22	24	16
22	14	26	20	15
17	18	19	18	18

$$\frac{\text{Average Particles}}{\text{16 Squares}} = 20$$

$$\text{Average Powder Constant} = 5.96 \times 10^{9} \frac{\text{Particles}}{\text{Gram}}$$

Particle Size (Micron)

8.0	9.0	7.5	8.0	5.0
9.0	7.5	7.0	6.0	5.5
7.0	8.0	8.0	7.0	9.0
5.0	9.0	5.0	9.0	9.0
9.0	8.0	7.0	9.0	9.5
6.5	7.0	8.0	8.5	11.0

Average Particle Size = 7.8 Micron

TABLE 8 --- Continued

PARTICLE COUNT DATA AND SIZE DATA

CARBON

1	3	3	1
2	4	5	3
1	5	1	1
1	1	4	4

$$\frac{\text{Average Particles}}{\text{16 Squares}} = 2.56$$

$$\text{Average Powder Constant} = \frac{4.9 \times 10^{8} \text{ Particles/Gram}}{\text{Particle Size (Micron)}}$$

30.0	22.5	5.0	5.0	20.0
20.0	5.0	7.5	5.0	15.0
22.5	2.5	20.0	5.0	5.0
15.0	20.0	25.0	2.5	15.0
20.0	7.5	10.0	2.5	7.5
20.0	7.5	17.5	2.5	10.0
22.5	7.5	15.0	2.5	5.0
5.0	7.5	5.0	2.5	10.0
7.5	2.5	5.0	15.0	17.5
12.5	5.0	15.0	17.5	12.5

Average Particle Size 11.245

TABLE 8 --- Continued

PARTICLE COUNT DATA AND SIZE DATA

CARBON

75 ml. of 95 Per Cent Ethanol
0.0976 gms. Powder

Count of Particles in 16 Squares Section			
3	1	2	3
1	1	4	4
2	7	1	2
4	2	5	1
	$\frac{\text{Average Particles}}{\text{16 Squares}}$ = 2.69		
3	4	1	2
1	2	1	3
1	1	2	0
0	1	3	0
	$\frac{\text{Average Particles}}{\text{16 Squares}}$ = 1.50		
2	6	3	2
4	2	2	1
1	4	1	1
0	2	1	3
	$\frac{\text{Average Particles}}{\text{16 Squares}}$ = 2.18		
2	1	0	3
4	1	6	1
6	6	2	1
2	0	0	0
	$\frac{\text{Average Particles}}{\text{16 Squares}}$ 2.18		

TABLE 8 --- Continued

PARTICLE COUNT DATA AND SIZE DATA

IRON

8	8	7	7
7	5	5	4
4	5	6	4
5	5	5	6

$$\frac{\text{Average Particles}}{\text{16 Squares}} = 5.75$$

$$\text{Average Powder Constant} = \frac{7.36 \times 10^{8} \text{ Particles}}{\text{Gram}} \times \text{Particle Size (Micron)}$$

2.0	3.5	4.0	4.5	3.0
2.3	3.5	2.5	2.0	2.5
2.5	4.0	3.0	2.0	3.0
4.0	3.0	3.4	3.0	3.3
3.5	3.3	3.0	3.5	4.0
4.0	3.7	2.7	3.0	2.0

Average Particle Size 3.75 Micron

TABLE 8 --- Continued

PARTICLE COUNT DATA AND SIZE DATA

IRON

75 ml. of 95 Per Cent Ethanol
0.1431 gms. Powder

Count of Particles in 16 Squares Section

10	5	9	3
8	10	4	8
3	3	3	10
4	6	5	9

$$\frac{\text{Average Particles}}{\text{16 Squares}} = 6.2$$

7	5	4	6
5	6	2	5
9	3	5	3
8	8	8	4

$$\frac{\text{Average Particles}}{\text{16 Squares}} = 5.5$$

4	1	5	6
2	4	7	8
3	3	4	5
3	6	6	7

$$\frac{\text{Average Particles}}{\text{16 Squares}} = 4.5$$

TABLE 8 --- Continued

PARTICLE COUNT DATA AND SIZE DATA

SILICA			
4	4	2	5
6	3	3	2
3	6	8	2
5	3	4	6

$$\frac{\text{Average Particles}}{\text{16 Squares}} = 4.125$$

$$\text{Average Powder Constant} = 3.4 \times 10^{8} \frac{\text{Particles}}{\text{Gram}}$$

Particle Size (Micron)

2.5	7.5	7.5	5.0	7.5
2.5	7.5	2.5	5.0	5.0
2.5	2.5	2.5	5.0	12.5
5.0	5.0	12.5	2.5	2.5
3.8	5.0	10.0	2.5	2.5
20.0	12.5	2.5	2.5	15.0
5.0	5.0	2.5	2.5	5.0
2.5	2.5	2.5	2.5	2.5
10.0	5.0	7.5	10.0	10.5
2.5	5.0	5.0	5.0	7.5

Average Particle Size = 5.4 Micron

TABLE 8 --- Continued

PARTICLE COUNT DATA AND SIZE DATA

SILICA

75 ml. of 95 Per Cent Ethanol
0.220 gms. Powder

Count of Particles in 16 Squares Section			
3	7	3	2
4	2	8	5
2	3	5	2
4	3	6	1

$$\frac{\text{Average Particles}}{\text{16 Squares}} = 3.75$$

5	8	2	3
5	5	3	2
5	5	1	3
1	6	3	1

$$\frac{\text{Average Particles}}{\text{16 Squares}} = 3.75$$

2	8	5	1
2	3	2	1
8	6	4	5
10	2	7	2

$$\frac{\text{Average Particles}}{\text{16 Squares}} = 4.25$$

REFERENCES

1. Aden, A. L., and Kerker, M. "Scattering of Electromagnetic Waves from Two Concentric Spheres," J. Appl. Phys., XX (1951), p. 1242.

2. Albini, F. A. "Scattering of a Plane Wave by an Inhomogeneous Sphere under the Born Approximation," J. Appl. Phys., XXX (1962), pp. 3032-3036.

3. American Machine and Foundry Company. "Cloud Chamber Measurements of Visible and Infrared Absorptivity of Aerosols," Infrared Phys., II, 1962 (Report CRL-T-33, 1961).

4. Arnulf, A., and Bricard, J. "Transmission by Haze and Fog in the Spectral Region 0.35 to 10 Microns," J. Opt. Soc. Am., XLVII (1957), pp. 491-498.

5. Askley, T. E., and Coff, C. M. "Single Particle Scattering Function for Latex Spheres in Water," J. Opt. Soc. Am., XLVIII (1958), pp. 261-268.

6. Barnes, R. B. "Notes on the Preparation of Reststrahlen Plates and the Reflection Power of Powders," Phys. Rev., XLVIII (1933), p. 31.

7. Baum, F. J., and Billmeyer, F. W., Jr. "Automatic Photometer for Measuring the Angular Dissymmetry of Light Scattering," J. Opt. Soc. Am., LI (1961), pp. 452-456.

8. Biber, E., and Levy, S. "Spectrographic Procedure for Analysis of Powdered Samples of Unknown Origin," J. Opt. Soc. Am., XLVII (1957), pp. 381-385.

9. Billmeyer, Fred W., Jr. "Measurement of Optical Clarity by Low-Angle Light Scattering," J. Opt. Soc. Am., XLIX (1959), pp. 368-371.

10. Blevin, W. R., and Brown, W. J. "Light-Scattering Properties of Pigment Suspensions," J. Opt. Soc. Am., LI (1961), pp. 975-982.

11. Boll, R. H., Gumprecht, R. O., and Sliepcevich, C. M.. "Theoretical Light-Scattering Coefficients for Relative Refractive Indexes Less than Unity and for Totally Reflecting Spheres," J. Opt. Soc. Am., XLIV (1954), pp. 18-21.

12. Brown, J., and Blevin, W. R. "Total Reflectance of Opague Diffusers," J. Opt. Soc. Am., LII (1962), pp. 1250-1255.

13. Cairns, J. H. "Apparatus for Investigating Total Hemispherical Emissivity," J. Sci. Instr., XXXVII (1960), pp. 84-87.

14. Caulfield, Daniel, and Ullman, Robert. "High-Angle Limit in Low-Angle Scattering and Its Effect on the Determination of Surface Area," J. Appl. Phys., XXXIII (1962), pp. 1737-1740.

15. Chromey, Fred C. "Evaluation of Mie Equations for Colored Spheres," J. Opt. Soc. Am., L (1960), pp. 730-737.

16. Chu, Chiao-Min, Churchill, S. W. "Numerical Solution of Problems in Multiple Scattering of Electromagnetic Radiation," J. Phys. Chem., LIX (1955), pp. 855-863.

17. Chu, Chiao-Min, Churchill, S. W. "Representation of the Angular Distribution of Radiation Scattering by a Spherical Particle," J. Opt, Soc. Am., XLV (1955), pp. 958-962.

18. Churchill, S. W., Clark, G. C., and Sliepcevich, C. M. "Light-Scattering by Very Dense Monodispersions of Latex Particles," Faraday Society Discussions, XXX (1960), pp. 192-199.

19. Ciobanu, G. "The Light Scattering on Hemispherical Particles," Stud. Cercetari Fiz., X (1959), pp. 449-456.

20. Ciobanu, G., Toma, E. "Some Contributions to the Theory of Light Scattering by Systems of Particles," Stud. Cercetari Fiz., X (1959), pp. 825-836.

21. Clark, George C., Chu, Chiao-Min, Churchill, Stuart W. "Angular Distribution Coefficients for Radiation Scattering by a Spherical Particle," J. Opt. Soc. Am., XLVII (1957), pp. 81-84.

22. Clark, George L. The Encyclopedia of Spectroscopy. New York: Reinhold Publishing Corporation, 1961.

23. Clebsch, A. Z. Math., LX (1863), pp. 195-262.

24. Cleveland, E. Lynn, Raymond, Richard. "Scattering of Visible and Near Infrared Radiation by Layered Distributions of Small Metal Spheres," J. Opt. Soc. Am., XLII (1952), pp. 183-186.

25. Clewell, Dayton H. "Scattering of Light by Pigment Particles," J. Opt. Soc. Am., XXXI (1941), pp. 521-527.

26. Crosby, Peter, and Koerber, Brian W. "Scattering of Light in the Lower Atmosphere," J. Opt. Soc. Am., LIII (1963), pp. 358-361.

27. Curcio, Joseph A. "Evaluation of Atmospheric Aerosol Particle Size Distribution from Scattering Measurements in the Visible and Infrared," J. Opt. Soc. Am., LI (1961), pp. 548-551.

28. Curcio, Joseph A., and Petty, C. C. "The Near Infrared Absorption Spectrum of Liquid Water," J. Opt. Soc. Am., XLI (1951), pp. 302-304.

29. Debye, P. Ann. Physik., XXX (1909), pp. 57-136.

30. Deirmendjian, Diran, Sekera, Zdenek. "Quantitative Evaluation of Multiply Scattered and Diffusely Reflected Light in the Direction of a Stellar Source in a Rayleight Atmosphere," J. Opt. Soc. Am., XLIII (1953), pp. 1158-1165.

31. Deirmendjian, Diran. "Temperature Dependence of the Rayleight Scattering Coefficient in the Atmosphere," J. Opt. Soc. Am., XLVIII (1958), p. 1018.

32. Deirmendjian, D., Clasen, R., and Vilzee, W. "Mie Scattering with Complex Index of Refraction," J. Opt. Soc. Am., LI (1961), pp. 620-633.

33. Denisyuk, Yu. N. "Representation of Optical Properties of an Objective by Means of Wave Pattern of Light Scattered by It," Sov. Phys., VII (1962), pp. 543-545.

34. De Vore, J. R. "Optical Scattering by Dielectric Powders of Uniform Particle Size," J. Opt. Soc. Am., XXXVII (1947), pp. 826-832.

35. Downie, A. R., Magoon, M. C., Purcell, Thomasine, and Crawford, Byrce, Jr. "The Calibration of Infrared Prism Spectrometers," J. Opt. Soc. Am., XLIII (1953), pp. 941-951.

36. Ellison, J. McK. "Light Scattering by Polydesperse Dust Clouds," Brit. J. Appl. Phys., Suppl. 3 (1954), pp. 66-71.

37. _____. "The Scattering of Light by Dust and its Application to the Evaluation of Industrial Dust Clouds." Ph.D. Thesis, London University (1954).

38. _____. "Extinction of Light by Suspensions of Silica Dust," Phys. Soc. (London), B 70 (1957), pp. 102-111.

39. _____. "The Forward Scattering of Light by Spheres According to Geometric Optics," Proc. Phys. Soc., LXXIV, Pt. 1 (1959), pp. 105-123.

40. Fedorova, E. O. Optics Inst., XXV (1957).

41. Filler, A. S., and Indyk, L. "Calibration of Infrared Prism Spectrometer," J. Opt. Soc. Am., LI (1961), pp. 572-574.

42. Florence, J. M., Glaze, F. W., and Black, M. H. "Transmission of Near-Infrared Energy by Some Two and Three Component Glasses," J. Res. Nat'l. Bur. Std., L (1953), pp. 187-189.

43. Filler, A. S., and Indyk, L. "Calibration of Infrared Prism Spectrometer," J. Opt. Soc. Am., LI, No. 5 (May, 1961), pp. 572-574.

44. Foster, W. W. "Attenuation of Light by Wood Smoke," Brit. J. Appl. Phys., X (1959), pp. 416-420.

45. Fraser, Robert S. "Computed Intensity and Polarization of Light Scattered Outwards from the Earth and an Overlying Herosol," J. Opt. Soc. Am., LIV (1964), pp. 157-168.

46. Gates, L. W, Habell, K. L., and Lackson, A. "The Refractive Index of Materials from 0.2 to 5μ," Optica Acta (Internat.), VIII (1961), pp. 323-327.

47. Gates, David M., and Shaw, Clyde C. "Infrared Transmission of Clouds," J. Opt. Soc. Am., L (1960), pp. 876-882.

48. Gibbons, Mathew G. "Wavelength Dependence of the Scattering Coefficient for Infrared Radiation in Natural Haze," J. Opt. Soc. Am., XLVIII (1958), pp. 172-176.

49. Giese, R. H. "Light Scattering by Spherical Metal Particles," F. Naturforsch, XIVa (1959), pp. 1058-1088.

50. Gillham, E. J., and King, R. J. "New Design of Spectropolarimeter," J. Sci. Instr., XXXVIII (1961), pp. 21-25.

51. Grechushnikov, B. N., and Petrov, I. P. "A Polarizer for the Infrared Region of the Spectrum," Opt. and Spectroscopy, XIV (1963), pp. 160-161.

52. Greenberg, J. Mayo, Pedersen, Norman E., and Pedersen, Jeanne C. "Microwave Analog to the Scattering of Light by Nonspherical Particles," J. Appl. Phys., XXXII (1961), pp. 233-242.

53. Gucku, F. T., and Egan, J. J. "Measurement of the Angular Variation of Light Scattered from Single Aerosol Droplets," J. Colloid Sci., XVI (1961), pp. 68-84.

54. Gucker, F. T., and Rowell, R. L. "The Angular Variation of Light Scattered by Single Deoctyl Phthalate Aerosol Droplets," Faraday Society Discussions, No. 30 (1960), pp. 185-191.

55. Guinier, A., Fournet, G., Walker, C., and Yudowitch, K. Small - Angle Scattering of X-Rays. New York: John Wiley and Sons, Inc., 1955.

56. Gumprecht, R. O., and Sliepcevich, C. M. "Scattering of Light by Large Sperical Particles," J. Phys. Chem., LVII (1953), pp. 90-95.

57. Hales, J. J. "Double-Beam Infrared Grating Spectrometer," J. Sci. Instr., XXXVI (1959), pp. 264-266.

58. Hammard, H. "Scattering and Rescattering Sunlight," J. Opt. Soc. Am., XXXIX (1949), pp. 157-161.

59. Harris, E. J. "Use of a Photomultiplier in the Flame Photometric Analysis of Substances with Emission Bands in the Red," J. Sci. Instr., XXXVI (1959), p. 369.

60. Hawkins, H. M., Lang, Y. S., Gary, J. H., and Wikman, H. O. "A Special Analytical Study of Heat Transfer Phenomena with Clouds of Small Particles in Air at High Temperatures." University of Florida Engineering and Industrial Experiment Station Report (1950).

61. Heddle, D. W. O. "Photon-Scattering Processes," J. of Quantitative Spectroscopy and Radiation Transfer, Session A, II (1962), p. 349.

62. Heller, W. "Anisotropic Light Scattering of Streaming Suspensions and Solutions," Rev. Mod. Phys., XXXI (1959), pp. 1072-1077.

63. Heller, W., and McCarty, H. J. "Theoretical Investigations on the Light Scattering of Colloidal Spheres," J. Chem. Phys., XXIX (1958), pp. 78-80.

64. Heller, W., and Nakagaki, M. "Theoretical Investigations on the Light Scattering of Colloidal Spheres," J. Chem. Phys., XXXI (1959), pp. 1189-1195.

65. Heller, W., Nakagaki, M., and Wallach, M. L. "Theoretical Investigations on the Light Scattering of Colloidal Spheres," J. Chem. Phys., XXX (1959), pp. 444-450.

66. Henery, W. G., and Meharry, M. R. "Calibration of a Prism Spectrometer," J. Opt. Soc. Am., LI (1961), pp. 356-359.

67. Hodkinson, J. R. "Dust Measurements by Light Scattering and Absorption." Ph.D. Thesis, University of London (1962).

68. Hodkinson, J. Raymond. "Light Scattering and Extinction by Irregular Particles Larger than the Wavelength," International Series of Monographs on Electromagnetic Waves. New York: Macmillan Company, 1963.

69. Hodkinson, J. Raymond, and Greenleaves, I. "Computations of Light-Scattering and Extinction by Spheres According to Diffraction and Geometrical Optics, and some Comparisons with the Mie Theory," J. Opt. Soc. Am., LIII (1963), pp. 577-588.

70. Hulburt, E. O. "Optics of Atmospheric Haze," J. Opt. Soc. Am., XXXI (1941), pp. 467-476.

71. Ivanov, H. P. "Nonlinear Optical Phenomena in Scattering Media," Opt. and Spectroscopy, XIV (1963), pp. 142-147.

72. James, J. F. "Method of Double-Beam Spectrophotometry in the Vacuum Ultra-Violet," J. of Sci. Instr., XXXVI (1959), pp. 188-190.

73. Johnson, Peter D. "Optical Absorption and Diffuse Reflectance of Powders," J. Appl. Phys., XXXV (1964), pp. 334-336.

74. Jones, R. Clark. "Energy Detectable by Radiation Detectors," J. Opt. Soc. Am., L (1960), pp. 883-886.

75. Kerker, Milton. "Scattering Functions for Spherical Particles of Refractive Index of 1.46 - 4.30i," J. Opt. Soc. Am., XLII (1955), p. 1081.

76. Kerker, Milton, and Cox, A. Lucile. "Eleven Additional Light Scattering Functions for Spherical Particles of Refractive Index 2," J. Opt. Soc. Am., XLV (1955), p. 1080.

77. Kerker, Milton, and Hampton, Merle I. "The Use of Unfiltered Light in Determining Particle Radius by the Polarization Ratio of the Scattered Light," J. Opt. Soc. Am., XLIII (1953), pp. 370-372.

78. Kerker, Milton, Kratohvil, J. P., and Matyevic, E. "Light Scattering Functions for Concentric Spheres," J. Opt. Soc. Am., LII (1962), pp. 551-561.

79. Kerker, Milton, and Malyevie, Egon. "Mie Scattering Functions for Refractive Index of 2.105," J. Opt. Soc. Am., LI (1961), pp. 87-92.

80. _____. "Light Scattering of Monodispersed Polystyrene Latexes," J. Opt. Soc. Am., L (1960), pp. 722-729.

81. Kerker, Milton, and Perlee, Henry E. "Additional Light Scattering Functions for Spherical Particles of Refractive Index of 2," J. Opt. Soc. Am., XLIII (1953), pp. 49-50.

82. Knestrick, G. L., Cosden, T. H., and Cwicio, J. A. "Atomospheric Scattering Coefficients in the Visible and Infrared Regions," J. Opt. Soc. Am., LII (1962), pp. 1010-1016.

83. Kubo, K. "On the Intensity of Light Scattered by Fine Particles," J. Sci. Res. Inst. (Tokyo), L (1956), pp. 10-18.

84. Lamb, H. "Theory of Hydrodynamics," Proc. London Math. Soc., XXX (1881), pp. 189-212.

85. Larkin, Bert K., and Churchill, S. W. "Scattering and Absorption of Electromagnetic Radiation by Infinite Cylinders," J. Opt. Soc. Am., XLIX (1959), pp. 188-190.

86. Leibfried, G., and Oen, O. S. "A Simple Approximation for Classical Scattering at Large Angles," J. Appl. Phys. XXX, No. 77, pp. 2257-2262.

87. Levine, S., and Kerker, Milton. "Scattering of Electromagnetic Waves from Two Concentric Spheres, When the Outer Shell Has a Variable Refractive Index," International Series of Monographs on Electromagnetic Waves. New York: Macmillan Company, 1963.

88. Lorenz, L., and Selskàles, Videnskab. Skrifter, VI (1890); Scientifiques I (1898), pp. 405-502.

89. Love, Tom J., Jr. An Investigation of Radiant Heat Transfer in Absorbing, Emitting and Scattering Media, Norman, Oklahoma. University of Oklahoma Research Inst. 1963 (Contract AF 33 (657) - 8859) (ARL 63-3).

90. Love, Tom J., Jr., and Wheasler, R. A. An Experimental Study of Infra-Red Scattering by Clouds of Particles, USAF Office of Aerospace Research (ARL 64-109), June, 1964.

91. Macrae, J. C. "Significance of the Properties of Materials in the Packing of Real Spherical Particles," Brit. J. Appl. Phys., XII (1961), pp. 164-172.

92. Malijevic, E., Kerker, Milton, and Schulz, K. F. "Light Scattering of Coated Aerosols," Faraday Society Discussions, No. 30 (1960), pp. 178-184.

93. Maron, S. H., Elder, Mac E., and Pierce, P. E. J. Colloid Sci., XVIII, No. 2 (1963), pp. 107-119.

94. _____. J. Colloid Sci., XVIII, No. 3 (1963), pp. 199-208.

95. _____. J. Colloid Sci., XVIII, No. 4 (1963), pp. 391-399.

96. _____. J. Colloid Sci., XVIII, No. 8 (1963), pp. 733-744.

97. Maron, S. H., Pierce, P. E., and Vlevitch, I. N. J. Colloid Sci., XVIII, No. 5 (1963), pp. 470-482.

98. Meehan, E. V., and Beattie, W. H. "Light Scattering Functions for Spherical Particles with m = 1.75," J. Opt. Soc. Am., XLIX (1959), p. 735.

99. Melamed, N. T. "Optical Properties of Powders," J. Appl. Phys., XXXIV (1963), pp. 560-70.

100. Mcilraith, H. H. "A Soft-x-ray Spectrometer with Pulsed Source, and Synchronous Phosphor-photomultiplier Detector," J. Sci. Inst., XXXIX (1962), pp. 505-508.

101. Mie, G. Ann. Physik., XXV (1908), p. 377.

102. Millikan, Roger C. "Measurements of Particles and Gas Temperature in a Slightly Tuminous Premixed Plane," J. Opt. Soc. Am., LI (1961), pp. 535-542.

103. Mori, N., and Kekuchi, H. "Scattering of Light by Spherical Particles I," Bull. Electrotech. Lab.(Tokyo), XXI (1957), pp. 561-567.

104. _____. "Scattering of Light by Spherical Particles II," Bull. Electrotech. Lab. (Tokyo), XXII (1958), pp. 209-224.

105. Murley, R. D. "Mie Theory of Light Scattering. Limitations on Accuracy of Approximate Methods of Computation," J. Phys. Chem., LXIV (1960), pp. 161-162.

106. Nakagaki, M., and Heller, W. "Theoretical Investigations on the Light Scattering of Colloidal Spheres," J. Chem. Phys., XXX (1959), pp. 783-786.

107. _____. "Theoretical Investigations on the Light Scattering of Colloidal Spheres," J. Chem. Phys., XXXII (1960), pp. 835-842.

108. Napper, D. H., and Ottewill, R. H. "Multiple Scattering Effects in Polystyrene Latex Dispersions," J. Colloid Sci., XIX (1964), pp. 72-80.

109. Nelson, C. M., and Weeks, R. A. "Vacuum - Ultraviolet Absorption Studies of Irradiated Silica and Quartz," J. Appl. Phys., XXXII (1961), pp. 883-886.

110. Nonxira, Y., and Takaku, K. Res. Inst. Elec. Comm., VIIB (1955), p. 107.

111. Olson, O. H., and Katz, S. "Emusivity Absorptivity, and High-Temperature Measurements at Armour Research Foundation." First Symposium, Surface Effects on Spacecraft Materials.

112. Penndorf, Rudolf. "Angular Mie Scattering," J. Opt. Soc. Am., LII (1962), pp. 402-408.

113. _____. "An Approximation Method to the Mie Theory for Clloidal Spheres," J. Phys. Chem., LXII (1958), pp. 1537-42.

114. _____. "Approximation Formulas for Forward Scattering," J. Opt. Soc. Am., LII (1962), pp. 797-800.

115. Penndorf, Rudolf. "Scattering Coefficients for Absorbing and Nonabsorbing Spheres." AFCRL-TN60-667 (Technical Report RAD-TR-60-27, Avco Co.), Wilmington, Mass., October, 1960, 92 pages.

116. _____. "Scattering and Extinction Coefficients for Small Absorbing and Nonabsorbing Aerosols," J. Opt. Soc. Am., LII (1962), pp. 896-904.

117. _____. "Tables of the Refractive Index for Standard Air and the Rayleigh Scattering Coefficient for the Spectral Region between 0.2 and 20.0μ and their Application to Atmospheric Optics," J. Opt. Soc. Am., XLVII (1957), pp. 176-182.

118. Prebytkova, N. N., and Agrosken, L. A. "Optic Properties of some Dyes in a 'Massive' State by the Method of Mirror Reflection," Opt. Spectroscopy, II (1957), p. 623.

119. Preshwalko, A. P. "Study of Light Scattering from Large Highly Absorbing Spherical Particles," Opt. Spectroscopy, XIV (1963), pp. 139-141.

120. Reynolds, P. M. "Spectral Emissivity of 99.7% Aluminium between 200 and 540° C.," Brit. J. Appl. Phys., XII (1961), pp. 111-114.

121. Rodney, W. S., and Spindler, R. J. "Index of Refraction of Fired-Quartz Glass for Ultraviolet, Visible, and Infrared Wavelengths," J. Res. Nat'l. Bur. St., LIII (1954), R.P. 2531, p. 185.

122. Romanova, L. M. "Radiation Field in Plane Layers of a Turbid Medium with Highly Anisotropic Scattering," Opt. Spectroscopy, XIV (1963), pp. 135-138.

123. _____. "The Solution of the Radiation-Transfer Eq. for the Case When the Indicatrix of Scattering Greatly Differs from the Spherical One," Opt. Spectroscopy, XIII (1962), pp. 238-241.

124. Schiff, L. I. "Scattering of Waves and Particles by Inhomogeneous Regions," J. Opt. Soc. Am., LII (1962), pp. 140-144.

125. Sexl, R. "Theory of Multiple Scattering," Acta Phys. Ausbiaca, XIV (1961), pp. 180-184.

126. Shatilov, A. V. "Anomalous Scattering as a Case of Scattering by a System of Particles," Opt. Spectroscopy, XIII (1962), pp. 412-414.

127. Sinclair, David. "Light Scattering by Spherical Particles," J. Opt. Soc. Am., XXXVII (1947), pp. 475-480.

128. Sloan, Raymond, Shaw, John H., and Williams, Dudley. "Infrared Emission Spectrum of the Atomosphere," J. Opt. Soc. Am., XLV (1955), pp. 455-460.

129. Slutsker, A. I., and Marikhin, V. A. "Measurements of the Transmittance of a Light Scattering Medium as a Method of Studying Inhomogeneities in It," Opt. Spectroscopy, X (1961), pp. 263-266.

130. Speyer, E. "Cloud Chamber for Optical Measurements of Aerosols," Appl. Opt., II (1963), pp. 207-215.

131. Stein, R. S., Wilson, P. R., and Stidham, S. N. "Scattering of Light by Heterogeneous Spheres," J. Appl. Phys., XXXIV (1963), pp. 46-50.

132. Straffon, J. H. Electromagnetic Theory. New York: McGraw-Hill Book Company, Inc., 1941, p. 563.

133. Stull, V. Robert, and Plass, Gilbert N. "Emissivity of Dispersed Carbon Particles," J. Opt. Soc. Am., L (1960), pp. 121-129.

134. Sturge, M. D. "A Differential Absorption Spectrometer for the Infrared," J. Sci. Instr., XXXVIII (1961), pp. 96-98.

135. Tayor, J. H., and Yates, H. W. "Atmospheric Transmission in the Infrared," J. Opt. Soc. Am., XLVII (1957), pp. 223-226.

136. Tears, P. W. "Low-Angle Geiger Diffractometer for Use with Monochromatic Radiation," J. Sci. Instr., XXXVII (1960), pp. 132-134.

137. Theissing, H. H. "Macrodistribution of Light Scattered by Dispersions of Spherical Dielectric Particles," J. Opt. Soc. Am., XL (1950), pp. 232-243.

138. Timofieva, V. A. Dokl. Akad. Nauk SSSR 113 (1957), p. 556.

139. Tiversky, Victor. "Multiple Scattering of Waves and Optical Phenomena," J. Opt. Soc. Am., LII (1962), pp. 145-171.

140. Tourin, Richard H. "Measurements of Infrared Spectral Emissivities of Hot Carbon Dioxide in the 4.3μ Region," J. Opt. Soc. Am., LI (1961), p. 175.

141. Tourin, Richard H. "Some Spectral Emissivities of Water Vapor in the 2.7μ Region," J. Opt. Soc. Am., LI (1961), pp. 1225-1228

142. Tyler, John E. "Measurement of the Scattering Properties of Hydrosols," J. Opt. Soc. Am., LI (1961), pp. 1289-1293.

143. Urbach, Franz. "Notes on Specular Densities and Forward Scattering," J. Opt. Soc. Am., XXXIV (1944), pp. 592-594.

144. Van de Hulst, H. C. Light Scattering by Small Particles. New York: John Wiley & Sons, Inc., 1957.

145. _____. "Formation of Solid Particles in Intersellar Gas," Recherches Astronomiques de l'Observatoire d'Vtrecht, XI (1946).

146. Waterman, P. C., and Truell, R. "Multiple Scattering of Waves," J. of Math. Phys., II (1961), pp. 512-537.

147. Wheasler, Robert A. "Measurements of the Angular Distribution of Scattered Monochromatic Intensity from an Aerosol Containing Particles of Irregular Size and Shape for Wavelength in the Infrared." Ph.D. Dissertation, University of Oklahoma, 1964.

148. Wyatt, P. S. "Quasi - Random Model of Band Absorbtion," Opt. Soc. Am., LII (1962).

149. Wyatle, P. J. Phys. Rev., XCCVII (1962), p. 1837.

150. _____. "Light Scattering from Objects with Spherical Symmetry," International Series of Monographs on Electromagnetic Waves. New York: Macmillan Company, 1963.

151. Yokobori, S. "Study on the Emissivity of a Gas which Contains Particles." 1961 International Heat Transfer Conference Proceedings.

152. Yokota, T. "Expansion Theorem of Density Matrix, Virial Expansion and Neo Formula of Multiple Scattering," J. Phys. Soc. Japan, XV (1960), pp. 779-794.

NOMENCLATURE

English Symbols

a_j = Quadrature weight factor

c = Velocity of light, $(ft)\ (hr)^{-1}$

d = Particle diameter, (ft)

h = Planck's constant, $(Btu)\ (hr)^{-1}$

I = Monochromatic intensity of radiation, $(Btu)\ (ft)^{-2}\ (stearadian)^{-1}$

K^e = Extinction cross section

k = Boltzman's constant, $(Btu)\ (R)^{-1}$

M = Complex index of refraction

s = Scattering function

s = Distance along a ray, (ft)

x = Normal coordinate distance, (ft)

Greek Symbols

α = Particle size parameter

β = Monochromatic mass extinction coefficient, $(ft)^2\ (lb_m)^{-1}$

θ = Polar angle, radians

Θ = Angle between incident and leaving ray, radians

κ = Monochromatic mass absorption coefficient, $(ft)^2\ (lb_m)^{-1}$

λ = Radiation wave length, (ft)

μ = Cosine θ

ν = Frequency of radiation, $(hr)^{-1}$

π = 3.1416

ρ = Mass density, $(lb_m)\ (ft)^{-3}$

σ = Monochromatic mass scattering coefficient, $(ft)^2\ (lb_m)^{-1}$

τ = Optical depth

ϕ = Azimuthal angle, radians

ω = Solid angle, stearadian

Subscripts

i = Iteration index

j = Iteration index